Time- and gender- dependent differences in neuronal behaviors in culture

Dissertation

for the award of the degree

“Doctor rerum naturalium”

of the Georg-August-Universität Göttingen

within the doctoral program *IMPRS Neuroscience*

of the Georg-August University School of Science (GAUSS)

submitted by

Sinem Meleknur Sertel

from Istanbul, Turkey

Göttingen, March 2020

Examination Board:

Thesis committee

Prof. Dr. Silvio O. Rizzoli

Institute for Neuro-and Sensory Physiology, University Medical Center Göttingen

Prof. Dr. Hannalore Ehrenreich

Max Planck Institute for Experimental Medicine, Göttingen

Prof. Dr. Henrik Bringmann

Neurobiology, Department of Biology, Philipps-University Marburg

Extended Examination Board:

Prof. Dr. Siegrid Löwel

Systems Neuroscience, Georg-August University, Göttingen

Prof. Dr. Dörthe Katschinski

Department of Cardiovascular Physiology, University Medical Center Göttingen

Prof. Dr. Markus Bohnsack

Department of Molecular Biology, University Medical Center Göttingen

Date of oral examination: 13.05.2020

Affidavit

I hereby declare that this thesis has been written independently and with no other sources and aids than quoted.

Sinem Meleknur Sertel

Göttingen, 31.03.2020

Table of Contents

1| Summary

Isolating cells from a living organism and growing them in a Petri dish allowed scientists to study the physiology and biochemistry of healthy and diseased cells. Today we have cell cultures from almost any tissue type, including the brain. One brain region has been fundamental for understanding neuronal and synaptic dynamics, both *in vivo* and in culture: the hippocampus. Since the H.M. case, the hippocampus drew attention to itself with the promise of understanding molecular and electrical mechanisms behind learning and memory. This made the primary culture from hippocampus tissue one of the most commonly used models in the neuroscience field. Despite being a very common preparation, it is still imperfectly known.

For example, during preparation, multiple animals are sacrificed, and tissues are pooled, regardless of their sex. That creates a female-male mixed culture in which the female to male neuron ratio is unknown. It is still unclear whether the neurons of different genders behave differently in these cultures. To address this question, I performed a systematic investigation on cultured female and male neurons. I found differences in their electrical activity as well as in their synaptic translation rate. First, I compared the firing rates with a calcium indicator and found higher spontaneous electrical activity and larger response capacity to electrical stimulation in male neurons than in female neurons. The following step was investigating the dynamics of synaptic compartments with a synaptotagmin 1 (Syt1) uptake assay. It also proved that male neurons have a larger active synaptic vesicle pool size and dynamics than female neurons. An immunostaining survey with a focus on synaptic proteins did not show major differences between the two sexes. Their transcriptomes also shown substantial differences. Finally, I also examined the local translation, and found higher translation rate at the male synapse, which could, at least in part, explain the functional differences. These results present an extensive comparison for functional behavior and synaptic structure between female and male neurons and encourage a first discussion on primary hippocampal culture preparation in respect to female-male neuron ratio.

Another overlooked aspect of the primary hippocampal culture is the circadian effects on cellular biology. It is now well established that circadian rhythm is kept in every mammalian cell via the molecular clock, which consists of several transcription factors. However, without a central pacemaker, which *in vivo* is located in the suprachiasmatic nucleus (SCN) of the hypothalamus, it would be difficult to maintain a 24-hour rhythmicity in cell cultures. Therefore, we expect that primary hippocampal neurons in culture will maintain a form of rhythmus in culture, but this has never been studied. I performed a series of experiments indicating the existence of a weak circadian rhythm in the firing patterns, the synaptic activity and mRNA localization at the synapse, even after 20 day-long deprivation of external stimuli. I found a

rhythmically expressed transcript, RNA-binding motif 3 (RBM3), whose knock-down results in significant changes in the firing pattern and in the reduction of the active synaptic vesicle pool dynamics, the post-synapse size, and the post-synaptic translation rate. This implies that RBM3 is involved in sustaining the rhythmic abundance of synaptic proteins, and therefore in sustaining rhythmic synaptic function.

Overall, these findings change the impression of the primary hippocampal culture. It is essential to be aware of the female-male ratio and the timing of experiments.

2| General Introduction

In the late 19th century, while Ramon Y Cajal was studying the nerve endings on the smooth muscles and Charles Scott Sherrington was introducing the term ‘synapse’, Ross Granville Harrison cultured the nerve fibers from a tadpole in a lymphatic fluid and grew them for several weeks (Harrison et al., 1907a). His achievement was a milestone for the cell culture and neuroscience. The rapidly developing neuron culturing techniques and growing information on neurobiology have helped Gary Banker and W. Maxwell Cowan to establish a dispersed hippocampal neuron culture protocol (Banker and Cowan, 1977) that is even used today. It allowed neuroscientists to focus on the electrical properties of hippocampal neurons, study the development of neuronal processes and synaptic connections. There are many different versions of primary hippocampal culture preparation. However, the concept is mainly the same. The procedure starts with the hippocampi isolation from the brain and continues with cell dissociation. The dissociated cells are seeded on a glass coverslip that was treated with an adherent molecule for better cell attachment. Neurons are cultured up to four weeks in a medium that is specialized for the neuron growth. Despite being a widely used method over almost half a century, there are still overlooked steps in the procedure.

There has been accumulating strong evidence that female and male neurons show fundamental differences for instance in the biosynthesis and actions of steroid hormones (Hojo and Kawato, 2018) and the responds to metabolic challenges (Chowen et al., 2018; Reisert et al., 1989) and to hypoxic conditions (Heyer et al., 2005). Yet, it is common practice to pool isolated hippocampi into one tube for their dissociation regardless of the sex of sacrificed animals during the primary hippocampal culture preparation. Another important aspect is understanding the cellular and synaptic circadian behavior of dissociated hippocampal cultures. Many studies have shown oscillations in the molecular clock gene expressions in the cell culture, even in the absence of external stimuli (Balsalobre et al., 1998; Nagoshi et al., 2004). However, the culture synchronicity has been found to be lost in time, and it is expected to happen in any kind of cell culture. Nevertheless, the hippocampus, whose function relies on the sleep-wake cycle, has not been investigated in details neither *in vivo* nor *in vitro*. The endogenous rhythmicity of hippocampal neurons could explain the mechanisms behind the importance of the sleep-wake cycle during memory formation or retrieval and help to identify proteins that play a role in this process. Therefore, I studied the primary hippocampal culture with respect to functional and structural differences between the two sexes, and the different time points throughout the day.

In the following subsections, I will introduce the primary hippocampal culture briefly. Further, I will continue with an overview of the sexual differentiation in the brain. Lastly, I will present the mammalian-time keeping mechanism *in vivo* and *in vitro* with a focus on the neuronal tissue.

2.1| Brief history of the primary rat hippocampal culture

Culturing tissues and cells, isolated from an animal, was a long-lasting wish of scientists. It has allowed performing biochemical, pharmaceutical, and electrophysiological methods on a large scale. The journey of the cell culture has started with the development of a saline solution. In 1882 Sydney Ringer managed to keep a heart beating after it had been removed from a frog and placed into the saline solution. The saline solution can mimic the physiological conditions with the correct adjustments of the salt concentration, pH values, and osmotic pressure (Ringer, 1882). In the 1920s, it was possible to grow heart tissue in the cell culture by mixing chicken blood and Ringer solution (Carrel, 1923). This experiment pointed out the necessity of nutrients in the saline solution. A systematic investigation on the essential nutrients to supplement the saline solution gave rise to today's most used cell culture media at the end of the 1950s (Eagle, 1955, 1959). These improvements made it possible to grow almost any cell type, isolated from a living tissue (Yao and Asayama, 2017).

Neurons have been part of the cell culture journey since the beginning. In the 1890s, Ross Granville Harrison isolated nerve fibers from a tadpole and grew them in a lymphatic fluid for several weeks (Harrison et al., 1907b). Till the 1950s, scientists were performing *ex vivo* experiments, where a tissue is isolated from a living animal. To observe the developmental stages, methods on how to separate cells from the tissue had been discussed. It was possible to dissociate tissues from invertebrate animals with a mechanical force, but vertebrate cells were not surviving such treatment (Moscona and Moscana, 1952). In 1952, Moscona A. found a pancreatic protease enzyme, namely trypsin, to be used as a dissociating reagent, and he dissociated the limb buds from a chick embryo (Moscona, 1952). In 1956, the dorsal root was dissociated from the chick embryo and grown in the culture (Nakai, 1956). The only remaining problem for the dissociated culture was the cell body attachment to the surface. The solution was introduced in the 1970s by Yavin E. and Yavin Z.. They took advantage of the electrostatic interaction between poly-lysine coated surfaces and dissociated cells from rat embryonic brain (Yavin and Yavin, 1974). Having a positively charged surface will increase the interaction with the negatively charged membrane of a cell. While physiologists were improving the protocol for dissociated cultures, others were working on specializing the basal medium for neuron growth. To promote the development of a cell in a culture dish, serums, which were processed from animal blood, have been used. The serum contains growth factors, nutrients, essential vitamins and amino acids. However, it was challenging to adjust concentrations of these elements, as it depends on the metabolism of the animal. Together with the discovery of growth factors, serum-free media has been started to be tailored according to the cell type. In the late 20th century, Brewer G.J. supplemented the serum-free basal media with vitamin E, progesterone, bovine serum albumin, fatty acids, and glutathione (Brewer et al., 1993). His

recipe maintained the differentiated growth of many different neuron types, such as cortical and hippocampal neurons (Brewer, 1995).

In the meantime, the famous case study of H.M. patient, who developed a loss of short-term memory formation upon a bilateral hippocampal lesions in 1957 was published (Scoville and Milner, 1957). The research interest in the hippocampus structure and its role in memory formation has grown since, and the hippocampus has become one of the most-well studied brain regions. On the mission to capturing the molecular signature of learning and memory, Banker G.A. and Cowan W.M. published their protocol for culturing rat hippocampal neurons in 1977 (Banker and Cowan, 1977). It allowed neuroscientists to focus on the electrical properties of hippocampal neurons, study the development of neuronal processes and synaptic connections.

Since then, the dissociated hippocampal culture has been modified heavily. The medium has been optimized, different enzymes have been suggested for the tissue dissociation, and alternative coating materials have been found. However, the main concept remained the same (**Figure 1**). Briefly, the brain is removed either from an embryonic 18 day (E18) rat or a newborn rat (postnatal day 0, P0). The hippocampi are isolated from the brain. After collecting all hippocampi in a single tube, cells are dissociated with an enzyme. Historically, this enzyme is trypsin, but for the experiments in this thesis, papain was used. To complete the dissociation process, cells are repeatedly passed through the pipette. Then the cells are counted and seeded on top of a glass coverslip. The glass coverslips are coated with a positively charged polymer, poly-L-lysine (PLL) to increase the attachment of a negatively charged membrane. Today there are many alternative adherent molecules optimized for the cell type and the surface. Furthermore, cells are grown in a basal medium that is specialized for neuron growth. In essence the medium provides essential hormones, vitamins, amino acids, glucose, inorganic salts, and a pH buffer. Overall, with this technique, it is possible to maintain dissociated cells up to 4 weeks in the incubator at 37ºC with the support of 5% CO_2 gas and full humidity. On day 1, they present short arbors. On day 8, they have multiple long arbors trying to find partner neurons. Till day 15, they grow very rapidly and form a very intricate network (**Figure 1**) (Dotti et al., 1988).

The primary hippocampal culture is not completely homogenous in terms of cell types. Three different types of cells have been identified: glia, excitatory, and inhibitory neurons (Benson et al., 1994). Glia cells have been found throughout the central nervous system, including the P0 rat hippocampus (Freeman and Rowitch, 2013). In our preparations, glia cells take up to ~70% of the culture (**Chapter 3 Supplementary Figure 1**). Mainly their function is to keep the homeostasis in the culture by maintaining ionic balance, collecting excess neurotransmitters from the extracellular space, and supporting neurons with energy and neurotransmitter

substrates. While glia cells make up the largest portion of the culture, excitatory neurons (glutamatergic neurons) make up the majority among neuronal cells. As it has been described in the literature before, only 5-6% of the neurons in the primary rat hippocampal culture are inhibitory neurons (γ-aminobutyric acid (GABA)ergic neurons) (Benson et al., 1994). Having glia and neurons in one culture helps to maintain neurons healthy, and the low GABAergic neuron percentage sustains a stable network activity during the lifetime of the culture.

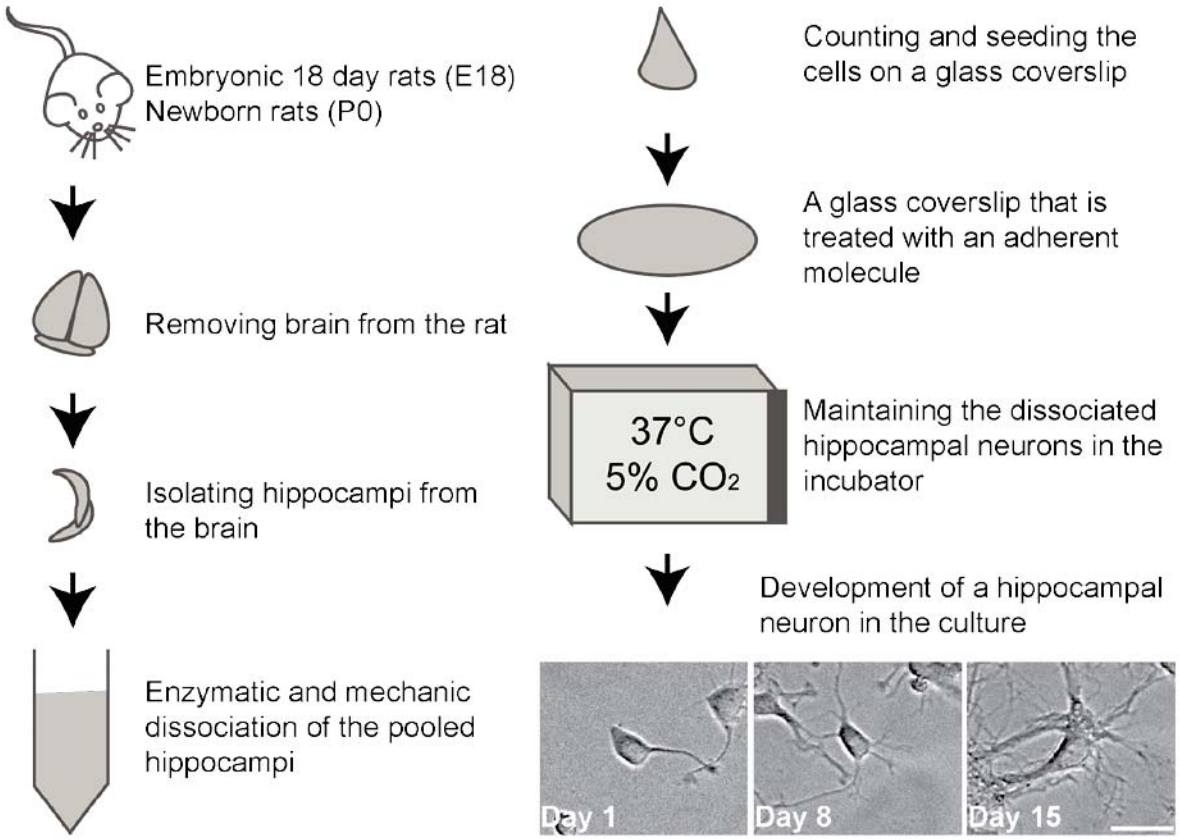

Figure 1. The schematic representation of the primary rat hippocampal culture preparations. The rats from embryonic 18 day (E18) and later stages (up to P0) can be used for the culture preparation. The brain is removed from the rat and the hippocampi are isolated. Later the cells are completely dissociated with an enzymatic treatment and a mechanic force. The dispersed cells are counted and seeded accordingly on the glass coverslip. For better attachment, the glass coverslips are treated with an adherent molecule prior to the cell plating. The cells are kept in the incubator up to 4 weeks with a basal medium that is specialized for neuron growth. The primary rat hippocampal neurons were kept in BioSpa 8 automated incubator (Biotek, Germany), and representative images were taken by Cytation Gen 5 plate reader (Biotek, Germany) with 20X phase objective (1320517, BioTek, Germany). Scale bar: 200 µm.

Another heterogeneous aspect of the primary hippocampal culture is being a mixture of female and male hippocampi. In a traditional sense, the sex of the sacrificed animal has been seen as irrelevant, and hippocampi have been pooled into one tube without knowing the female-

male hippocampi ratio. In the following subsection, I will discuss the physiological and morphological differences between female and male neurons. Notably, the primary hippocampal cultures throughout the thesis have an equal contribution from both sex, except exclusive female and exclusive male cultures that are presented in the Chapter 2.

Although the morphology and physiology of hippocampal neurons *in vitro* are relevant to the hippocampal neurons *in vivo*, primary cultures certainly lack daily external input. For example, animals can anticipate changes in environmental cues by a time-keeping mechanism called circadian clock. This mechanism organizes daily rhythms from molecular level to behavior such as sleep-wake cycle. Many cellular processes have been linked to circadian rhythm and having external stimuli, like the light intensity, helps to sustain these rhythms. However, external stimuli do not exist in an isolated environment such as an incubator. Taken together with the major effects of the molecular clock on cellular biology, the remaining circadian rhythm in the primary hippocampal culture has been addressed in this thesis. Therefore, in the last subsection, I will explain the mammalian time-keeping mechanism *in vivo* and *in vitro*.

2.2| Sexual differentiation in the brain

Observations on sex-dependent behavior and physiology in vertebrates have been reported over the decades. Sex-specific hormones have been thought to be the driving force for the sexual differentiation or in another term, sexual dimorphism. While sex-specific hormones are at the core of the research, overwhelming evidence has been accumulating that these differences are present even before the secretion of sex-specific hormones (Gegenhuber and Tollkuhn, 2020). Such findings indicate that sexual dimorphism starts to occur during embryonic development. Moreover, primary cultures, which are widely in use, are in question of having female-male mixed neurons with sex-specific differences in their morphology and physiology.

Genetic and epigenetic factors are the origin of sexual differentiation.

The genetic difference between female and male mice is mostly found in the sex chromosome pair. Female cells contain two X chromosomes, while male cells have an X and a Y chromosome as a sex chromosome pair (Mclaren, 1988). The epigenetic and genetic information on these chromosomes is the origin of sexual differentiation. For example, female cells start the differentiation with an X chromosome inactivation and male cells start with SRY-dependent transcription.

Firstly, to compensate for the X chromosome dosage, one of the X chromosomes in female cells is randomly selected to become silent (Chow et al., 2005). The X inactivation center (XIC) is a region on the X chromosome (Lee and Jaenisch, 1997), which consists of non-coding RNAs like Xist, Tsix, Jpx, and Ftx (Mercer et al., 2009). The expression of these non-coding RNAs indicates the X-chromosome dosage and determines which X chromosome to inactivate. To initiate the inactivation, the Xist non-coding RNA coats the randomly selected X chromosome (**Figure 2a**) and induces a high level of DNA methylation together with low levels of histone acetylation among many other gene silencing modifications (Costanzi and Pehrson, 1998).

Conversely, male cells do not undergo X inactivation. They initiate male sex differentiation because of a sex-specific transcription factor, called sex-determining region Y (SRY) (Koopman et al., 1991). SRY is essential for male phenotype development. (**Figure 2a**). Its absence on the Y chromosome leads to a female phenotype, and its insertion onto the X chromosome pair results in a male phenotype. SRY-induced gene expression directs the gonadal development from a female to a male gonadal differentiation. Once the gonadal development is completed, sex-specific hormones that are secreted from the gonads will play a major role in sexual differentiation.

Sexual differentiation in such early stages is permanent for the animal. Not only the gonadal development is affected by the sexual differentiation but also the brain development, which will be described in the upcoming subsection.

Sex-specific hormones promote sexual differentiation.

During development, female and male gonads are the main source of sex-specific hormones. The female gonads secrete progesterone and estrogen, whereas male gonads secrete low amounts of progesterone but high quantities of testosterone and dihydrotestosterone (DHT) (**Figure 2b**). These hormones are referred to as steroid hormones because of their similarity to cholesterol. The mechanism of action is either through nuclear steroid hormone receptors or non-nuclear steroid hormone receptors. Nuclear steroid receptors are transcription factors, which will be localized at the nucleus upon steroid hormone binding where they induce gene expression (**Figure 2c**). Since they can pass through the membrane due to their lipid-like structure, they can directly take part in cell signaling. Tissue and sex specificity are then achieved by regulating the abundance of steroid hormone receptors and their distribution in the cell.

The sexual dimorphic nucleus-preoptic area (SDN-POA) and the anteroventral periventricular nucleus (AVPV) are great examples of tissue and sex specificity. Although both of these

regions are located in the hypothalamus, their development is completely different. The neurogenesis in the SDN-POA starts earlier in the female fetus than male (Jacobson and Gorski, 1981). In the later stages, however, estrogen triggers apoptosis in this region. Androgen receptor activation in the male SDN-POA has been found to block the apoptosis signal (Döhler et al., 1982; Murakami and Arai, 1989). In turn, female SDN-POA after birth has less neurons than the male SDN-POA (Jacobson et al., 1980). In contrast to SDN-POA development, at birth AVPV has more neurons in a female mouse than a male mouse (Simerly et al., 1985b, 1985a). The high abundance of aromatase in the AVPV converts testosterone into the 17ß-estradiol, an estrogen, which activates cellular apoptosis signal (Lephart et al., 2001). This results in more cell loss in the male AVPV.

Sexual differentiation in the brain starts even before the sex-specific hormone secretion.

Testosterone secretion starts at E15 (Picon, 1976) and it can be found in the plasma on E18 onwards (Ward and Weisz, 1980). Sexual differentiation in the brain has been observed even before testosterone secretion. The neurogenesis in the SDN-POA has started earlier in female mice and it has already more cells than male SDN-POA on E14 (Jacobson and Gorski, 1981). Moreover, the dissociated hypothalamus culture from E14 female mice has been found to have more dopaminergic neurons than male ones. These female dopaminergic neurons also exhibit longer neurites in their morphology and more dopamine uptake in comparison to the male dopaminergic neurons (Reisert et al., 1989). These observations suggest that neurons have already initiated sexual differentiation before sex-specific hormone secretion. It is an indication that neurons, which are used in primary cultures, have already undergone to sexual differentiation. As female and male neurons are mixed during culture preparations, these differences might be found in the primary culture too.

The sexual differentiation in the hippocampus also contributes to the sex-specific behavior.

Hypothalamus was one of the first brain regions that was playing role in sexually dimorphic behavior. Together with the enhancements in the technology, it was possible to track sex-specific hormones (Pfaff, 1968; Stumpf, 1968) and detect their receptors (Stumpf and Sar, 1976; Toft and Gorski, 1966) in other brain regions (Pfaff and Keiner, 1973). Reports on sex-specific memory performance (Bowman et al., 2003; Luine et al., 1994, 1996; Sherwin, 1988) drew attention on the hippocampus. Non-nuclear steroid receptors along the dendrites, at synapses and glia processes have been found in the hippocampus (McEwen and Milner, 2007). Nevertheless, the underlying molecular mechanism for sex-specific memory performances is still remained unclear.

As it has been shown for the hypothalamus, the hippocampus is also subjected to sexual differentiation in molecular level. Pyramidal hippocampal neurons found to have non-nuclear steroid receptors at the dendrites regardless of their sex (Weiland et al., 1997). On the other hand, early studies employing electron microscopy showed nuclear estrogen receptors being localized in female, but not in male GABAergic neurons (Loy et al., 1988; Nakamura et al., 2004). Nuclear androgen receptor has been exclusively found in male pyramidal hippocampal neurons (Kerr et al., 1995; Tabori et al., 2005). Such cell type and sex dependent differences in the receptor distribution will contribute to sexually dimorphic behavior.

Estrogen has been found to play a major role in neurogenesis, synaptic density, and plasticity. In the 1990s, the spine number in the CA1 region of the hippocampus was shown to be cyclic throughout the estrous cycle in female mice. The highest number of spines was detected at the proestrus stage where the estrogen level peaks (Woolley et al., 1990). In another study, bath-applied estrogen increased the kainite-induced currents in female and male dissociated hippocampal cultures via non-nuclear steroid receptors (**Figure 2d**) (Gu and Moss, 1996; Gu et al., 1999). Application of estrogen receptor α and ß agonists induced PSD95 and GluR1 gene expression (Waters et al., 2009). Multiple studies have repeatedly shown that through nuclear or non-nuclear receptors, estrogen is modulating the electrophysiological response, and can induce long-term potentiation (LTP) (Foy et al., 1999; Fugger et al., 2001; Kumar et al., 2015; Smith and McMahon, 2005). LTP is a long-lasting strengthening of the synapse due to a steady increase in the synaptic excitability (Citri and Malenka, 2008). These findings suggest that sexual differentiation is manifested by the abundance of steroid receptors and their localization in the neuron according to the cell type with downstream effects via steroid receptor activation contribute to sexually dimorphic neuronal activity and behavior.

Does the incomplete organization of sexual differentiation affect the morphology and physiology of primary hippocampal neurons?

The previous section describes how sexual differentiation influences cell fate and neuronal physiology. While it is evident that P0 rats have already initiated sexual differentiation, it is still unknown whether there is a sex-specific behavior in the primary hippocampal culture. It is important to remember that the basal medium used for maintaining the culture contains estrogen, and progesterone (Brewer et al., 1993). Having sex-specific hormones in the medium could organize as well as activate the sexual differentiation in primary cultures. Another critical role is played by the cell types in the culture. There are glia cells, inhibitory, and excitatory neurons, which have been shown to have sex-specific steroid receptor expression and distribution (McEwen and Milner, 2017). Overall it is essential to investigate

sex-specific behavior in one of the most common *in vitro* models, the primary hippocampal neurons, before drawing major conclusions regarding the physiology and morphology.

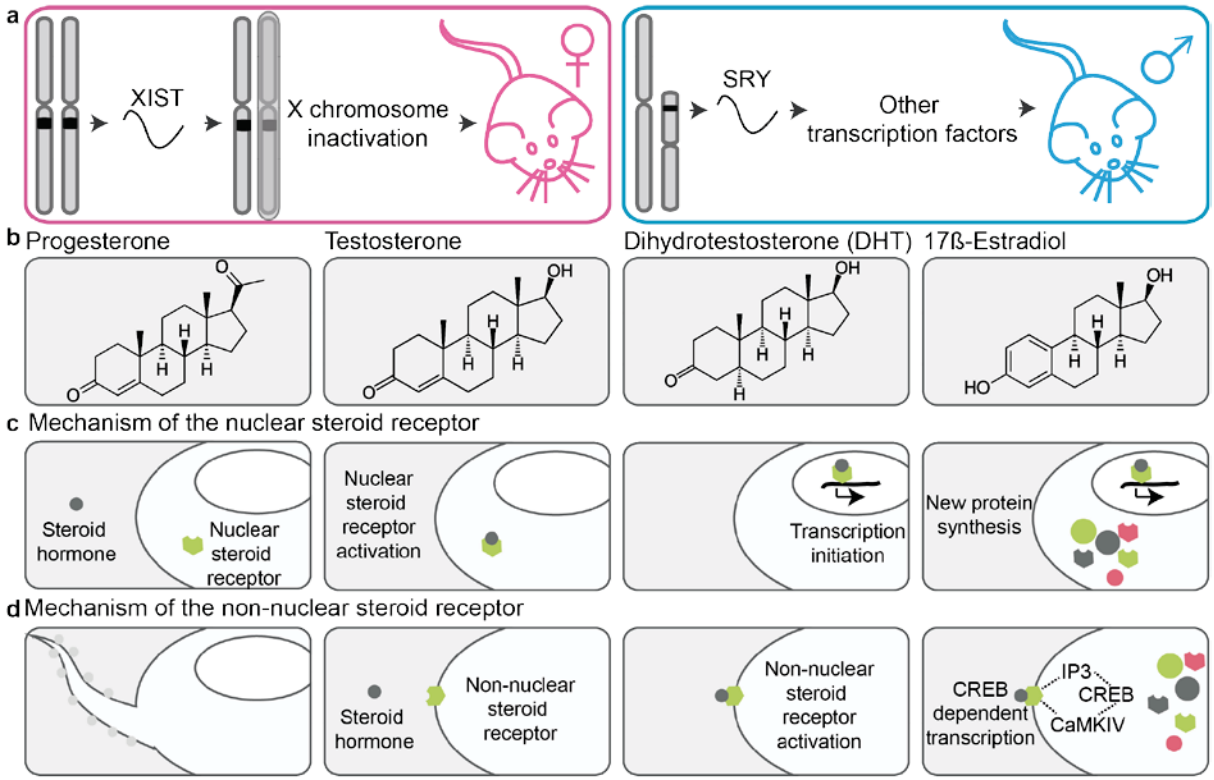

Figure 2. The origin and mechanisms of sexual differentiation. (a) The illustration indicates the sex chromosome pair differences between female and male mammals, including mice, rats, and humans. The sex of the cell is determined according to the number of X chromosomes and the Y chromosome. One of multiple copies of the X chromosome has to be inactivated for the dosage compensation. The inactivation starts with the expression of non-coding RNAs like Xist from the X chromosome inactivation center (XIC). They randomly select an X chromosome and silence it by coating with Xist and promoting epigenetic modifications (Chow et al., 2005). For male differentiation, it is necessary to have a sex-determining region Y (SRY) gene. This transcription factor induces gene expressions, some of which can initiate male differentiation (Koopman et al., 1991). **(b)** The structures of sex-specific hormones are depicted. Progesterone and estrogen (17ßestradiol) are found in female animals in high-quantities. Male animals secrete mainly testosterone and dihydrotestosterone (DHT) from their gonads. **(c)** The illustration depicts the mechanism of steroid hormones through nuclear steroid receptors. Nuclear steroid receptors are transcription factors. Upon activation through steroid hormone binding, they localize to the nucleus and promotes gene expression (Frick et al., 2015). **(d)** Similar to c, the illustration depicts the mechanism of action for steroid hormones through non-nuclear steroid receptors. Even the distal parts of a neuron have been shown to have non-nuclear steroid receptors. Non-nuclear steroid receptor activation leads to CREB dependent gene expression via the ERK or the adenyl cyclase signaling pathway (Frick et al., 2015).

A recent study addressed the effects of sexual differentiation on the neuronal morphology of primary hippocampal cultures (Keil et al., 2017). Male P0 hippocampal neurons were shown

to have longer primary neurites and develop more arbors on their dendrites than female neurons at day *in vitro* (DIV) 9. Interestingly, such differences have not been observed in cultured cortical neurons. These findings encouraged our study to investigate sex-specific physiological differences in the primary hippocampal neurons.

I explored sexual differentiation in the primary hippocampal culture in many different levels. Firstly, to identify differentially expressed transcripts, we performed mRNA sequencing. Our findings suggest that female neurons have slightly more transcripts that are playing a role in the synaptic organization. These transcripts, however, were not found in the proteome as differentially abundant between primary hippocampal cultures from the two sexes. Later, to determine whether there is a sex-specific firing rate, we explored the calcium dynamics and synaptic activity. In contrast to the transcriptome data, male neurons have higher global and synaptic activity as well as larger active recycling synaptic vesicle pool than female neurons at DIV 15. Finally, we investigated the local translation rate, to understand the relation between electrical behavior and transcriptome data. Our assay reported that the synaptic translation rate was significantly higher in male neurons than in female neurons. In summary, male neurons have higher global and synaptic activity, supported by higher rates of local synaptic translation. The results suggest that primary hippocampal neurons do exhibit sex-specific physiology.

2.3| The mammalian time-keeping mechanism

The theory of the 'survival of the fittest' has highlighted the importance of adaption throughout evolution. Animals have survived by adapting and anticipating the 24 hours rhythmic changes in the surrounding environment, like the temperature, light, and food availability. To achieve such fitness, time-keeping mechanism has evolved to coordinate 24 hour-long oscillations of external and internal cues is called the circadian clock.

Reports on circadian behavior go back to the 18th century. Jean Jacques d'Ortous de Mairan reported his observation on the daily rhythmic up and down movement of heliotrope plants' leaves (De Mairan, 1729). His observation, however, was not followed further. Two centuries later, together with the discovery of the *period gene* in the fruit fly *Drosophila melanogaster* (Konopka and Benzer, 1971), the interest in a new research field has grown. Today the time-keeping mechanism is subject to behavioral, physiological, and molecular studies (Dibner et al., 2010; Hastings et al., 2003).

A circadian behavior consists of three essential elements. The main component is the endogenous rhythmicity. The circadian behavior should generate a rhythmicity even in the absence of external stimuli. For example, light is a very powerful environmental cue for the

entrainment. In constant darkness, the sleep-wake cycle of a mouse is forced to be generated by an endogenous rhythmicity or internal clock. Even after 23 days, the locomotor behavior has been reported to be rhythmic (Gutman et al., 2011). The second component of a circadian behavior is the entrainment by external cues. Input from any environmental factor can help the circadian clock to be entrained. The food shock is a very common external cue to synchronize the molecular clock in an *ex vivo* tissue (Balsalobre et al., 1998). The last component of a circadian behavior is to generate 24 hour-long rhythmicity. In summary, a true circadian behavior is a daily endogenous rhythmicity that can be entrained by environmental factors.

The molecular clock is the representation of the circadian clock on the cellular level.

Every mammalian cell has the molecular signature for the circadian clock, which is at the heart of endogenous rhythmicity. The fundamental mechanism of the molecular clock is based on an auto-regulatory feedback loop (Young and Kay, 2001). Approximately 5% of the genes are rhythmically expressed across the tissues, and they form multiple transcriptional-translation feedback (TTF) loops. I will introduce the four clock genes that are part of the core TTF loop.

The core clock components are CLOCK (Circadian Locomotor Output Cycles Kaput), BMAL (Brain and Muscle ARNT (Aryl hydrocarbon Receptor Nuclear Translocator) Like), Per (Period), and Cry (Cryptochrome). BMAL and CLOCK are transcription factors that dimerize in the cytoplasm. After the BMAL-CLOCK dimerization, they are transported to the nucleus. The dimer binds to the *cis*-regulatory E-box (Enhancer box) on the promoters of *Per* and *Cry* genes. Upon BMAL-CLOCK induced transcription, mRNA levels of *Per* and *Cry* genes are increased. After translation, the mature Per and Cry proteins heterodimerize at the cytoplasm and are transported to the nucleus to repress their own transcription. As the abundance of Per and Cry decreases due to their life-time, the BMAL-CLOCK heterodimer can induce Per and Cry gene expression again (Gekakis et al., 1998). This cycle takes roughly 24 hours.

Together with the molecular clock, approximately half of the genes are rhythmically expressed in mammals (Yan et al., 2008). The targets of the molecular clock are tissue specific to allow various metabolisms and physiologies (Doherty and Kay, 2010; Zhang et al., 2014).

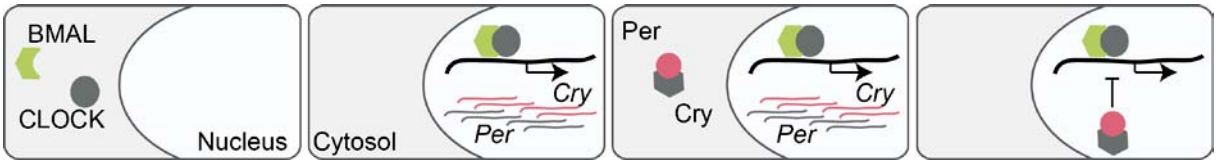

Figure 3. The molecular signature of the circadian clock is a transcriptional-translational feedback loop. As the transcription factors BMAL and CLOCK heterodimerize, the complex is translocated to the nucleus. The dimer induces the Per and Cry gene expression by binding to their upstream promoter sequence. The mRNA levels for Per and Cry will increase, and they will be translated

into proteins in the cytoplasm. The mature Per and Cry proteins heterodimerize like BMAL-CLOCK and are transported to the nucleus. By suppressing their own gene expression, the transcriptional-translational feedback loop is complete. While Per and Cry proteins are degrading within their life-time, the abundances of BMAL and CLOCK are increasing. Once the abundance of Per-Cry versus BMAL-CLOCK dimers is out of balance, BMAL-CLOCK will induce the expression of Per and Cry genes again.

The master clock SCN synchronizes the molecular clock across tissues.

There are several external cues that can help the entrainment, and light is substantially the strongest entrainer for the circadian behavior. Studies on the light–dark cycle have shown that the light has a great capacity to shift the phase and to extend or shorten the period of the circadian behavior. Therefore, scientists have come up with the idea that there should be a master clock in the brain that integrates the sensory information that brings the external input and governs the internal circadian rhythmicity across tissues (Pittendrigh, 1960). In the following years, neural tracing studies have discovered the connection between the eye and the brain: the retino-hypothalamic tract (RHT) (Hendrickson et al., 1972; Moore and Lenn, 1972). At the recipient end of the tract there was the suprachiasmatic nucleus (SCN) of the hypothalamus. Many circadian behaviors such as locomotor behavior and adrenal corticosterone secretion were disrupted by SCN lesions (Moore and Eichler, 1972; Stephan and Zucker, 1972), and the SCN transplantation restores the rhythmicity (Lehman et al., 1987). These findings demonstrated the importance of the SCN as a master clock.

The anatomical location of SCN can explain the strong light influence on the circadian rhythm. The SCN is located atop of the optic-chiasm and receives the majority of its inputs from the retina. The other main inputs are projections from the geniculohypothalamic tract (GHT), and raphe nuclei (van Esseveldt et al., 2000; Meyer-Bernstein and Morin, 1996). These are thought to be non-photic inputs for internal cues such as body temperature and food intake. Retrograde tracking methods have found several efferent pathways of the SCN (van Esseveldt et al., 2000; Meyer-Bernstein and Morin, 1996). They project to the arcuate nucleus that organizes the food intake behavior, the preoptic area that coordinates the sexual behavior, the amygdala that controls decision-making processes, and many other regions of the brain (Dibner et al., 2010). However, circadian behavior is not only governed by direct connections from the SCN but also by indirect connections from other brain regions. By coordinating the timing of the hypothalamus hormone secretion, the SCN can maintain synchronicity across many tissues (Guilding and Piggins, 2007).

Another remarkable feature of the SCN is having a very-well coupled neuron network. There are 20,000 neurons in the nucleus (Abrahamson and Moore, 2001), and their connections are heavily depending on gap junctions (Colwell, 2000; Jiang et al., 1997). Together with this tight

network, the firing pattern in the SCN exhibits circadian rhythmicity (Paul et al., 2019). The firing rate of the SCN is thought to communicate the time information and generate a coherent rhythm in the central and peripheral tissues.

The circadian rhythm is cell-autonomous and self-sustained, even in the absence of an entrainment.

After the discovery of SCN and the presence of molecular clock genes in the periphery, the master clock was thought to entrain damped rhythmicity in peripheral tissues. In parallel to this notion, the first observations on explant periphery tissues demonstrated that skeletal muscle, liver, and lung explants exhibit rhythmic but damped *Per1* (Period 1) gene expression up to 7 days without any external cues or the SCN input (Yamazaki et al., 2000). In the following years, many studies have reported that the rhythmic molecular clock gene expression is self-sustained in the periphery (Yamamoto et al., 2004; Yoo et al., 2004). These reports clearly indicate the presence of an endogenous rhythmicity in the peripheral tissue.

Such rhythmic but damped molecular clock gene expression has been found also in dispersed and cell line cultures (Balsalobre et al., 2000a). Instead of complete synchrony, in the absence of tight interactions and external cues, cultured cells exhibit desynchronized individual rhythms (Nagoshi et al., 2004). This wide distribution of the period length can be synchronized by external stimulations such as a serum shock (Balsalobre et al., 1998), a temperature shock (Brown et al., 2002; Ohnishi et al., 2014) and activation of cell signaling with glucocorticoid treatments (Balsalobre et al., 2000b; Yoo et al., 2004). These findings suggest that every tissue has a cell-autonomous self-sustained rhythmicity, but the SCN maintains the synchronicity.

The SCN encodes the time information through its firing pattern.

The SCN is responsible for the synchronization of molecular clock across tissues. Its remarkable firing pattern is thought to be the underlying mechanism of how the SCN is delivering time of day information. In the SCN, the firing rate is low during the night, whereas it is high during the day (Inouye and Kawamura, 1979). Furthermore, the membrane potential has been found to be time-dependent (Kuhlman and McMahon, 2004). These effects on the membrane properties are due to the activity and expression of ion. Briefly, high sodium (Paul et al., 2016; Pennartz et al., 1997) and calcium currents (Pennartz et al., 2002) are the excitatory drive for a high firing frequency during the day. A higher potassium current (Meredith et al., 2006; Montgomery and Meredith, 2012) is responsible for the nightly silencing.

Such robust and rhythmic firing patterns have been seen in different preparations ranging from freely moving hamsters (Yamazaki et al., 1998) to dispersed SCN cultures (Green and Gillette, 1982; Herzog et al., 1998). The SCN firing pattern in mice is resistant to the absence of rhythmic environmental light cues (Nakamura et al., 2011). In contrast to *in vivo* experiments, the synchronicity in firing patterns was lost in dispersed cultures. Dissociated SCN cells exhibited rhythmicity but in a desynchronized fashion (Welsh et al., 1995). Culturing SCN neurons with a high density generated synchronous firing patterns (Aton et al., 2005; Honma et al., 1998; Liu et al., 1997). Furthermore, blocking synaptic communication by a TTX (tetrodotoxin, a sodium channel blocker) treatment in the high density dispersed SCN cultures and in acute slices showed that network activity is necessary for the SCN synchronicity (Honma et al., 2000; Yamaguchi et al., 2003). As in the peripheral tissue, the circadian rhythmicity of the SCN is cell-autonomous and self-sustained. Moreover, the tightly coupled network is essential to maintain a coherent firing pattern.

The molecular clock is rhythmically expressed in the hippocampus.

The hippocampus is one of the most-well characterized brain regions due to its role in memory consolidation. Interestingly, the hippocampus expresses the whole pallet of molecular clock genes in a rhythmic manner (Besing et al., 2017; Chun et al., 2015; Harbour et al., 2014; Jilg et al., 2010). In contrast to the SCN expression pattern, *Per2* gene expression in the hippocampus is peaking in the late night (Wang et al., 2009). The rhythmic gene expressions of *Cry1* and *Per2* have been found to be resistant to the constant dark condition (Mei et al., 2018; Wang et al., 2009). Moreover, the organotypic hippocampus sustained the rhythmicity of *Per2* gene expression over several cycles (Wang et al., 2009). Overall, these reports suggest that the hippocampus has self-autonomous circadian rhythmicity.

Synaptic plasticity is a time-dependent process in the hippocampus.

There is overwhelming evidence that can link the molecular clock to hippocampus-dependent memory formation (Snider et al., 2018). For example, knocking out *Cry1* and *Cry2* genes exhibited impairment of time-place learning (Van der Zee et al., 2008). *Per1* knock-out (KO) mice had problems with spatial learning in the radial arm maze (Jilg et al., 2010).

Synaptic plasticity has been shown to be the molecular mechanism of memory process. It is a biological process that describes modulations on the synaptic strength depending on the synaptic activity. It has been explored mainly in the hippocampus tissue. The excitatory postsynaptic potential (EPSP) has been found with the greatest amplitude at night (Barnes et al., 1977; Cauller et al., 1985). However, this difference in the EPSP amplitude was not

observed in other studies (West and Deadwyler, 1980). In the following years, many studies tried to find a consensus on the topic without much success (Besing et al., 2017; Chaudhury et al., 2005; Harris and Teyler, 1983). The differences seen across these findings could be attributed to the animal models and different LTP induction protocols.

Several studies have tried to explain the molecular connection between the synaptic plasticity and molecular clock. BMAL-CLOCK heterodimer has been found to bind to the promoter of CREB (Travnickova-Bendova et al., 2002). Another study has reporterd that MAPK inhibits BMAL-CLOCK heterodimerization by phosphorylating BMAL protein (Sanada et al., 2002). These findings suggest that molecular clock genes, especially ones expressed in the hippocampus, can influence memory formation (Gerstner and Yin, 2010; Smarr et al., 2014).

2.4| Aims of this work

The overall objective of this work was to characterize the primary hippocampal culture from a new angle: sex-specific differences and temporal dynamics. These perspectives have never been systematically addressed in such a common *in vitro* model, the primary culture. Due to overwhelming evidence on sexual differentiation in the brain, I set out to investigate whether there are sex-specific differences between female and male neurons in the hippocampal culture. To achieve this goal, I first established sex-specific dissociated hippocampal cultures. Further, I compared the two sexes in the mRNA and protein levels. I performed functional assays to determine the electrical activity, synaptic vesicle dynamics and size. Later, I surveyed the synaptic proteins with immunostainings to determine distribution and abundance of synaptic proteins. Lastly, to investigate the synaptic plasticity I studied the local protein translation rate at the synapse. Overall, I compared sexual differentiation of the two sexes on multiple levels.

I have also investigated the temporal dynamics of primary hippocampal neurons. I performed various imaging assays at different time-points of the day to determine rhythms in electrical activity, synaptic vesicle dynamics and synapse size. Furthermore, time-series transcriptome pointed out a robust rhythmic expression of an mRNA called RNA-binding motif 3 (RBM3). I characterized this protein with a short-hairpin RNA (shRNA) method to understand its influence on the electrical activity, synaptic vesicle dynamics and local translation in synapses. In summary, I studied the temporal dynamics of primary hippocampal cultures and characterized a protein that might play a role in sustaining a rhythm in firing patterns via local translation in synapses. This work provides insights into how sex-specific differences and temporal dynamics can affect the cellular biology in the hippocampus.

3| Sex-specific differences in the primary hippocampal culture

Sinem M. Sertel[1], Wiebke Blumenstein[1], Sunit Mandad, Silvio O. Rizzoli[1,2*]

Author contribution of Sinem Meleknur Sertel:

- Design (together with Silvio O. Rizzoli), performance and analysis (together with Silvio O. Rizzoli) of experiments shown in the following figures: Figure 1a-e (together with Wiebke Blumenstein), Figure 1f-h, Supplementary Figures 1-3, Supplementary Figure 4 (together with Sunit Mandad), Figure 2,5-8 (together with Wiebke Blumenstein)
- Preparation of the manuscript together with Silvio O. Rizzoli.

This article has not been submitted yet.

Sex-specific differences in the primary hippocampal culture

Sinem M. Sertel[1], Wiebke Blumenstein[1], Sunit Mandad, Silvio O. Rizzoli[1,2*]

[1]Institute for Neuro- and Sensory Physiology, University Medical Center Göttingen, Göttingen, Germany
[2]Lead Contact
*Correspondence: srizzol@gwdg.de (S.O.R.)

3.1| Abstract

The rat hippocampal culture has been a standard model for studies of neuronal function for more than four decades. The typical protocol involves the dissociation of multiple hippocampi from newborn rats, which are then combined and plated. This typically results in cultures containing mixtures of male and female hippocampal neurons. To test whether gender affects neuronal function in these cultures, we plated male and female neurons separately and analyzed them by tools ranging from molecular biology to functional imaging assays. We found very few differences at the transcriptome or proteome levels. Nevertheless, male neurons displayed stronger levels of both spontaneous and stimulated activity, had larger active vesicle pools, and they also showed higher levels of local translation in synapses. This implies that experiments involving such cultures should take the sex of the newborn rats into account, to ensure that experiments can be reproduced well across cultures.

3.2| Introduction

The primary hippocampal culture has been one of the most common systems in neurobiology, used for studies of neuronal morphology (Kapitein et al., 2010), synaptic function (Matteoli et al., 1995; Molnár, 2011), and neurodegenerative disease (Imahori and Uchida, 1997; Landfield, 1996) for several decades. The cultures are prepared from enzymatically and mechanically dissociated hippocampi of newborn rats. The sex of the sacrificed animals has not been taken into account during this procedure, and it results in female-male mixed neuronal cultures. This means that the female to male neuron ratio is unknown, and it may vary from culture to culture. As sexual differentiation in the brain is well documented in behavior and on cellular levels, female-male mixed cultures raise a question about whether neurons from female and male hippocampi act differently in the primary culture.

Several studies have shown that cell lines and primary cultures exhibit functional differences between female- and male-derived cells. Even before gonadal hormone secretion, female neurons take up more dopamine than male neurons in primary hypothalamic cultures (Reisert et al., 1989). Primary hippocampal cultures are also subjected to sexual differentiation. Female neurons have been reported being more resistant to hypoxic conditions than male neurons (Heyer et al., 2005). On the other hand, male neurons have been shown to have more elaborated dendritic arbors than female neurons (Keil et al., 2017). These findings, taken together with sex-specific differences in hippocampus function (Hojo and Kawato, 2018) draw attention on how sexual differentiation influences the physiology of primary hippocampal neurons.

Despite being a standard *in vitro* culture model, the effects of sex in the primary hippocampal neurons have not been systematically studied. Here we compared female and male hippocampal cultures with experiments ranging from RNA sequencing to calcium imaging. While female and male hippocampal neurons have a similar transcriptome and proteome in primary cultures, we found a slightly but significantly higher electrical activity and synaptic translation rate in male neurons. We conclude that it is important to be aware of the sex-dependent functional differences and keep the female to male ratio constant in mixed hippocampal cultures for reproducibility. Moreover, sex-specific primary hippocampal cultures provide an opportunity to study sexual differentiation in the hippocampus.

3.3| Methods

Hippocampal cultures. We prepared the primary dissociated hippocampal from newborn rats (Kaech and Banker, 2006). The dissected hippocampi were washed with Hank's balanced salt solution (HBSS, Thermo Fisher, US). To dissociate the tissue, hippocampi were incubated in the enzyme solution (1.6 mM cysteine, 100 mM $CaCl_2$, 50 mM EDTA, and 25 units papain in 10 ml Dulbecco's modified eagle medium (DMEM)) for 1 hour. The hippocampi were incubated 15 more minutes after the addition of 5 ml DMEM (Thermo Fisher, US) that contains 10% fetal calf serum, 0.5% albumin, and 0.5% trypsin inhibitor to inactivate the enzymes in the solution. The enzymatic dissociation was followed with a mechanical disruption. 80,000 cells were seeded on poly-L-lysine (Sigma-Aldrich, Germany) coated circular coverslips (1.8 cm in diameter). To optimize the cell attachment, seeded neurons were kept in plating medium (3.3 mM glucose, 2 mM glutamine, and 10% horse serum in DMEM) at 37°C. After 1 hour incubation, the medium was changed to Neurobasal-A medium (with B27 supplement, 1% GlutaMax, and 0.2% penicillin/streptomycin mixture). The cultures were kept at 37°C and 5% CO_2 for ~20 days.

Transfection. The cultures were transfected at DIV5 with lipofectamine 2000 (Thermo Fisher, USA) according to the manufecturer's protocol. The plasmid was designed by Sinem M Sertel, and synthesized by Genscript (US). It has a pUC57 as a backbone, a ubiquitin C (UBC) promoter and a membrane-bound GFP sequence as a reporter.

Immunostaining. The cultured neurons were washed once with the cold tyrode buffer (124 mM NaCl, 5mM KCl, 2 mM $CaCl_2$, 1 mM $MgCl_2$, 30 mM D-glucose, and 25 mM HEPES), and fixed for 30 min at room temperature with 4% PFA (Sigma-Aldrich, Germany). Fixed cells were quenched with a solution (100 mM NH_4Cl in phosphate buffer solution (PBS)) for 30 min at room temperature. Later on, cells were washed three times with the permeabilization solution (3% bovine serum albumin (BSA), 0.01% Triton-X-100 in PBS). Cells were stained during 1 hour incubation with 0.2% of the primary antibody in the permeabilization solution, and they were subsequently washed three times with the permeabilization solution. Afterwards, cells were incubated with 0.5% of the secondary antibody in the permeabilization solution for 1 hour. Subsequently, cells were washed three times with high salt PBS which is supplemented with 0.38 M NaCl on a shaker and two times with PBS. If it is specified, cultures were stained with Hoechst dye. To stain the nucleus, cells were incubated for 5 min with 1:1000 Hoechst in PBS. Lastly, coverslips were mounted in 8 µl Mowiol (Merck Millipore, Germany) and stored at 4°C. Unless otherwise specified, imaging was performed with the IX83 inverted Olympus (Japan) confocal microscope (Abberior, Germany) that is equipped with a 100X super-apochromat and coverslip corrected oil objective (Olympus, Japan). The analysis was performed on Matlab (MathWorks, US) and plotted with Graphpad (US).

Half of the immunostaining survey on synaptic proteins was performed with a confocal microscope called LSM 780 laser scanning microscope (Zeiss, Germany), which is equipped with an Examiner Z1 microscope (Zeiss, Germany), a 20X water objective (Plan-apochromat, Zeiss, Germany) and an AxioCam camera (Zeiss, Germany).

Calcium imaging. A genetically encoded calcium indicator NeuroBurst Orange Lentivirues (Sartorius, Germany) was used for the calcium imaging. Neurons were incubated with 3 µl of NeuroBurst from day *in vitro* (DIV) 10 till DIV20. The glass coverslips were placed into the imaging chamber and imaged at 37°C with an inverted Nikon Ti eclipse epifluorescence microscope (Nikon, Japan) with a 20X Plan Apo (Nikon, Japan) objective, an HBO-100W lamp, an IXON X3897 Andor camera (Andor, UK) and a cage-incubator (Okolab, Italy). A calcium dye was used for the electrically stimulated neurons. Prior to imaging, cells were incubated with 1.8 µg/ml of Fluo-4 AM (F14201, Thermo Fisher, US) for 30 minutes. After the wash with 1 ml of cold tyrode buffer, the coverslip was placed in imaging chamber with the electrical stimulator and imaged in the Nikon microscope which is described above. Cells were imaged

for 5 minutes. Within that time, they were subjected to 3 and 30 seconds long 20 Hz electrical stimulations.

Synaptotagmin1 (Syt1) Uptake assay. To determine the synaptic vesicle dynamics, we performed the Syt1 Uptake assay. Syt1 is a calcium sensor protein on a synaptic vesicle. Its luminal domain is exposed to the medium when the synaptic vesicle exocytose during recycling. A fluorescently-conjugated antibody targets the exposed luminal domain of Syt1 and is taken up with recycling of the vesicle. For this assay, neurons were incubated with 2.5 µg/ml Syt1-Atto647N antibody (105311AT1, Synaptic Systems, Germany) in 300 µl of their own Neurobasal-A medium for 45 min. This incubation was followed the addition of 16.7 nM anti-mouse secondary nanobody (N2002-At542-S, Nanotag, Germany) conjugated to Atto542 into the medium. 15 min later, neurons were washed with ice-cold tyrode buffer and fixed with 4% PFA. To label the complete presynaptic vesicle pool, Synaptophysin (Syph) immunostaining with Syph antibody (101004, Synaptic Systems, Germany) was performed as described in the immunostaining section. To estimate the Syt1 surface pool and spontaneous vesicle fusion, we performed the Syt1 assay with a Na^+ channel blocker tetrodotoxin (TTX, Tocris Bioscience, UK) and with the 'on-ice' condition that slows down the metabolism. The assay was imaged with a n inverted Nikon Ti eclipse epifluorescence microscope (Nikon, Japan) that has a 20X Plan Apo (Nikon, Japan) objective, an HBO-100W lamp, an IXON X3897 Andor camera (Andor, UK), and was analyzed using Matlab (MathWorks, US).

Puromycin assay. To determine the translation rate at a particular location, we performed the puromycin assay. It takes advantage of an antibiotic called puromycin (ant-pr-1, InvivoGen, US) that stops an ongoing translation by incorporating itself into the premature poly-peptide chain and then releases it. The coverslips were incubated with 1 µg/ml of puromycin in the incubator. 10 min later, neurons were washed twice with the ice-cold tyrode buffer, and fixed with 4% PFA. To estimate the background signal, we added 0.13 µM anisomycin A5862, Sigma-Aldrich, Germany) which halts the translation complex by inhibiting tRNA-transferase activity into the cultures for 10 min before the puromycin treatment. At the end of the assay, neurons were immunostained for Synaptophysin (101004, Synaptic Systems, Germany), Homer1 (160011, Synaptic Systems, Germany), and puromycin (MABE343, Merck Millipore, Germany) as described in the immunostaining section.

The FUNCAT (Fluorescent Non-Canonical Amino Acid Tagging) assay. To determine the protein turnover rate and localization of newly synthesized proteins at a particular location, we performed the FUNCAT assay (Tom Dieck et al., 2015). Neurons were incubated with 0.2 mM HPG (C10186, Thermo Fisher, US) in DMEM medium that is supplemented with 6.5 mM HEPES, B27 supplement, 0.25mM L-cysteine, and 0.81 mM $MgCl_2$ for 4 hours in an incubator. The metabolically labeled neurons were washed with ice-cold tyrode buffer and fixed with 4%

PFA. Fluorescent STAR635P-azide (Abberior, Germany) was conjugated to the HPG with a Click reaction (Click-iT reaction buffer kit, Thermo Fisher, US) as described in the manufecturer's protocol. To verify the specificity of the reaction, we incubated the coverslips in a media without HPG. The following Homer1 and Syph staining were performed as described in the immunostaining section.

Transcriptomics. RNA was isolated from the culture with the miRNeasy Kit (Qiagen, France). The mRNAseq experiments were performed by Transcriptome and Genome Analysis Laboratory (TAL, Göttingen, Germany). Limma package was used for differential expression analysis (Ritchie et al., 2015), and Webgestalt database was used for gene ontology analysis with Ensemble gene IDs of differentially expressed transcripts and difference folds between the two sexes (Wang et al., 2017). The result of gene set enrichment analysis indicates the pathways with a p-value <0.05 and a false-discovery rate (FDR)<0.05. The transcripts with significant differences between the sexes are listed in **Supplementary Table 1**.

Sample processing for iBAQ. The protein lysate was collected by scraping cultures with 100 µl of tyrode buffer. All the samples were subjected to protein estimation using standard BCA protocol (Smith et al., 1985) as provided by the Thermo Scientific online. 10 µl of 1% RapiGest was added to 20 ug of protein sample (male, female and UPS2 standard protein in separate vials) and heated to 95°C for 5 min. All subsequent steps were performed at 750 rpm on a thermomixer at room temperature. 10 µl of 100 mM ammonium bicarbonate solution was added to the sample and incubated for 5 min. To reduce cysteines, 10 µl of 10 mM dithiothreitol in 100 mM ammonium bicarbonate was added and incubated for 1 hour. Reduced cysteines were alkylated by adding 10 µl of 100 mM iodoacetamide in 100 mM ammonium bicarbonate and incubated for 20 min in dark. 180 µl of 100 mM ammonium bicarbonate was added to dilute the detergent percentage to 0.1%. Finally, trypsin (1:20, ProMega) was added to the protein samples for digestion. Trypsin was quenched by adding 20 µl of 5% formic acid solution. The protein samples were incubated in 20 µl of 5% trifluoro-acetic acid for 2 hours to deteriorate the detergent RapiGest. The protein samples were further desalted using StageTips. Briefly, at least four C_{18} plugs were filled in a micropipette tip to make one column. Prior to use, the column was washed twice with 50 µl of methanol. The column was equilibrated by passing 50 µl of 0.1% formic acid solution twice. The supernatant containing peptides was loaded on a pre-equilibriated column. While passing the supernatant through column, the peptides being hydrophobic bound to the C_{18} matix. The column was washed four times with 50 µl of 0.1% formic acid solution. Finally, bound peptides were eluted by 50 µl of 80% acetonitrile, 0.1% formic acid solution twice. The eluted peptide solution was dried using SpeedVac. 1 µg of digested protein sample (male or female or UPS2 standard protein) were injected and processed for LC-MS on a 90 min gradient on Q-Exactive HF Mass Spectrometer

(Thermo Scientific). UPS2 standard protein was analysed between the samples to estimate the abundance of protein in the sample by label-free intensity based absolute quantification (iBAQ) approach.

Liquid chromatography mass spectrometry (LC-MS). The resuspended peptides in sample loading buffer (5% acetonitrile and 0.1% trifluoroactic acid) were fractionated and analysed by an online UltiMate 3000 RSLCnano HPLC system (Thermo Fisher Scientific) coupled online to the Q Exactive HF or Orbitrap Fusion Lumos Tribrid Mass Spectrometer (Thermo Fisher). Firstly, the peptides were desalted on a reverse phase C18 pre-column (3 cm long, 100µm inner diameter 360 mm outer diameter) for 3 minutes. After 3 minutes the pre-column was switched online with the analytical column (30 cm long, 75 µm inner diameter) prepared in-house using ReproSil-Pur C18 AQ 1.9 µm reversed phase resin (Dr. Maisch GmbH). The peptides separated with a linear gradient of 5–30% buffer B (80% acetonitrile (Lichrosolv) and 0.1% formic acid) at flow rate of 10 nL/min gradient of 88 min on Q-Exactive HF. The pre-column and the column temperature was set to 50°C during the chromatorgraphy. The precursors were scanned in the mass range from 350 to 1600 Da at a resolution of 60,000 at m/z 200. Top 30 precursor ion were chosen for MS1 by using data-dependent acquisition (DDA) mode at a resolution of 15,000 at m/z 200 with maximum IT of 50 ms. For MS2, HCD fragmentation was performed with the AGC target fill value of 1e5 ions. The precursors were isolated with a window of 1.4 Da. The lock mass option (m/z 445.1200 (Olsen et al., 2005)) was used for internal recalibration.

Database search and data analysis. Proteins were identified using MaxQuant software (Cox and Mann, 2008) version 1.5.3.8 or 1.6.0.16 using the Andromeda search engine (Cox et al., 2011) with rat SwissProt (December 2016; containing 29795 entries) and Human Universal Proteome Standard (UPS2, Sigma-Aldrich) protein databases. For the database search, tolerance of 6 ppm (for MS) and 10 ppm (for MS/MS) were set. Oxidation of methionine and carbamidomethylation of cysteines were set as variable and fixed modifications respectively. Tryptic specificity with no proline restriction and up to 2 missed cleavages was used. False discovery rate (FDR) was set at 1%. Additionally, the LFQ and iBAQ option were enabled for quantification (using the log10 fit). Perseus was used for further data analysis and volcano-plot. The proteins with significant differences between the sexes are listed in **Supplementary Table 2**.

3.4| Results

Female and male derived primary hippocampal cultures have similar transcriptome and proteome.

To investigate whether sex is affecting the function of primary hippocampal neurons, we cultured female and male neurons separately and tested them after they have mature synaptic connections at *day in vitro* (DIV) 20. We started the culture characterization by analyzing the cell types and concentrations. We found that the cell concentration for glia and neurons were similar across cultures and the two sexes (**Supplementary Fig. 1**). To investigate the neuronal volume, we expressed membrane-bound GFP (mGFP) in neurons and compared the GFP positive areas. There were no differences in neuronal volumes depending on the sex of the cultures (**Supplementary Fig 2**).

We followed these observations with an analysis of the transcriptome (**Supplementary Table 1**) and the proteome (**Supplementary Table 2**). We found few significant differentially expressed mRNAs (**Supplementary Fig. 3 and 4**), including transcripts from sex chromosomes such as male enriched Y chromosome-linked genes. The pathway enrichment analysis with differentially expressed mRNAs showed that neuronal function related transcripts have a slightly higher expression in female cultures (**Supplementary Fig. 3b**), albeit this tendency did not propagate to the protein amounts (**Supplementary Fig. 4**).

Male hippocampal neurons have higher calcium activity than female neurons.

To determine the functional differences, we first compared the electrical activity between female and male neurons with a genetically-encoded calcium indicator, NeuroBurst (Sartorius, Germany). We imaged neurons for 5 minutes on DIV 21 (**Fig. 1a and b**), and calculated the normalized mean intensity of somas throughout the video (**Fig. 1c and d**). To compare the spontaneous electrical activity, we measured the activity scores which are the areas under the peaks of the normalized mean intensity. According to our measurements, male neurons are significantly more active than female neurons (**Fig. 1e**). To test whether the firing capacity is different, we electrically stimulated the neurons for 3 and 30 seconds with 20 Hz frequency (**Fig. 1f**). We found that the male neurons respond to stimulations with a larger calcium influx (**Fig. 1g and h**). We conclude that even the differences are not more than 40%, the male neurons have a higher spontaneous firing rate as well as a bigger firing capacity than the female primary hippocampal neurons.

Male hippocampal neurons have more synaptic vesicle recycling and a bigger actively-recycling pool.

To investigate whether the electrical activity differences are reflected at the synaptic level, we measured synaptic vesicle dynamics with the Synaptotagmin 1 (Syt1) uptake assay. It is possible to detect recycling vesicles with an antibody that targets the luminal domain of a calcium sensor Syt1 (Kraszewski et al., 1995; Matteoli et al., 1992). The recycling vesicles take up the Syt1 antibody since the luminal domain of Syt1 is available to the antibody after exocytosis (**Fig. 1i**). To examine the active vesicle pool size, we incubated neurons with fluorescently-conjugated Syt1 antibodies for 45 minutes, which is sufficient enough to label all active synaptic vesicles (Truckenbrodt et al., 2018). We then incubated cells for 15 minutes with fluorescently-conjugated secondary nanobodies (NB) that detect the Syt1 antibody. The NB will be taken up by a recycling vesicle that is labeled with the Syt1 antibody. The short incubation of NB enables to measure the synaptic activity rather than the pool size (**Fig. 1i**). To validate this assay, we blocked action potential generation by using a Na^+ channel blocker: tetrodotoxin (TTX). Blocking action potential generation significantly decreased the active vesicle recycling and thus reduced both the Syt1 antibody and NB stainings (**Fig. 1k and l**). To confirm the results, we also performed the assay on ice to slow the cellular metabolism, and as expected, we found similar results (**Supplementary Fig. 5**). We marked the presynapse with a Synaptophysin (Syph) immunostaining and measured the intensity of the Syt1 antibody as well as NB in Syph positive areas (**Fig. 1j**). Our measurements suggest that male neurons have a bigger actively-recycling vesicle pool (**Fig. 1k**) as well as a higher synaptic activity (**Fig. 1l**). Overall these experiments confirm that male neurons have a slightly (~40%) but significantly bigger actively-recycling vesicle pool and have more frequent synaptic vesicle recycling.

Synaptic organization is similar between female and male hippocampal neurons, despite their global and synaptic activity differences.

To investigate the synaptic organization in more detail, we surveyed synaptic proteins with immunostainings (**Supplementary Fig. 6**). Among many pre- and postsynaptic markers, we found that Bassoon has significantly higher, but Synaptophysin (Syph) has less intensity in female neurons in the culture (**Supplementary Fig. 6a**). To check whether the number of synapses varies between female and male cultures, we calculated the number of detected objects in each immunostaining. However, we have not found any substantial differences between the two sexes (**Supplementary Fig. 6b**). The activity differences were not accompanied by the changes in the synaptic organization.

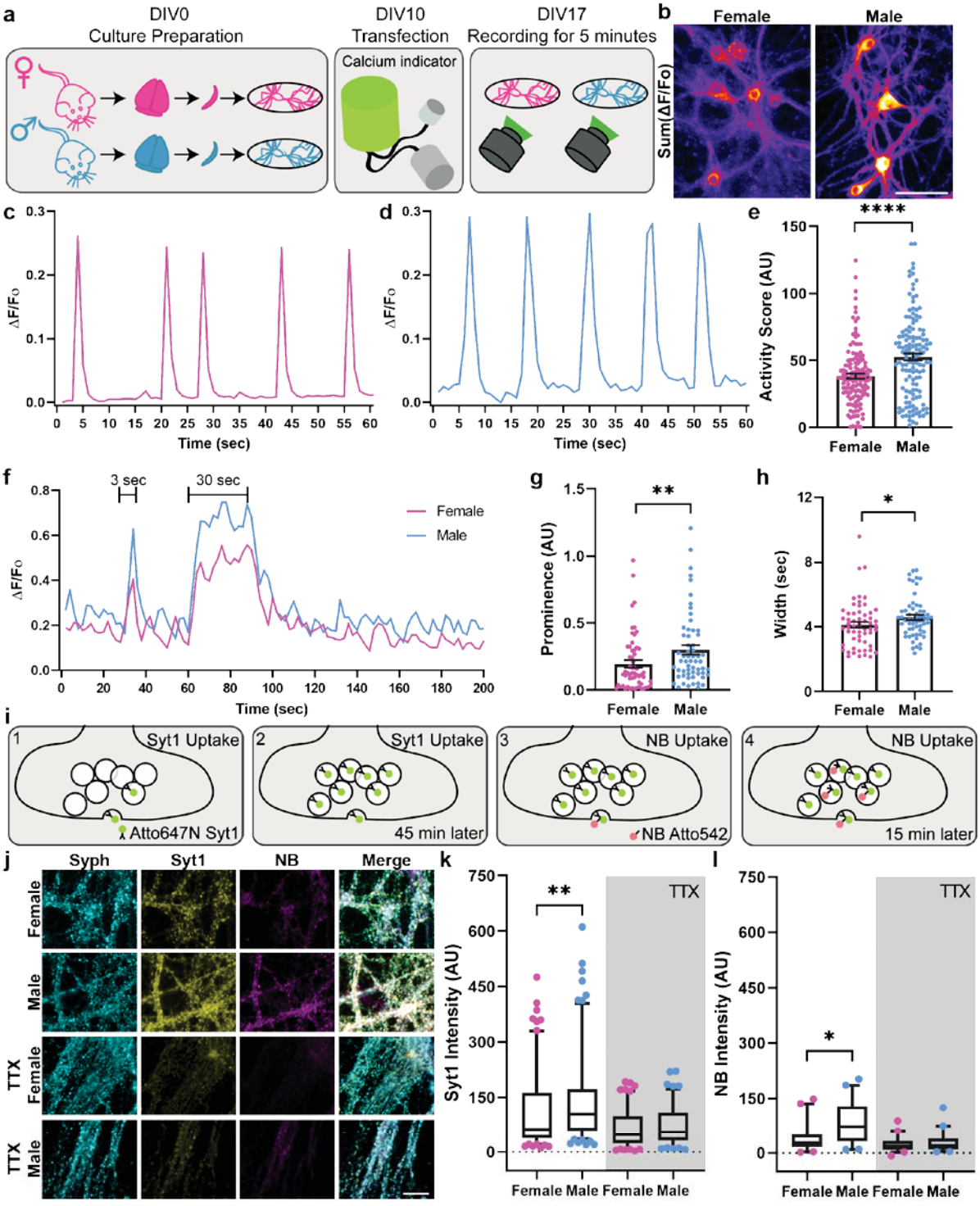

Figure 4. Male hippocampal neurons have a higher firing rate and more synaptic activity than female hippocampal neurons in the primary culture. (a) To be able to study the effects of sex on the primary culture, we separated the female and male neurons during the primary culture preparation. To determine the spontaneous firing rate, we transfected cultured hippocampal neurons at DIV10 with the genetically-encoded Ca^{2+} indicator Neuroburst. At DIV17, we imaged neurons for 5 minutes. **(b)** To visualize the overall activity, we summed frames of 5-minute-long videos and presented them as heatmaps to demonstrate the total activity. Scale bar: 50 µm. **(c and d)** To measure the activity in a neuron, we selected the neuronal cell bodies. We calculated the mean fluorescence intensity and normalized it to the baseline ($\Delta F/F_0$). The graphs show the exemplary normalized intensity for female and male hippocampal neurons. **(e)** To compare the spontaneous electrical activity of the two

sex, we calculated the area under the curve from the intensity graphs, which we termed “activity score”. We performed calcium imaging with 3 independent culture preparations that have 6 coverslips for each condition, and a maximum of 10 neurons were selected from a coverslip. We analyzed 135 neurons for both sexes. The graph indicates the average activity score (± SEM), and each symbol represents a neuron. The statistical comparison between the two sexes was performed with the Mann-Whitney test. ****p<0.0001. **(f)** To determine the firing capacity of the neurons, we electrically stimulated them with 20 Hz frequency for 3 and 30 seconds. We selected the cell bodies and measured the normalized mean intensities over time. The line graph presents the average of 58 female and 59 male hippocampal neurons from 4 independent culture with 6 coverslips measured per experiment. **(g and h)** To compare the responses to electrical stimulations, we calculated the prominence and the width of each response. The graphs illustrate the mean (± SEM) of the prominence and the width, respectively. Each dot represents a neuron. The statistical comparisons between the two sexes were performed with the Mann-Whitney test. *p<0.05 and **p<0.005. **(i)** To determine whether the presynaptic activity of male neurons depicts a similar trend to the calcium imaging, we used a Synaptotagmin 1 (Syt1) uptake assay (Kraszewski et al., 1995; Matteoli et al., 1992) at DIV18. To visualize the recycling vesicle pool, we incubated the neurons with an Atto647N-conjugated Syt1 antibody for 45 minutes (1). The antibody detects a luminal (intravesicular) domain of calcium sensor synaptic vesicle protein Syt1, and will be taken up during the synaptic vesicle recycling. To saturate the recycling vesicle pool and estimate its size, it is sufficient to incubate neurons with the Syt1 antibody for 45 minutes (2). To estimate the overall synaptic activity of the neurons, we added Atto532-conjugated secondary nanobodies (NB), which detect the Syt1 antibody, for 15 minutes (3). Since a 15 minute-long incubation is not enough to label the complete recycling vesicle pool, the subset of NB labeled vesicles represents the synaptic activity level (4). To mark the presynapse, the cultures were subsequently fixed and were immunostained for Synaptophysin (Syph). To verify the assay, we stopped action potential generation with a tetrodotoxin (TTX) treatment. Not having action potential allows the Syt1 antibodies to bind only to the surface epitopes (Truckenbrodt et al., 2018). **(j)** Exemplary images of female and male neurons, along with a TTX treatment, are shown. Scale bar: 50 µm **(k** and **l)** The Syt1 and NB intensities in Syph positive areas were calculated, with and without TTX treatment. The bar graph indicates the mean ± SEM. Each symbol represents the average intensity in one image. For Syt1 staining N=7 independent experiments, for NB staining N=4 independent experiments. To compare the intensities between female and male neurons, we performed one-way ANOVA test, followed by the Holm-Sidak multiple comparison test. *p<0.05, **p<0.005.

Male neurons have a higher translation rate at the synapse.

As activity is strongly linked to cellular and synaptic turnover (Sutton and Schuman, 2006), we tested whether the differences in the activity could also be observed at the protein turnover and the translation level. We first performed an assay that investigates the protein turnover rate (Kos et al., 2016). We incubated the neurons with a Methionine substitute called HPG (L-Homopropargylglycine) for four hours. HPG will be incorporated into newly synthesized proteins in the meantime. After the incubation, we conjugated fluorescent probes on each HPG-labeled newly synthesized protein with a particular reaction called Click reaction (Tornøe et al., 2002) (**Supplementary Fig. 7a**). To study the protein turnover rate in the soma, we imaged neurons with an epifluorescence microscope. We did not find any profound difference between the two sexes (**Supplementary Fig. 7c**). To test the protein turnover at the synapse, we marked the pre- and postsynapse with Syph and Homer1 stainings, respectively

(**Supplementary Fig. 7b**). Our measurements did not show any protein turnover rate differences between female and male synapses (**Supplementary Fig. 7d and e**).

Recent studies suggest that the translation rate at the synapse is essential for maintaining synaptic function. To determine whether the synaptic translation rate is different between the two sex, we relied on an assay called the puromycin assay (Hafner et al., 2019) that reports the translation sites. Puromycin is an antibiotic that stops ongoing translation by incorporating itself into the polypeptide chain and causing the premature release of it. The premature polypeptide chains can be detected with a puromycin antibody, and thereby it is possible to obtain an accurate estimate of the translation rate at a particular position in the cell (**Fig. 2a**). To be able to detect the background level of the puromycin assay, we treated the culture with another antibiotic called anisomycin prior to the puromycin treatment. Anisomycin blocks the tRNA-transferase activity, and thus the puromycin cannot be incorporated into the polypeptide chain (**Fig. 2b**). First, we took a look at the translation sites in the soma with the epifluorescence microscopy. We did not find any differences between female and male neurons (**Fig. 2d**). Later, we imaged the puromycin intensity at the synapse, and we found that male neurons have ~40% more translation sites than female neurons at both pre- and postsynapses in the primary culture (**Fig. 2c, e and f**).

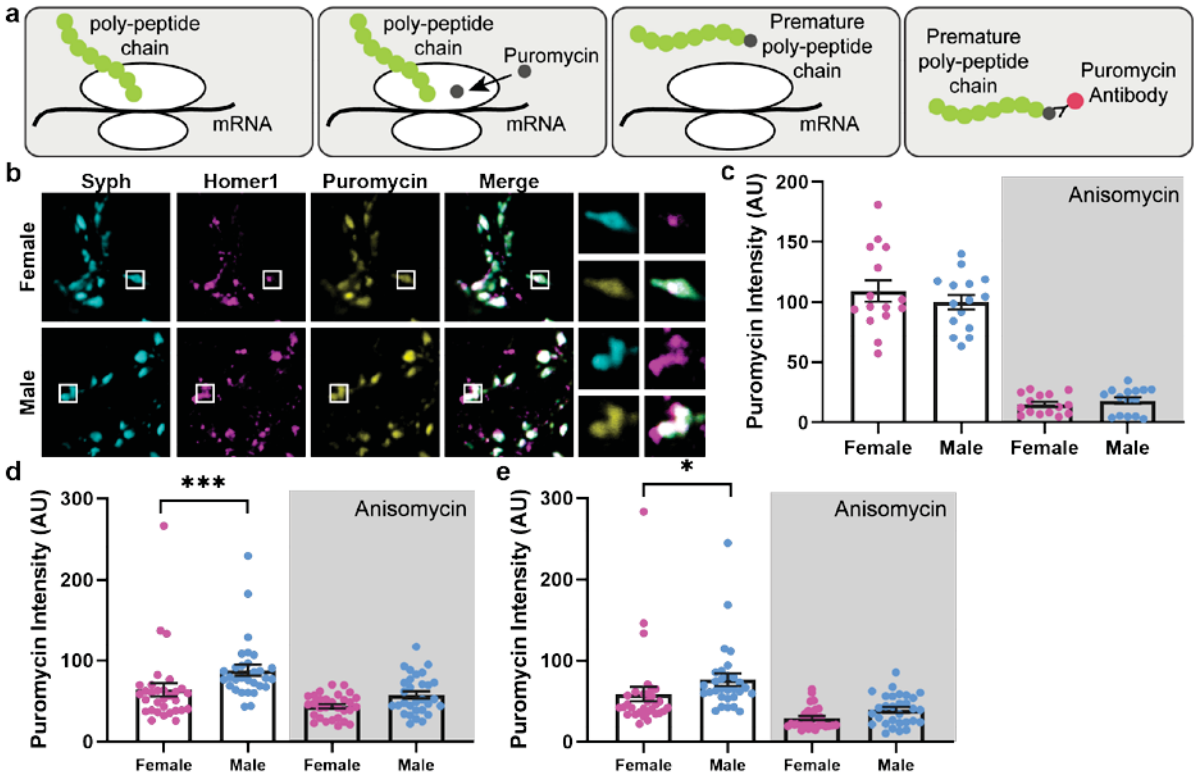

Figure 2. Male hippocampal neurons have a higher local translation rate at synapses compared to female hippocampal neurons in the primary culture. (a) To report local translation rates, we performed a puromycin

assay. Puromycin binds to the P site in the ribosome and incorporates itself into the polypeptide chain. This will release the premature polypeptide chain from the ribosome. The following immunostaining with a puromycin antibody reports the amount of local translation. To calculate the background of the puromycin treatment, we used another antibiotic called anisomycin, which prevents the incorporation of puromycin to a polypeptide chain (not shown). **(b)** The puromycin assay is shown, along with Syph and Homer1 stainings, to indicate pre- and postsynaptic sites. Scale bar: 2.5 µm. **(c)** The puromycin intensity at the cell body is not different between female and male neurons. Each dot represents the mean of an image, and the bar graph shows the mean ± SEM. N=3 independent experiments. **(d and e)** Puromycin antibody intensities are shown, calculated for pre- and post synapse, respectively. Each dot represents the mean of an image, and the bar graph shows the mean ± SEM. N=3 independent experiments. The male neurons show significantly more translation at the synapse (Kruskal-Wallis test, followed by Dunn's multiple comparison test). *$p<0.05$, ***$p<0.0005$.

3.5| Discussion

We conclude that there are significant behavioral differences between male and female hippocampal neurons in the culture. Although female hippocampal neurons have more synaptic transmission-related transcripts, male neurons have a higher global and synaptic activity. Despite finding similar protein turnover rates between the two sexes, we found that the local translation rate at the synapse is larger in male neurons than in female neurons. Overall, our observations suggest that in comparison to female neurons, male hippocampal neurons have a higher neuronal activity, which is supported by a higher local translation rate.

Reports on dissociated cultures from the brain suggest that sexual differentiation has started even before the sex-specific hormone secretion (Reisert et al., 1989). Recently a study showed the similarity between *in vivo* and *in vitro* morphological developments of hippocampal neurons (Keil et al., 2017). They also showed that male neurons have longer and more elaborate dendrites both *in vivo* and *in vitro*. Together with our findings, this indicates that primary hippocampal cultures have a great potential for studying sexual differentiation in order to understand sex-biased diseases such as Alzheimer's disease and autism spectrum disorder (Yagi and Galea, 2019).

Another implication is evident at an experimental level: reproducibility across cultures. Typically, the hippocampal primary culture is prepared from multiple hippocampi without knowing the sex of the sacrificed animals. This results in female-male mixed cultures where the female to male neuron ratio is not known and can vary with each preparation. Since we found substantial functional differences in the primary culture between the two sexes, it is essential to keep the female-male ratio constant in a culture.

Acknowledgements

We would like to thank Roya Yousefi and Prof. Peter Rehling for their generous gift of puromycin, anisomycin and puromycin antibody. We also would like to thank the Transcriptome and Genome Analysis Laboratory (TAL, Göttingen, Germany) for mRNA sequencing and Prof. Henning Urlaub for mass spectrometry experiments. The work was supported by a grant from the Deutsche Forschungsgemeinschaft (DFG) to S.O.R., SFB1286/A03.

Author Contributions

Study design by S.M.S. and S.O.R. Data collection by S.M.S., W.B. and S.M. Data analysis and interpretation by S.M.S. and S.O.R. Manuscript preparation by S.M.S. and S.O.R.

Competing interests

The authors declare that they have no competing interests.

Materials & Correspondence

S.O.R. : srizzol@gwdg.de

3.6| Supplementary Data

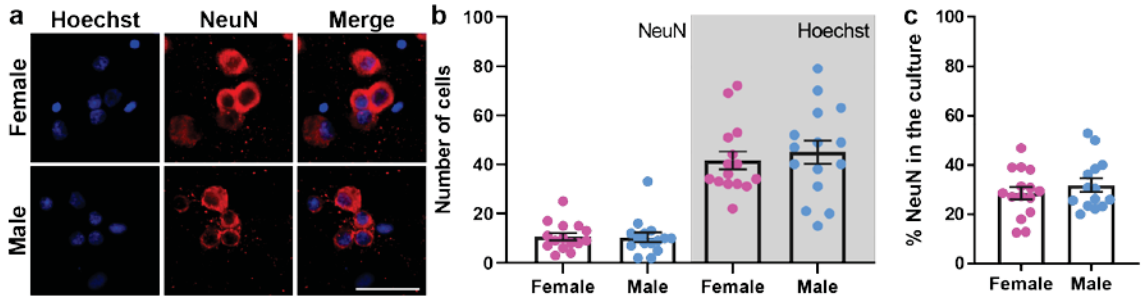

Supplementary Figure 1. Female and male primary hippocampal cultures have the same glia and neuron concentration. (a) To estimate the number of neurons and glia in the culture, we performed immunostaining for the DNA stain Hoechst and neuronal nuclei (NeuN). Exemplary images are shown for female and male cultures. Scale bar: 50 µm. **(b and c)** The amount of Hoechst and NeuN positive nuclei in female and male cultures are shown, respectively.

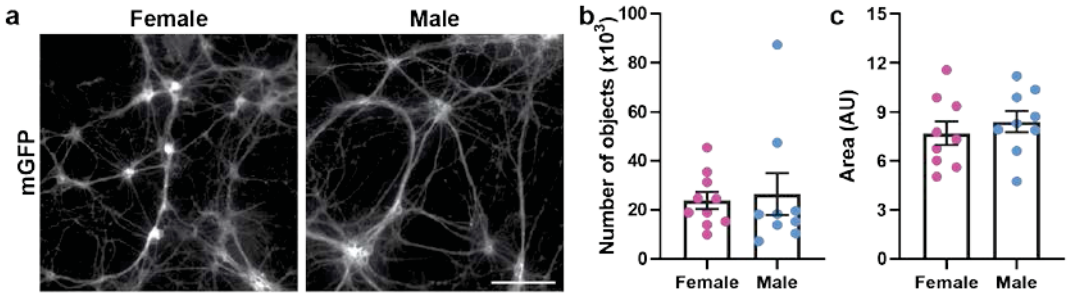

Supplementary Figure 2. Neuronal volumes are similar across female, and male primary hippocampal cultures. (a) To estimate the volume of neuronal processes, we expressed membrane-bound GFP (mGFP) in the cultures. Exemplary images of mGFP positive female and male neurons are shown. Scale bar: 100 µm. **(b)** To compare the number of processes, we calculated the number of mGFP positive objects in an image. The bar graph indicates the mean ± SEM. Each symbol represents the mean of an image. Unpaired t-test suggests there are no differences between female and male cultures. **(c)** To determine whether the mGFP positive objects have a similar area between female and male neurons, we calculated the area of mGFP positive objects. The bar graph indicates the mean ± SEM. Each symbol represents the mean of an image. An unpaired t-test suggests that there are no differences between female and male cultured hippocampal neurons.

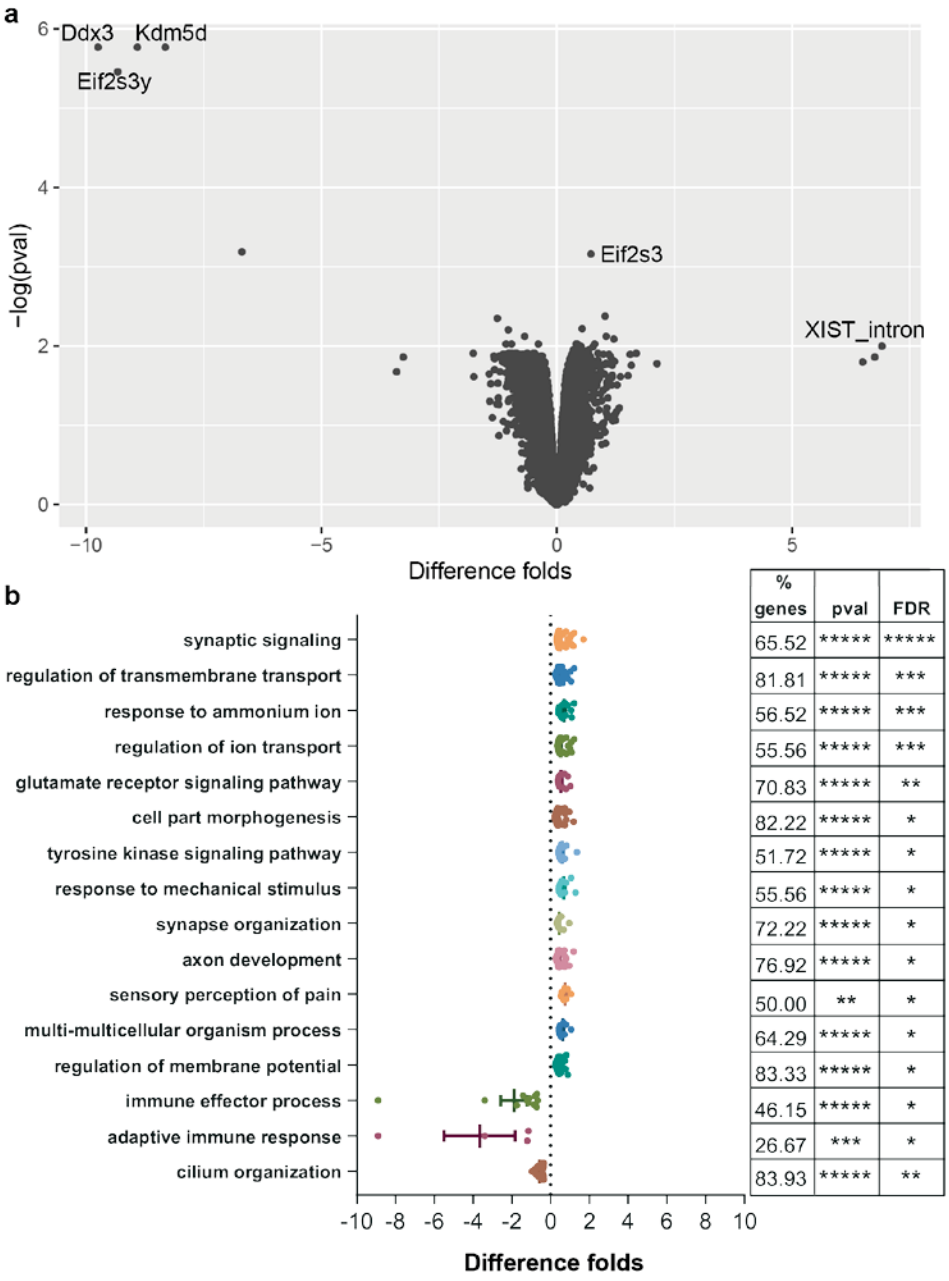

Supplementary Figure 3. Neuronal function-related pathways are slightly but significantly enriched in female hippocampal neurons. (a) To determine differentially expressed mRNAs between female and male cultures, we performed mRNA sequencing. N=5 independent experiments. The analysis is performed with an R package called limma (Ritchie et al., 2015). Each symbol represents a transcript and they are plotted difference folds versus –log(p-value). **(b)** To determine whether the differentially expressed transcripts enriched in a pathway, we performed a gene set enrichment analysis (GSEA) with a website called Webgestalt (Wang et al., 2017) by analyzing the fold change of differentially expressed transcripts. The graph shows the mean ± SEM of the fold change of the pathway. Each dot represents a differentially expressed transcript that is part of the pathway. The table shows the percentage of differentially expressed genes that are part of the pathway, the p-value, and the false discovery rate (FDR) value of GSEA analysis. * <0.05, **<0.01, ***<0.005, ****<0.0001, *****<0.00001.

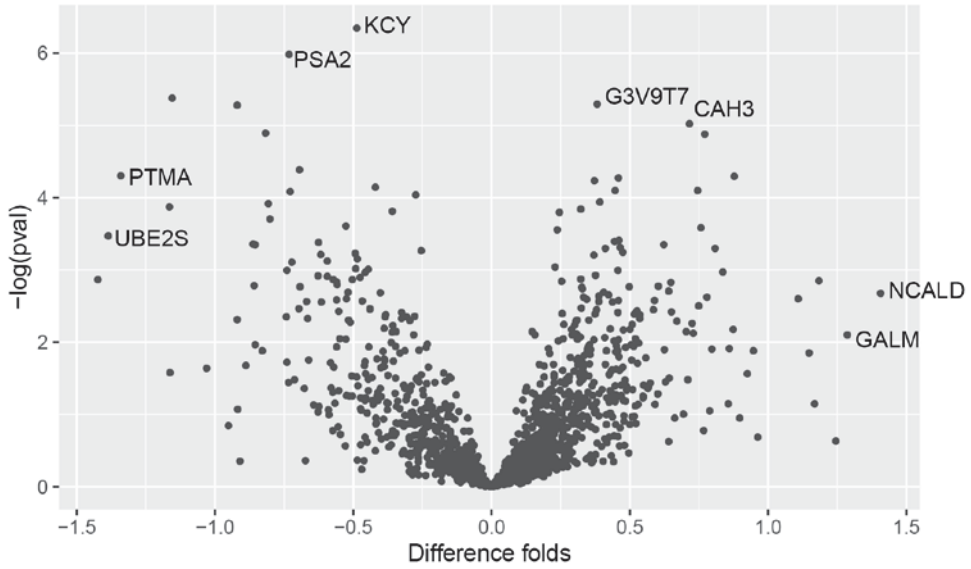

Supplementary Figure 4. The differential protein abundance was not enriched in a single pathway. To compare the protein abundance between female and male cultures, we performed mass-spectrometry with protein lysates. We calculated the male to female ratio in logarithmic scale 10 (difference folds), and performed statistical tests with the limma package (Ritchie et al., 2015) between the two sex. Each dot represents a protein that is detected, and they are plotted according to –log(p-value) and difference folds. N=4 independent experiments. A gene set enrichment analysis (GSEA) was performed with the Webgestalt database, but a significant enrichment was not found.

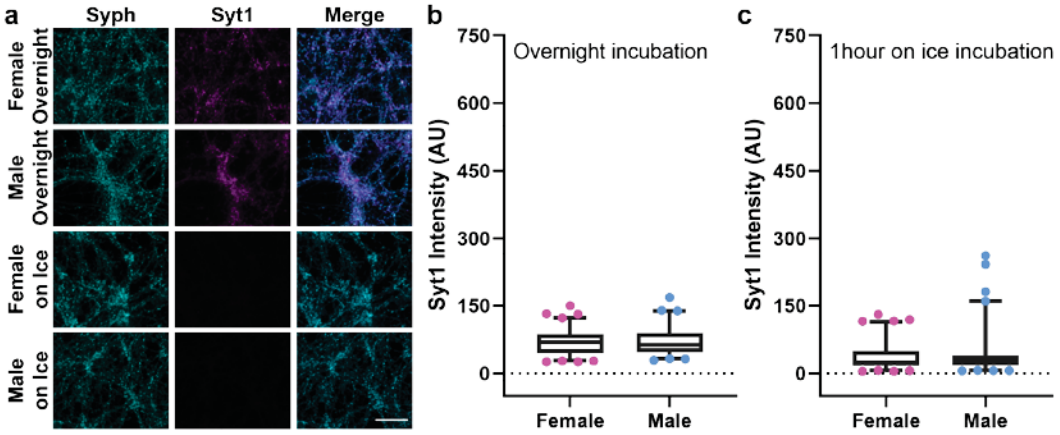

Supplementary Figure 5. Synaptotagmin 1 labeling does not show any significant difference between female and male hippocampal neurons with overnight or on ice incubation. (a) To check the active synaptic vesicle pool, we performed overnight incubations with a Syt1 antibody. To verify the Syt1 surface pool and control whether the Syt1 labeling, which is described in Figure 1, is due to exocytosis, we blocked the Na^+ channels, thus exocytosis, with tetrodotoxin (TTX), but also performed on ice incubation. The cellular metabolism slows down with low temperature. Thus, the frequency of synaptic vesicle exocytosis drops. The exemplary images are shown for female and male hippocampal neurons with overnight or on ice incubation. Scale bar: 50 µm **(b)** and **(c)** The means of the Syt1 intensity after overnight incubation and 1 hour on ice incubation were plotted as boxplots, respectively. The Syt1 intensity in the Syph area in every image is calculated. The boxplots show the first and third quartiles. The line in the box indicates the median of the distribution, and the whiskers indicate the 5-95 percentile. The dots are the outliers of the distribution. Each symbol represents the mean of an image. N=3 independent experiments.

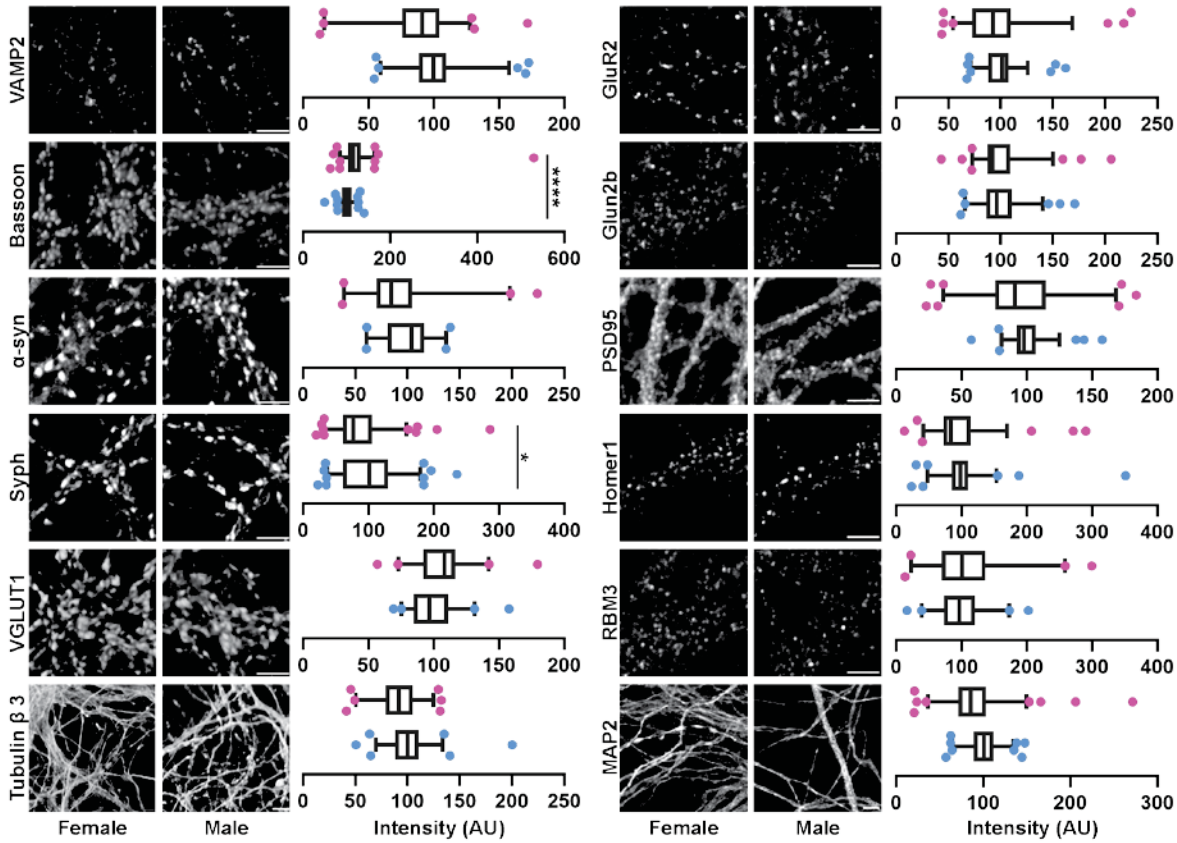

Supplementary Figure 6. The synaptic organization does not show a substantial difference between the two sex. To determine whether the synaptic organization is the reason for functional differences between the two sex, we surveyed the synapse with multiple immunostainings. Exemplary images for each staining are shown. Scale bar: 3.5 µm. We analyzed the intensity and plotted them as boxplots. The boxplot shows the first and third quartiles. The line in the box indicates the median of the distribution, and the whiskers indicate the 5-95 percentile. The dots are the outliers of the distribution. Each symbol represents the mean of an image. N=4 independent experiments. The statistical comparison was performed either with the unpaired t-test or the Mann-Whitney test. However, we have found a substantial difference only in the Bassoon staining.

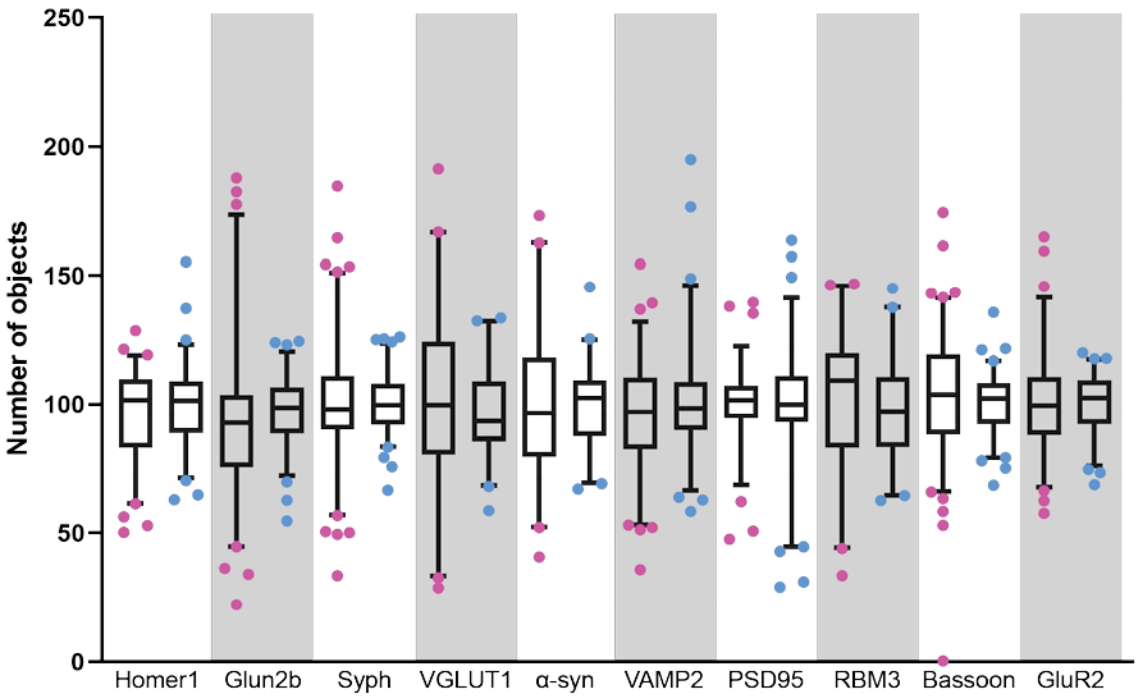

Supplementary Figure 7. The number of synapses is not different between the two sexes. To determine whether the synapse number differ between the two sex, we calculated the number of objects detected in each immunostaining. We plotted them as boxplots. The boxplot shows the first and third quartiles. The line in the box indicates the median of the distribution, and the whiskers indicate the 5-95 percentile. The dots are the outliers of the distribution. Each symbol represents the number of objects in an image. N=7 independent experiments. The statistical comparison was performed either with the unpaired t-test or the Mann-Whitney test.

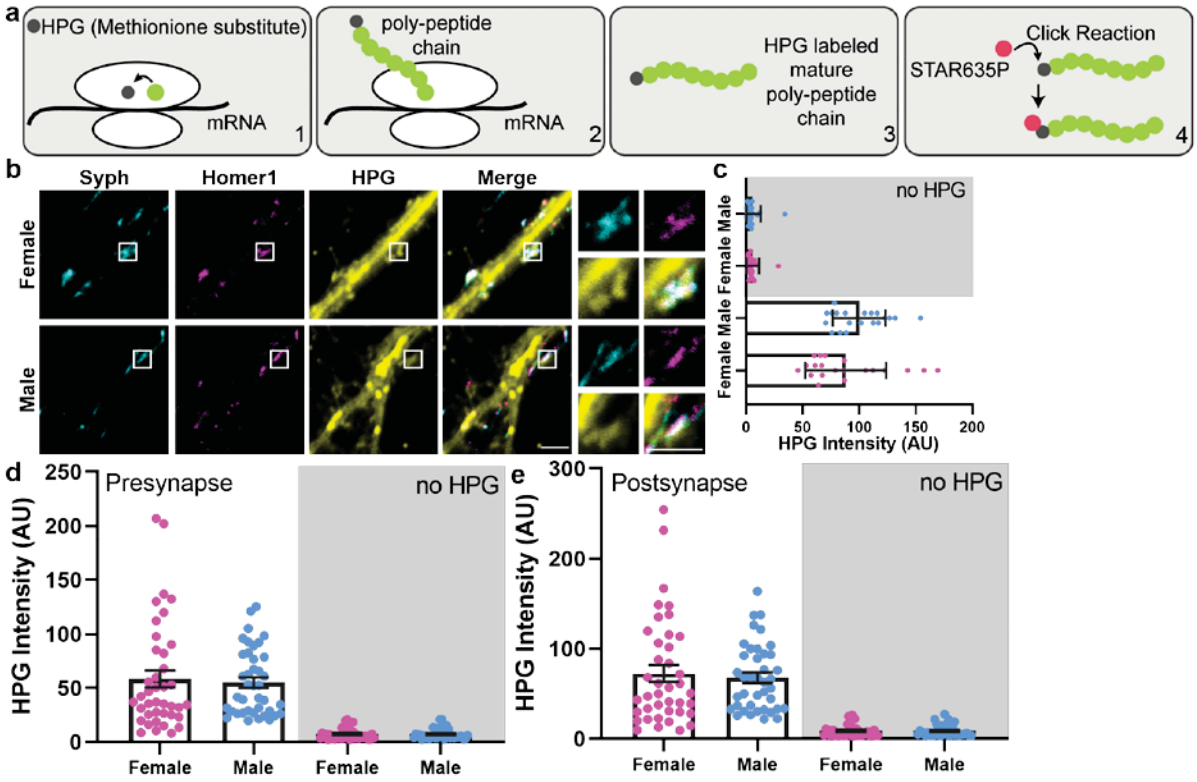

Supplementary Figure 8. Female and male primary hippocampal cultures have a similar protein turnover rate. (a) To investigate whether the protein turnover rate is different between the two sex, we performed the HPG assay. HPG is a Methionine substitute. We incubated the cells with a media that has HPG instead of Methionine (1), and thereby, neurons will incorporate HPG during the translation (2). HPG does not cause any problem during and after translation (3). To label the HPG incorporated proteins, we performed a Click reaction and conjugated Star635P fluorescent probes to the HPG molecule (4). To test the specificity of the Click reaction, we also performed the HPG assay without adding HPG into the media and called the condition as "no HPG". **(b)** The HPG assay is shown, along with Syph and Homer1 stainings, to indicate pre- and postsynaptic sites. Scale bar: 2.5 µm. **(c)** To determine the protein turnover rate in female and male neurons, we calculated the HPG intensity for each image. Each dot represents the summation of an image, and the bar graph shows the mean ± SEM. N=4 independent experiments. **(d** and **e)** The HPG intensities are shown, calculated for pre- and postsynapse, respectively. Each dot represents the mean of an image, and the bar graph shows the mean ± SEM. N=4 independent experiments. The global and synaptic protein turnover rate is not different between female and male neurons according to the Kruskal-Wallis test, which is followed by a Dunn's multiple comparison test.

Supplementary Table 1. The mRNA sequencing suggests differentially expressed transcripts between the two sexes. The transcripts that are significantly different between the two sexes, are listed together with -log(adjusted p-value) and difference folds (log_2(female/male)). The statistical test was performed by the limma package (Ritchie et al., 2015) on the R Studio.

Gene name	Description	Difference folds	-log(P-value)
Gad1	glutamate decarboxylase 1	0,612064387	1,650793711
Steap1	STEAP family member 1	-0,404816697	1,462788219
Tmcc2	transmembrane and coiled-coil domain family 2	0,43757448	1,911720438
Idua	iduronidase, alpha-L-	-0,319413657	1,830935884
Cplx1	complexin 1	0,736143609	1,830935884
Cplx2	complexin 2	0,410219548	1,711154338
Dnajb5	DnaJ heat shock protein family (Hsp40) member B5	0,200028333	1,412683009
Txndc15	thioredoxin domain containing 15	-0,183529526	1,340030656
Lamp2	lysosomal-associated membrane protein 2	-0,213864747	1,462788219
Fam13c	family with sequence similarity 13, member C	0,376855718	1,699600456
Prodh1	proline dehydrogenase 1	-0,32679373	1,877410501
Cd24	CD24 molecule	-0,446334085	1,830935884
Hace1	HECT domain and ankyrin repeat containing, E3 ubiquitin protein ligase 1	0,238735005	1,559369764
Slc35f1	solute carrier family 35, member F1	0,256718392	1,732044204
Psmb8	proteasome subunit beta 8	-0,57406298	1,408528447
Psmb9	proteasome subunit beta 9	-0,474066902	1,527964891
Rgl2	ral guanine nucleotide dissociation stimulator-like 2	-0,191802377	1,342843091
Tspyl4	TSPY-like 4	0,275932909	1,56533424
RGD1306739	similar to RIKEN cDNA 1700040L02	-0,76497486	1,799599454
Acacb	acetyl-CoA carboxylase beta	-0,334245208	1,643653253
Hps4	Hermansky-Pudlak syndrome 4	-0,229704626	1,669509893
Svop	SV2 related protein	0,396067005	1,911720438
Coro1c	coronin 1C	0,158991472	1,31963453
RT1-S3	RT1 class Ib, locus S3	-1,140488777	1,799599454
Smpdl3a	sphingomyelin phosphodiesterase, acid-like 3A	-0,339563385	1,467238841
Atp6v1g2	ATPase H+ transporting V1 subunit G2	0,273287945	1,484031428
Slc44a4	solute carrier family 44, member 4	-0,959541551	1,766941492
Slc9a6	solute carrier family 9 member A6	0,239803129	1,513238513
Asl	argininosuccinate lyase	-0,217440866	1,382565378
Phkg1	phosphorylase kinase, gamma 1	-0,758559855	1,689751918
Sumf2	sulfatase modifying factor 2	-0,237812006	1,409455863
Glt1d1	glycosyltransferase 1 domain containing 1	0,420021899	1,466443595
Stxbp2	syntaxin binding protein 2	-0,490000086	1,323629101
Evi5l	ecotropic viral integration site 5-like	0,20797298	1,548092038
Rsph10b	radial spoke head 10 homolog B	-0,771070948	1,643653253
Ctxn1	cortexin 1	0,240714181	1,576123972
Rilpl2	Rab interacting lysosomal protein-like 2	-0,265574196	1,689751918
Tesc	tescalcin	0,278786331	1,486851905

Nos1	nitric oxide synthase 1	1,051831178	1,47499596
Wsb2	WD repeat and SOCS box-containing 2	0,216884756	1,509904365
RGD1311899	similar to RIKEN cDNA 2210016L21 gene	0,176915407	1,333933463
Pttg1ip	pituitary tumor-transforming 1 interacting protein	-0,278412762	1,701776837
Ift81	intraflagellar transport 81	-0,367318246	1,445407678
Pdgfa	platelet derived growth factor subunit A	0,245815375	1,470686839
Gnaz	G protein subunit alpha z	0,302515152	1,340550376
Rtdr1	rhabdoid tumor deletion region gene 1	-0,778688812	1,534362711
Il3ra	interleukin 3 receptor subunit alpha	-0,531370888	1,637641423
Wdr66	WD repeat domain 66	-0,741181462	1,566629682
Aldh2	aldehyde dehydrogenase 2 family (mitochondrial)	-0,449253383	1,508264693
Rph3a	rabphilin 3A	0,624784352	1,877410501
Oas1a	2'-5' oligoadenylate synthetase 1A	-1,756040747	1,611478922
Rasal1	RAS protein activator like 1 (GAP1 like)	0,568228277	1,897007127
Mettl7a	methyltransferase like 7A	-0,411919727	1,468167582
Iqcd	IQ motif containing D	-0,569272834	1,531034125
Actl6b	actin-like 6B	0,403022812	1,757078164
Ywhag	tyrosine 3-monooxygenase/tryptophan 5-monooxygenase activation protein, gamma	0,318029059	1,689751918
Srrm3	serine/arginine repetitive matrix 3	0,404246533	1,711154338
Rapgef4	Rap guanine nucleotide exchange factor 4	0,528789801	1,516637644
Dlx2	distal-less homeobox 2	1,17358214	1,605955585
Dlx1	distal-less homeobox 1	1,109422975	1,897007127
Tomm70	translocase of outer mitochondrial membrane 70	0,217145927	1,317311075
Kcnj6	potassium voltage-gated channel subfamily J member 6	0,438195298	1,830935884
Ttc3	tetratricopeptide repeat domain 3	0,248627654	1,368816971
Kalrn	kalirin, RhoGEF kinase	0,277435093	1,520332638
Ap2m1	adaptor-related protein complex 2, mu 1 subunit	0,168574791	1,358231212
Hrasls	HRAS-like suppressor	-0,797577804	1,758676133
Opa1	OPA1, mitochondrial dynamin like GTPase	0,20366833	1,47499596
Sst	somatostatin	1,590287654	1,759614516
Lrrc74b	leucine rich repeat containing 74B	-0,892074478	1,897007127
P2rx6	purinergic receptor P2X 6	-0,679961064	2,121067527
Map6d1	MAP6 domain containing 1	0,358490058	1,633666403
Fgf12	fibroblast growth factor 12	0,436727132	1,681512209
Mx2	MX dynamin like GTPase 2	-0,963077028	1,897007127
Tmprss2	transmembrane protease, serine 2	-1,395034844	1,525228034
Prdm8	PR/SET domain 8	0,275087946	1,330690083
Epha5	EPH receptor A5	0,406391564	1,384522877
Evi5	ecotropic viral integration site 5	-0,268405624	1,500466038
Spata18	spermatogenesis associated 18	-1,016659755	1,879710229
Sgcb	sarcoglycan, beta	-0,268588856	1,559369764
Tmprss7	transmembrane protease, serine 7	-0,844193916	1,387865527
Dcun1d4	defective in cullin neddylation 1 domain containing 4	0,250438683	1,391765661
Coq2	coenzyme Q2, polyprenyltransferase	0,217685167	1,341282308
Hsd17b11	hydroxysteroid (17-beta) dehydrogenase 11	-0,201939303	1,349393833

Klhl8	kelch-like family member 8	0,316065844	1,456473696
Scarb2	scavenger receptor class B, member 2	-0,303427519	1,711154338
Adcy5	adenylate cyclase 5	0,240909577	1,498747514
Tmem150c	transmembrane protein 150C	0,495875785	1,760777114
Enoph1	enolase-phosphatase 1	0,266512775	1,757078164
Hlx	H2.0-like homeobox	-0,667065301	1,582961216
Gabra4	gamma-aminobutyric acid type A receptor alpha4 subunit	0,266815999	1,3938137
Uchl1	ubiquitin C-terminal hydrolase L1	0,395414733	1,647493296
Rnf112	ring finger protein 112	0,433187532	1,827973956
Mmd	monocyte to macrophage differentiation-associated	0,262112702	1,684276272
Ifi47	interferon gamma inducible protein 47	-0,974451876	1,527964891
Stxbp5l	syntaxin binding protein 5-like	0,419703178	1,490391966
Spata17	spermatogenesis associated 17	-0,825533838	1,778093331
Parm1	prostate androgen-regulated mucin-like protein 1	0,371776451	1,582081492
Esrrg	estrogen-related receptor gamma	0,509361268	1,438240015
Hnf1b	HNF1 homeobox B	-1,034520448	1,585084141
Rap1gap2	RAP1 GTPase activating protein 2	0,417052217	1,509498727
Magee1	MAGE family member E1	0,491388242	1,911720438
Pbdc1	polysaccharide biosynthesis domain containing 1	0,511378803	1,911720438
Emp2	epithelial membrane protein 2	0,456339001	1,336964243
Vps4b	vacuolar protein sorting 4 homolog B	-0,20677051	1,310373134
Dlg3	discs large MAGUK scaffold protein 3	0,34831278	1,825014164
Gdpd2	glycerophosphodiester phosphodiesterase domain containing 2	-0,477025555	1,343791177
Mapk9	mitogen-activated protein kinase 9	0,235220325	1,428537915
Rbfox1	RNA binding protein, fox-1 homolog 1	0,389909692	1,476117633
Pdzd11	PDZ domain containing 11	-0,285851786	1,481545013
Ccdc181	coiled-coil domain containing 181	-0,338552611	1,548092038
Fam183b	family with sequence similarity 183, member B	-0,794696858	1,711154338
Nme7	NME/NM23 family member 7	-0,332885542	1,365545881
Wdr19	WD repeat domain 19	-0,351002616	1,67486188
P2ry4	pyrimidinergic receptor P2Y4	-0,923278852	1,780790003
Stim2	stromal interaction molecule 2	0,220414028	1,486775936
Itpkb	inositol-trisphosphate 3-kinase B	-0,335199219	1,711154338
Maats1	MYCBP associated and testis expressed 1	-0,638825839	1,634446082
Efhc2	EF-hand domain containing 2	-0,627026465	1,689751918
Rn50_X_0749.3	0	0,380459455	1,757270081
Plcd3	phospholipase C, delta 3	-0,239453268	1,435273797
Rbms2	RNA binding motif, single stranded interacting protein 2	-0,204122097	1,382387044
Ribc1	RIB43A domain with coiled-coils 1	-0,592696486	1,711154338
Trpv2	transient receptor potential cation channel, subfamily V, member 2	0,638998938	1,697344548
Kif19	kinesin family member 19	-0,861795449	1,633455613
Hdac8	histone deacetylase 8	-0,308174912	1,470904198
Gprc5c	G protein-coupled receptor, class C, group 5, member C	-0,73422507	1,471259905
Timp2	TIMP metallopeptidase inhibitor 2	0,193554213	1,582081492
Ldb2	LIM domain binding 2	1,175538856	1,757078164

Lgals3bp	galectin 3 binding protein	-0,908794903	1,629521887
B3galt2	Beta-1,3-galactosyltransferase 2	0,513107786	1,557956217
Map3k14	mitogen-activated protein kinase kinase kinase 14	-0,288529577	1,333933463
Fbxw10	F-box and WD repeat domain containing 10	-0,523779054	1,511690985
Cadm3	cell adhesion molecule 3	0,384198227	1,780790003
Rbfox3	RNA binding protein, fox-1 homolog 3	0,321847485	1,476705146
Mcf2	MCF.2 cell line derived transforming sequence	0,622865465	1,308621422
MAST1	microtubule associated serine/threonine kinase 1	0,409720575	1,827973956
Ppfia4	PTPRF interacting protein alpha 4	0,2321623	1,490391966
Tbc1d9	TBC1 domain family member 9	0,33354331	1,701776837
Gabra1	gamma-aminobutyric acid type A receptor alpha1 subunit	0,755352824	1,676902309
Mr1	major histocompatibility complex, class I-related	-0,6980162	1,768758989
Smyd2	SET and MYND domain containing 2	0,209061528	1,34596196
Tmem183a	transmembrane protein 183A	0,187451174	1,343791177
Tuba4a	tubulin, alpha 4A	0,243036989	1,524253833
Arhgap44	Rho GTPase activating protein 44	0,331593822	1,350583688
Gabrb2	gamma-aminobutyric acid type A receptor beta 2 subunit	0,613489076	1,310251152
Prox1	prospero homeobox 1	0,342358065	1,486904074
Fam184b	family with sequence similarity 184, member B	0,64110094	1,516175038
Cdkl5	cyclin-dependent kinase-like 5	0,297587675	1,419031513
Galc	galactosylceramidase	-0,41862826	1,711154338
Usp43	ubiquitin specific peptidase 43	-0,580076535	1,305367244
Map2k4	mitogen activated protein kinase kinase 4	0,31141719	1,408528447
Med12	mediator complex subunit 12	-0,184487942	1,420775628
Sod3	superoxide dismutase 3, extracellular	-0,41114172	1,34596196
Lgi2	leucine-rich repeat LGI family, member 2	0,727967555	1,554522956
Uck2	uridine-cytidine kinase 2	0,348131488	1,542068118
Asnsd1	asparagine synthetase domain containing 1	0,253263837	1,757270081
Map3k19	mitogen-activated protein kinase kinase kinase 19	-0,749038545	1,684276272
Adcy3	adenylate cyclase 3	0,281030264	1,438240015
Grip1	glutamate receptor interacting protein 1	0,494675317	1,834794779
Atp2b1	ATPase plasma membrane Ca2+ transporting 1	0,279350108	1,487364554
Aldh9a1	aldehyde dehydrogenase 9 family, member A1	-0,237418917	1,312708734
Lrrk2	leucine-rich repeat kinase 2	0,229271737	1,67486188
Kcnc2	potassium voltage-gated channel subfamily C member 2	1,219845898	1,807165803
Frmpd4	FERM and PDZ domain containing 4	0,372615152	1,685766058
Abca8a	ATP-binding cassette, subfamily A (ABC1), member 8a	-0,253324957	1,799599454
Cdk17	cyclin-dependent kinase 17	0,17251237	1,508264693
Lrp12	LDL receptor related protein 12	0,260329698	1,71338915
Samd14	sterile alpha motif domain containing 14	0,298741045	1,526001032
Dnah9	dynein, axonemal, heavy chain 9	-0,575771248	1,689751918
Rims2	regulating synaptic membrane exocytosis 2	0,333000717	1,534362711
Glrx5	glutaredoxin 5	0,187088588	1,442085086
Dohh	deoxyhypusine hydroxylase/monooxygenase	0,22995711	1,669509893
Myt1l	myelin transcription factor 1-like	0,469149927	1,807165803

Tcn2	transcobalamin 2	-0,475754027	1,43350273
Tor3a	torsin family 3, member A	-0,314822997	1,619659914
Sh3kbp1	SH3 domain-containing kinase-binding protein 1	0,330133968	1,50635229
Chrdl1	chordin-like 1	-0,461378163	1,897007127
Fam20b	FAM20B, glycosaminoglycan xylosylkinase	0,196747837	1,360992234
Parp10	poly (ADP-ribose) polymerase family, member 10	-0,396825949	1,629521887
Rps6ka5	ribosomal protein S6 kinase A5	-0,345560556	1,647493296
Aatk	apoptosis-associated tyrosine kinase	0,25044848	1,731867267
RGD1311756	similar to hypothetical protein FLJ20950	-0,326369381	1,465485008
Ston2	stonin 2	-0,255431624	1,526218562
Ccdc88c	coiled-coil domain containing 88C	-0,322916619	1,689751918
Adgre5	adhesion G protein-coupled receptor E5	-0,646310741	1,724814579
Cacnb1	calcium voltage-gated channel auxiliary subunit beta 1	0,191227609	1,405612758
Wdr60	WD repeat domain 60	-0,416774211	1,360992318
Fam69b	family with sequence similarity 69, member B	0,23528913	1,509904365
Ttc8	tetratricopeptide repeat domain 8	-0,294978829	1,502311707
Dhx40	DEAH-box helicase 40	-0,217192095	1,438240015
Cacna1b	calcium voltage-gated channel subunit alpha1 B	0,428838673	1,758676133
Lrriq1	leucine-rich repeats and IQ motif containing 1	-0,574630519	1,488991519
Begain	brain-enriched guanylate kinase-associated	0,323267385	1,34841041
Rbm43	RNA binding motif protein 43	-0,455545066	1,394492809
Kif5c	kinesin family member 5C	0,298833856	1,447760609
Rbfox2	RNA binding protein, fox-1 homolog 2	0,242285746	1,678674894
Celf5	CUGBP, Elav-like family member 5	0,324494239	1,516532422
Aard	alanine and arginine rich domain containing protein	-0,590136283	1,341035359
Napb	NSF attachment protein beta	0,488777497	1,552262958
Syt2	synaptotagmin 2	1,692047968	1,911720438
Crmp1	collapsin response mediator protein 1	0,275293311	1,778093331
Rtn1	reticulon 1	0,252219753	1,404800374
Plcb1	phospholipase C beta 1	0,450165102	1,720313286
Sntb1	syntrophin, beta 1	-0,307331181	1,650793711
Dock4	dedicator of cytokinesis 4	0,271095007	1,310620462
B4galnt1	beta-1,4-N-acetyl-galactosaminyl transferase 1	0,32954442	1,574721009
Akap6	A-kinase anchoring protein 6	0,390155033	1,47499596
Mpped2	metallophosphoesterase domain containing 2	0,325861966	1,611478922
Dyrk3	dual specificity tyrosine phosphorylation regulated kinase 3	-0,470357981	1,516637644
Flrt3	fibronectin leucine rich transmembrane protein 3	0,232080265	1,388081194
Slc4a1ap	solute carrier family 4 member 1 adaptor protein	0,218786921	1,467448865
Sdc2	syndecan 2	-0,282361335	1,442995267
Csmd3	CUB and Sushi multiple domains 3	0,408275028	1,897007127
Jakmip1	janus kinase and microtubule interacting protein 1	0,535941957	1,765740972
Ptprn2	protein tyrosine phosphatase, receptor type N2	0,265084201	1,594952973
Tmed4	transmembrane p24 trafficking protein 4	-0,170562789	1,395903174
Scn2a	sodium voltage-gated channel alpha subunit 2	0,383053959	1,649805466
Trhr	thyrotropin releasing hormone receptor	0,976350542	1,440317196

Tbr1	T-box, brain, 1	0,374206349	1,34050607
Bzw2	basic leucine zipper and W2 domains 2	0,292832599	1,711154338
Mapt	microtubule-associated protein tau	0,227087957	1,312768424
Ccdc157	coiled-coil domain containing 157	-0,3859921	1,62948979
Map7d2	MAP7 domain containing 2	0,245901996	1,349841496
Vstm2a	V-set and transmembrane domain containing 2A	0,771652571	1,996359989
Kcnq3	potassium voltage-gated channel subfamily Q member 3	0,40255331	1,37819374
Itpka	inositol-trisphosphate 3-kinase A	0,475601051	1,618117208
Coch	cochlin	1,089037908	1,34596196
Kif5a	kinesin family member 5A	0,400637358	1,738829265
Slc4a10	solute carrier family 4 member 10	0,470957701	1,69232475
Scn8a	sodium voltage-gated channel alpha subunit 8	0,420063535	1,637641423
Galnt13	polypeptide N-acetylgalactosaminyltransferase 13	0,299514321	1,382052609
Elf4	E74 like ETS transcription factor 4	-0,734418849	1,402890574
Rybp	RING1 and YY1 binding protein	0,267568103	1,5949826
Ctc1	CST telomere replication complex component 1	-0,220638646	1,387780684
Csrnp3	cysteine and serine rich nuclear protein 3	0,609088709	1,654920157
Kcnip1	potassium voltage-gated channel interacting protein 1	0,565177625	1,344315162
Lrrc9	leucine rich repeat containing 9	-0,683174031	1,689751918
Zhx2	zinc fingers and homeoboxes 2	-0,165783409	1,306562256
Lsm11	LSM11, U7 small nuclear RNA associated	0,488014867	1,911720438
Dnah11	dynein, axonemal, heavy chain 11	-0,709769442	1,596665441
Lamp5	lysosomal-associated membrane protein family, member 5	0,938400342	1,685766058
Lrfn5	leucine rich repeat and fibronectin type III domain containing 5	0,354185968	1,365540325
Phospho1	phosphoethanolamine/phosphocholine phosphatase 1	0,358298631	1,352376072
Itgb4	integrin subunit beta 4	-0,771713438	1,518426143
Dhrs7	dehydrogenase/reductase 7	-0,298851583	1,696748851
Cntn4	contactin 4	0,363118171	1,392776974
Runx1t1	RUNX1 translocation partner 1	0,626604972	1,575950116
Nsg1	neuron specific gene family member 1	0,307833943	1,702412232
Pclo	piccolo (presynaptic cytomatrix protein)	0,395413817	1,720313286
Bcl11b	B-cell CLL/lymphoma 11B	0,60787443	1,733627747
Lyz2	lysozyme 2	-0,581692261	1,453897482
Gdap1	ganglioside-induced differentiation-associated-protein 1	0,294727883	1,313170408
Maml2	mastermind-like transcriptional coactivator 2	-0,282067185	1,340550376
Tle1	transducin like enhancer of split 1	0,384956556	1,382387044
Nek10	NIMA-related kinase 10	-0,397026559	1,569662205
Fsip1	fibrous sheath interacting protein 1	-0,677886579	1,516532422
Them6	thioesterase superfamily member 6	0,336838889	1,699600456
Yap1	yes-associated protein 1	-0,284683341	1,551255357
Cfap46	cilia and flagella associated protein 46	-0,876032085	1,782458213
Rrbp1	ribosome binding protein 1	-0,207949784	1,395903174
RGD1311744	similar to RIKEN cDNA 5830475I06	-0,221815814	1,509498727
Rab2a	RAB2A, member RAS oncogene family	0,219551534	1,508264693
Gpr176	G protein-coupled receptor 176	0,52950754	1,586510509

Lhx6	LIM homeobox 6	1,560173204	1,897007127
Snap25	synaptosomal-associated protein 25	0,486974998	1,763240386
Lynx1	Ly6/neurotoxin 1	0,607942257	1,830935884
Jph1	junctophilin 1	0,396600045	1,43350273
Cfap69	cilia and flagella associated protein 69	-0,447290069	1,724814579
St18	suppression of tumorigenicity 18	0,324830102	1,350777348
Slc30a3	solute carrier family 30 member 3	0,438628242	1,582081492
Cacng2	calcium voltage-gated channel auxiliary subunit gamma 2	0,606442402	1,897007127
Ptpro	protein tyrosine phosphatase, receptor type, O	0,2108284	1,446498639
Alg2	ALG2, alpha-1,3/1,6-mannosyltransferase	0,202945553	1,54008332
Ddx58	DEXD/H-box helicase 58	-0,530956494	1,684276272
Nectin1	nectin cell adhesion molecule 1	0,297638914	1,622800884
Akap5	A-kinase anchoring protein 5	0,448548727	1,417475182
Kcnk16	potassium two pore domain channel subfamily K member 16	-0,994335938	1,650793711
Syt1	synaptotagmin 1	0,538868521	1,530199435
Ift27	intraflagellar transport 27	-0,3615929	1,382387044
Hspa2	heat shock protein family A member 2	-0,286024831	1,522488479
Thnsl2	threonine synthase-like 2	-0,378219093	1,669509893
Vezt	vezatin, adherens junctions transmembrane protein	0,234078524	1,562518805
Tmem107	transmembrane protein 107	-0,453986191	1,438240015
Atp6v0c	ATPase H+ transporting V0 subunit C	0,169713244	1,341035359
Cyfip2	cytoplasmic FMR1 interacting protein 2	0,354378361	1,778093331
Htr3a	5-hydroxytryptamine receptor 3A	0,601101907	1,55058347
Thy1	Thy-1 cell surface antigen	0,370663783	1,837926977
Cntnap2	contactin associated protein-like 2	0,642352017	1,582081492
Slc38a4	solute carrier family 38, member 4	1,108108715	1,596610422
Sh3gl2	SH3 domain-containing GRB2-like 2	0,241692736	1,326113827
Rbm18	RNA binding motif protein 18	0,15122011	1,31351724
Sema4f	ssemaphorin 4F	0,384389469	1,596665441
Dhcr24	24-dehydrocholesterol reductase	0,371290961	1,548092038
Tmem246	transmembrane protein 246	0,290853533	1,737586133
Ano4	anoctamin 4	0,505580911	1,75931642
Elavl2	ELAV like RNA binding protein 2	0,48343256	1,737586133
Akap14	A-kinase anchoring protein 14	-0,76964232	1,711154338
Pou3f2	POU class 3 homeobox 2	-0,28790633	1,431492707
Sptb	spectrin, beta, erythrocytic	0,32554028	1,897007127
Adamtsl1	ADAMTS-like 1	-0,521991719	1,750594197
Gria4	glutamate ionotropic receptor AMPA type subunit 4	0,408895001	1,826012297
Stk32c	serine/threonine kinase 32C	0,319667943	1,748072267
Wdr78	WD repeat domain 78	-0,585390679	1,322852445
Slc3a1	solute carrier family 3 member 1	0,304727508	1,565157506
Galm	galactose mutarotase	-0,289392923	1,40109479
Epha7	Eph receptor A7	0,44464238	1,454904633
Cfap57	cilia and flagella associated protein 57	-0,803872234	1,720313286
Cfap70	cilia and flagella associated protein 70	-0,701422379	1,531369534

Bcl11a	B-cell CLL/lymphoma 11A	0,395524494	1,351541051
Dhx33	DEAH-box helicase 33	-0,216515853	1,307502985
March10	membrane associated ring-CH-type finger 10	-0,827941477	1,633666403
Cacna1c	calcium voltage-gated channel subunit alpha1 C	0,267084196	1,463570698
Plxnb2	plexin B2	-0,231568103	1,404157789
Atp5g1	ATP synthase, H+ transporting, mitochondrial Fo complex, subunit C1 (subunit 9)	0,176168557	1,452306759
Ttc9	tetratricopeptide repeat domain 9	0,353398319	1,650793711
Necab1	N-terminal EF-hand calcium binding protein 1	0,495720874	1,484031428
Ccdc134	coiled-coil domain containing 134	-0,533590535	1,768202909
Slc2a1	solute carrier family 2 member 1	-0,449395157	1,691883395
Herc3	HECT and RLD domain containing E3 ubiquitin protein ligase 3	0,363656591	1,557956217
Mroh8	maestro heat-like repeat family member 8	-0,483697924	1,329799834
Grasp	general receptor for phosphoinositides 1 associated scaffold protein	0,302265887	1,45157359
Rab15	RAB15, member RAS oncogene family	0,330846752	1,701776837
Slit3	slit guidance ligand 3	0,343867607	1,655497556
Tmem132e	transmembrane protein 132E	0,297942795	1,42848315
Ndufaf4	NADH:ubiquinone oxidoreductase complex assembly factor 4	0,243913893	1,305054854
Lrtm2	leucine-rich repeats and transmembrane domains 2	0,354241024	1,45338331
Rsad2	radical S-adenosyl methionine domain containing 2	-1,198526167	1,67486188
Glb1l2	galactosidase, beta 1-like 2	-0,448168038	1,316704411
Pygb	glycogen phosphorylase B	-0,218617559	1,669509893
Tcp11l2	t-complex 11 like 2	-0,341753494	1,333408771
C1qtnf5	C1q and tumor necrosis factor related protein 5	-0,305741812	1,505705802
B3galt1	Beta-1,3-galactosyltransferase 1	0,385280893	1,559769393
Cadps2	calcium dependent secretion activator 2	0,995434536	1,895068937
Kcnj9	potassium voltage-gated channel subfamily J member 9	0,260163104	1,314326512
Gria3	glutamate ionotropic receptor AMPA type subunit 3	0,281589745	1,830935884
Sept3	septin 3	0,273274502	1,699600456
Ift52	intraflagellar transport 52	-0,286075066	1,597825273
Lhfpl4	lipoma HMGIC fusion partner-like 4	0,271998627	1,682695134
Arhgef9	Cdc42 guanine nucleotide exchange factor 9	0,305501402	1,534362711
Ehd3	EH-domain containing 3	0,247470942	1,650793711
Zmynd19	zinc finger, MYND-type containing 19	0,347667611	1,305054854
Plod1	procollagen-lysine, 2-oxoglutarate 5-dioxygenase 1	-0,261555879	1,724814579
Nap1l5	nucleosome assembly protein 1-like 5	0,804052861	2,030793234
Kdm3a	lysine demethylase 3A	-0,161701668	1,378265437
Vgll4	vestigial-like family member 4	-0,235268967	1,668683638
Slc16a7	solute carrier family 16 member 7	0,348989982	1,377347998
Ablim2	actin binding LIM protein family, member 2	0,217156581	1,379630112
Tmed10	transmembrane p24 trafficking protein 10	-0,18858926	1,493658921
Itga7	integrin subunit alpha 7	-0,301578625	1,565177308
Tmem178a	transmembrane protein 178A	0,431845277	1,5743345
Cldn19	claudin 19	-0,483625691	1,358421153
Cgref1	cell growth regulator with EF hand domain 1	0,503188584	1,766941492

Elfn2	extracellular leucine-rich repeat and fibronectin type III domain containing 2	0,331724135	1,757078164
Timp4	tissue inhibitor of metalloproteinase 4	-0,368550534	1,405917321
Syt13	synaptotagmin 13	0,272253878	1,689751918
Akna	AT-hook transcription factor	-0,342805755	1,340550376
Atp8a2	ATPase phospholipid transporting 8A2	0,66670668	1,818329099
Naga	N-acetyl galactosaminidase, alpha	-0,326547014	1,393363558
Rgs6	regulator of G-protein signaling 6	-0,33498584	1,312708734
RGD1309108	similar to hypothetical protein FLJ23554	-0,731233333	1,750965409
Irf1	interferon regulatory factor 1	-0,329654465	1,311460267
Traf3	Tnf receptor-associated factor 3	0,242959533	1,353206955
Syn2	synapsin II	0,357608686	1,508264693
Ubash3b	ubiquitin associated and SH3 domain containing, B	0,371410484	1,649805466
Pnpla7	patatin-like phospholipase domain containing 7	-0,268771628	1,462788219
Cnr1	cannabinoid receptor 1	0,719136594	1,84615826
Fnbp1	formin binding protein 1	-0,191711737	1,321818541
Pitpnm3	PITPNM family member 3	-0,572534024	1,64707996
Crocc	ciliary rootlet coiled-coil, rootletin	-0,607554472	1,720313286
Gjd2	gap junction protein, delta 2	0,250516634	1,312588016
Cep63	centrosomal protein 63	-0,381108166	1,753015761
Sec23b	Sec23 homolog B, coat complex II component	-0,286151419	1,45157359
Nab2	Ngfi-A binding protein 2	0,237240339	1,552175485
Nav1	neuron navigator 1	0,247195155	1,473975255
Necap2	NECAP endocytosis associated 2	-0,258021215	1,682695134
Gabbr2	gamma-aminobutyric acid type B receptor subunit 2	0,473354683	1,799599454
LOC303140	up-regulator of carnitine transporter, OCTN2	-0,266053344	1,664663019
Tmem132d	transmembrane protein 132D	0,503889448	1,85179005
Rundc3b	RUN domain containing 3B	0,458168115	1,711154338
Agbl2	ATP/GTP binding protein-like 2	-0,765787217	1,689751918
Slc8a1	solute carrier family 8 member A1	0,209483239	1,356500253
Reep1	receptor accessory protein 1	0,465076894	1,534209154
Cfap45	cilia and flagella associated protein 45	-0,729412534	1,518426143
Ccdc30	coiled-coil domain containing 30	-0,419101173	1,575352716
Nkiras1	NFKB inhibitor interacting Ras-like 1	0,273078284	1,496589768
Cadps	calcium dependent secretion activator	0,427163553	1,508264693
Cdk16	cyclin-dependent kinase 16	0,23888157	1,68465649
Ttc12	tetratricopeptide repeat domain 12	-0,662401783	1,84615826
Ttll9	tubulin tyrosine ligase like 9	-0,609648933	1,640705567
Mal2	mal, T-cell differentiation protein 2	0,497360064	1,650793711
Ubr3	ubiquitin protein ligase E3 component n-recognin 3	0,251398634	1,510647721
Agtrap	angiotensin II receptor-associated protein	-0,283170121	1,804803971
Rimkla	ribosomal modification protein rimK-like family member A	0,540127313	1,479253691
Alk	anaplastic lymphoma receptor tyrosine kinase	0,866073274	1,551255357
Nefh	neurofilament heavy	1,053398718	2,121067527
Tp53i11	tumor protein p53 inducible protein 11	0,482366939	1,487364554
Tmem218	transmembrane protein 218	-0,367685821	1,778093331

Ncs1	neuronal calcium sensor 1	0,367957878	1,701776837
Grin2b	glutamate ionotropic receptor NMDA type subunit 2B	0,424280727	1,877410501
Lrguk	leucine-rich repeats and guanylate kinase domain containing	-0,723705696	1,748072267
Gdap1l1	ganglioside-induced differentiation-associated protein 1-like 1	0,327710746	1,689751918
Rp1	retinitis pigmentosa 1	-0,789738887	1,440775854
Nsmf	NMDA receptor synaptonuclear signaling and neuronal migration factor	0,230696956	1,345347917
Fkbp1a	FK506 binding protein 1a	0,22937966	1,462788219
Hcn2	hyperpolarization activated cyclic nucleotide-gated potassium channel 2	0,429417437	1,877410501
Abcg4	ATP binding cassette subfamily G member 4	0,329734656	1,35986003
Parp2	poly (ADP-ribose) polymerase 2	-0,233043869	1,309467925
Fggy	FGGY carbohydrate kinase domain containing	-0,444638166	1,487669535
Draxin	dorsal inhibitory axon guidance protein	-0,705156494	1,724814579
Hbp1	HMG-box transcription factor 1	-0,184454656	1,449368238
Nxph1	neurexophilin 1	0,56159693	1,946967741
Mapre3	microtubule-associated protein, RP/EB family, member 3	0,17330101	1,306598632
Pcdh17	protocadherin 17	0,33131397	1,34511263
Dpysl5	dihydropyrimidinase-like 5	0,529383964	1,780790003
Slc6a6	solute carrier family 6 member 6	0,311365095	1,684276272
Nptn	neuroplastin	0,231992911	1,412683009
Ttll3	tubulin tyrosine ligase like 3	-0,787964381	1,877410501
Elmod1	ELMO domain containing 1	0,315775475	1,557956217
Cfap206	cilia and flagella associated protein 206	-0,843020367	1,701776837
Prkar2b	protein kinase cAMP-dependent type 2 regulatory subunit beta	0,368226568	1,518086719
C1qtnf4	C1q and tumor necrosis factor related protein 4	0,619584353	1,897007127
Dmxl2	Dmx-like 2	0,24007671	1,517247243
Foxp1	forkhead box P1	0,370600009	1,325707654
Rab6b	RAB6B, member RAS oncogene family	0,395655204	1,707360265
RGD1561795	similar to RIKEN cDNA 1700012B09	-0,916869398	1,699600456
Slitrk1	SLIT and NTRK-like family, member 1	0,360438223	1,586559548
Tmem17	transmembrane protein 17	-0,46329681	1,322974657
Entpd8	ectonucleoside triphosphate diphosphohydrolase 8	-1,059753409	1,488991519
Timm29	translocase of inner mitochondrial membrane 29	0,162241432	1,395788457
Ifi27	interferon, alpha-inducible protein 27	-0,795710025	1,897007127
Erc1	ELKS/RAB6-interacting/CAST family member 1	0,184144157	1,397138861
Kcnk9	potassium two pore domain channel subfamily K member 9	0,606015597	1,639298692
Adra2c	adrenoceptor alpha 2C	0,526785993	1,711154338
Mapk15	mitogen-activated protein kinase 15	-1,027670331	1,897007127
Fbxo2	F-box protein 2	-0,46951926	1,697785357
Mob3b	MOB kinase activator 3B	-0,447425305	1,509498727
Erich3	glutamate-rich 3	-0,541328771	1,664663019
Pgp	phosphoglycolate phosphatase	0,175750778	1,475097609
Krt2	keratin 2	0,616128392	1,758676133
Pdxp	pyridoxal phosphatase	0,309889627	1,597825273
Wipf3	WAS/WASL interacting protein family, member 3	0,702667444	1,738829265

Snph	syntaphilin	0,279575989	1,711154338
Dpysl2	dihydropyrimidinase-like 2	0,208141927	1,629521887
Ankrd42	ankyrin repeat domain 42	-0,378981278	1,341035359
Dync1i1	dynein cytoplasmic 1 intermediate chain 1	0,31648732	1,454564213
Chd3	chromodomain helicase DNA binding protein 3	0,369613935	1,554522956
Grip2	glutamate receptor interacting protein 2	0,637701854	1,830935884
Cyp7b1	cytochrome P450, family 7, subfamily b, polypeptide 1	-0,311702932	1,655173266
Elovl4	ELOVL fatty acid elongase 4	0,310587157	1,651387588
Zbbx	zinc finger, B-box domain containing	-0,858375644	1,780790003
LOC100362176	hypothetical protein LOC100362176	0,685740832	1,354360809
Wasf2	WAS protein family, member 2	-0,31444125	1,549740721
Olfm1	olfactomedin 1	0,434654141	1,897007127
Prrt3	proline-rich transmembrane protein 3	0,218835945	1,438240015
Kcnh2	potassium voltage-gated channel subfamily H member 2	0,379173306	1,639298692
Fam161a	family with sequence similarity 161, member A	-0,708737006	1,618117208
Ppp3ca	protein phosphatase 3 catalytic subunit alpha	0,325844533	1,618117208
Lrrc46	leucine rich repeat containing 46	-0,659820114	1,582081492
Swap70	SWAP switching B-cell complex 70	-0,252955353	1,408528447
Plch1	phospholipase C, eta 1	-0,440532741	1,689751918
Pih1d2	PIH1 domain containing 2	-0,71808803	1,7656552
Otof	otoferlin	0,604899479	1,310388589
Akap11	A-kinase anchoring protein 11	0,175789034	1,310678182
Atr	ATR serine/threonine kinase	-0,316750825	1,494086586
Wdfy2	WD repeat and FYVE domain containing 2	-0,304423322	1,585427406
Panx1	Pannexin 1	0,302553114	1,602146759
Dgkh	diacylglycerol kinase, eta	0,423308713	1,330690083
Spag1	sperm associated antigen 1	-0,5506712	1,518426143
Magix	MAGI family member, X-linked	-1,016842106	1,582961216
Kcnmb2	potassium calcium-activated channel subfamily M regulatory beta subunit 2	0,878557673	1,8191646
Trim2	tripartite motif-containing 2	0,254269069	1,443281205
RGD1306233	similar to hypothetical protein MGC29761	-0,763381219	1,84605841
Tubb4b	tubulin, beta 4B class IVb	-0,28848449	1,492637062
Glrb	glycine receptor, beta	0,324523705	1,778093331
Timp1	TIMP metallopeptidase inhibitor 1	-0,200523139	1,390920345
Serpini1	serpin family I member 1	0,685617121	1,874318128
Hexa	hexosaminidase subunit alpha	-0,246930033	1,454564213
Htr1a	5-hydroxytryptamine receptor 1A	0,460740499	1,47499596
Col20a1	collagen type XX alpha 1 chain	-0,437581224	1,34596196
Syn1	synapsin I	0,317746303	1,689751918
Mknk1	MAP kinase-interacting serine/threonine kinase 1	-0,22978974	1,355848542
Agbl3	ATP/GTP binding protein-like 3	-0,601489215	1,770119411
Ccdc180	coiled-coil domain containing 180	-0,942542518	1,895068937
Ptbp1	polypyrimidine tract binding protein 1	-0,293114506	1,306181746
Slc34a3	solute carrier family 34 member 3	-1,323945473	1,844039254
LOC500712	Ab1-233	-1,320456988	1,707078717

Cyp39a1	cytochrome P450, family 39, subfamily a, polypeptide 1	-0,645647479	1,528149159
Cdh18	cadherin 18	0,803732875	1,479977543
Tspo	translocator protein	-0,778702252	1,416587071
Intu	inturned planar cell polarity protein	-0,43577882	1,516532422
Smarcd2	SWI/SNF related, matrix associated, actin dependent regulator of chromatin, subfamily d, member 2	-0,229011771	1,301162155
Acot7	acyl-CoA thioesterase 7	0,486485951	1,780790003
Igfbp4	insulin-like growth factor binding protein 4	0,533256595	1,720313286
Tmem229b	transmembrane protein 229B	0,389893526	1,84605841
Terf2ip	TERF2 interacting protein	-0,287499397	1,314326512
Efcab10	EF-hand calcium binding domain 10	-0,779322409	1,438240015
Arrdc4	arrestin domain containing 4	-0,487835542	1,469681504
Dusp7	dual specificity phosphatase 7	0,184584662	1,355848542
Spryd3	SPRY domain containing 3	0,297533699	1,608877008
Noct	nocturnin	0,451751774	1,897007127
Ankrd54	ankyrin repeat domain 54	-0,300005631	1,442834699
Mpped1	metallophosphoesterase domain containing 1	0,806133357	1,516532422
Krt222	keratin 222	0,60320422	1,513922712
Chrna7	cholinergic receptor nicotinic alpha 7 subunit	0,465822243	1,414506329
Rims4	regulating synaptic membrane exocytosis 4	0,338067178	1,487669535
Gpr27	G protein-coupled receptor 27	0,616383899	1,547358667
Trak2	trafficking kinesin protein 2	0,315169777	1,766941492
RGD1309534	similar to RIKEN cDNA 4931406C07	-0,226428064	1,390572314
Mbd4	methyl-CpG binding domain 4 DNA glycosylase	-0,41610383	1,509498727
Spa17	sperm autoantigenic protein 17	-0,689415304	1,56442015
Acad11	acyl-CoA dehydrogenase family, member 11	-0,31909722	1,313170408
Ift122	intraflagellar transport 122	-0,411576888	1,720313286
Rims1	regulating synaptic membrane exocytosis 1	0,447948654	1,475097609
Stoml3	stomatin like 3	-1,005480254	1,50661285
Hivep2	human immunodeficiency virus type I enhancer binding protein 2	0,245728968	1,531667664
Rn50_3_1467.1	0	-0,618491259	1,335835253
Tekt2	tektin 2	-0,680791024	1,442085086
Ttbk2	tau tubulin kinase 2	0,258205882	1,499606087
Clstn3	calsyntenin 3	0,333093771	1,669509893
Sv2b	synaptic vesicle glycoprotein 2b	0,589052755	1,701776837
Pex5l	peroxisomal biogenesis factor 5-like	0,633666831	1,508264693
Layn	layilin	-0,407765107	1,877410501
Cntnap4	contactin associated protein-like 4	0,90107955	1,591125842
Chd5	chromodomain helicase DNA binding protein 5	0,406984344	1,766941492
Tmem63c	transmembrane protein 63c	0,29764705	1,702412232
Kif3c	kinesin family member 3C	0,364117835	1,650793711
Prag1	PEAK1 related kinase activating pseudokinase 1	-0,264120545	1,351211248
Aldh6a1	aldehyde dehydrogenase 6 family, member A1	-0,225489772	1,34596196
Ptpn3	protein tyrosine phosphatase, non-receptor type 3	0,374870057	1,408528447
Ccdc39	coiled-coil domain containing 39	-0,360271366	1,383874603
Tpd52	tumor protein D52	0,208369677	1,561473385

Kif6	kinesin family member 6	-0,744648934	1,701776837
Slc36a4	solute carrier family 36 member 4	0,33672661	1,522964331
Arfgef3	ARFGEF family member 3	0,340847655	1,382387044
Fgf9	fibroblast growth factor 9	0,731968905	1,596665441
Srcin1	SRC kinase signaling inhibitor 1	0,377717296	1,897007127
Tnfrsf21	TNF receptor superfamily member 21	0,237060254	1,357457852
Dusp26	dual specificity phosphatase 26	0,362689099	1,312708734
Filip1	filamin A interacting protein 1	0,809757114	1,651387588
Cygb	cytoglobin	0,584115351	1,343791177
Kcnab2	potassium voltage-gated channel subfamily A regulatory beta subunit 2	0,338135822	1,619659914
Klc1	kinesin light chain 1	0,241425026	1,455430032
Gldc	glycine decarboxylase	-0,259959881	1,341035359
Myo9a	myosin IXA	0,183031416	1,34596196
Rab3c	RAB3C, member RAS oncogene family	0,338361839	1,711154338
Kcnq2	potassium voltage-gated channel subfamily Q member 2	0,363653823	1,62948979
Auh	AU RNA binding methylglutaconyl-CoA hydratase	0,240064828	1,629521887
Fbxo34	F-box protein 34	0,188981689	1,34596196
Stmn2	stathmin 2	0,469557874	1,56442015
Grin1	glutamate ionotropic receptor NMDA type subunit 1	0,29519063	1,47499596
Ncdn	neurochondrin	0,324129311	1,512699651
Oplah	5-oxoprolinase (ATP-hydrolysing)	-0,375248301	1,690536738
Got2	glutamic-oxaloacetic transaminase 2	0,206420074	1,516532422
Lzts1	leucine zipper tumor suppressor 1	0,258563134	1,759614516
Unc5d	unc-5 netrin receptor D	0,557062577	1,763240386
Abhd14a	abhydrolase domain containing 14A	-0,378476029	1,317311075
Lrrc7	leucine rich repeat containing 7	0,406614223	1,836970288
Abhd14b	abhydrolase domain containing 14b	-0,431582815	1,569153984
Nmbr	neuromedin B receptor	1,063712713	1,54227317
Plppr2	phospholipid phosphatase related 2	0,317344254	1,880992377
Sox2	SRY box 2	-0,222542033	1,474852707
Dmtn	dematin actin binding protein	0,324312658	1,629521887
Cfap161	cilia and flagella associated protein 161	-0,827339805	1,689751918
Gucy1a3	guanylate cyclase 1 soluble subunit alpha 3	0,718209956	1,871203654
Ttc29	tetratricopeptide repeat domain 29	-0,720234282	1,681512209
Slc36a1	solute carrier family 36 member 1	0,263946846	1,681512209
Cacng3	calcium voltage-gated channel auxiliary subunit gamma 3	0,451964774	1,34596196
S100a1	S100 calcium binding protein A1	-0,303798167	1,534362711
Adam23	ADAM metallopeptidase domain 23	0,33483334	1,343791177
Dynlrb2	dynein light chain roadblock-type 2	-0,796380206	1,516532422
Eef1a2	eukaryotic translation elongation factor 1 alpha 2	0,357841248	1,948911923
Ndrg4	NDRG family member 4	0,336916175	1,650793711
Amph	amphiphysin	0,295372524	1,34596196
Ephb2	Eph receptor B2	0,257328446	1,487669535
Madd	MAP-kinase activating death domain	0,285668998	1,473991435
Aamdc	adipogenesis associated, Mth938 domain containing	-0,407818497	1,592008995

Tmem212	transmembrane protein 212	-1,019295912	1,780790003
Ppt1	palmitoyl-protein thioesterase 1	-0,177007309	1,488741725
Efhb	EF hand domain family, member B	-0,854392516	1,911720438
Syngr3	synaptogyrin 3	0,323518903	1,314047265
Lgals9	galectin 9	-0,913138395	1,817393541
Spaca9	sperm acrosome associated 9	-0,864595851	1,633666403
RGD1564149	similar to Protein C21orf58	-1,231309616	1,877410501
Kif24	kinesin family member 24	-0,468788641	1,442874633
Spock1	sparc/osteonectin, cwcv and kazal like domains proteoglycan 1	0,341862436	1,347447868
Ak8	adenylate kinase 8	-0,824785729	1,691448225
Nqo1	NAD(P)H quinone dehydrogenase 1	-0,349478977	1,462069186
Grhpr	glyoxylate and hydroxypyruvate reductase	-0,358442515	1,669509893
C1qa	complement C1q A chain	-3,401834347	1,675538095
Mlf1	myeloid leukemia factor 1	-0,837868042	1,724638644
Ccdc146	coiled-coil domain containing 146	-0,742561808	1,724814579
Themis2	thymocyte selection associated family member 2	-0,666533843	1,442834699
Acadl	acyl-CoA dehydrogenase, long chain	-0,280439611	1,513922712
Ggcx	gamma-glutamyl carboxylase	-0,230632082	1,534362711
Rgl3	ral guanine nucleotide dissociation stimulator-like 3	-0,527490036	1,509498727
Pip4k2b	phosphatidylinositol-5-phosphate 4-kinase type 2 beta	0,248304144	1,711154338
Lrp8	LDL receptor related protein 8	0,220838717	1,344212407
Nkain3	Sodium/potassium transporting ATPase interacting 3	0,660675423	1,34596196
Tmem179	transmembrane protein 179	0,425469813	1,595390816
Grm2	glutamate metabotropic receptor 2	0,698984915	1,4938794
Cmip	c-Maf-inducing protein	0,205866971	1,534362711
Rnaset2	ribonuclease T2	-0,322734399	1,379826999
Barhl1	BarH-like homeobox 1	-1,072905324	1,782458213
Ccdc151	coiled-coil domain containing 151	-0,780529391	1,682695134
Helz2	helicase with zinc finger 2, transcriptional coactivator	-0,505778562	1,542268488
Kcnt2	potassium sodium-activated channel subfamily T member 2	0,373328789	1,521251022
Nceh1	neutral cholesterol ester hydrolase 1	0,234687171	1,407414955
Ccdc150	coiled-coil domain containing 150	-0,919190517	1,655497556
RGD1561916	similar to testes development-related NYD-SP22 isoform 1	-0,723294538	1,707078717
Cdhr1	cadherin-related family member 1	-0,7173703	1,720457588
0	0	0,545020541	1,394492809
Gsta1	glutathione S-transferase alpha 1	-0,428259789	1,67486188
Rpl31	ribosomal protein L31	0,293506861	1,379521362
Ptpru	protein tyrosine phosphatase, receptor type, U	0,55096591	1,731010224
Slc31a2	solute carrier family 31 member 2	-0,369170099	1,356500253
Myo7a	myosin VIIA	-0,635267835	1,629521887
Stmn3	stathmin 3	0,455063511	1,797151145
Nefl	neurofilament light	0,386506282	1,404450574
Erich6	glutamate-rich 6	0,756490662	1,355848542
LOC499240	similar to predicted gene ICRFP703B1614Q5.5	-0,67957186	1,455430032
Dnai1	dynein, axonemal, intermediate chain 1	-0,712634989	1,54008332

Large1	LARGE xylosyl- and glucuronyltransferase 1	0,277766006	1,711154338
Elavl3	ELAV like RNA binding protein 3	0,350631625	1,799599454
Dmc1	DNA meiotic recombinase 1	-0,905258673	1,719412906
Cmas	cytidine monophosphate N-acetylneuraminic acid synthetase	0,309531524	1,626237195
Cby1	chibby family member 1, beta catenin antagonist	-0,24297412	1,499606087
Nefm	neurofilament medium	0,729322372	1,834019545
Ift46	intraflagellar transport 46	-0,382177118	1,500466038
Zc3hav1	zinc finger CCCH-type containing, antiviral 1	-0,347555807	1,387780684
Idh2	isocitrate dehydrogenase (NADP(+)) 2, mitochondrial	-0,31279422	1,462788219
Skor1	SKI family transcriptional corepressor 1	0,788986898	1,467448865
Creg2	cellular repressor of E1A-stimulated genes 2	0,376665845	1,487669535
Kif2a	kinesin family member 2A	0,20553064	1,454564213
Neto1	neuropilin and tolloid like 1	0,52028251	1,994650432
Gfod1	glucose-fructose oxidoreductase domain containing 1	0,523441194	1,897007127
Rasgrf1	RAS protein-specific guanine nucleotide-releasing factor 1	0,677529773	1,948911923
Sertm1	serine-rich and transmembrane domain containing 1	0,742896234	1,595867138
Clybl	citrate lyase beta like	-0,306356895	1,488314156
Stat1	signal transducer and activator of transcription 1	-0,35487197	1,500660945
Retsat	retinol saturase	-0,259633153	1,384670311
Wdr38	WD repeat domain 38	-0,792552006	1,62948979
Myo5b	myosin Vb	1,179566286	1,830935884
Omg	oligodendrocyte-myelin glycoprotein	0,290788747	1,622800884
Npy1r	neuropeptide Y receptor Y1	0,568454439	1,686297263
Smoc2	SPARC related modular calcium binding 2	-0,79825616	1,340030656
Dbn1	drebrin 1	0,235332462	1,689751918
Zfp395	zinc finger protein 395	-0,402163666	1,766941492
Plch2	phospholipase C, eta 2	0,808601523	1,390920345
Map1a	microtubule-associated protein 1A	0,202007418	1,525734368
Erbb4	erb-b2 receptor tyrosine kinase 4	0,679476297	1,844389761
Phactr1	phosphatase and actin regulator 1	0,336107763	1,650793711
Elof1	elongation factor 1 homolog	-0,389117865	1,534362711
Ssh2	slingshot protein phosphatase 2	0,36535518	1,669509893
Grm1	glutamate metabotropic receptor 1	0,664494994	1,830935884
Dlgap3	DLG associated protein 3	0,446498714	1,895068937
Gne	glucosamine (UDP-N-acetyl)-2-epimerase/N-acetylmannosamine kinase	0,267253363	1,450081636
Slc27a4	solute carrier family 27 member 4	0,263238843	1,702412232
Anxa5	annexin A5	-0,465034685	1,382052609
Evl	Enah/Vasp-like	0,271112497	1,684276272
Celf4	CUGBP, Elav-like family member 4	0,435536123	1,877410501
Sacs	sacsin molecular chaperone	0,319322274	1,720313286
Cdc14a	cell division cycle 14A	-0,541230397	1,85179005
Dock3	dedicator of cyto-kinesis 3	0,24268129	1,555833548
Cfap53	cilia and flagella associated protein 53	-0,436668131	1,492637062
Arpin	actin-related protein 2/3 complex inhibitor	-0,300204901	1,322417361
Sgcg	sarcoglycan, gamma	-0,866815013	1,62948979

Grk6	G protein-coupled receptor kinase 6	0,212761845	1,446375162
Morn1	MORN repeat containing 1	-0,501648389	1,488991519
Zfp423	zinc finger protein 423	-0,331443393	1,830935884
Ebpl	emopamil binding protein-like	-0,355436155	1,516532422
Kcnd3	potassium voltage-gated channel subfamily D member 3	0,286617808	1,780790003
Raph1	Ras association (RalGDS/AF-6) and pleckstrin homology domains 1	0,247442082	1,440317196
Cbfa2t3	CBFA2/RUNX1 translocation partner 3	0,466016256	1,586559548
Ankrd13b	ankyrin repeat domain 13B	0,290559963	1,629521887
Glis3	GLIS family zinc finger 3	-0,506750988	1,739471227
Ccne1	cyclin E1	0,361675304	1,548092038
Peg3	paternally expressed 3	0,240405935	1,516532422
Slc1a1	solute carrier family 1 member 1	0,249593604	1,35860056
Kif21a	kinesin family member 21A	0,227696391	1,408528447
Gabrg3	gamma-aminobutyric acid type A receptor gamma 3 subunit	0,516722601	1,479253691
Wdr31	WD repeat domain 31	-0,378850819	1,479520273
Ttc7a	tetratricopeptide repeat domain 7A	-0,42609366	1,753015761
Wdr63	WD repeat domain 63	-0,808310703	1,669509893
Apba1	amyloid beta precursor protein binding family A member 1	0,416614154	1,911720438
Lrrc71	leucine rich repeat containing 71	-0,65313868	1,405131631
Tekt1	tektin 1	-0,66025273	1,389937964
Scn5a	sodium voltage-gated channel alpha subunit 5	0,759177389	1,629521887
Golga7b	golgin A7 family, member B	0,336418284	1,467448865
Il11ra1	interleukin 11 receptor subunit alpha 1	-0,215969603	1,326526533
Stc1	stanniocalcin 1	0,439837754	1,438366032
Ifitm3	interferon induced transmembrane protein 3	-0,707050684	1,350650433
Necab2	N-terminal EF-hand calcium binding protein 2	0,456087012	1,499606087
Mak	male germ cell-associated kinase	-0,790428015	1,62948979
Erc2	ELKS/RAB6-interacting/CAST family member 2	0,515106229	1,649805466
Smtnl2	smoothelin-like 2	-0,469665475	1,469463078
Crtac1	cartilage acidic protein 1	0,382229623	1,768057547
Pip5k1b	phosphatidylinositol-4-phosphate 5-kinase type 1 beta	0,305624082	1,659326208
Cul2	cullin 2	0,210787754	1,408528447
Tmem160	transmembrane protein 160	0,25417944	1,353813467
Aox1	aldehyde oxidase 1	-0,505350965	1,757078164
Npas1	neuronal PAS domain protein 1	0,881510027	1,911720438
Slc32a1	solute carrier family 32 member 1	1,129769942	1,877410501
Stxbp1	syntaxin binding protein 1	0,290530294	1,488991519
Nlgn2	neuroligin 2	0,183708676	1,428537915
Ubxn11	UBX domain protein 11	-0,464270169	1,689751918
Prkcz	protein kinase C, zeta	0,24766322	1,484382552
Tead1	TEA domain transcription factor 1	-0,229954305	1,4938794
Otud7a	OTU deubiquitinase 7A	0,41651595	1,799599454
RGD1307235	similar to RIKEN cDNA 2310035C23	0,223886425	1,661969028
Bcat1	branched chain amino acid transaminase 1	0,404618101	1,38575219
Pja2	praja ring finger ubiquitin ligase 2	0,197444254	1,305054854

Abcd2	ATP binding cassette subfamily D member 2	0,407489988	1,449368238
Ctbs	chitobiase	-0,223438342	1,310388589
Dnah6	dynein, axonemal, heavy chain 6	-0,919802056	1,650793711
Dnaaf1	dynein, axonemal, assembly factor 1	-0,824808899	1,85179005
Prkce	protein kinase C, epsilon	0,312069429	1,766941492
Wdr27	WD repeat domain 27	-0,474980985	1,496589768
MGC116202	hypothetical protein LOC688735	0,595262845	1,799599454
Wdr34	WD repeat domain 34	-0,316717811	1,516532422
Ugcg	UDP-glucose ceramide glucosyltransferase	0,246412221	1,450081636
Slc2a13	solute carrier family 2 member 13	0,329993043	1,911720438
Wnt7b	wingless-type MMTV integration site family, member 7B	0,247191263	1,31650344
Pyroxd2	pyridine nucleotide-disulphide oxidoreductase domain 2	-0,47300589	1,651387588
Bbs7	Bardet-Biedl syndrome 7	-0,35373057	1,412392461
Cacna2d2	calcium voltage-gated channel auxiliary subunit alpha2delta 2	0,811293994	1,782458213
Hint2	histidine triad nucleotide binding protein 2	-0,254419935	1,525263705
Add2	adducin 2	0,34646098	1,650793711
Rap1gds1	Rap1 GTPase-GDP dissociation stimulator 1	0,299462471	1,689751918
Npr2	natriuretic peptide receptor 2	-0,298280897	1,586559548
Gprc5b	G protein-coupled receptor, class C, group 5, member B	-0,357376262	1,750965409
Kank1	KN motif and ankyrin repeat domains 1	-0,240112942	1,622800884
Hecw1	HECT, C2 and WW domain containing E3 ubiquitin protein ligase 1	0,220522883	1,306181746
Macf1	microtubule-actin crosslinking factor 1	-0,22379186	1,332927383
Tab2	TGF-beta activated kinase 1/MAP3K7 binding protein 2	-0,26399048	1,43350273
P3h3	prolyl 3-hydroxylase 3	-0,328504487	1,444650583
Tmem169	transmembrane protein 169	0,392073486	1,488991519
Neurl4	neuralized E3 ubiquitin protein ligase 4	0,209087638	1,56442015
Nptxr	neuronal pentraxin receptor	0,348805667	1,689751918
Spata2L	spermatogenesis associated 2-like	0,237834543	1,479433266
Tmem67	transmembrane protein 67	-0,37825988	1,442834699
Scn2b	sodium voltage-gated channel beta subunit 2	0,352891156	1,421530765
Casq2	calsequestrin 2	-0,477113699	1,376658979
Daw1	dynein assembly factor with WD repeats 1	-0,71584376	1,498747514
Mblac2	metallo-beta-lactamase domain containing 2	0,293423886	1,328351313
Acsl5	acyl-CoA synthetase long-chain family member 5	0,295318627	1,720313286
Itm2b	integral membrane protein 2B	-0,25117743	1,509498727
Camk2n1	calcium/calmodulin-dependent protein kinase II inhibitor 1	0,491966155	1,646626534
Cx3cl1	C-X3-C motif chemokine ligand 1	0,253252677	1,470686839
Got1	glutamic-oxaloacetic transaminase 1	0,366095326	1,513922712
Fgfr2	fibroblast growth factor receptor 2	-0,266674465	1,317311075
Gabrd	gamma-aminobutyric acid type A receptor delta subunit	0,413557152	1,358231212
Rps12	ribosomal protein S12	0,531790822	1,311725935
Eef2k	eukaryotic elongation factor-2 kinase	-0,460433841	1,84605841
Clu	clusterin	-0,473100409	1,778093331
Vangl1	VANGL planar cell polarity protein 1	-0,332248506	1,546518176
Myo16	myosin XVI	0,456415003	1,911720438

Pltp	phospholipid transfer protein	-0,65528934	1,487669535
Dscaml1	DS cell adhesion molecule-like 1	0,206126933	1,348247787
Fam169a	family with sequence similarity 169, member A	0,346390194	1,701776837
Ift140	intraflagellar transport 140	-0,383928652	1,674387212
Vwa5b1	von Willebrand factor A domain containing 5B1	-0,521904626	1,728175607
Dgat2	diacylglycerol O-acyltransferase 2	0,215656238	1,414506329
Rtn2	reticulon 2	0,271600436	1,509498727
Hras	Harvey rat sarcoma virus oncogene	0,330990747	1,757270081
LOC361646	similar to K04F10.2	-0,293910134	1,646626534
Dner	delta/notch-like EGF repeat containing	0,335870652	1,782458213
Pla2g2c	phospholipase A2, group IIC	-0,413810725	1,534362711
Ssc5d	scavenger receptor cysteine rich family member with 5 domains	-0,372872955	1,420775628
Lrrc56	leucine rich repeat containing 56	-0,525474721	1,651387588
Epb41l3	erythrocyte membrane protein band 4.1-like 3	0,585612905	1,682695134
Slc14a1	solute carrier family 14 member 1	-0,310496441	1,681512209
Oprl1	opioid related nociceptin receptor 1	0,349699683	1,306978582
Phyhd1	phytanoyl-CoA dioxygenase domain containing 1	-0,488756585	1,911720438
Stmn1	stathmin 1	0,229047421	1,520332638
Slc38a3	solute carrier family 38, member 3	-0,342163567	1,711154338
Wdr37	WD repeat domain 37	0,200778417	1,409455863
Pifo	primary cilia formation	-0,765338834	1,701776837
Pnmal2	paraneoplastic Ma antigen family-like 2	0,230351255	1,651387588
Plppr4	phospholipid phosphatase related 4	0,294567085	1,324126197
Shisa7	shisa family member 7	0,323700498	1,614506019
Plppr5	phospholipid phosphatase related 5	0,431908921	2,030793234
Tppp3	tubulin polymerization-promoting protein family member 3	-0,850968751	1,456010656
Stk36	serine/threonine kinase 36	-0,431670279	1,685766058
Nadk	NAD kinase	-0,260485561	1,548092038
Nhlrc2	NHL repeat containing 2	-0,233732699	1,453897482
Grp	gastrin releasing peptide	2,131774408	1,782458213
Plxna1	plexin A1	0,193795265	1,555833548
Zdhhc1	zinc finger, DHHC-type containing 1	-0,331434929	1,47499596
Fbxo36	F-box protein 36	-0,751596787	1,387865527
Ryr2	ryanodine receptor 2	0,375476315	1,634446082
Mark4	microtubule affinity regulating kinase 4	0,224218944	1,62948979
Pgm2l1	phosphoglucomutase 2-like 1	0,309015326	1,699600456
Syngr1	synaptogyrin 1	0,273371335	1,522488479
B2m	beta-2 microglobulin	-0,307966304	1,877410501
Rhd	Rh blood group, D antigen	-0,877843703	1,765740972
Snx30	sorting nexin family member 30	0,288267931	1,355848542
Pfkp	phosphofructokinase, platelet	0,23253766	1,452781854
Mycbp	Myc binding protein	-0,371331402	1,408087394
Hydin	Hydin, axonemal central pair apparatus protein	-0,909090674	1,701776837
Trim30c	tripartite motif-containing 30C	-0,368415707	1,573124398
Lingo1	leucine rich repeat and Ig domain containing 1	0,296128402	1,853318039

Tubb3	tubulin, beta 3 class III	0,535560456	1,758478369
Tcirg1	T-cell immune regulator 1, ATPase H+ transporting V0 subunit A3	-0,392921345	2,030793234
Sord	sorbitol dehydrogenase	-0,229839343	1,340030656
Apobr	apolipoprotein B receptor	-0,545989658	1,314326512
Atrnl1	attractin like 1	0,320605353	1,534209154
Map1b	microtubule-associated protein 1B	0,443987144	1,827986613
Nrsn1	neurensin 1	0,600074167	1,341035359
Vstm2b	V-set and transmembrane domain containing 2B	0,677993526	1,911720438
C1ql3	complement C1q like 3	0,546680372	1,724814579
Anxa1	annexin A1	-0,715835292	1,406250686
Ttc25	tetratricopeptide repeat domain 25	-0,852039278	1,758478369
Snx24	sorting nexin 24	-0,259722449	1,621080523
Mmp9	matrix metallopeptidase 9	0,793625865	1,420812473
Tubb2a	tubulin, beta 2A class IIa	0,257155978	1,649805466
Bphl	biphenyl hydrolase like	-0,280194331	1,335340827
C2cd3	C2 calcium-dependent domain containing 3	-0,317020249	1,547358667
Nedd4l	neural precursor cell expressed, developmentally down-regulated 4-like, E3 ubiquitin protein ligase	0,199719485	1,516532422
Hs3st2	heparan sulfate-glucosamine 3-sulfotransferase 2	0,708144996	1,618117208
Brsk1	BR serine/threonine kinase 1	0,334705433	1,544348887
Unc93b1	unc-93 homolog B1 (C. elegans)	-0,495168621	1,766941492
Katnal2	katanin catalytic subunit A1 like 2	-0,815701995	1,723598698
Cd14	CD14 molecule	-0,506029938	1,56442015
Ucp2	uncoupling protein 2	-0,537335854	1,438240015
Irf8	interferon regulatory factor 8	-1,016009937	1,768202909
Tcaf1	TRPM8 channel-associated factor 1	0,183700453	1,312708734
Cfap100	cilia and flagella associated protein 100	-0,950087075	1,84605841
Serpinb6	serpin family B member 6	-0,33934215	1,678674894
Gprin1	G protein-regulated inducer of neurite outgrowth 1	0,358244556	1,782458213
Dnajb13	DnaJ heat shock protein family (Hsp40) member B13	-0,503334668	1,519248138
Ranbp10	RAN binding protein 10	-0,182680369	1,371796806
Hspa12a	heat shock protein family A (Hsp70) member 12A	0,531381334	1,897007127
Sncb	synuclein, beta	0,387143296	1,724814579
Phyh	phytanoyl-CoA 2-hydroxylase	-0,303930164	1,384670311
Neu3	neuraminidase 3	-0,464243861	1,322154782
Slc12a5	solute carrier family 12 member 5	0,403082008	1,911720438
Acadvl	acyl-CoA dehydrogenase, very long chain	-0,230370082	1,701337428
Tspan17	tetraspanin 17	0,343417936	1,686297263
Abca1	ATP binding cassette subfamily A member 1	-0,338621407	1,596554745
Slc27a1	solute carrier family 27 member 1	-0,274400284	1,701260919
Oprm1	opioid receptor, mu 1	0,894610334	1,748072267
Gad2	glutamate decarboxylase 2	1,174675838	1,637641423
Abhd17a	abhydrolase domain containing 17A	0,23522799	1,4938794
Slc45a1	solute carrier family 45, member 1	0,310142228	1,582081492
Ank1	ankyrin 1	0,420627618	1,605955585
Camkk1	calcium/calmodulin-dependent protein kinase kinase 1	0,301980588	1,567947127

Dhx58	DEXH-box helicase 58	-0,785221824	1,67486188
Tnni3	troponin I3, cardiac type	-1,060987644	1,877410501
Hhip	Hedgehog-interacting protein	0,813326073	1,799599454
St8sia3	ST8 alpha-N-acetyl-neuraminide alpha-2,8-sialyltransferase 3	0,507920607	1,543686203
Eno4	enolase family member 4	-0,573431803	1,585084141
Aak1	AP2 associated kinase 1	0,293842255	1,338471524
Cnppd1	cyclin Pas1/PHO80 domain containing 1	-0,283506732	1,547358667
Fank1	fibronectin type 3 and ankyrin repeat domains 1	-0,676910404	1,637641423
Shtn1	shootin 1	0,404159726	1,766941492
Chrm1	cholinergic receptor, muscarinic 1	0,273785796	1,548092038
Cpne6	copine 6	0,388815843	1,817393541
Sfi1	SFI1 centrin binding protein	-0,299884787	1,34596196
Per3	period circadian clock 3	-0,245766859	1,340550376
Ttbk1	tau tubulin kinase 1	0,335654754	1,518796954
Stab1	stabilin 1	-3,262117596	1,859688645
Tctex1d4	Tctex1 domain containing 4	-1,037769831	1,537566888
Trim21	tripartite motif-containing 21	-0,332400646	1,323629101
Ezr	ezrin	-0,248423735	1,651387588
Dlg4	discs large MAGUK scaffold protein 4	0,242630077	1,548092038
Ahcyl1	adenosylhomocysteinase-like 1	-0,172201805	1,312708734
Fam134a	family with sequence similarity 134, member A	0,161528268	1,353206955
Plekhb1	pleckstrin homology domain containing B1	-0,290008209	1,537566888
Enkur	enkurin, TRPC channel interacting protein	-0,567977992	1,468167582
Slc6a7	solute carrier family 6 member 7	0,529966418	1,559369764
Ap3m2	adaptor-related protein complex 3, mu 2 subunit	-0,178945508	1,494714574
Agtpbp1	ATP/GTP binding protein 1	0,336506689	1,678674894
Camk2a	calcium/calmodulin-dependent protein kinase II alpha	0,408558964	1,567947127
Zfp474	zinc finger protein 474	-0,817933254	1,895068937
Rad9a	RAD9 checkpoint clamp component A	-0,307334957	1,375643283
Ugt1a5	UDP glucuronosyltransferase family 1 member A5	-0,370486832	1,413144644
Rsph3	radial spoke 3 homolog	-0,403554024	1,386573587
Jph3	junctophilin 3	0,268928904	1,454904633
Tekt4	tektin 4	-0,551754656	1,408528447
Herpud1	homocysteine inducible ER protein with ubiquitin like domain 1	-0,359730716	1,50661285
Fam65b	family with sequence similarity 65, member B	0,591401622	1,350583688
Ntrk2	neurotrophic receptor tyrosine kinase 2	-0,268995187	1,321818541
Ttc9b	tetratricopeptide repeat domain 9B	0,419077641	1,711154338
Pik3ip1	phosphoinositide-3-kinase interacting protein 1	-0,265094333	1,674387212
Ssh3	slingshot protein phosphatase 3	-0,266135017	1,500466038
Hcrt	hypocretin neuropeptide precursor	-1,001259044	1,572617303
Armc4	armadillo repeat containing 4	-1,005032177	1,711154338
Sprn	shadow of prion protein homolog (zebrafish)	0,455779712	1,825014164
Gstm7	glutathione S-transferase, mu 7	-0,289889462	1,517247243
Tsnaxip1	translin-associated factor X interacting protein 1	-0,890871068	1,807165803
Mt3	metallothionein 3	-0,310372006	1,397778445

Syne1	spectrin repeat containing nuclear envelope protein 1	-0,409714967	1,31506598
Entpd3	ectonucleoside triphosphate diphosphohydrolase 3	0,510530154	1,651387588
Fbxl19	F-box and leucine-rich repeat protein 19	0,282548655	1,633666403
Myh7b	myosin heavy chain 7B	-0,458093123	1,759614516
Plat	plasminogen activator, tissue type	-0,555488689	1,550887713
Habp4	hyaluronan binding protein 4	0,335292642	1,877410501
Ola1	Obg-like ATPase 1	0,254659488	1,356500253
Ankzf1	ankyrin repeat and zinc finger domain containing 1	-0,254428287	1,782458213
Bap1	Brca1 associated protein 1	0,175355286	1,340030656
Hmgcs2	3-hydroxy-3-methylglutaryl-CoA synthase 2	-0,47393521	1,911720438
Jakmip2	janus kinase and microtubule interacting protein 2	0,31683047	1,689751918
Syt6	synaptotagmin 6	1,219715943	2,090474573
Taf10	TATA-box binding protein associated factor 10	0,249340739	1,62948979
Acsl4	acyl-CoA synthetase long-chain family member 4	0,43056323	1,525263705
Acat2	acetyl-CoA acetyltransferase 2	0,337694323	1,711154338
Stx1b	syntaxin 1B	0,283979933	1,649805466
Shank1	SH3 and multiple ankyrin repeat domains 1	0,42185039	1,650793711
Tpp1	tripeptidyl peptidase 1	-0,329581268	1,731010224
Vamp1	vesicle-associated membrane protein 1	0,501006295	1,493466259
Rnf220	ring finger protein 220	0,189306778	1,43350273
Glb1l	galactosidase, beta 1-like	-0,269181704	1,799599454
Kif27	kinesin family member 27	-0,677561375	1,711154338
Ulk4	unc-51 like kinase 4	-0,486675119	1,689751918
Edem2	ER degradation enhancing alpha-mannosidase like protein 2	-0,229390884	1,462788219
Eid2	EP300 interacting inhibitor of differentiation 2	0,433225972	1,711154338
Syt3	synaptotagmin 3	0,295084155	1,382387044
Cck	cholecystokinin	0,808679148	1,4938794
Hipk1	homeodomain interacting protein kinase 1	-0,243369543	1,492388962
Inpp5j	inositol polyphosphate-5-phosphatase J	0,334257636	1,586559548
Ablim3	actin binding LIM protein family, member 3	0,377373503	1,509498727
Coro1a	coronin 1A	0,34414516	1,682695134
Rab3a	RAB3A, member RAS oncogene family	0,376595213	1,765740972
Psd	pleckstrin and Sec7 domain containing	0,296004877	1,469681504
Ecel1	endothelin converting enzyme-like 1	0,685835742	1,368816971
Rsph9	radial spoke head 9 homolog	-0,496978822	1,597825273
Agap1	ArfGAP with GTPase domain, ankyrin repeat and PH domain 1	0,190565218	1,527197678
Irf9	interferon regulatory factor 9	-0,489007471	1,413144644
Psmb10	proteasome subunit beta 10	-0,392850362	1,676902309
Stat5a	signal transducer and activator of transcription 5A	-0,544142911	1,689751918
LOC100910979	interferon-inducible GTPase 1-like	-1,038701592	1,844389761
Cd9	CD9 molecule	-0,510532324	1,562518805
Pde2a	phosphodiesterase 2A	0,441602156	1,778093331
Jund	JunD proto-oncogene, AP-1 transcription factor subunit	0,212821364	1,435273797
Iqca1	IQ motif containing with AAA domain 1	-0,720958537	1,895068937
Pld2	phospholipase D2	-0,362422744	1,48450127

Gpr61	G protein-coupled receptor 61	0,335242825	1,602886302
Stat3	signal transducer and activator of transcription 3	-0,163059571	1,3131808
Kcna1	potassium voltage-gated channel subfamily A member 1	0,319584603	1,322974657
Sil1	SIL1 nucleotide exchange factor	-0,291019119	1,488314156
Bbs1	Bardet-Biedl syndrome 1	-0,289246641	1,650793711
Gng7	G protein subunit gamma 7	0,426849942	1,668633435
Lrfn1	leucine rich repeat and fibronectin type III domain containing 1	0,333744126	1,682695134
Folr1	folate receptor 1	-0,850831211	1,629521887
Fam57b	family with sequence similarity 57, member B	0,321552887	1,539412296
Xrcc1	X-ray repair cross complementing 1	-0,288391511	1,748072267
Ramp1	receptor activity modifying protein 1	-0,868120778	1,669226379
Tmem151b	transmembrane protein 151B	0,434222312	1,911720438
Kcnc3	potassium voltage-gated channel subfamily C member 3	0,223380389	1,315959499
Tcte1	t-complex-associated testis expressed 1	0,262482625	1,428430876
Spata24	spermatogenesis associated 24	-0,631683719	1,552175485
Asic4	acid sensing ion channel subunit family member 4	0,374061453	1,456473696
Slc16a1	solute carrier family 16 member 1	-0,28268557	1,699600456
Tmem198	transmembrane protein 198	0,289840505	1,493658921
Lrrc18	leucine rich repeat containing 18	-1,075171855	1,661501376
Pcdha4	protocadherin alpha 4	0,401996616	1,687031769
Ttll10	tubulin tyrosine ligase like 10	-0,856570086	1,582961216
Slc4a3	solute carrier family 4 member 3	0,196697343	1,547940063
Tinf2	TERF1 interacting nuclear factor 2	-0,295200235	1,585084141
Ptpn20	protein tyrosine phosphatase, non-receptor type 20	-0,698425273	1,585084141
Dlgap4	DLG associated protein 4	0,155425821	1,398198424
Cnih2	cornichon family AMPA receptor auxiliary protein 2	0,383088648	1,689751918
Ina	internexin neuronal intermediate filament protein, alpha	0,521853551	1,757270081
Atp1a3	ATPase Na+/K+ transporting subunit alpha 3	0,4312288	1,897007127
Slc25a20	solute carrier family 25 member 20	-0,200237122	1,349841496
Klc2	kinesin light chain 2	0,311065396	1,499606087
RGD1309139	similar to CG5435-PA	-0,783119018	1,534362711
Ech1	enoyl-CoA hydratase 1	-0,395803671	1,804942506
Grik5	glutamate ionotropic receptor kainate type subunit 5	0,193247808	1,491648748
Asb1	ankyrin repeat and SOCS box-containing 1	0,326615009	1,487617366
Wdr47	WD repeat domain 47	0,217754804	1,45157359
Neurl1	neuralized E3 ubiquitin protein ligase 1	0,415611442	1,897007127
Atcay	ATCAY, caytaxin	0,256844943	1,664663019
Gsk3a	glycogen synthase kinase 3 alpha	0,223012346	1,545001516
Fndc7	fibronectin type III domain containing 7	-0,583505422	1,765740972
Apc	APC, WNT signaling pathway regulator	0,325081266	1,600202021
Camk4	calcium/calmodulin-dependent protein kinase IV	0,340012424	1,504514031
Plekha1	pleckstrin homology domain containing A1	0,274232545	1,58465783
Tjp3	tight junction protein 3	-0,598063765	1,757270081
Khnyn	KH and NYN domain containing	-0,397574787	1,669509893
Prrg2	proline rich and Gla domain 2	-0,403898967	1,368816971

Fam189b	family with sequence similarity 189, member B	0,316914415	1,474956038
Olfm2	olfactomedin 2	0,265878643	1,36820448
Pip5k1c	phosphatidylinositol-4-phosphate 5-kinase type 1 gamma	0,259891987	1,336220061
Ppp1r32	protein phosphatase 1, regulatory subunit 32	-0,877785411	1,826012297
Nsg2	neuron specific gene family member 2	0,256390619	1,392776974
Slc17a7	solute carrier family 17 member 7	0,400573353	1,699600456
Pbxip1	PBX homeobox interacting protein 1	-0,321614871	1,701776837
Ifi35	interferon-induced protein 35	-0,470238892	1,719412906
Dpf1	double PHD fingers 1	0,268778636	1,597825273
Cpeb3	cytoplasmic polyadenylation element binding protein 3	0,440194926	1,830935884
Tmem216	transmembrane protein 216	-0,407484663	1,529558923
Icam5	intercellular adhesion molecule 5	0,278364481	1,516175038
Sipa1l3	signal-induced proliferation-associated 1 like 3	0,281412555	1,479433266
Ppfia3	PTPRF interacting protein alpha 3	0,26098673	1,368816971
Lin7b	lin-7 homolog B, crumbs cell polarity complex component	0,479012347	1,821107891
Dhcr7	7-dehydrocholesterol reductase	0,22739705	1,31351724
Chrnb2	cholinergic receptor nicotinic beta 2 subunit	0,322385233	1,306181746
Hipk4	homeodomain interacting protein kinase 4	0,458371106	1,54008332
Coq8b	coenzyme Q8B	-0,249466752	1,364471447
Aplp1	amyloid beta precursor like protein 1	0,282714313	1,68649236
Kif9	kinesin family member 9	-0,820721021	1,826012297
Hspb6	heat shock protein family B (small) member 6	-0,324324779	1,556237203
Sac3d1	SAC3 domain containing 1	0,270881573	1,513922712
Ppp2r5b	protein phosphatase 2, regulatory subunit B', beta	0,26838707	1,552175485
Fam171a2	family with sequence similarity 171, member A2	0,283027943	1,635545286
Lmtk3	lemur tyrosine kinase 3	0,215743186	1,685766058
Grin2d	glutamate ionotropic receptor NMDA type subunit 2D	1,019656971	1,646491247
Fxyd7	FXYD domain-containing ion transport regulator 7	0,472002315	1,342843091
Sema6c	semaphorin 6C	0,37892129	1,457826737
Scn1b	sodium voltage-gated channel beta subunit 1	0,280358661	1,522488479
Nrxn2	neurexin 2	0,275446781	1,780790003
Ccdc114	coiled-coil domain containing 114	-0,764951959	1,731867267
Mllt11	myeloid/lymphoid or mixed-lineage leukemia; translocated to, 11	0,414550445	1,830935884
Nomo1	nodal modulator 1	0,20884651	1,516175038
Kcnj11	potassium voltage-gated channel subfamily J member 11	0,451698715	1,465485008
Abcc8	ATP binding cassette subfamily C member 8	0,508782835	1,702078113
Macrod1	MACRO domain containing 1	-0,371626036	1,379630112
Sv2a	synaptic vesicle glycoprotein 2a	0,355169618	1,724814579
Rtn3	reticulon 3	0,200277125	1,333408771
Slc4a11	solute carrier family 4 member 11	-0,779273809	1,757270081
Spef1	sperm flagellar 1	-0,417285627	1,454564213
Cds2	CDP-diacylglycerol synthase 2	0,293331518	1,516263706
Celsr1	cadherin, EGF LAG seven-pass G-type receptor 1	-0,484702193	1,711154338
RGD1306954	similar to RIKEN cDNA 1110004E09	-0,298263382	1,321161586
Pptc7	PTC7 protein phosphatase homolog	0,227791348	1,404157789

Reln	reelin	0,733729932	1,518664794
Tpd52l1	tumor protein D52-like 1	0,388354286	1,306978582
Akt3	AKT serine/threonine kinase 3	0,28835154	1,317311075
Rtn4rl2	reticulon 4 receptor-like 2	0,414463653	1,821107891
Tmem231	transmembrane protein 231	-0,370215664	1,604811062
Tiam1	T-cell lymphoma invasion and metastasis 1	0,42088003	1,681512209
RGD1561931	similar to KIAA2022 protein	0,241426155	1,413220507
Zmynd10	zinc finger, MYND-type containing 10	-0,688811327	1,585804241
Cdk5r1	cyclin-dependent kinase 5 regulatory subunit 1	0,235998391	1,341282308
Fam149a	family with sequence similarity 149, member A	-0,422195243	1,387865527
Atp8b5p	ATPase, class I, type 8B, member 5, pseudogene	-0,629363365	1,701776837
Fam92b	family with sequence similarity 92, member B	-0,671906043	1,685425675
Iqub	IQ motif and ubiquitin domain containing	-0,506863902	1,701776837
Bhlhe22	basic helix-loop-helix family, member e22	0,542663354	1,707078717
Fam227a	family with sequence similarity 227, member A	-0,882313176	1,897007127
Isg15	ISG15 ubiquitin-like modifier	-0,856942831	1,751789185
Cep126	centrosomal protein 126	-0,567103232	1,68465649
Fam216b	family with sequence similarity 216, member B	-0,969885094	1,711154338
Cntrl	centriolin	-0,388811168	1,68649236
Paqr7	progestin and adipoQ receptor family member 7	-0,360458844	1,778093331
LOC685680	similar to TPA-induced transmembrane protein	-0,979549501	1,582961216
Zmynd12	zinc finger, MYND-type containing 12	-0,731463783	1,780790003
Ifi44	interferon-induced protein 44	-0,491106563	1,531667664
Fbxl16	F-box and leucine-rich repeat protein 16	0,318164361	1,442834699
Lhfpl5	lipoma HMGIC fusion partner-like 5	1,28090046	1,508264693
Ccdc78	coiled-coil domain containing 78	-1,260126513	2,352696509
Hspb8	heat shock protein family B (small) member 8	-0,262676887	1,531667664
St8sia5	ST8 alpha-N-acetyl-neuraminide alpha-2,8-sialyltransferase 5	0,811196142	1,54008332
RGD1562029	similar to KIAA2012 protein	-0,77803986	1,830935884
Rubcnl	RUN and cysteine rich domain containing beclin 1 interacting protein like	-0,724976364	1,335218142
Elfn1	extracellular leucine-rich repeat and fibronectin type III domain containing 1	0,470153078	1,674387212
Fgfbp3	fibroblast growth factor binding protein 3	0,419544495	1,897007127
Rimbp2	RIMS binding protein 2	0,312761704	1,557956217
Slc25a12	solute carrier family 25 member 12	0,235463966	1,324394631
Slc35d1	solute carrier family 35 member D1	-0,278146586	1,450258457
Tctex1d1	Tctex1 domain containing 1	-0,732834385	1,527197678
Lonrf2	LON peptidase N-terminal domain and ring finger 2	0,223576565	1,445648765
Parp14	poly (ADP-ribose) polymerase family, member 14	-0,412319425	1,313170408
Styxl1	serine/threonine/tyrosine interacting-like 1	-0,746608404	1,719412906
Ddx3x	DEAD-box helicase 3, X-linked	0,309226532	1,863659497
Dtx3l	deltex E3 ubiquitin ligase 3L	-0,441738593	1,34596196
Parp9	poly (ADP-ribose) polymerase family, member 9	-0,347093421	1,419031513
Fam168b	family with sequence similarity 168, member B	0,181278839	1,391779153
Map3k10	mitogen activated protein kinase kinase kinase 10	0,27163083	1,629521887

Ankfn1	ankyrin-repeat and fibronectin type III domain containing 1	-0,729916341	1,711154338
Vwa3b	von Willebrand factor A domain containing 3B	-0,75246109	1,572617303
Elavl4	ELAV like RNA binding protein 4	0,607649563	1,697344548
Cfap74	cilia and flagella associated protein 74	-0,86155883	1,911720438
Mmp17	matrix metallopeptidase 17	0,282067609	1,317311075
Celf2	CUGBP, Elav-like family member 2	0,163925223	1,424574501
LOC502684	hypothetical protein LOC502684	-0,806703852	1,711154338
NEWGENE_1305560	neuronal tyrosine-phosphorylated phosphoinositide-3-kinase adaptor 2	0,745298382	1,817393541
Mei4	meiotic double-stranded break formation protein 4	-0,68322405	1,724814579
Pak1ip1	PAK1 interacting protein 1	0,254013861	1,355580011
Snap91	synaptosomal-associated protein 91	0,36157696	1,711154338
Man2b1	mannosidase, alpha, class 2B, member 1	-0,274328163	1,551016067
Tbc1d30	TBC1 domain family, member 30	0,454043252	1,696748851
Ndfip2	Nedd4 family interacting protein 2	0,193057213	1,419689951
Lemd3	LEM domain containing 3	0,210306627	1,482400353
Slain1	SLAIN motif family, member 1	0,252232452	1,513922712
T2	brachyury 2	-1,015005244	1,646491247
Cenpt	centromere protein T	-0,434784594	1,520332638
Tnfaip8l3	TNF alpha induced protein 8 like 3	0,805396948	1,537566888
Ccdc170	coiled-coil domain containing 170	-0,634016211	1,572617303
AABR07019083.1	0	0,643856276	1,911720438
LOC690276	hypothetical protein LOC690276	-0,733547768	1,586626478
Carmil2	capping protein regulator and myosin 1 linker 2	0,344688058	1,765740972
Tarsl2	threonyl-tRNA synthetase-like 2	0,303385138	1,711154338
Traf3ip1	TRAF3 interacting protein 1	-0,389406759	1,575950116
Ap1ar	adaptor-related protein complex 1 associated regulatory protein	0,231173112	1,31351724
AABR07056633.1	0	-0,791745527	1,685766058
Dnai2	dynein, axonemal, intermediate chain 2	-0,583823097	1,318178772
Ttc34	tetratricopeptide repeat domain 34	-0,81216607	1,826012297
Ganc	glucosidase, alpha; neutral C	-0,212582226	1,388928771
Wdr49	WD repeat domain 49	-0,792930284	1,733115406
Gpr85	G protein-coupled receptor 85	0,307274841	1,470686839
Arhgap33	Rho GTPase activating protein 33	0,371999116	1,699600456
Hopx	HOP homeobox	-0,508360255	1,307848774
Tp73	tumor protein p73	-0,909830019	1,711154338
Ppm1e	protein phosphatase, Mg2+/Mn2+ dependent, 1E	0,420276522	1,479809529
Col22a1	collagen type XXII alpha 1 chain	-0,716134073	1,804942506
Gpr158	G protein-coupled receptor 158	0,311279584	1,517768321
Anks1b	ankyrin repeat and sterile alpha motif domain containing 1B	0,355929499	1,520332638
Pla2g4e	phospholipase A2, group IVE	1,518680707	1,62948979
Drc1	dynein regulatory complex subunit 1	-0,699843532	1,757270081
Als2cr12	amyotrophic lateral sclerosis 2 chromosome region, candidate 12	-0,85195268	1,778093331
Mgat5b	mannosyl (alpha-1,6-)-glycoprotein beta-1,6-N-acetyl-glucosaminyltransferase, isozyme B	0,275749139	1,711154338
Dnali1	dynein, axonemal, light intermediate chain 1	-0,736516348	1,681512209

Ccdc190	coiled-coil domain containing 190	-0,596059345	1,364471447
Vwa3a	von Willebrand factor A domain containing 3A	-0,814301755	1,633666403
Icam2	intercellular adhesion molecule 2	-0,931756679	1,347863065
Tmem130	transmembrane protein 130	0,301110872	1,438240015
Ccdc87	coiled-coil domain containing 87	-0,728526763	1,413144644
RGD1565611	RGD1565611	-0,853889476	1,611478922
Slc2a10	solute carrier family 2 member 10	-0,426955908	1,521251022
Map3k13	mitogen-activated protein kinase kinase kinase 13	0,339844215	1,301162155
Crb2	crumbs 2, cell polarity complex component	-0,491431263	1,387865527
Tvp23a	trans-golgi network vesicle protein 23A	0,354948752	1,38433524
Rgs22	regulator of G-protein signaling 22	-0,723126492	1,550330124
Agap2	ArfGAP with GTPase domain, ankyrin repeat and PH domain 2	0,350143597	1,682695134
Jph4	junctophilin 4	0,48579225	1,750594197
Scrt1	scratch family transcriptional repressor 1	0,520809587	1,911720438
Pla2g7	phospholipase A2 group VII	-0,459647138	1,568502927
Armcx2	armadillo repeat containing, X-linked 2	0,276040662	1,753015761
LOC499770	similar to LOC495800 protein	-0,262510766	1,518796954
Tcf23	transcription factor 23	-1,240645534	1,348204581
Spag6l	sperm associated antigen 6-like	-0,775988903	1,603898558
Ccdc102a	coiled-coil domain containing 102A	-0,334896116	1,582081492
Drc7	dynein regulatory complex subunit 7	-0,910018603	1,699600456
Aim1	absent in melanoma 1	-0,718729044	1,314326512
Grem1	gremlin 1, DAN family BMP antagonist	1,358543672	1,616787105
Slit1	slit guidance ligand 1	0,95374495	1,666346368
Cetn4	centrin 4	-0,667090296	1,543686203
Syde2	synapse defective Rho GTPase homolog 2	-0,319235304	1,699600456
Armc2	armadillo repeat containing 2	-0,636763309	1,580696635
Saxo2	stabilizer of axonemal microtubules 2	-0,706032686	1,534209154
Fam179a	family with sequence similarity 179, member A	-0,889340487	1,877410501
Iqcg	IQ motif containing G	-0,715701216	1,578733541
Syt7	synaptotagmin 7	0,213204104	1,479253691
Gpd1l	glycerol-3-phosphate dehydrogenase 1-like	0,29382206	1,724814579
Lrrtm3	leucine rich repeat transmembrane neuronal 3	0,412083518	1,557956217
Gltpd2	glycolipid transfer protein domain containing 2	-0,763248447	1,557964673
Dnm3	dynamin 3	0,475003012	1,911720438
Xrra1	X-ray radiation resistance associated 1	-0,86316367	1,582961216
Wdr93	WD repeat domain 93	-0,969972245	1,526218562
Vrk3	vaccinia related kinase 3	-0,191667857	1,438219462
Glipr1l1	GLI pathogenesis-related 1 like 1	-0,923947214	1,711154338
Dgki	diacylglycerol kinase, iota	0,324993282	1,724814579
Dennd2a	DENN domain containing 2A	-0,264501442	1,445648765
Disp2	dispatched RND transporter family member 2	0,367803841	1,487364554
Pgbd5	piggyBac transposable element derived 5	0,35654227	1,85179005
Arhgap42	Rho GTPase activating protein 42	-0,330876647	1,697785357
Dnah1	dynein, axonemal, heavy chain 1	-0,965731489	1,799599454

Osbpl8	oxysterol binding protein-like 8	0,304817027	1,643653253
Gas8	growth arrest specific 8	-0,391239634	1,586559548
Tmem140	transmembrane protein 140	-0,49779675	1,557964673
Dbndd1	dysbindin domain containing 1	0,365210486	1,335923845
Oscp1	organic solute carrier partner 1	-0,402028365	1,438240015
Igtp	interferon gamma induced GTPase	-0,493270166	1,355848542
Ube2k	ubiquitin-conjugating enzyme E2K	0,170484285	1,312688527
Sez6l2	seizure related 6 homolog like 2	0,341989289	1,534362711
Zc2hc1c	zinc finger, C2HC-type containing 1C	-0,678688017	1,711154338
Map6	microtubule-associated protein 6	0,268961161	1,766941492
Tekt3	tektin 3	-0,799499963	1,341035359
Trpc5	transient receptor potential cation channel, subfamily C, member 5	0,728270627	1,611478922
Faxdc2	fatty acid hydroxylase domain containing 2	-0,687228765	1,525263705
Dagla	diacylglycerol lipase, alpha	0,190025695	1,506844943
Xkr4	XK related 4	0,501420193	1,763695767
Tenm2	teneurin transmembrane protein 2	0,502158893	1,825014164
Cfap46	cilia and flagella associated protein 46	-0,891345028	1,818329099
Ccdc187	coiled-coil domain containing 187	-0,985083684	1,739471227
Adamts3	ADAM metallopeptidase with thrombospondin type 1, motif 3	0,642084223	1,565157506
Mn1	meningioma 1	0,27788901	1,702412232
Nmi	N-myc (and STAT) interactor	-0,401721902	1,516175038
Tapbpl	TAP binding protein-like	-0,407134751	1,699600456
Dpysl4	dihydropyrimidinase-like 4	0,228544197	1,341035359
Jakmip3	janus kinase and microtubule interacting protein 3	0,277126294	1,62948979
Ttc26	tetratricopeptide repeat domain 26	-0,27726877	1,386680101
Casc1	cancer susceptibility candidate 1	-0,539824302	1,701776837
Ubxn10	UBX domain protein 10	-0,753104954	1,817393541
Ptk2b	protein tyrosine kinase 2 beta	0,522023005	1,651387588
Rapgefl1	Rap guanine nucleotide exchange factor like 1	0,421716243	1,897007127
Lrrc34	leucine rich repeat containing 34	-0,862816763	1,799599454
Crip1	cysteine rich protein 1	-0,766424828	1,34596196
Tnnt1	troponin T1, slow skeletal type	-1,250085909	1,534209154
Fhad1	forkhead associated phosphopeptide binding domain 1	-0,773880876	1,830935884
Cfap44	cilia and flagella associated protein 44	-1,162893861	1,840759334
Tmem35b	transmembrane protein 35B	-0,363709384	1,467448865
Slc7a14	solute carrier family 7, member 14	0,409474451	1,397778445
Pld1	phospholipase D1	-0,266794072	1,558970741
Ankrd13d	ankyrin repeat domain 13D	0,231432369	1,593630972
Lca5l	LCA5L, lebercilin like	-0,973570544	1,830935884
Tppp	tubulin polymerization promoting protein	0,272210628	1,586626478
Unc80	unc-80 homolog, NALCN activator	0,365067987	1,758478369
Npepl1	aminopeptidase-like 1	-0,391981491	1,504785446
Ppp1r1b	protein phosphatase 1, regulatory (inhibitor) subunit 1B	-0,622899884	1,911720438
Neurod2	neuronal differentiation 2	0,485704022	1,724814579
Tctn1	tectonic family member 1	-0,459850515	1,763240386

Mansc1	MANSC domain containing 1	-0,309705451	1,559369764
Pcnx2	pecanex homolog 2 (Drosophila)	0,459983962	1,711154338
Ccdc138	coiled-coil domain containing 138	-0,655392595	1,341035359
Ksr2	kinase suppressor of ras 2	0,290493946	1,531543609
Prkar1b	protein kinase cAMP-dependent type 1 regulatory subunit beta	0,330313087	1,782458213
Gal3st3	galactose-3-O-sulfotransferase 3	0,468175851	1,840759334
Gbp4	guanylate binding protein 4	-0,710529249	1,340030656
Cfap77	cilia and flagella associated protein 77	-0,800921548	1,543686203
Oasl2	2'-5' oligoadenylate synthetase-like 2	-1,095319341	1,834794779
Sorcs3	sortilin-related VPS10 domain containing receptor 3	0,330333424	1,699600456
Rtp4	receptor (chemosensory) transporter protein 4	-1,034349739	1,306978582
RGD1565536	similar to hypothetical protein	-0,337985364	1,421918432
AABR07024637.1	0	-1,026000334	2,208516677
Adgrl1	adhesion G protein-coupled receptor L1	0,196624271	1,322974657
Epha6	Eph receptor A6	0,761661276	1,724814579
Uba7	ubiquitin-like modifier activating enzyme 7	-0,92897576	1,72681633
Dusp8	dual specificity phosphatase 8	0,2584385	1,496589768
Bai1	0	0,229958988	1,523294228
Tapbp	TAP binding protein	-0,403592242	1,588904814
Nrbp2	nuclear receptor binding protein 2	-0,455623878	1,720313286
Eci2	enoyl-CoA delta isomerase 2	-0,192469549	1,38145736
Cdhr4	cadherin-related family member 4	-1,03767064	1,879710229
Clec2l	C-type lectin domain family 2, member L	0,438380234	1,720313286
Rnf213	ring finger protein 213	-0,476581739	1,554522956
Gstm1	glutathione S-transferase mu 1	-0,562839394	1,669509893
Diras1	DIRAS family GTPase 1	0,403385364	1,766941492
Maob	monoamine oxidase B	-0,690444036	1,534209154
Lrrc4c	leucine rich repeat containing 4C	0,330043648	1,757078164
Cfap54	cilia and flagella associated protein 54	-0,760537379	1,85179005
Gucy1a2	guanylate cyclase 1 soluble subunit alpha 2	0,40498096	1,522488479
Gp1bb	glycoprotein Ib platelet beta subunit	0,387270639	1,899224437
Zbtb16	zinc finger and BTB domain containing 16	0,26441401	1,391835313
Vamp3	vesicle-associated membrane protein 3	-0,27460623	1,373557871
Cerkl	ceramide kinase-like	-0,688579231	1,64707996
Tango2	transport and golgi organization 2 homolog	0,282732105	1,689751918
Atp2b2	ATPase plasma membrane Ca2+ transporting 2	0,329223335	1,707360265
Pcdh11x	protocadherin 11 X-linked	0,349068384	1,684276272
Tf	transferrin	-0,339980027	1,609695989
RT1-A2	RT1 class Ia, locus A2	-0,653641051	1,430897628
Bsn	bassoon (presynaptic cytomatrix protein)	0,421796659	1,948911923
Adarb2	adenosine deaminase, RNA-specific, B2	0,703245381	1,877410501
Stat2	signal transducer and activator of transcription 2	-0,355016856	1,527033446
Ergic3	ERGIC and golgi 3	-0,185493357	1,444650583
RT1-CE7	RT1 class I, locus CE7	-0,589444705	1,394217764
Irgm	immunity-related GTPase M	-0,545459803	1,454564213

LOC500035	hypothetical protein LOC500035	0,836091562	1,640705567
Siae	sialic acid acetylesterase	-0,394503765	1,604236657
Ift22	intraflagellar transport 22	-0,252368006	1,527197678
Stk32b	serine/threonine kinase 32B	0,667674222	1,711154338
AC097129.1	0	-0,948377034	1,897007127
Stpg1	sperm-tail PG-rich repeat containing 1	-0,715270452	1,711154338
RGD1563714	RGD1563714	-0,756482	1,780790003
0	0	-0,749484611	1,460526203
Syndig1	synapse differentiation inducing 1	0,372460413	1,391765661
Rasgef1a	RasGEF domain family, member 1A	0,475108326	1,548092038
Gbp2	guanylate binding protein 2	-0,576866685	1,669226379
Rangap1	RAN GTPase activating protein 1	0,184024446	1,324126197
Nkain4	Sodium/potassium transporting ATPase interacting 4	-0,460824108	1,54008332
Ttll7	tubulin tyrosine ligase like 7	0,369654617	1,689751918
Hapln1	hyaluronan and proteoglycan link protein 1	0,706650765	1,724814579
Dlec1	deleted in lung and esophageal cancer 1	-1,076461272	2,030793234
Cyp2d4	cytochrome P450, family 2, subfamily d, polypeptide 4	-0,529954201	1,897007127
AABR07058658.1	0	-0,406833168	1,643653253
Mtus2	microtubule associated tumor suppressor candidate 2	0,456539539	1,3938137
Usp22	ubiquitin specific peptidase 22	0,214230089	1,651387588
Spag8	sperm associated antigen 8	-0,887903122	1,897007127
Foxo6	forkhead box O6	0,741852521	1,462788219
Ube2e2	ubiquitin-conjugating enzyme E2E 2	0,258922484	1,664663019
Stxbp4	syntaxin binding protein 4	-0,332750078	1,462788219
Mapk8ip2	mitogen-activated protein kinase 8 interacting protein 2	0,27134473	1,516532422
Mlc1	megalencephalic leukoencephalopathy with subcortical cysts 1	-0,331674799	1,40109479
Cyp4f4	cytochrome P450, family 4, subfamily f, polypeptide 4	-0,566516065	1,395903174
Mef2c	myocyte enhancer factor 2C	0,357027592	1,509498727
Fbxo41	F-box protein 41	0,373736283	1,84605841
Oas1b	2-5 oligoadenylate synthetase 1B	-1,431788523	1,650793711
LOC501110	similar to Glutathione S-transferase A1 (GTH1) (HA subunit 1) (GST-epsilon) (GSTA1-1) (GST class-alpha)	-0,416312434	1,585084141
Cib1	calcium and integrin binding 1	-0,316986374	1,766941492
Ribc2	RIB43A domain with coiled-coils 2	-0,604591343	1,603798447
Ldlrad2	low density lipoprotein receptor class A domain containing 2	-0,773679968	1,467448865
Cacna2d1	calcium voltage-gated channel auxiliary subunit alpha2delta 1	0,399045047	1,701776837
AY172581.21	0	0,856464093	1,629521887
Osbpl9	oxysterol binding protein-like 9	-0,189063094	1,550330124
Cep170b	centrosomal protein 170B	0,288094919	1,655830417
Ccdc81	coiled-coil domain containing 81	-0,998054789	1,911720438
Ankrd34a	ankyrin repeat domain 34A	0,30834288	1,479671561
Dnm1	dynamin 1	0,414566397	1,877410501
RGD1560470	similar to Gene model 996	0,324920385	1,308502943
Cacna1h	calcium voltage-gated channel subunit alpha1 H	0,256007868	1,440229118
Fcho1	FCH domain only 1	0,32539315	1,394492809
Als2cl	ALS2 C-terminal like	-0,304107183	1,42848315

Grin2a	glutamate ionotropic receptor NMDA type subunit 2A	0,427602499	1,45614877
Vstm2l	V-set and transmembrane domain containing 2 like	1,032472589	2,37856714
Ube2ql1	ubiquitin-conjugating enzyme E2Q family-like 1	0,380270533	1,799599454
Ttc21a	tetratricopeptide repeat domain 21A	-0,894135861	1,699600456
Pcdhga2	protocadherin gamma subfamily A, 2	-0,214491869	1,634446082
Cfap126	cilia and flagella associated protein 126	-0,714072256	1,711154338
Cfap43	cilia and flagella associated protein 43	-0,916816727	1,586626478
Rab40b	Rab40b, member RAS oncogene family	0,302350427	1,650793711
Foxk2	forkhead box K2	0,177849942	1,321161586
Iqck	IQ motif containing K	-0,679385015	1,766941492
Snhg11	small nucleolar RNA host gene 11	0,605257779	1,449701644
Wls	wntless Wnt ligand secretion mediator	-0,406598568	1,306978582
RGD1309621	similar to hypothetical protein FLJ10652	-0,236767798	1,348204581
Etfbkmt	electron transfer flavoprotein beta subunit lysine methyltransferase	-0,658109022	1,586559548
Odf3b	outer dense fiber of sperm tails 3B	-0,99060967	1,766941492
Spag17	sperm associated antigen 17	-0,995560061	1,911720438
Usp18	ubiquitin specific peptidase 18	-1,017835279	1,321054061
Riiad1	regulatory subunit of type II PKA R-subunit (RIIa) domain containing 1	-0,617112281	1,534209154
XAF1	XIAP associated factor-1	-0,615713882	1,34596196
Tmem196	transmembrane protein 196	0,858413064	1,505197308
Galnt9	polypeptide N-acetylgalactosaminyltransferase 9	0,552179948	1,669509893
Cd68	Cd68 molecule	-0,868648633	1,330690083
Kdm6b	lysine demethylase 6B	-0,20986213	1,336964243
LOC688553	hypothetical protein LOC688553	-0,945358661	1,689751918
Ak9	adenylate kinase 9	-0,829591467	1,69988277
Cfap52	cilia and flagella associated protein 52	-0,652576448	1,689751918
Rita1	RBPJ interacting and tubulin associated 1	0,317185383	1,539412296
Cdk5r2	cyclin-dependent kinase 5 regulatory subunit 2	0,508186954	1,999345788
Catip	ciliogenesis associated TTC17 interacting protein	-0,612146753	1,582081492
AABR07065353.1	0	-1,334137278	1,877410501
LOC100912028	olfactory receptor 19-like	-0,754818931	1,388928771
LOC680227	LRRGT00193	6,761768803	1,865675952
Fam155b	family with sequence similarity 155, member B	0,370421341	1,689751918
Elmod3	ELMO domain containing 3	-0,225351809	1,319108337
Dok6	docking protein 6	0,48099414	1,605955585
Calml4	calmodulin-like 4	-0,654225208	1,689751918
Serp2	stress-associated endoplasmic reticulum protein family member 2	0,276668094	1,531667664
AABR07015812.1	0	0,669006897	1,689751918
Ppp1r36	protein phosphatase 1, regulatory subunit 36	-0,541283115	1,551148958
Rassf9	Ras association domain family member 9	-0,515091193	1,650793711
Dnaaf3	dynein, axonemal, assembly factor 3	-0,74774651	1,669509893
RGD1564308	similar to LOC495042 protein	-0,620356247	1,355321826
Ccdc153	coiled-coil domain containing 153	-0,890640505	1,689751918
Ahcyl2	adenosylhomocysteinase-like 2	0,347226605	1,592008995
Pcdhgb7	protocadherin gamma subfamily B, 7	-0,412715905	1,582081492

Aass	aminoadipate-semialdehyde synthase	0,372704631	1,484031428
Dydc2	DPY30 domain containing 2	-0,941893254	1,516532422
Orai3	ORAI calcium release-activated calcium modulator 3	-0,359921618	1,62948979
Ttf1	transcription termination factor 1	-0,346340268	1,596610422
Lrrc73	leucine rich repeat containing 73	0,251487827	1,629521887
Mfsd12	major facilitator superfamily domain containing 12	0,253303868	1,496589768
LOC681766	hypothetical protein LOC681766	-0,757584299	1,782458213
Ankrd34b	ankyrin repeat domain 34B	0,590690825	1,388928771
Cdkl4	cyclin-dependent kinase-like 4	-0,577078336	1,580696635
Mir770	microRNA 770	0,526014049	1,508079385
Efs	embryonal Fyn-associated substrate	-0,339251699	1,4611588
Tmem240	transmembrane protein 240	0,415807515	1,572617303
LOC100912642	cytochrome P450 2J3-like	-0,392949215	1,306978582
AC130035.1	0	-0,810413635	1,646626534
Fbxo31	F-box protein 31	0,226370724	1,384522877
Soga3	SOGA family member 3	0,210176517	1,544348887
Adam22	ADAM metallopeptidase domain 22	0,389460961	1,696748851
Smim17	small integral membrane protein 17	1,007897668	1,766941492
Rgs10	regulator of G-protein signaling 10	0,38228065	1,582081492
Rhof	ras homolog family member F, filopodia associated	0,366080092	1,412258263
Trim34	tripartite motif-containing 34	-0,575130864	1,317329314
Efhc1	EF-hand domain containing 1	-0,743167772	1,500466038
Slc25a18	solute carrier family 25 member 18	-0,537500421	1,85179005
Adgb	androglobin	-0,85119319	1,766941492
Fgf13	fibroblast growth factor 13	0,415442508	1,419031513
LOC688801	hypothetical protein LOC688801	-0,788697649	1,830935884
RT1-T24-4	RT1 class I, locus T24, gene 4	-0,644922055	1,513922712
Mycbpap	Mycbp associated protein	-0,659002203	1,488991519
Fbxl13	F-box and leucine-rich repeat protein 13	-0,555789213	1,479671561
Fam43b	family with sequence similarity 43, member B	0,749045122	1,768202909
Cntnap5c	contactin associated protein-like 5C	0,933966236	1,40109479
Ppil6	peptidylprolyl isomerase like 6	-0,485037393	1,516532422
LOC688613	hypothetical protein LOC688613	-0,320004494	1,45157359
Ppp3r1	protein phosphatase 3, regulatory subunit B, alpha	0,307338648	1,607785128
Zfp771	zinc finger protein 771	0,315755659	1,757270081
Cyp4f6	cytochrome P450, family 4, subfamily f, polypeptide 6	-0,352868692	1,853318039
Fdps	farnesyl diphosphate synthase	0,289928866	1,349841496
LOC100359479	rCG58364-like	-0,807011848	1,558970741
Samd12	sterile alpha motif domain containing 12	0,497200142	1,817393541
LOC654482	hypothetical protein LOC654482	-0,688381074	1,629521887
Cyp4x1	cytochrome P450, family 4, subfamily x, polypeptide 1	0,53602598	1,493658921
Morn3	MORN repeat containing 3	-0,658534062	1,353206955
Rnf14	ring finger protein 14	0,235872685	1,329799834
Cxxc4	CXXC finger protein 4	0,397394643	1,462788219
Gria1	glutamate ionotropic receptor AMPA type subunit 1	0,361457782	1,319938534

Hps1	HPS1, biogenesis of lysosomal organelles complex 3 subunit 1	-0,40030006	1,487669535
Rfx2	regulatory factor X2	-0,564464217	1,763240386
AABR07030823.1	0	-0,692930998	1,548092038
Slc22a5	solute carrier family 22 member 5	-0,590068871	1,807165803
Basp1	brain abundant, membrane attached signal protein 1	0,552835398	1,897398857
Ablim1	actin-binding LIM protein 1	0,302649263	1,322154782
Ankrd66	ankyrin repeat domain 66	-0,946424093	1,85179005
Lrrc75b	leucine rich repeat containing 75B	-0,316907544	1,611415134
LOC100361018	rCG22048-like	-0,707850669	1,689751918
Abcc2	ATP binding cassette subfamily C member 2	0,666169667	1,508264693
Cecr6	cat eye syndrome chromosome region, candidate 6	0,698823403	1,827986613
Ak5	adenylate kinase 5	0,455365521	1,313170408
Cbx6	chromobox 6	0,209329829	1,509904365
Sult4a1	sulfotransferase family 4A, member 1	0,386481871	1,547073313
Unc93a	unc-93 homolog A (C. elegans)	-1,423947161	1,306562256
Lhb	luteinizing hormone beta polypeptide	-0,668998256	1,689751918
Lrrtm2	leucine rich repeat transmembrane neuronal 2	0,427149776	1,715296669
Fkbp1b	FK506 binding protein 1B	0,364232578	1,397778445
Zfp551	zinc finger protein 551	0,44481713	1,302673253
Pja1	praja ring finger ubiquitin ligase 1	0,294927269	1,395903174
Krt18	keratin 18	-0,659615679	1,343791177
Pot1b	protection of telomeres 1B	-0,717879026	1,766941492
Wasf1	WAS protein family, member 1	0,386523486	1,766941492
AABR07037520.1	0	0,301464856	1,629521887
Tubb4a	tubulin, beta 4A class IVa	0,374601647	1,877410501
Ccdc57	coiled-coil domain containing 57	-0,293123774	1,447302298
Nrxn3	neurexin 3	0,467044369	1,720313286
Pou3f1	POU class 3 homeobox 1	0,713851465	1,765740972
Plin5	perilipin 5	-0,68643038	1,897007127
LOC682102	hypothetical protein LOC682102	-0,843363464	1,797600427
Sstr1	somatostatin receptor 1	0,797377421	1,739895894
Rac3	ras-related C3 botulinum toxin substrate 3 (rho family, small GTP binding protein Rac3)	0,311469977	1,332927383
Nlrc5	NLR family, CARD domain containing 5	-0,657128462	1,707360265
Dnah5	dynein, axonemal, heavy chain 5	-0,792917564	1,778093331
Iqcc	IQ motif containing C	-0,495550224	1,394492809
Nek5	NIMA-related kinase 5	-0,884393874	1,829940766
LOC100909954	uncharacterized LOC100909954	0,50832145	1,347426487
Smap1	small ArfGAP 1	0,26656702	1,487617366
Rnf187	ring finger protein 187	0,241165692	1,765740972
Tcf7l2	transcription factor 7 like 2	-0,270318206	1,323732926
Nat8l	N-acetyltransferase 8-like	0,345797055	1,701776837
Gas7	growth arrest specific 7	0,395232958	1,836970288
Adamtsl4	ADAMTS-like 4	-0,435078709	1,486904074
Chrm3	cholinergic receptor, muscarinic 3	0,335235182	1,559369764
Slc35f3	solute carrier family 35, member F3	0,329303058	1,306673113

Atp9a	ATPase phospholipid transporting 9A (putative)	0,229685439	1,701776837
Adcy9	adenylate cyclase 9	0,399448312	1,610431022
Gstt1	glutathione S-transferase theta 1	-0,49387041	1,582961216
AABR07031533.1	0	0,420371097	1,680466346
Rnf157	ring finger protein 157	0,291997702	1,508264693
Hapln4	hyaluronan and proteoglycan link protein 4	0,394461977	1,310388589
Gprasp1	G protein-coupled receptor associated sorting protein 1	0,178372675	1,306680055
Efcab1	EF hand calcium binding domain 1	-0,657757449	1,400898193
Rfng	RFNG O-fucosylpeptide 3-beta-N-acetylglucosaminyltransferase	0,210564736	1,551114798
Pcdha4	protocadherin alpha 4	0,494256971	1,582081492
Dnah3	dynein, axonemal, heavy chain 3	-0,923225212	1,757270081
Gcnt1	glucosaminyl (N-acetyl) transferase 1, core 2	-0,724855095	1,450081636
Ttc16	tetratricopeptide repeat domain 16	-0,668698796	1,768202909
Pdlim4	PDZ and LIM domain 4	-0,257943659	1,596610422
Ache	acetylcholinesterase	0,381823906	1,759614516
C2	complement C2	-0,725510649	1,766941492
Rn50_X_0752.3	0	6,50479669	1,799599454
Cables2	Cdk5 and Abl enzyme substrate 2	0,302452656	1,325166077
LOC103689961	selenoprotein W-like	0,282838678	1,643653253
Ccdc113	coiled-coil domain containing 113	-0,728587267	1,738829265
Tep1	telomerase associated protein 1	-0,336431458	1,85179005
AABR07070161.1	0	-0,947969049	1,911720438
Camk2b	calcium/calmodulin-dependent protein kinase II beta	0,356599533	1,689751918
Ppp1r9b	protein phosphatase 1, regulatory subunit 9B	0,248039639	1,470686839
Nav3	neuron navigator 3	0,36910773	1,836970288
AABR07067728.1	0	-1,774452303	1,911720438
Tbc1d24	TBC1 domain family, member 24	0,285247171	1,456473696
Gm2a	GM2 ganglioside activator	-0,166387551	1,3028797
Celf6	CUGBP, Elav-like family member 6	0,487475074	1,699600456
Dact3	dishevelled-binding antagonist of beta-catenin 3	0,411408999	2,030793234
Cnot10	CCR4-NOT transcription complex, subunit 10	-0,19437204	1,450118572
Bend6	BEN domain containing 6	0,356006476	1,586559548
AABR07071395.1	0	0,408977611	1,509498727
Cdh4	cadherin 4	-0,269724102	1,531667664
Kcna6	potassium voltage-gated channel subfamily A member 6	0,411233341	1,582961216
Grb14	growth factor receptor bound protein 14	0,467744423	1,639298692
Chga	chromogranin A	0,519351227	1,681512209
Aff2	AF4/FMR2 family, member 2	0,338449707	1,605955585
Dnah2	dynein, axonemal, heavy chain 2	-0,962308859	1,830935884
Cacna1a	calcium voltage-gated channel subunit alpha1 A	0,265918702	1,529558923
Kdm6a	lysine demethylase 6A	0,54027841	2,218791514
Ccpg1os	cell cycle progression 1, opposite strand	-0,533623041	1,662784372
Ccdc173	coiled-coil domain containing 173	-0,688376397	1,408528447
Ccdc189	coiled-coil domain containing 189	-0,43299469	1,567947127
B4galnt4	beta-1,4-N-acetyl-galactosaminyl transferase 4	0,330131852	1,340086954

Scn1a	sodium voltage-gated channel alpha subunit 1	0,581944382	1,509498727
Faim2	Fas apoptotic inhibitory molecule 2	0,403273658	1,546518176
Chi3l1	chitinase 3 like 1	-0,327803651	1,711154338
Ank3	ankyrin 3	0,36183026	1,66886009
Ccpg1	cell cycle progression 1	-0,218809809	1,436519599
AABR07029417.1	0	0,792010348	1,559369764
Zfp192	zinc finger protein 192	-0,164315498	1,379143092
Kcng2	potassium voltage-gated channel modifier subfamily G member 2	0,431497505	1,45157359
AC096809.1	0	1,048767597	1,787100211
Tesk1	testis-specific kinase 1	0,218500145	1,479253691
Akain1	A-kinase anchor inhibitor 1	0,957993124	1,312708734
Rdh5	retinol dehydrogenase 5	-0,730006131	1,371968398
AABR07019086.1	0	0,781498116	1,316216563
Scamp5	secretory carrier membrane protein 5	0,246015646	1,479433266
Tbc1d8b	TBC1 domain family member 8B	0,256252605	1,350583688
Adap1	ArfGAP with dual PH domains 1	0,463344366	1,517054225
Pde1a	phosphodiesterase 1A	0,594475332	1,812783718
Cacnb3	calcium voltage-gated channel auxiliary subunit beta 3	0,317086599	1,895068937
Capsl	calcyphosine-like	-0,617506424	1,438240015
Wdpcp	WD repeat containing planar cell polarity effector	-0,393813666	1,397778445
Prkcg	protein kinase C, gamma	0,416704226	1,397020593
AABR07070161.2	0	-0,934581552	1,895068937
Pacsin1	protein kinase C and casein kinase substrate in neurons 1	0,330033738	1,757078164
Lmbrd2	LMBR1 domain containing 2	0,284189876	1,701776837
Renbp	renin binding protein	-0,276197399	1,440317196
Ppp3cb	protein phosphatase 3 catalytic subunit beta	0,3643334	1,622800884
AABR07041096.1	0	-0,644049528	1,47499596
AABR07005593.1	0	-0,995561548	1,701776837
Pih1d3	PIH1 domain containing 3	-0,829505501	1,384522877
LOC100909709	short transient receptor potential channel 1-like	0,341975951	1,488991519
Rhbdd1	rhomboid domain containing 1	-0,336175291	1,534362711
NEWGENE_2319083	epithelial cell transforming 2 like	-0,870306731	1,782458213
AABR07024641.1	0	-1,106985718	1,897007127
AABR07070161.3	0	-0,957074614	2,030793234
XIST_intron	XIST 3' intron conserved motif	6,906257419	1,999345788
AABR07053500.1	0	0,415797595	1,347291453
Sptbn4	spectrin, beta, non-erythrocytic 4	0,307121296	1,550330124
Hcn1	hyperpolarization-activated cyclic nucleotide-gated potassium channel 1	0,524050066	1,554522956
Eif4ebp2	eukaryotic translation initiation factor 4E binding protein 2	-0,239721219	1,522488479
Kcnc1	potassium voltage-gated channel subfamily C member 1	0,496117284	1,550887713
Trim46	tripartite motif-containing 46	0,362407749	1,550330124
Ywhah	tyrosine 3-monooxygenase/tryptophan 5-monooxygenase activation protein, eta	0,332631135	1,440229118
LOC102546862	uncharacterized LOC102546862	-1,006582454	1,332900126
Dkc1	dyskerin pseudouridine synthase 1	-0,230415708	1,355848542

Ak7	adenylate kinase 7	-0,880292751	1,711154338
Myb	MYB proto-oncogene, transcription factor	-0,679584171	1,490391966
AABR07030901.1	0	-0,835953802	1,684276272
Trnp1	TMF1-regulated nuclear protein 1	0,582634974	1,897007127
Erich2	glutamate-rich 2	-0,712200047	1,43350273
Purb	purine rich element binding protein B	0,264503652	1,465463985
0	0	0,487766728	1,699600456
Gls	glutaminase	0,324851302	1,336918689
Ttll13	tubulin tyrosine ligase-like family, member 13	-0,415985228	1,689751918
AC096600.1	0	0,593715401	1,548544391
Kcnab1	potassium voltage-gated channel subfamily A member regulatory beta subunit 1	0,734933613	1,799599454
Zbtb20	zinc finger and BTB domain containing 20	-0,182841489	1,306181746
Cfap221	cilia and flagella associated protein 221	-1,039658984	1,778093331
Abr	active BCR-related	0,218056435	1,494714574
Bicdl1	BICD family like cargo adaptor 1	0,442374365	1,684276272
Cfap65	cilia and flagella associated protein 65	-0,930378967	1,757270081
Spns2	spinster homolog 2	0,359021995	1,758676133
Slc12a3	solute carrier family 12 member 3	-0,656091814	1,34596196
Gnai1	G protein subunit alpha i1	0,307960769	1,558970741
Ddr1	discoidin domain receptor tyrosine kinase 1	-0,322505293	1,494714574
Ddx3	DEAD (Asp-Glu-Ala-Asp) box polypeptide 3	-9,326711233	5,464331373
AABR07067355.1	0	-0,36806725	1,462788219
Efna3	ephrin A3	0,36946294	1,305367244
Fam81a	family with sequence similarity 81, member A	0,27182355	1,454564213
Kdm5c	lysine demethylase 5C	0,361142632	1,911720438
Nup62cl	nucleoporin 62 C-terminal like	-0,928871179	1,450258457
Ccdc191	coiled-coil domain containing 191	-0,437220575	1,516532422
Epb41l1	erythrocyte membrane protein band 4.1-like 1	0,356494699	1,837926977
Cacng8	calcium voltage-gated channel auxiliary subunit gamma 8	0,366166419	1,827986613
Rsph1	radial spoke head 1 homolog	-0,774447374	1,608877008
Mns1	meiosis-specific nuclear structural 1	-0,646042686	1,618117208
Ppp2r2c	protein phosphatase 2, regulatory subunit B, gamma	0,417164202	1,830935884
Rfx8	RFX family member 8, lacking RFX DNA binding domain	-0,656648215	1,420775628
Asic2	acid sensing ion channel subunit 2	0,61236877	1,724814579
Cfap99	cilia and flagella associated protein 99	-0,93402678	1,897007127
Mapk8ip1	mitogen-activated protein kinase 8 interacting protein 1	0,19608196	1,521251022
AABR07024542.1	0	0,54124928	1,911720438
Nek9	NIMA-related kinase 9	-0,194790219	1,534209154
Sptbn2	spectrin, beta, non-erythrocytic 2	0,359664671	1,513928579
Myo5a	myosin VA	0,332097481	1,557319
Mroh7	maestro heat-like repeat family member 7	-0,664063303	1,469681504
Camkv	CaM kinase-like vesicle-associated	0,470155556	1,470686839
Socs7	suppressor of cytokine signaling 7	0,221858193	1,378267069
Ccdc40	coiled-coil domain containing 40	-0,842094074	1,724814579
Ttc30b	tetratricopeptide repeat domain 30B	-0,392493803	1,724814579

B4galt1	beta-1,4-galactosyltransferase 1	-0,533023539	1,330554719
AABR07005596.1	0	-0,957438317	1,844039254
LOC100910792	amphiphysin-like	0,27766784	1,534362711
Bbox1	gamma-butyrobetaine hydroxylase 1	-0,703069334	1,479253691
Cetn2	centrin 2	-0,333353204	1,348247787
AABR07012274.1	0	1,169547653	1,509498727
Tex9	testis expressed 9	-0,324378563	1,54008332
Cc2d2a	coiled-coil and C2 domain containing 2A	-0,283254567	1,516175038
Syp	Synaptophysin	0,360882739	1,699600456
AABR07041411.1	0	0,857915441	1,596610422
Unc5a	unc-5 netrin receptor A	0,392784458	1,877410501
Dnah12	dynein, axonemal, heavy chain 12	-0,979953426	1,780790003
Bst2	bone marrow stromal cell antigen 2	-0,816330467	1,651387588
AABR07070161.4	0	-1,015879293	1,911720438
Pi4ka	phosphatidylinositol 4-kinase alpha	0,183489907	1,438240015
Eif2s3y	eukaryotic translation initiation factor 2, subunit 3, structural gene Y-linked	-9,738722323	5,768214065
Sowaha	sosondowah ankyrin repeat domain family member A	0,568281811	1,508264693
Adra1b	adrenoceptor alpha 1B	0,595763326	1,306598632
Prr29	proline rich 29	-1,006897771	1,527197678
AABR07070161.5	0	-1,040808559	1,877410501
Pcdh1	protocadherin 1	0,234669426	1,640735353
Rn60_Y_0001.2	0	-6,692852154	3,191596621
Kdm5d	lysine demethylase 5D	-8,909758021	5,768214065
Gabrb3	gamma-aminobutyric acid type A receptor beta 3 subunit	0,352764326	1,573124398
Rn60_Y_0010.2	0	-8,310057461	5,768214065
AABR07070161.6	0	-1,14732155	1,895068937
Slc24a3	solute carrier family 24 member 3	0,315294279	1,54227317
Eif2s3	eukaryotic translation initiation factor 2 subunit gamma	0,729976725	3,160674616
Ccm2	CCM2 scaffolding protein	0,166154736	1,306181746
AABR07017145.1	0	0,464284884	1,565157506
Qars	glutaminyl-tRNA synthetase	-0,208413971	1,531543609
Dnah7	dynein, axonemal, heavy chain 7	-0,94106209	1,649805466
Hrh3	histamine receptor H3	1,080481645	1,782458213
L1cam	L1 cell adhesion molecule	0,456939118	1,54008332
Selenom	selenoprotein M	0,342341133	1,598325794
AABR07011996.1	0	-0,368352307	1,757270081
Atp2b3	ATPase plasma membrane Ca2+ transporting 3	0,412475295	1,750594197
Rph3al	rabphilin 3A-like (without C2 domains)	-0,659543165	1,720313286
Reps2	RALBP1 associated Eps domain containing protein 2	0,483762152	1,343156702
AC128059.3	0	-1,066920087	1,897007127
Cttnbp2	cortactin binding protein 2	0,283220769	1,836970288
Aqp9	aquaporin 9	-0,630912728	1,462788219
Myo1e	myosin IE	-0,24695578	1,374433791

Supplementary Table 2. iBAQ suggests differentially abundant proteins between the two sexes. The differentially abundant proteins are listed together with –log(adjusted p-value) and difference folds (log(male/female)). The statistical test was performed by the limma package (Ritchie et al., 2015) on the R Studio.

Protein Id	Protein Name	-log(P-value)	Difference folds
REEP5	Receptor expression-enhancing protein 5	4,90	-0,82
UBE2S	Ubiquitin-conjugating enzyme E2 S	3,48	-1,39
ITPA	Inosine triphosphate pyrophosphatase	2,45	0,59
DDAH1	N(G),N(G)-dimethylarginine dimethylaminohydrolase 1	3,02	-0,49
MSMO1	Methylsterol monooxygenase 1	2,18	0,87
PUR9	Bifunctional purine biosynthesis protein PURH	4,24	0,37
TRXR1	Thioredoxin reductase 1, cytoplasmic	2,92	-0,63
Q6P6G9	Heterogeneous nuclear ribonucleoprotein A1	4,39	-0,69
PTMA	Prothymosin alpha	4,30	-1,34
A0A0G2JYW3	Clathrin light chain A	3,61	-0,53
B4F773	Protein tweety homolog	2,71	0,64
HS71B	Heat shock 70 kDa protein 1B	2,99	0,46
Q8SEZ0	NADH-ubiquinone oxidoreductase chain 5	2,98	0,84
G3V6I9	60S ribosomal protein L26	2,33	-0,67
IBP2	Insulin-like growth factor-binding protein 2	3,71	-0,80
CAH3	Carbonic anhydrase 3	5,03	0,72
ACADL	Long-chain specific acyl-CoA dehydrogenase, mitochondrial	2,56	-0,62
PIPNA	Phosphatidylinositol transfer protein alpha isoform	3,35	-0,85
PSA2	Proteasome subunit alpha type-2	5,99	-0,73
NB5R3	NADH-cytochrome b5 reductase 3	2,69	-0,52
ATP5E	ATP synthase subunit epsilon, mitochondrial	2,80	-0,56
EAA2	Excitatory amino acid transporter 2	2,57	-0,67
A0A0G2K890	Ezrin	2,35	-0,74
PPAC	Low molecular weight phosphotyrosine protein phosphatase	3,25	0,48
USO1	General vesicular transport factor p115	3,42	0,46
VATF	V-type proton ATPase subunit F	3,30	0,41
IPP2	Protein phosphatase inhibitor 2	2,87	-0,57
AL1A1	Retinal dehydrogenase 1	2,78	-0,86
UK114	Ribonuclease UK114	2,99	-0,74
PP1A	Serine/threonine-protein phosphatase PP1-alpha catalytic subunit	2,77	-0,69
PRS8	26S protease regulatory subunit 8	2,84	-0,56
TMOD2	Tropomodulin-2	3,31	0,46
FIS1	Mitochondrial fission 1 protein	3,11	-0,72
6PGL	6-phosphogluconolactonase	3,40	0,44
A0A140TAB4	Core histone macro-H2A	2,10	1,29
ATIF1	ATPase inhibitor, mitochondrial	2,87	-1,42
VAT1	Synaptic vesicle membrane protein VAT-1 homolog	4,11	0,45
SARNP	SAP domain-containing ribonucleoprotein	4,27	0,46
KCY	UMP-CMP kinase	6,35	-0,49
LZTL1	Leucine zipper transcription factor-like protein 1	1,91	0,86

PIR	Pirin	2,51	0,75
CAPR1	Caprin-1	3,94	0,39
ITM2C	Integral membrane protein 2C	3,35	0,62
NCALD	Neurocalcin-delta	2,68	1,41
SIR2	NAD-dependent protein deacetylase sirtuin-2	2,58	0,59
SV2B	Synaptic vesicle glycoprotein 2B	3,59	0,76
Q6P136	Hyou1 protein	3,23	-0,49
A0A0G2K6H7	Uncharacterized protein	3,21	-0,62
COPD	Coatomer subunit delta	2,87	-0,50
GALM	Aldose 1-epimerase	2,61	1,11
CYBP	Calcyclin-binding protein	3,88	-1,16
ABHEB	Protein ABHD14B	2,83	0,65
DDAH2	N(G),N(G)-dimethylarginine dimethylaminohydrolase 2	2,90	-0,48
CLIC1	Chloride intracellular channel protein 1	4,10	0,75
AP4A	Bis(5-nucleosyl)-tetraphosphatase [asymmetrical]	2,60	-0,53
SFXN5	Sideroflexin-5	2,78	0,60
PHOCN	MOB-like protein phocein	1,91	0,80
09. Sep	Septin-9	4,09	-0,73
A0A0G2JT93	Catenin (Cadherin associated protein), beta 1, isoform CRA	4,15	-0,42
KAD4	Adenylate kinase 4, mitochondrial	2,15	0,70
F1LP21	Protein Timm8a1	2,77	0,50
PRDX4	Peroxiredoxin-4	2,13	0,73
A0A096MJG7	Protein Nebl (Fragment)	5,28	-0,92
A0A0G2JTG7	Heterogeneous nuclear ribonucleoprotein H	4,30	0,88
A0A0G2JWS2	Protein Nebl	2,91	-0,59
Q6PW38	Neuronal cell adhesion molecule	1,97	-0,85
A0A0U1RRV7	Protein Srsf3	2,63	0,78
B2RZD6	Ndufa4 protein	3,12	-0,59
B4F7A3	Galectin	2,26	0,73
D3ZD11	Protein Spcs2	3,38	-0,63
D3ZDH8	Platelet glycoprotein Ib beta chain	2,46	-0,70
D3ZY02	Protein Athl1	5,38	-1,15
D3ZZP2	Protein Rab39a	2,29	0,67
D4A8U7	Dynactin 1, isoform CRA	3,36	-0,86
D4AD05	Protein Crocc	2,86	1,18
F1LPV8	Succinyl-CoA ligase subunit beta	2,43	0,65
G3V8G2	Proteasome (Prosome, macropain) 26S subunit, non-ATPase, 5 (Predicted), isoform CRA	2,59	-0,56
G3V9T7	ATPase Asna1	5,30	0,38
M0R7G4	MICOS complex subunit	4,88	0,77
Q3KRE2	Methyltransferase like 7A	1,89	0,95
Q4G079	Protein Aimp1	3,15	-0,49
Q5RK17	Diablo homolog (Drosophila)	3,92	-0,81
Q6AY58	B-cell receptor-associated protein 31	2,32	-0,92
Q6MGB8	Protein RT1-A2	1,85	1,15
Q6PDV8	Protein LOC100360057	3,30	0,81

4| The mRNA-binding protein RBM3 regulates the activity rhythms and local synaptic translation in cultured hippocampal neurons

Sinem M. Sertel[1], Malena S. von Elling-Tammen[1], Silvio O. Rizzoli[1,2*]

Author contribution of Sinem Meleknur Sertel:

- Design (together with Silvio O. Rizzoli), performance and analysis (together with Silvio O. Rizzoli) of experiments shown in the following figures: Figure 1a-d, Figure 2a-f (together with Malena S. von Elling-Tammen), Figure 2g-i, Figure 3a-b, Figure 4a-c (together with the Transcriptome Analysis Laboratory (TAL)), Figure 4d-e (together with Malena S. von Elling-Tammen), Figure 5a-d, Figure 6a-d (together with Malena S. von Elling-Tammen), Figure 6e-f (together with Janina Pasch), Figure 7a-b, Figure 7c-e (together with Janina Pasch), Supplementary Figure 1a-b, Supplementary Figure 2a-b, Supplementary Figure 3a-c (together with Malena S. von Elling-Tammen), Supplementary Figure 3d, Supplementary Figure 4a-e, Supplementary Figure 5a-c, Supplementary Figure 6a-d (together with Malena S. von Elling-Tammen), Supplementary Figure 7a-b, Supplementary Figure 8a-f (together with Janina Pasch), Supplementary Figure 9a,f,g, Supplementary Figure 9b-e (together with Malena S. von Elling-Tammen), Supplementary Figure 9h-j (together with Janina Pasch).
- Preparation of the manuscript together with Silvio O. Rizzoli.

This article has been submitted to the Cell Reports on 10/03/2020.

The mRNA-binding protein RBM3 regulates activity rhythms and local synaptic translation in cultured hippocampal neurons

Sinem M. Sertel[1], Malena S. von Elling-Tammen[1], Silvio O. Rizzoli[1,2*]

[1]Institute for Neuro- and Sensory Physiology, University Medical Center Göttingen, Göttingen, Germany
[2]Lead Contact
*Correspondence: srizzol@gwdg.de (S.O.R.)

4.1| Abstract

The activity and the metabolism of the brain change rhythmically during the day. Such rhythmicity is also observed in cultured neurons from the suprachiasmatic nucleus, which is a critical center in rhythm maintenance. However, this issue has not been extensively studied in cultures from areas less involved in timekeeping, as the hippocampus. We found that cultured hippocampal neurons exhibit rhythmic changes in global activity, in synaptic vesicle dynamics, in synapse size, and in synaptic mRNA amounts. A transcriptome analysis of the neurons, performed at different times of day, revealed significant changes only for RNA-binding motif 3 (RBM3). RBM3 amounts changed throughout the day, especially in synapses. RBM3 knock-down altered synaptic vesicle dynamics and changed the neuronal activity rhythms. This procedure also altered local translation in synapses, albeit it left the global cellular translation unaffected. We conclude that hippocampal cultured neurons can exhibit endogenous rhythmicity, in an RBM3-dependent fashion.

4.2| Introduction

Maintaining a synchronous pattern of day and night activity is critical for the function of all of the tissues of a mammalian organism. This is ensured by several well-established mechanisms, the first of which is the daily rhythmic expression of molecular clock genes in every cell (Partch et al., 2014). These genes control the timing of many biological functions, such as glucose metabolism and electrical activity (Dibner et al., 2010). A second fundamental mechanism is provided by the function of the suprachiasmatic nucleus (SCN), a central pacemaker of the hypothalamus, which is in charge of the molecular clock synchronization among the cells of the animal (Welsh et al., 2010). The SCN achieves this goal by encoding time information in its spontaneous firing rate (which is low during the night, and high during the day (Colwell, 2011)), and by communicating this to other brain regions and tissues through synaptic projections, and hormones (Buijs et al., 2006).

The rhythmic expression of clock genes in the SCN controls the expression and function of ion channels as the BK channels (large-conductance calcium-activated potassium channels) or L-type voltage-gated calcium channels (Colwell, 2011). The function of these proteins induces oscillations in the resting membrane potential (Kononenko et al., 2008; Pennartz et al., 2002), thereby changing the firing rates. This ensures that the rhythmic firing activity of the SCN, which has been demonstrated in freely moving animals, in acute slices, and even in dispersed cultures (Green and Gillette, 1982; Herzog et al., 1998). The rhythmic firing is resistant to disturbances in the light-dark cycle (Kuhlman and McMahon, 2004; Nakamura et al., 2011), and it persists in SCN cultures that are not subjected to daily light or temperature changes. However, clock gene expression alone is not sufficient to maintain the synchronized firing of SCN neurons in the long term. In culture, they slowly become desynchronized, with every cell eventually assuming its own individual firing pattern that oscillates throughout the day (Welsh et al., 1995). The desynchronization is accelerated by blocking network activity, suggesting that neuronal communication is important in maintaining the rhythm synchronicity for long time intervals (Honma et al., 2000; Yamaguchi et al., 2003).

The observation of rhythmic activity in dispersed SCN cultures prompted research also in other cell types. Fibroblast cell lines were found to exhibit molecular clock rhythmicity, albeit they lose cell synchronicity rapidly (Nagoshi et al., 2004), unless they are re-synchronized by regular changes in temperature (Brown et al., 2002) or culture media (Balsalobre et al., 1998). However, many brain areas have been little investigated in relation to rhythmic activity (Paul et al., 2019). A prominent example is the hippocampus, which is involved in learning and memory, two processes that are strongly regulated by the circadian clock (Gerstner and Yin, 2010). Hippocampal activity *in vivo* oscillates throughout the day (Munn and Bilkey, 2012), and its ability to respond to plasticity-inducing stimuli is also dependent on the time of day (Harris and Teyler, 1983). These findings demonstrate that the hippocampus function is governed by the daily cycle, but leave open the question of whether this is exclusively due to the general rhythmicity induced by the SCN, or whether this is a fundamental hallmark of the hippocampal neuron, which would persist in dissociated cultures.

To solve this question, we turned to the rat hippocampal culture, which is a commonly-used model for neuronal and synaptic research. In principle, mature dissociated cultures should exhibit a relatively constant electrical activity throughout the day, as the molecular clocks of the different neurons should mostly be desynchronized. Surprisingly, we found that the culture activity exhibited significant oscillations throughout the day, which were accompanied by substantial changes in presynaptic activity and the synapse size. To find potential molecules involved in these processes, we analyzed the culture transcriptome at different times of day. Only one transcript showed robust significant changes, RNA-binding motif 3 (RBM3). This is

an RNA-binding protein whose expression was found to be induced by cold shock (Danno et al., 1997, 2000), and which is known to promote translation (Dresios et al., 2005), to protect synapses from hypothermia, and to control the alternative polyadenylation of core clock genes (Liu et al., 2013). In our experiments, RBM3 exhibited strong abundance changes according to the time of day, especially in synapses. Its knock-down changed the activity pattern of the neurons, as well as synapse activity and size. These effects may be related to local translation at synaptic sites, since this was significantly affected by the RBM3 knock-down, without changing the general cellular translation levels. Overall, these data suggest that hippocampal cultures exhibit endogenous activity rhythms, and that these rhythms are under the control of RBM3, possibly through local translational mechanisms.

4.3| Methods

Hippocampal cultures. Primary disassociated hippocampal cultures were prepared from newborn rats (Banker and Cowan, 1977). The hippocampi were dissected from rat brain. They were washed with Hank's balanced salt solution (HBSS, Thermo Fisher, US). Later on, hippocampi were kept in the enzyme solution (1.6 mM cysteine, 100 mM $CaCl_2$, 50 mM EDTA, and 25 units papain in 10 ml Dulbecco's modified eagle medium (DMEM)) for 1 hour. To inactivate the enzyme solution, 5 ml DMEM (Thermo Fisher, US) that contains 10% fetal calf serum, 0.5% albumin, and 0.5% trypsin inhibitor was added and incubated for 15 min. Cells were further separated by mechanical disruption and were seeded on poly-L-lysine (Sigma-Aldrich, Germany) coated circular coverslips (1.8 cm in diameter) with a density of 80,000 cells per coverslip. The neurons were kept in plating medium (3.3 mM glucose, 2 mM glutamine, and 10% horse serum in DMEM) for 1-2 hours at 37°C. Afterwards the medium was exchanged to Neurobasal-A medium (with B27 supplement, 1% GlutaMax, and 0.2% penicillin/streptomycin mixture). The cultures were maintained at 37°C and 5% CO_2 for ~20 days.

Calcium imaging. Neurons were transduced with 3 µl of NeuroBurst Orange Lentivirus (Sartorius, Germany) at day *in vitro* (DIV) 10, and kept in the incubator for 9 additional days. For imaging, the coverslips were placed into imaging chamber and imaged with and inverted Nikon Ti eclipse epifluorescence microscope (Nikon, Japan) that is equipped with a 20X Plan Apo (Nikon, Japan) objective, an HBO-100W lamp, an IXON X3897 Andor camera (Andor, UK) and a cage-incubator (Okolab, Italy). The temperature was set at 37°C and the atmosphere with 5% CO_2 throughout the imaging session. For long-term recordings, neurons were plated in a glass-bottom 24-well plate (Celvis, US) and imaged directly from the plate.

Promoter reporter imaging. The plasmid for the promoter reporter imaging was synthesized by Genscript (US), using pUC57 as a backbone. The promoter was selected as the sequence from 500 nucleotides in the upstream till 50 nucleotides in the downstream of the BMAL1 gene from *Rattus novergicus*. The plasmid expressed EGFP under the control of this promoter. The EGFP was destabilized by adding to its C terminus the residues 422-461 of mouse ornithine decarboxylase, which provides a 2-hour half-life time for the molecule (Li et al., 1998). Neurons were transfected with Lipofectamine 2000 (Thermo Fisher) at DIV5, according to the manufacturer's instructions.

Immunostaining. Neurons were washed with the tyrode buffer (124 mM NaCl, 5mM KCl, 2 mM $CaCl_2$, 1 mM $MgCl_2$, 30 mM D-glucose, and 25 mM HEPES) and then fixed with 4% PFA (Sigma-Aldrich, Germany) for 30 min at room temperature. Later on, cells were incubated in the quenching solution (100 mM NH_4Cl in phosphate buffer solution (PBS)) for 30 min at room temperature. Subsequently, neurons were washed with permeabilization solution (3% bovine serum albumin (BSA), 0.01% Triton-X-100 in PBS) three times for 5 min on a shaker. Permeabilized neurons were incubated for 1 hour, with 0.2% of the primary antibody in the permeabilization solution. Then, they were washed again with permeabilization solution three times for 5 min on a shaker. Neurons were incubated for 1 hour with 0.5% of the secondary antibody in permeabilization solution. Later on, they were washed with high salt PBS (supplemented with 0.38 M NaCl) solution three times for 5 min on a shaker and two times for 5 min with PBS. Lastly, coverslips were mounted in 8 µl Mowiol (Merck Millipore, Germany) and stored at 4°C. Unless otherwise specified, imaging was performed with IX83 inverted Olympus (Japan) confocal microscope (Abberior, Germany) that is equipped with a 100X super-apochromat and coverslip corrected oil objective (Olympus, Japan). The analysis was performed on Matlab (MathWorks, US) and plotted with Graphpad (US). The Syph (101004) and Homer1 (160011) antibodies were purchased from Synaptic Systems (Germany), and the RBM3 antibody (ab134946) was purchased from Abcam (UK).

Synaptotagmin1 Uptake assay. In order to study the synaptic vesicle usage, we took advantage of live staining with an antibody targeting the luminal domain of Synaptotagmin1. At DIV21 coverslips with neurons were placed in a new 12-well plate (Greiner Bio-One, Austria) with 300 µl of their own Neurobasal-A medium. Neurons were incubated with 2.5 µg/ml Syt1-Atto647N antibody (105311AT1, Synaptic Systems, Germany) for 45 min. Afterward, 16.7 nM anti-mouse secondary nanobody (N2002-At542-S, Nanotag, Germany) conjugated to Atto542 was added into the medium and incubated for15 min. Next, the neurons were washed with ice-cold tyrode buffer and fixed with 4% PFA. The immunostaining procedure for Synaptophysin is described in the immunostaining section. In order to see the spontaneous synaptic vesicle fusion, the action potential generation was blocked by adding 5 µM tetrodotoxin (TTX, Tocris

Bioscience, UK). In time-series experiments, the uptake assay was performed at different time points of the day. For the knocked down conditions, the uptake assay did not have secondary nanobody incubation. Instead, Syt1-Atto647N antibody was incubated for either 15 min or 1 hour. An inverted Nikon Ti eclipse epifluorescence microscope (Nikon, Japan) that has a 20X Plan Apo (Nikon, Japan) objective, an HBO-100W lamp, an IXON X3897 Andor camera (Andor, UK) was used for imaging, and the images were analyzed using Matlab (MathWorks, US).

Puromycin assay. Puromycin (ant-pr-1, InvivoGen, US) is an antibiotic that interferes with mammalian translation and incorporates itself into the polypeptide chain. Coverslips were placed in a new 12-well plate with 300 µl of their own Neurobasal-A medium and were incubated with 1 µl of 0.3 mg/ml puromycin for 10 min in the incubator. Later on, they were washed twice with ice-cold tyrode buffer and fixed with 4% PFA. As a control, another antibiotic called anisomycin was used. It halts the translation complex and does not allow puromycin to reach the binding site in the ribosome. Control groups were incubated with 0.13 µM anisomycin (A5862, Sigma-Aldrich, Germany) 10 min prior to puromycin treatment. Later, the immunostainings against Synaptophysin, Homer1, and puromycin (MABE343, Merck Millipore, Germany) were performed as described in the immunostaining section. Puromycin, anisomycin, and puromycin antibody were generous gifts from Prof. Peter Rehling, University Medical Center Göttingen, Germany.

Poly(A) staining. Oligo(dT) and oligo(dA) stainings were done as described before(Chou et al., 2018). Briefly, neurons were fixed and quenched, as stated in the immunostaining section. They were fixed one more time with ice-cold absolute Methanol for 10 min. Cells were rehydrated first with 70% EtOH and then with 1 M Tris buffer (pH 8) for 10 min. Later on, neurons were washed with hybridization buffer (1mg/ml yeast tRNA, 0.005% BSA, 10% Dextran sulfate, 25% formamide in finalized 2X SSC (0.3 M NaCl, 30 mM trisodium citrate in water)) once and then incubated with 1:1000 of 1 µg/µl 30 nucleotide long either oligo(dT) or oligo(dA) conjugated to Atto647N (Sigma-Aldrich, Germany) for 1 hour in hybridization buffer at 37ºC. Samples were washed two times with 4X SSC and two times 2X SSC. The following immunostainings against Synaptophysin and Homer1 were performed as specified in the immunostaining section.

Transcriptomics. The mRNAseq experiments as well as the analysis were performed by Transcriptome and Genome Analysis Laboratory (TAL, Göttingen, Germany). Samples were sequenced with HiSeq-4000 (Illumina, US) with 50 bp single-end design. The alignment was performed with STAR 2.5.2a (Dobin et al., 2013), and the assignment of reads to genes was done by using featureCounts 1.5.0 (Liao et al., 2019) with *rattus norvegicus* genome assembly rn6 and gene version 91. After the count calculation of each transcript, we used the limma

package to find differentially expressed transcripts (Ritchie et al., 2015). GO analysis was performed on the Webgestalt database with Ensembl gene IDs and difference folds between time points (Wang et al., 2017). The result of gene set enrichment analysis reports the pathways with p-value <0.05 and false-discovery rate (FDR)<0.05 (**Table S1**).

shRNA virus preparation. The sequence for short-hairpin RNA (shRNA) was prepared with the help of the BLOCK-iT RNAi Designer database (Thermo Fisher, US). The shRNA sequence was synthesized by Genscript (US) and placed in the pAAV-U6sgRNA (60958, Addgene)(Swiech et al., 2015). The plasmid of scrambled (Scr) shRNA was a generous gift of the Fornasiero lab(Keihani et al., 2019). Adeno-associated virus (AAV) was produced in human embryonic kidney (HEK) 293T (DSMZ, Germany) with 3 plasmids that have packaging proteins of recombinant (AAV), and are described before(McClure et al., 2011). HEK cells were transfected with Lipofectamine-2000 (Thermo Fisher, US) using the manufecturer's instructions. Three days later, transfected cells were harvested and centrifuged. The pellet was resuspended in 1 ml tyrode buffer and was exposed to freeze/thaw cycles three times in 70 % EtOH and dry ice mixture for lysis. After the addition of 1 µl of Nuclease (Thermo Fisher, US), the lysate was incubated at 37ºC for 30 min and was centrifuged with 1000xg for 5 min. The supernatant was aliquoted and stored at the -80ºC freezer. The virus titration was performed by observing the GFP signal from serial dilution on transfected hippocampal cultures. The virus was used on the primary hippocampal culture at DIV15. RBM3 shRNA sequence: CACCGCGTCTTCCCGCGCCGCAGTCCGAAGACTGCGGCGCGGGAAGACGCTTTTTTTT. BMAL1 shRNA sequence: CACCGCAAACTACAAGCCAACATTTCGAAAAATGTTGGCTTGTAGTTTGCTTTTTTTT

4.4| Results

Neuronal activity changes throughout the day in dissociated hippocampal cultures

Primary hippocampal cultures are widely used, as they are relatively simple to prepare and maintain most of the important functional features of the *in vivo* neurons (Dotti et al., 1988). We employed them here, relying on a classical protocol (Banker and Cowan, 1977) that dissociates the hippocampi of newborn rats, and results in mixed glia and neuron cultures. Most of the neurons are glutamatergic (more than 90%) (Benson et al., 1994) and have a mature morphology and synapse development already at ~12 days *in vitro* (DIV).

To determine whether primary hippocampal cultures show rhythmicity in their electrical activity, we performed long-term calcium imaging, using a genetically-encoded calcium indicator, NeuroBurst (Sartorius, Germany). To sample culture activity regularly, we imaged the neurons (starting at DIV18) every 4 hours, for 45 seconds (**Figure 1A**). This enabled us to obtain a fluorescence-based measure of the activity of the individual neurons at the particular time

points (**Figure 1B**), which we termed “activity score”. Individual neurons exhibited changes in the activity score throughout the day, with the examples shown in **Figure 1B** having strong peaks at 6:00 and 14:00. Such changes in activity were observed for all neurons investigated (see a selection in **Figure 1C**).

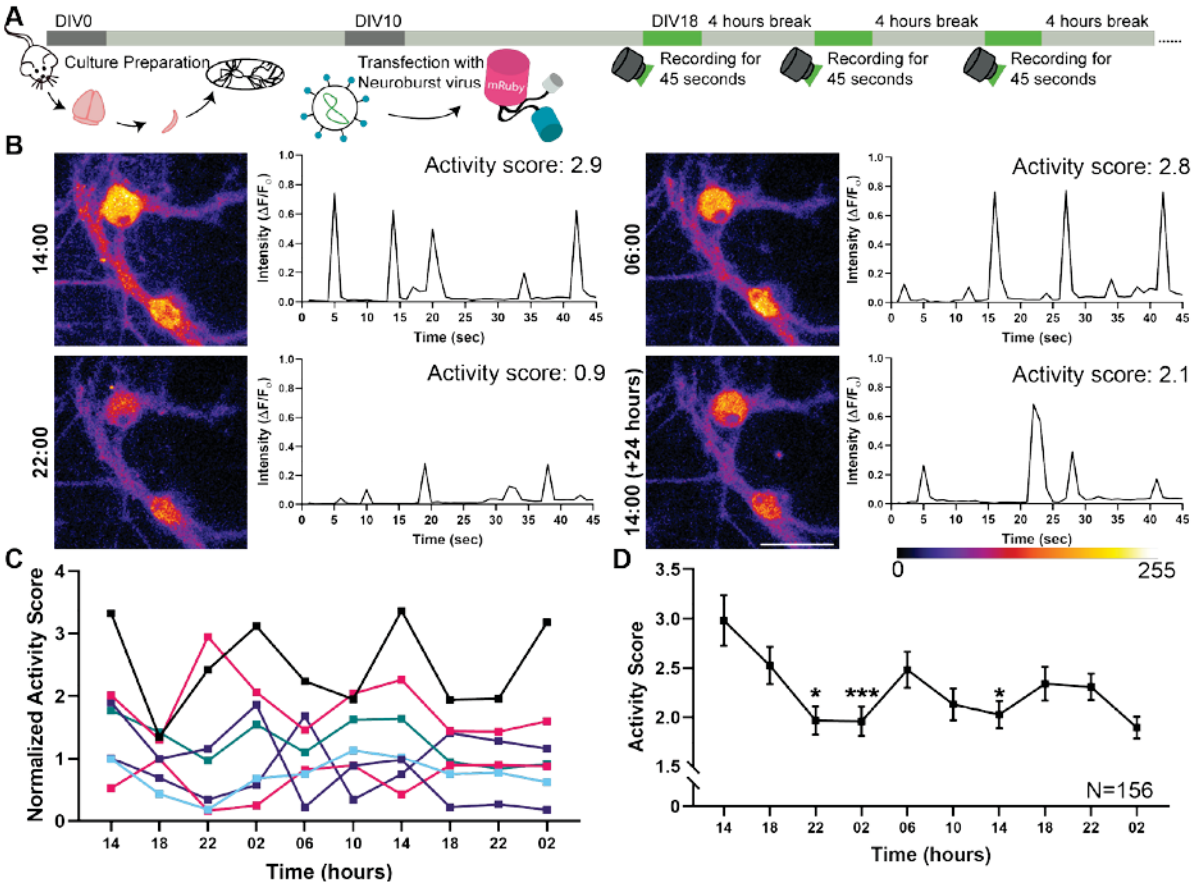

Figure 1. The average neuronal activity in dissociated hippocampal cultures oscillates during the day. (A) To determine the firing pattern of dissociated hippocampal neurons, we transfected cultured hippocampal neurons with the genetically-encoded Ca^{2+} indicator Neuroburst at DIV10. Starting at DIV18, we imaged neurons every 4 hours, relying on a continuous 45-second recording protocol. This provided a sample of activity at the particular time points, while being sufficiently mild to avoid phototoxicity. **(B)** To visualize the overall activity at every time point, we generated summed frames that illustrate the total activity along the 45-second-long videos. The activity in all movie frames, measured in the neuronal cell bodies, is shown in the graphs, in the form of fluorescence normalized to the baseline ($\Delta F/F_0$). To obtain a single numeric value that represents the activity along the whole movie, we calculated the area under the curve from these graphs, which we termed “activity score”. **(C)** Seven independent neurons are shown as examples. To enable a simple visual comparison of the traces, they were all normalized to their median activity score. **(D)** To reveal the average firing pattern of the hippocampal cultures, we analyzed 156 neurons, from 4 independent experiments (with 2-4 different wells measured per experiment). The graph indicates their average activity score (± SEM). The statistical significance of changes throughout the experiment was measured by the Friedman test, followed by Dunn’s multiple comparison test. The first time-point was the reference for the multiple comparison. *p<0.05, ***p<0.001. Scale bar: 50 μm.

To test whether the activity of the different neurons was synchronized, we performed this experiment with four different culture preparations, in which we tracked 156 different neurons. Their average activity score showed significant changes throughout the measurement (Figure 1D), with activity being high at 14:00, dropping until ~22:00, and rising again after 02:00, before dropping again for several hours, and finally rising one more time before the end of our measurements. Randomizing the timing of the individual neuronal measurements eliminates all significant changes (Figure S1), which suggests that the results obtained here are unlikely to be due to chance, but are rather due to synchronous culture activity. The rhythm observed does not conform to a precise 24-hour pattern (Figure 1D). Two possible interpretations could be made. First, the cultures exhibit their own pattern of activity, which does not relate to a 24-hour rhythm. Second, the activity of the individual neurons does conform to a 24-hour rhythm, but they are partially desynchronized, so that a 24-hour rhythm is no longer observed at the whole culture level, especially when averaging results across different cultures, as in Figure 1D. The second interpretation appeared probable, since 24-hour patterns are difficult to maintain with precision even in SCN cultures (Honma et al., 1998). To test this in more detail, we analyzed whether the activity patterns of individual neurons correlated significantly to the 24-hour pattern of a bona fide molecular clock gene. We expressed in our cultures a destabilized GFP molecule, relying on the promoter of the clock gene BMAL1. The fluctuations in the GFP amounts, which report the BMAL1 promoter activity, conformed to a 24-hour cycle, with peaks at night, and lower values during the day (Figure S2). In parallel, we analyzed the activity patterns of the GFP-expressing neurons (Figure S2). We found that their activity rhythms correlated significantly (albeit negatively) to the BMAL1 promoter activity. This implies that the activity of individual neurons in these cultures can be seen as exhibiting a daily (24-hour) rhythm, albeit this is difficult to observe when averaging many neurons and independent cultures, due to a partial desynchronization.

The dynamics of the synaptic vesicles also change throughout the day

Oscillations in neuronal activity should also be reflected at the synaptic level, especially in the synaptic vesicle dynamics. The vesicle behavior can be analyzed with precision by employing antibodies that detect the luminal (intravesicular) domain of the vesicular calcium sensor synaptotagmin 1 (Syt1) (Kraszewski et al., 1995; Matteoli et al., 1992). The antibodies are taken up by synaptic vesicles during their recycling, since they expose the luminal epitopes during exocytosis, and thus enable the antibody to penetrate into the vesicles, and to be endocytosed (**Figure 2A**). We incubated the cultures every six hours with fluorescently-conjugated Syt1 antibodies, for 45 minutes. This time interval is sufficient to label (saturate) all active synaptic vesicles, and therefore to provide a measure of the active vesicle pool size

(Truckenbrodt et al., 2018). We then applied to the cultures fluorescently-conjugated nanobodies that recognize the Syt1 antibodies, for 15 minutes. The nanobodies bind Syt1 antibodies that are exposed to the surface during vesicle activity (**Figure 2A**). This short incubation interval does not saturate all binding sites (Truckenbrodt et al., 2018), and therefore provides a measure of synaptic activity at the respective time point, rather than a measure of the vesicle pool size. To confirm the validity of this assay, we compared normal neurons with neurons in which network activity was blocked using the Na^+ channel inhibitor tetrodotoxin (TTX). TTX blocked active vesicle recycling, and therefore reduced both the antibody and nanobody stainings (**Figure 2B, C, E**), as expected.

These measurements suggested that the size of the actively-recycling vesicle pool is relatively constant throughout the day (**Figure 2D**), but that synaptic activity, as measured by the nanobody intensity, exhibits significant differences (**Figure 2F**). None of these measurements showed any changes in cultures maintained constantly in TTX, as expected (**Figure S3**).

Overall, these experiments confirm, at the synapse level, the idea that neurons show changes in their activity patterns throughout the day. As these measurements only targeted the active vesicles, which make up only ~50% of all vesicles (Rizzoli and Betz, 2005), we sought to also obtain a measurement of the entire vesicle pool, by immunostaining the synapses at different time points, relying on the vesicle marker Synaptophysin (Takamori et al., 2006a). This again showed changes during the day, with a substantial increase at 02:00 (**Figure 2G, H**). We observed similar behavior for a marker of the postsynaptic density, Homer1 (**Figure 2I**). No changes could be detected in the number of synapses (**Figure S3D**). These results suggest that not only neuronal and synapse activity, but also synapse size depends on the time of day.

Synaptic mRNA amounts are subject to change during the day

Along with brain activity, brain metabolism also changes throughout the day, including aspects as transcription and translation, which have been shown to exhibit strong circadian rhythmicity (Noya et al., 2019). We therefore proceeded to test whether such changes could also be observed in cultured hippocampal neurons. We analyzed the mRNA levels in the cultures, relying on fluorescence in situ hybridization (FISH), performed with fluorescently-conjugated oligonucleotides containing multiple thymidine (dT) moieties. These label specifically the polyadenylated tails of mRNAs, and showed measurable signals throughout the cells, including synaptic areas (**Figure 3A**). We analyzed the FISH signals, and found that they changed throughout the day, in a rhythmic fashion (**Figure 3B**). Nevertheless, these results demonstrate that dynamic changes of the mRNA levels take place over time in disassociated hippocampal cultures.

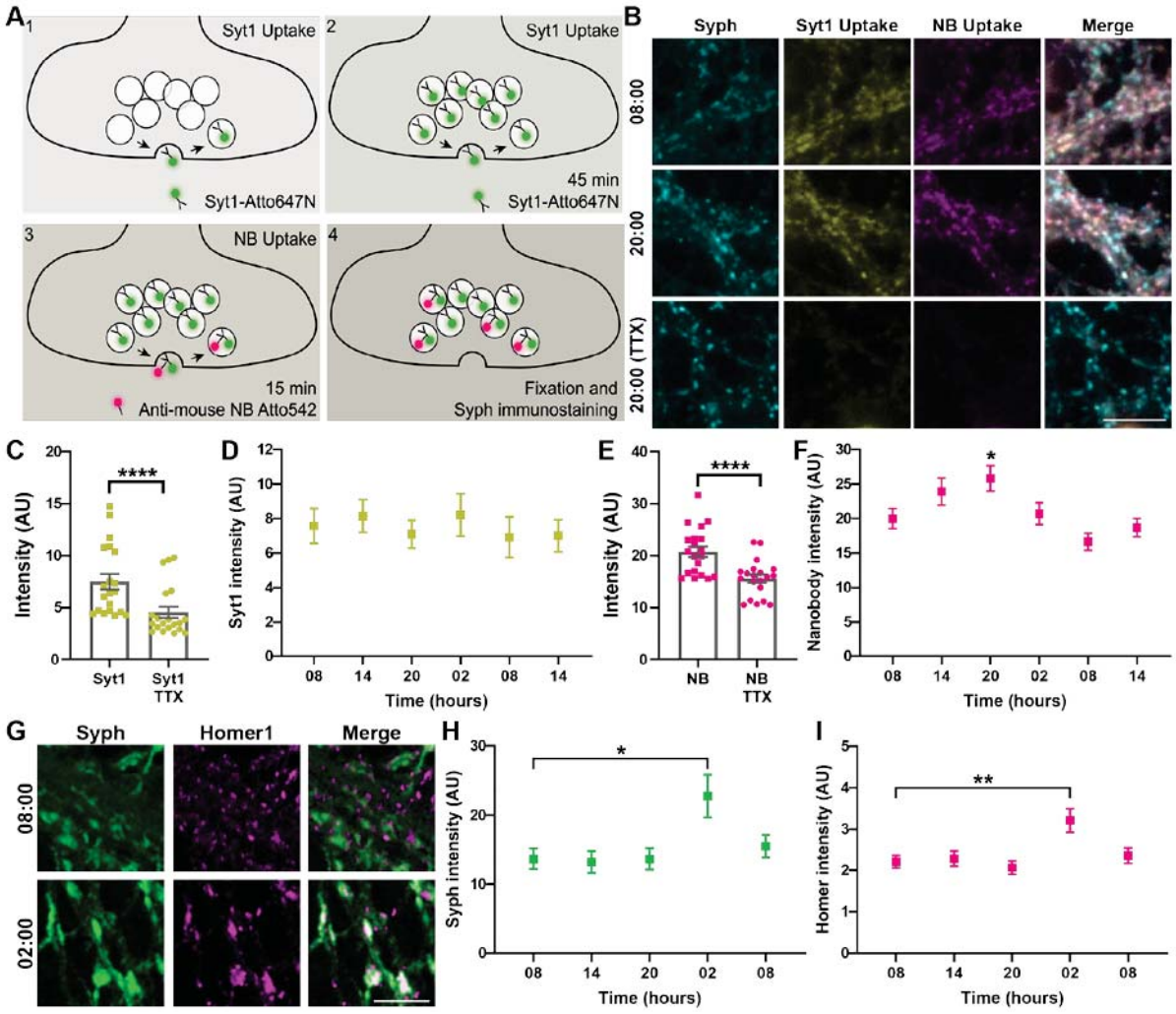

Figure 2. Synaptic vesicle recycling measurements confirm the existence of activity oscillations throughout the day. (A) To measure the presynaptic activity, we performed a Synaptotagmin 1 (Syt1) uptake assay (Kraszewski et al., 1995; Matteoli et al., 1992) at DIV18, at different times of day. To label the recycling vesicles, an Atto647N-conjugated Syt1 antibody was added to the cell culture medium for 45 minutes (1). The antibody recognizes a luminal (intravesicular) epitope, and is taken up during synaptic vesicle recycling. The 45-minute incubation is sufficient to saturate all of the recycling vesicles (2), and thereby provides an estimate for the total recycling pool. The non-recycling (reserve) pool of vesicles, which is larger than the recycling pool (Rizzoli and Betz, 2005), is not depicted here. To then obtain an estimate for the overall activity of the neurons at the particular time points we applied Atto532-conjugated secondary nanobodies (NB) that target the Syt1 antibody, for 15 minutes (3). The nanobodies label only a subset of the vesicles, in proportion to the activity levels (4). The neurons were subsequently fixed, and were immunostained for Synaptophysin (Syph) to label presynaptic compartments. To determine whether the assay indeed functioned, we blocked network activity with tetrodotoxin (TTX), which only allows the Syt1 antibodies to bind to surface epitopes, or to spontaneously recycling vesicles (Truckenbrodt et al., 2018). **(B)** Exemplary images of neurons tested at 08:00 or 20:00, along with a TTX treatment example. Scale bar: 10 µm. **(C)** and **(E)** The Syt1 and NB intensities were measured, with and without TTX treatment. Each symbol represents the average intensity of synapses in one image. N=4 independent experiments; the bar graph indicates the mean ± SEM. The mean intensities were significantly lower upon TTX treatment, in both C and E (2-way ANOVA test, followed by Tukey's multiple comparison test). **(D)** The Syt1 intensity over time. The symbols represent the mean ± SEM of each time point. No significant changes were observed (one-way ANOVA test, followed by Dunnet's multiple comparison test). **(F)** The NB intensity over time. The symbols represent the mean ± SEM of each time point. The activity at 20:00 is significantly different when compared to 08:00 (one-way ANOVA test, followed by Dunnet's multiple comparison test). **(G)** In order to test whether the variations in presynaptic activity are accompanied by morphological or size changes, neurons were immunostained at different time points for the presynaptic marker Syph and for the

postsynaptic marker Homer1. Scale bar: 5 µm. **(H)** and **(I)** show the intensity of Syph and Homer1 stainings over time (mean ± SEM; N=4 independent experiments). The intensities at 02:00 for both stainings are significantly higher in comparison to the stainings at 08:00 (one-way ANOVA test, followed by Dunnet's multiple comparison test). The first time-point was the reference for the multiple comparison. *p<0.05, **p<0.005, ****p<0.0001.

The abundance of RBM3 changes rhythmically, especially at synapses

To determine the molecular mechanisms responsible for the rhythmic changes in neuronal activity, synapse morphology and mRNA amounts, we analyzed the transcriptome of the cultures at different times of day, using mRNA sequencing (mRNAseq) (**Figure 4A**). Although several overall changes could be seen among the different sets of genes, relating to processes such as synaptic transmission and neuronal morphogenesis (**Table S1**), only one transcript showed a significant differential expression when the results from six different culture preparations were combined (**Figure 4B**), RNA-binding motif 3 (RBM3). This molecule showed the same general pattern of expression as *bona fide* clock genes like BMAL1 and Per2 (**Figure 4C**), but its variation among different cultures was small enough to result in significant differences between the time points, unlike BMAL1 or Per2. We assume that the desynchronization between different cell cultures is strong enough to mask the rhythmicity of BMAL1 or Per2, albeit at least the former is clearly exhibiting daily patterns in the cultured neurons (**Figure S2**).

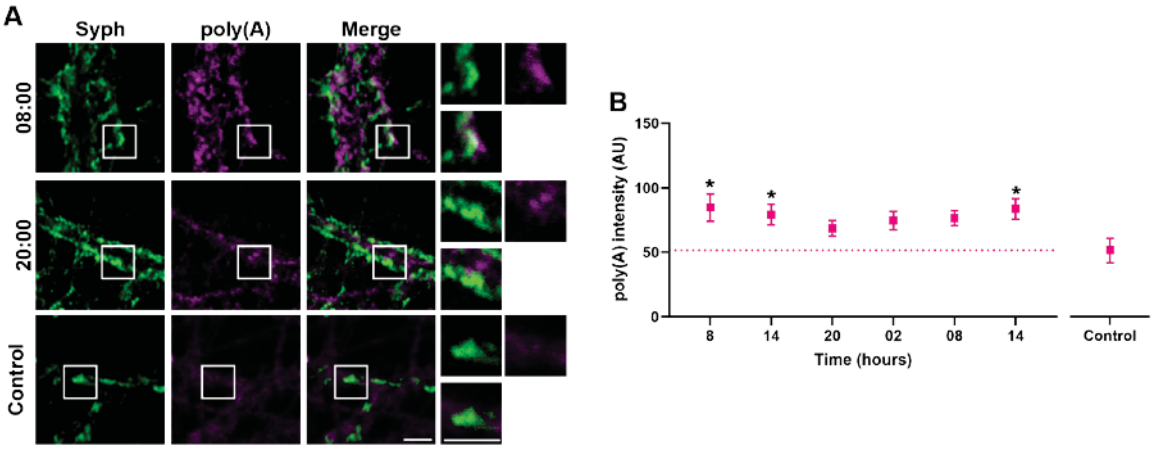

Figure 3. The amount of mRNA at the synapse is dynamic throughout the day. (A) To monitor the changes in the mRNA amounts throughout the day, we labeled the poly(A) tail of mRNAs with Atto647N-conjugated oligo(dT), at DIV18. We also immunostained the neurons for Syph, to determine synaptic locations. As a background staining control we relied on Atto647N-conjugated oligo(dA). Exemplary images for the stainings at 08:00 and 20:00 are shown, along with negative controls. Scale bars: 2.5 µm. **(B)** The synaptic signals were determined in regions-of-interest (ROIs) centered on the Syph spots, and broadened by 200 nm in each direction, to also include potential postsynaptic sites. The symbols show mean ± SEM of an image, N=3 independent experiments). The statistical significance was calculated with a Kruskal-Wallis test, followed by Dunn's multiple comparison test. The negative control signal was the reference for the multiple comparison. *p<0.05.

RBM3 is a cold-shock protein that is involved in translation, and which has been published as a potential biomarker for breast and colon cancer, due to this role (Sureban et al., 2008). However, RBM3 has also been connected to brain function, since it was discovered that it protects synapses from hypothermia (Peretti et al., 2015). More interestingly, it controls the alternative polyadenylation of core clock genes, which explains its connection to the circadian clock (Liu et al., 2013). A systematic transcriptomics analysis of the molecular circadian rhythm indicates that RBM3 is a rhythmically expressed transcript in the SCN tissue (Yan et al., 2008). To confirm this, we also surveyed circadian transcriptomics datasets that are available online at the Gene Expression Omnibus (GEO) repository (**Figure S4**). We found that RBM3 has a daily rhythmic expression in the SCN (GSE70391 and GSE70392, GSE72095 (Pembroke et al., 2015)), in liver (Almon, Richard R.; Yang, Eric; Lai, William; Androulakis, Ioannis P.; DuBois, Debra C.; Jusko, 2008; Terajima et al., 2017), cerebellum (GSE54651 (Zhang et al., 2014)), and even in cell cultures of wild-type and BMAL1 KO fibroblasts (GSE134333 (Ray et al., 2020)). Moreover, we found that RBM3 exhibits rhythmic expression throughout the day in the hippocampus tissue *in vivo* (GSE66875 (Renaud et al., 2015)). RBM3 appeared therefore as a strong candidate molecule, which may be involved in organizing rhythmic neuronal activity.

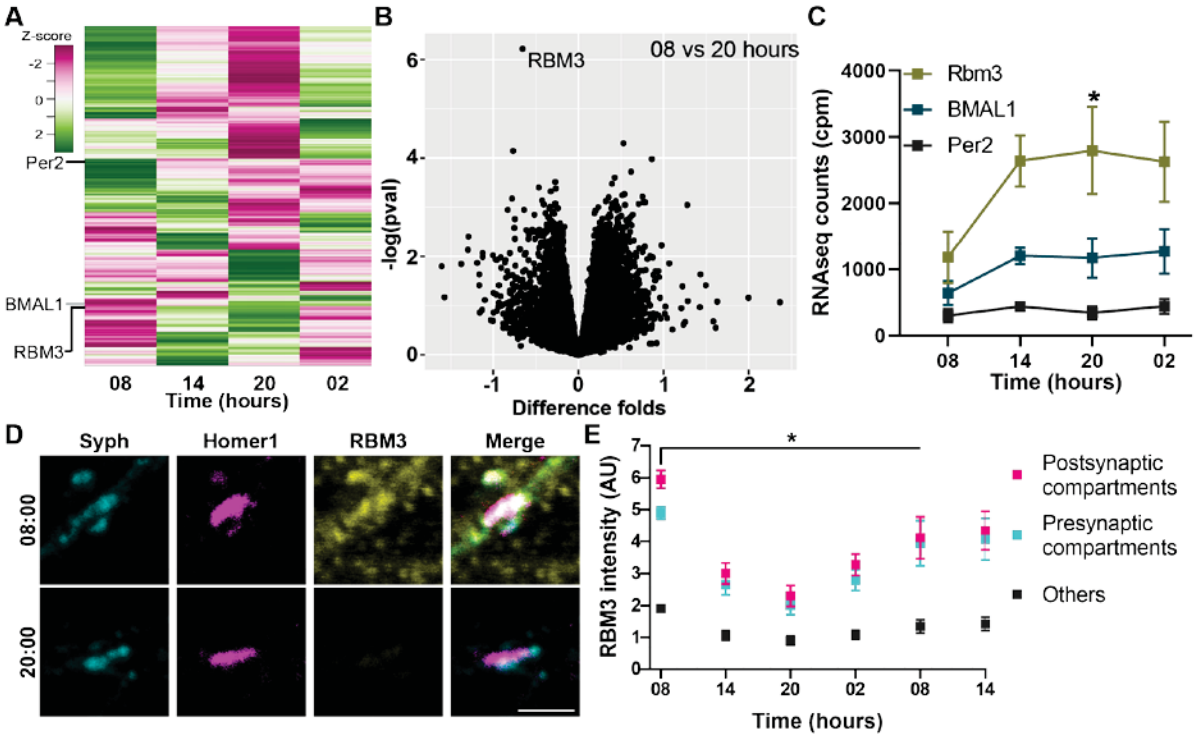

Figure 4. RBM3 abundance varies throughout the day in the hippocampal cultures. (A) To identify candidate genes that are responsible for the activity changes observed in the previous sections, we sequenced mRNAs collected from the cultures at different time points. Each row represents a gene. For expression profiling, a Z-score was calculated, and was scaled between -3 and 3. The Z-score describes the distance of the expression value at a given time point to the mean of the overall gene expression. **(B)** A volcano plot was generated to visualize the significance of the changes together with the fold difference. The graph plots –log(p-value) versus the ratio between

the amount of mRNAs that were collected at 08:00 and 20:00. The p-values are not adjusted for multiple comparisons in this graph. After correction for multiple comparisons (using the R package Limma(Ritchie et al., 2015)) only the changes in RBM3 appear significant. **(C)** The expression pattern of RBM3 is plotted along with that of the core clock genes Per2 and BMAL1. The symbols show the mean ± SEM of the counts per million (cpm) mapped reads. N=6 independent experiments. **(D)** To measure the RBM3 protein abundance we immunostained it at different time points, along with Syph and Homer1, to identify synapses. Scale bar: 2.5 μm. **(E)** The intensities of RBM3 at the presynaptic and postsynaptic locations, as well as in all other cell regions, were calculated (mean ± SEM). The statistical significance was calculated with a Kruskal-Wallis test, followed by Dunn's multiple comparison test. The first time point was the reference for the multiple comparison. *$p<0.05$.

Before pursuing this idea, we confirmed that its abundance is indeed cyclic in neurons. RBM3 immunostainings revealed that the protein has profound oscillations throughout the day, with minima in the evening, and maxima around 08:00 (**Figure 4D, E**). These changes were far more profound in synapses than in other compartments (**Figure 4E**), which again suggests that this molecule may be involved in synaptic function.

RBM3 controls the firing pattern in primary hippocampal cultures

To determine whether RBM3 affects neuronal activity, we resorted to long-term calcium imaging (as in **Figure 1**), in cultures subjected to RBM3 knock-down, or to the transfection of a scrambled oligonucleotide control (**Figure 5**). The RBM3 knock-down reduced the amounts of the protein significantly (**Figure S5**), albeit not completely. When analyzing in parallel the calcium signals from the knock-down cultures and their controls, it became obvious that activity could still be detected in both conditions (**Figure 5A, B**), but that the rhythms were different. The RBM3 knock-downs had peaks of activity at precisely the time points when the control cultures had their minimal activity (**Figure 5C, D**). This relation was significant (**Figure 5D**), implying that RBM3 has an important role in regulating the pattern of neuronal activity.

To test whether these effects also translated to synaptic vesicle activity, we relied on the Syt1 uptake assay used in **Figure 2**. We chose the time point that exhibited the highest difference in activity in calcium imaging (18:00, **Figure 5**), and incubated the cultures with Syt1 antibodies for 15 minutes, to determine the activity levels (**Figure 6A, B**), or for 60 minutes, in different coverslips, to measure the total size of the actively recycling vesicle pool (**Figure 6C, D)**. As cultures undergoing the knock-down treatment may be more fragile than unmodified cultures, we avoided the assay relying on mixtures of nanobodies and antibodies (from **Figure 2**), which involves multiple buffer changes that may harm the cultures, and we simply relied on separate 15 minute or 60 minute incubations. Both measurements showed significant differences, with RBM3 knock-down enhancing synaptic function, in agreement with the change in activity observed at 18:00 in calcium imaging (**Figure 5**). Performing these measurements in the

presence of TTX, which blocks network activity, resulted in no significant differences between the knock-downs and the controls (**Figure S6**).

Finally, immunostainings for Synaptophysin or Homer1, performed to determine the synapse size (as in **Figure 2**), suggested that RBM3 knock-down significantly influences the postsynapse size (**Figure 6E-G**). Overall, these results demonstrate that RBM3 is involved in the rhythm of synaptic and neuronal function.

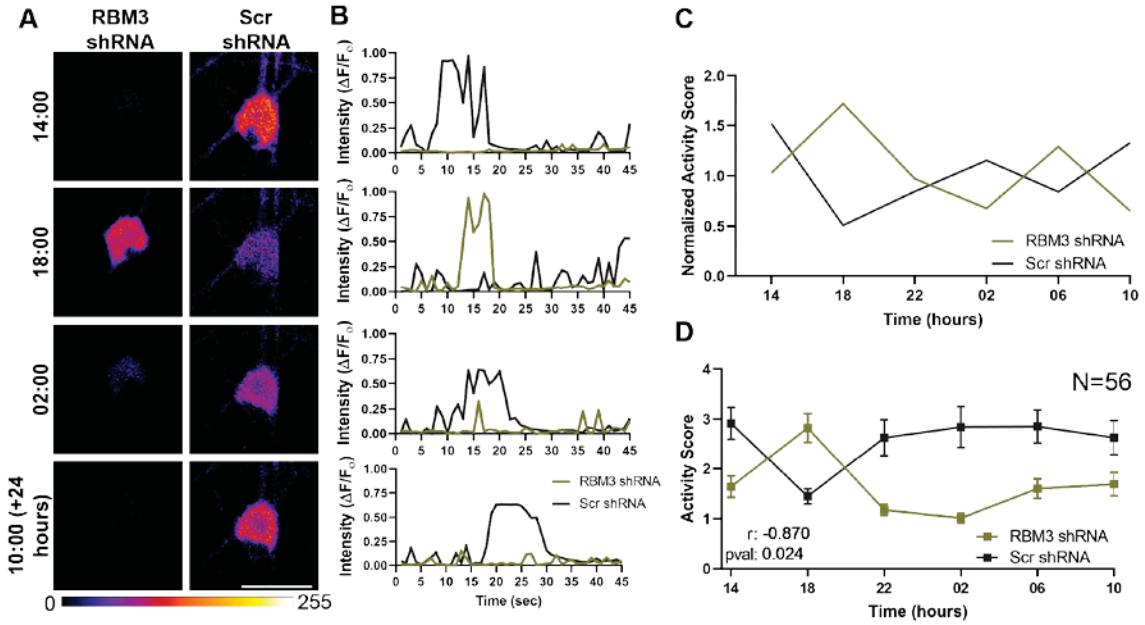

Figure 5. Knocking-down RBM3 alters the neuronal activity pattern throughout the day. (A) We knocked down RBM3 in the cultures by shRNA expression (see Methods). Alternatively, a scrambled shRNA was expressed (Scr), as a control. To determine the firing patterns, we performed Ca^{2+} experiments, exactly as in Fig.1. Scale bar: 50 µm. **(B)** The signals over the entire 45-second recordings from the cells shown in panel a are plotted, at the four different time points. **(C)** The activity score is plotted for the two exemplary neurons, normalized to their respective medians. **(D)** To reveal the average firing patterns, 56 neurons were measured in each condition, from 4 independent experiments (with 2-4 different wells measured per experiment; mean ± SEM). To calculate the correlation between two firing patterns, we performed a Pearson's correlation test. A significant anti-correlation was observed (r = -0.870, p = 0.024).

RBM3 controls local translation at the postsynapse

As mRNA amounts varied throughout the day (**Figure 3**), and as RBM3 is an mRNA binding protein, we next sought to determine whether the RBM3 knock-down influences the mRNA levels in synapses, where the highest RBM3 oscillations were observed (**Figure 4**). We repeated the FISH experiments performed in **Figure 3**, either in RBM3 knock-down neurons or in controls (**Figure 7a**). No significant changes could be observed (**Figure 7b**), neither when relying on Synaptophysin as a synaptic marker (**Figure 7**), nor when relying on the postsynaptic marker Homer1 (**Figure S7**). This suggests that RBM3 does not influence the synaptic mRNA levels, at least not sufficiently for detection with this FISH assay.

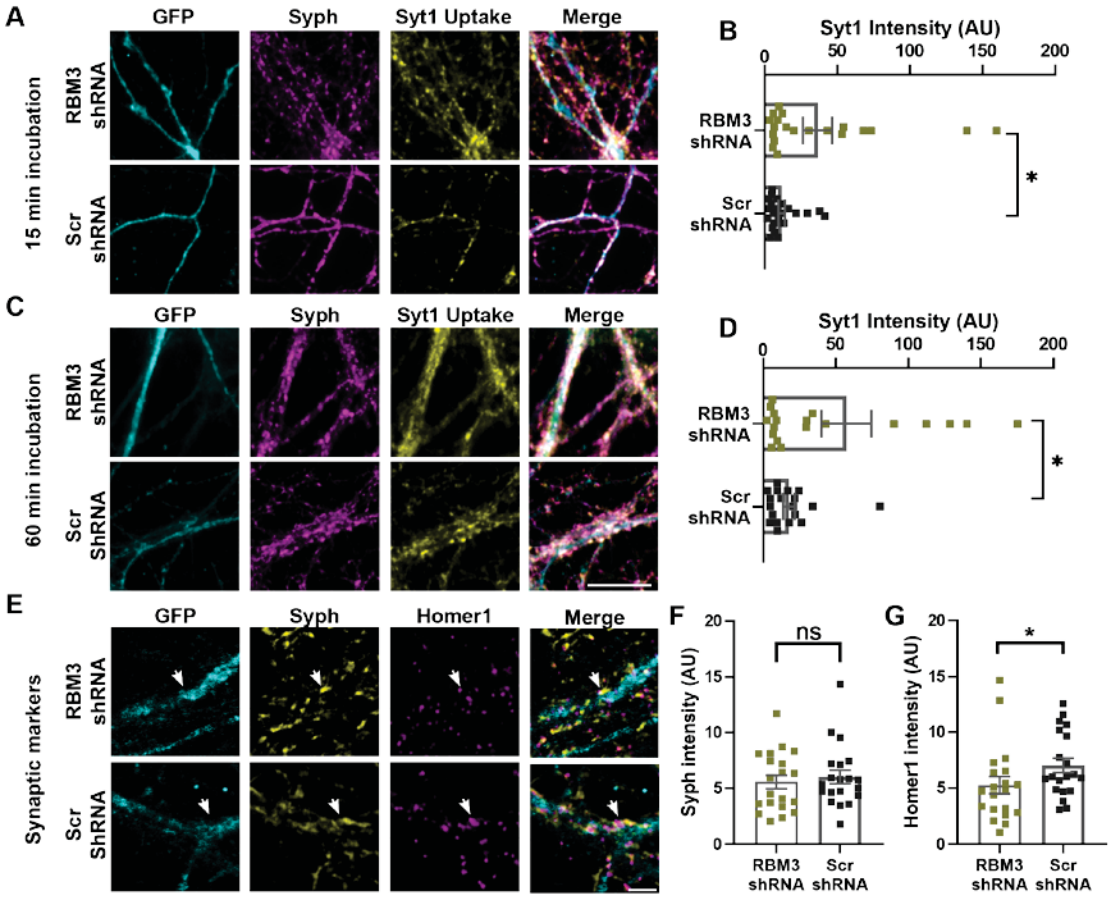

Figure 6. Synaptic activity and morphology are modified upon RBM3 shRNA treatment. (A) and **(C)** To measure synaptic vesicle recycling we relied on the Syt1 uptake assay, applying the antibodies for 15 or 60 minutes, in different experiments. Typical images are shown, obtained from DIV18 neurons, at 18:00. GFP is used as a reporter for the expression of shRNA or a scrambled control sequence. Scale bar: 20 µm. **(B)** and **(D)** The Syt1 intensity was measured. The symbols represent the mean of each image, and the bar graph shows the mean ± SEM; N=4 independent experiments. The recycling vesicle pool size (measured with 60-minute incubations), as well the synaptic activity (measured with 15-minute incubations) are significantly larger for the RBM3 knock-downs (Mann-Whitney tests). **(E)** To monitor changes in the size or morphology of synapses, neurons were immunostained for Syph and Homer1. Scale bar: 2.5 µm. Two synapses are indicated by the arrows. **(F)** and **(G)** show the intensity of the Syph and Homer1 stainings, respectively. The symbols indicate the mean intensity of each image, and the bar graph indicates the mean ± SEM. N=4 independent experiments. The Homer1 intensity of RBM3 KD is significantly lower than in the controls (Mann-Whitney tests). *p<0.05.

As RBM3 has been strongly linked to translation (Dresios et al., 2005; Smart et al., 2007a) we next analyzed its potential influence on this process. We relied on an assay that reports the translation sites, the so-called puromycin assay (Hafner et al., 2019). Puromycin is an antibiotic that binds to the P site of the ribosome and incorporates itself into the polypeptide chain. This results in the polypeptide chain being released from the ribosome prematurely (**Figure 7C**), thereby stopping the translation process. A subsequent immunostaining with a specific puromycin antibody reports all of the stopped translation sites, thereby providing an accurate estimate of ongoing translation in the particular cellular area. We combined this assay with the RBM3 knock-down (**Figure 7D**), and found that this treatment significantly reduced local

translation in postsynapses. The translation levels remaining in RBM3 knock-downs were close to the background levels, measured by pre-treating the cultures with anisomycin, an antibiotic that halts the ribosomal complex and prevents the incorporation of puromycin (**Figure 7E; Figure S 8A, B**). A similar trend was also observed in presynapses (**Figure S 8C, D, E**), albeit the local translation levels were too low for a clear differentiation between RBM3 knock-downs and controls (**Figure S 8E**). Importantly, when we analyzed the effects of the knock-down at the level of the whole cells, no significant difference could be measured (**Figure S8F**).

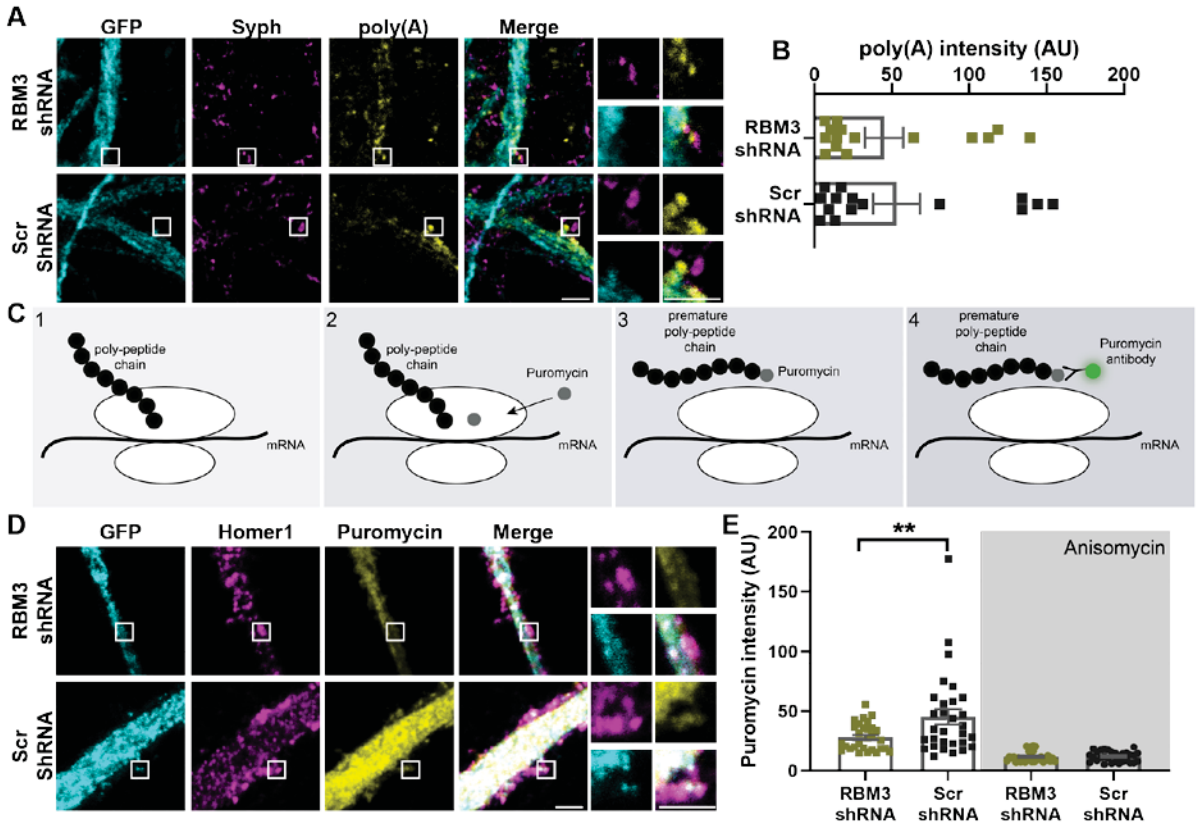

Figure 7. RBM3 knock-down decreases translation at the postsynapse, without affecting local mRNA levels. **(A)** To determine the effects of RBM3 on mRNA levels at the synapse, FISH with oligo(dT) was performed as in Fig 3. Scale bar: 2.5 µm. **(B)** An analysis of the FISH signal indicates no significant difference between RMB3 knock-downs and controls (Kruskal-Wallis, followed by Dunn's multiple comparison test). Each dot represents the mean of an image, and the bar graph shows the mean ± SEM. N=3 independent experiments. **(C)** To measure local translation at the postsynapse (1), we used the puromycin assay. Puromycin binds to the P site in the ribosome (2). It incorporates itself into the polypeptide chain and releases the polypeptide chain prematurely (3). A subsequent immunostaining for puromycin (4) enables an estimation of the amount of local translation. As a negative control, we treated the cultures with anisomycin (Supplementary Fig. 6), which prevents puromycin binding. **(D)** Puromycin immunostainings are shown, along with Homer1 stainings, to indicate postsynaptic sites. Scale bars: 2.5 µm. **(E)** Puromycin staining intensities are shown, calculated for the Homer1 areas; Each dot represents the mean of an image, and the bar graph shows the mean ± SEM. N=4 independent experiments. The RMB3 knock-downs show significantly less translation at postsynapses (one-way ANOVA, followed by Dunnet's multiple comparison test). **p<0.005.

This suggests that RBM3 controls local translation in postsynapses, and possibly also in presynapses, but its effects do not extend, under these conditions, to the organization of translation in the entire cell.

Importantly, to study the influence of molecular clock on the primary hippocampal culture, we repeated several of the assays presented above with a knocked-down for a core clock gene, Brain and muscle ARNT like 1 (BMAL1). The significant reduction in BMAL1 gene expression upon BMAL1 shRNA was verified using qPCR. Surprisingly, we have not observed any substantial changes in the BMAL1 knocked down neurons (**Figure S9**). This confirms that the observations we made above are specific for RBM3, which again underlines the importance of this protein for neuronal activity in these cultures.

4.5| Discussion

Our results suggest that hippocampal neurons in dissociated cultures maintain synchronized rhythms of activity, which are reproducible between independent coverslips and preparations, as demonstrated by both calcium imaging and measurements of synaptic vesicle dynamics. At the same time, their transcriptomes also show a tendency to synchronize, albeit only one protein, RBM3, showed significant differences between different time points, when multiple cultures were considered. RBM3 manipulations resulted in profound changes in the neuronal activity patterns. A potential mechanism for the RBM3 function may be through its modulation of local translation in synapses (**Figure 7**), which it appears to affect in a specific fashion, with less influence on global translation.

Rhythmic activity in dissociated hippocampal neurons

Primary hippocampal cultures are prepared from mechanically and enzymatically dissociated hippocampi. The loss of the third dimension is a dramatic change for the network dynamics. At the same time, not having hormonal and temporal input from other regions makes it more difficult to synchronize the neurons in a culture. This is already known from SCN cultures, where the neurons demonstrate individual rhythmicity (Welsh et al., 1995), and can maintain 24-hour rhythmicity when plated at high densities (Honma et al., 1998), but lose rhythmicity when the network communication is perturbed (Yamaguchi et al., 2003). Taken together, these findings suggest that network communication is essential for rhythmicity and synchronization in cultures, and that low-density cultures will lose synchronization relatively rapidly.

In view of these arguments, it was unclear whether hippocampal neurons would be able to synchronize over long periods in the culture, as the SCN neurons do (Watanabe et al., 1993).

Interestingly, our findings are consistent with the observations on SCN. Dissociated hippocampal neurons have a rhythmic activity, albeit a clear daily rhythmicity cannot be observed when averaging results across different cultures.

Neuronal activity was not the only factor that had rhythmicity. Presynaptic activity, synapse size, and mRNA amounts at the synapse also were changing throughout the day. These observations suggest that one of the most commonly used models for synaptic research, the primary hippocampal culture, has a time-dependent behavior. This makes it extremely important to acknowledge the timing of experiments performed with these cultures.

RBM3 connects molecular clock genes to neuronal function

It has been repeatedly demonstrated that the molecular clock regulates genes that control neuronal activity, as discussed in the Introduction. This makes them excellent candidates for the regulation of rhythmic activity in cultured neurons. Surprisingly, we did not find any of the core clock genes to have a very clear transcription pattern in these cultures, which implies that they may not be very well synchronized among different neurons and different cultures, unlike RMB3. This molecule has been found in many time-series transcriptomics datasets as a daily rhythmic gene (Almon, Richard R.; Yang, Eric; Lai, William; Androulakis, Ioannis P.; DuBois, Debra C.; Jusko, 2008; Noya et al., 2019; Pembroke et al., 2015; Ray et al., 2020; Renaud et al., 2015; Terajima et al., 2017; Yan et al., 2008; Zhang et al., 2014), and its oscillations in expression may be independent of at least some components of the molecular clock, as they still persist in BMAL1 KO cells (Ray et al., 2020). Overall, our work cannot state whether the RBM3 oscillations are controlled by the central molecular clock machinery in hippocampal cultures. However, its stronger synchronization (across cultures) than that of the canonical clock genes implies that RBM3 expression may be independent from them.

Other than being a rhythmically expressed gene, RBM3 is a cold-shock protein, whose expression is induced in hypothermia conditions. For example, keeping a culture at 32ºC instead of 37ºC for 24 hours induces RBM3 expression (Chappell et al., 2001; Yang et al., 2019). Such temperature changes are not possible in the wells of a closed plate in the incubator, which eliminates the possibility that RBM3 expression was synchronized by temperature changes in our experiments.

As a cold shock protein, RBM3 activates the translation machinery. Several studies have demonstrated that RBM3 enhances polysome formation, by phosphorylation of translation initiation factors and by changing the microRNA level (Chappell et al., 2001; Dresios et al., 2005). RBM3 has been described to enhance the translation of specific genes in hypothermia, thereby protecting synaptogenesis (Yan et al., 2019; Zhu et al., 2019). Moreover, although

RBM3 is primarily located at the nucleus, one isoform has been found in dendrites, where it colocalizes with a ribosomal protein (Smart et al., 2007a). In summary, these observations suggest that RBM3 is important for synaptic function, probably due to its role in translation, and possibly in local synaptic translation. Our findings suggest that RBM3 does not change the overall mRNA availability in synapses, but that it specifically changes local translation in synapses, without affecting the global translation. This effect may result in strong changes in synaptic activity, as explained below.

RBM3 may regulate synaptic function through local translation

Local translation appears to be an essential resource for neurons, since they need to strengthen or prune their connections in response to changes in synaptic activity. This implies that new proteins, as synaptic receptors, need to be incorporated dynamically in synapses. As neurons have extremely long neurites (Ishizuka et al., 1995), transport from the cell body would probably fail to satisfy the protein turnover needs of the synapses. To cope with this logistics challenge, neurons would need to place the translation machinery in synapses.

For a long time, electron microscopy images of synapse have demonstrated the presence of polyribosomes in the dendritic shaft and in the postsynapse (Ostroff et al., 2018; Steward and Levy, 1982). Later studies have shown that other components of the translational machinery, such as tRNAs, translation initiation factors, and elongation factors are present in synapses (Steward and Levy, 1982; Sutton and Schuman, 2006; Tiedge and Brosius, 1996). In spite of these observations, direct evidence for translation in all synaptic compartments, and especially in the presynapse, has been difficult to obtain until recent assays demonstrated this thoroughly for both synaptic boutons and dendritic spines (Hafner et al., 2019).

Functional data have also offered strong support to the idea that local translation is an important feature of the synapses. Synaptic plasticity has been shown to depend on local translation (Miller et al., 2002). This process has also been linked to memory formation (Jones et al., 2018). Furthermore, electrical activity can be affected by the local translation as well, as in the case of the calyx of Held (Scarnati et al., 2018), where the inhibition of protein synthesis enhances spontaneous activity.

Overall, these observations suggest that local translation has important effects on synaptic transmission, and hence on plasticity, which last for hours. It is therefore evident that disturbing local translation would affect synaptic transmission, which in turn would influence the general network activity, as we observed in RBM3 KD experiments.

To our knowledge, this is the first time that RBM3 has been linked to changes in local translation, or to long-term neuronal activity changes. At the same time, our work demonstrates

that broad changes take place in neuronal activity depending on the time of day, even in a simple model like dissociated hippocampal neurons in culture. This suggests that these cultures, which are far more common than SCN cultures, could become a useful model for daily rhythm studies. Finally, the link between RBM3 and local translation may provide substantial further insight in the future, especially as the local translation field is now rapidly progressing through numerous innovative tools and concepts (Holt et al., 2019).

Acknowledgements

We would like to thank Verena Klüver and Dr. Eugenio Fornasiero for their generous gift of the Scr shRNA plasmid, Roya Yousefi and Prof. Peter Rehling for their generous gift of puromycin, anisomycin and puromycin antibody, and Janina Pasch for her help throughout the puromycin experiments. We also would like to thank the Transcriptome and Genome Analysis Laboratory (TAL, Göttingen, Germany) for mRNA sequencing and analysis. We thank Prof. Christopher S. Colwell (Brain Research Institute, University of California, Los Angeles) for comments on the manuscript. The work was supported by a grant from the Deutsche Forschungsgemeinschaft (DFG) to S.O.R., SFB1286/A03.

Author Contributions

Study design by S.M.S. and S.O.R. Data collection by S.M.S. and M.S.ET. Data analysis and interpretation by S.M.S. and S.O.R. Manuscript preparation by S.M.S. and S.O.R.

Competing interests

The authors declare that they have no competing interests.

Materials & Correspondence

S.O.R. : srizzol@gwdg.de

4.6| Supplementary Data

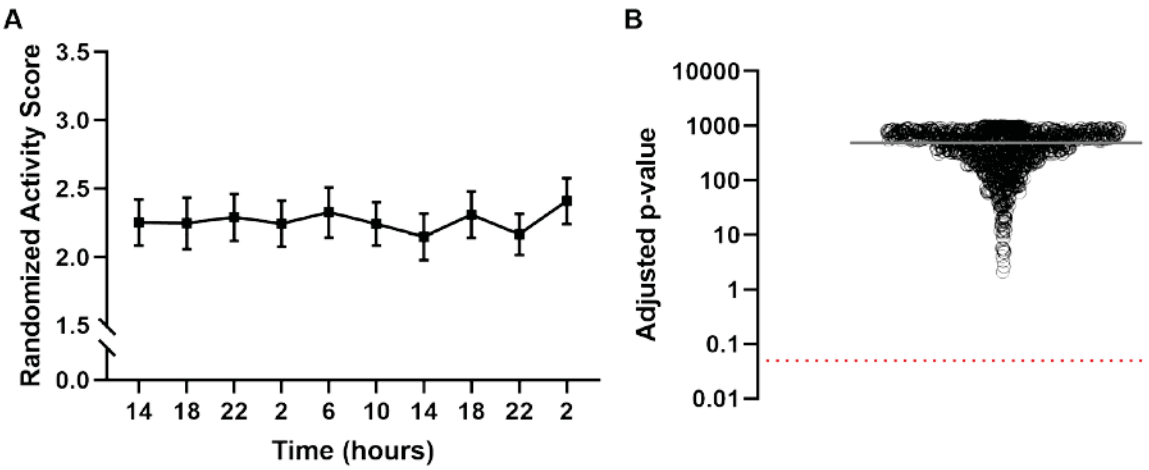

Supplementary Figure 1. Randomizing the activity scores failed to generate significant differences in the firing pattern of dissociated hippocampal cultures. (A) To confirm that the significant differences observed in the average firing pattern from Fig. 1D were not due to chance, the activity scores of the neurons were randomized, and the average activity was then investigated by Friedman tests, as in Fig. 1D. An exemplary randomized activity score is plotted, as mean ± SEM. **(B)** The randomization procedure was performed 1000 times, and the p-values that were obtained from the Friedman test were adjusted for the repeated multiple testing. The resulting p-values are shown as black circles. The gray line indicates the mean value, and the red dotted line shows the significance level (0.05).

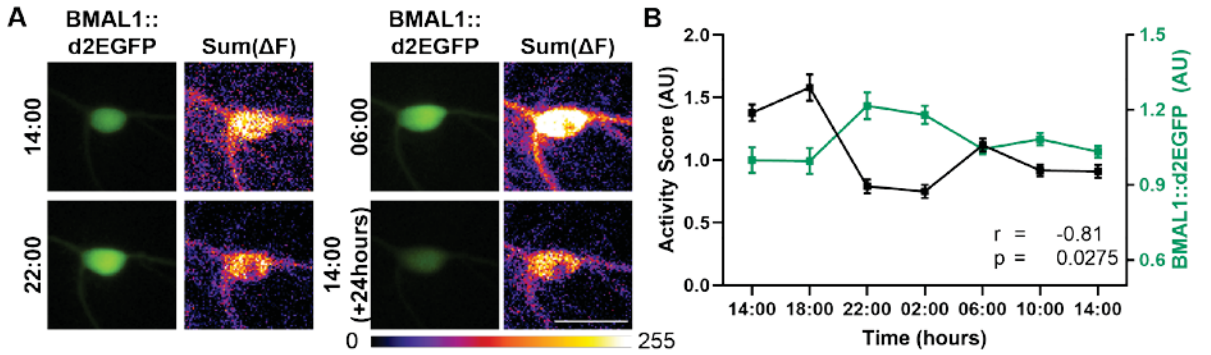

Supplementary Figure 2. The BMAL1 promoter activity is negatively correlated to the firing pattern in hippocampal culture. (B) We analyzed neuronal activity using the genetically-encoded Ca^{2+} indicator Neuroburst, as in Fig. 1. The neurons were also transfected with a destabilized EGFP (d2EGFP), under the control of the BMAL1 promoter, which enables us to analyze both BMAL1 rhythmicity and activity at the same time. The exemplary images show the d2EGFP fluorescence at different time points, as well as the overall activity at the respective time points, obtained by summing all frames collected in 45-second-long videos, as in Fig. 1. Scale bar: 50 µm. **(B)** The graph indicates the average activity scores (black) and d2EGFP signals (green), over 24 hours. The symbols indicate mean ± SEM, from 11 neurons tracked in 3 independent experiments. The correlation between the two curves is negative, as assessed by the Person's correlation test (r = -0.81, p=0.0275).

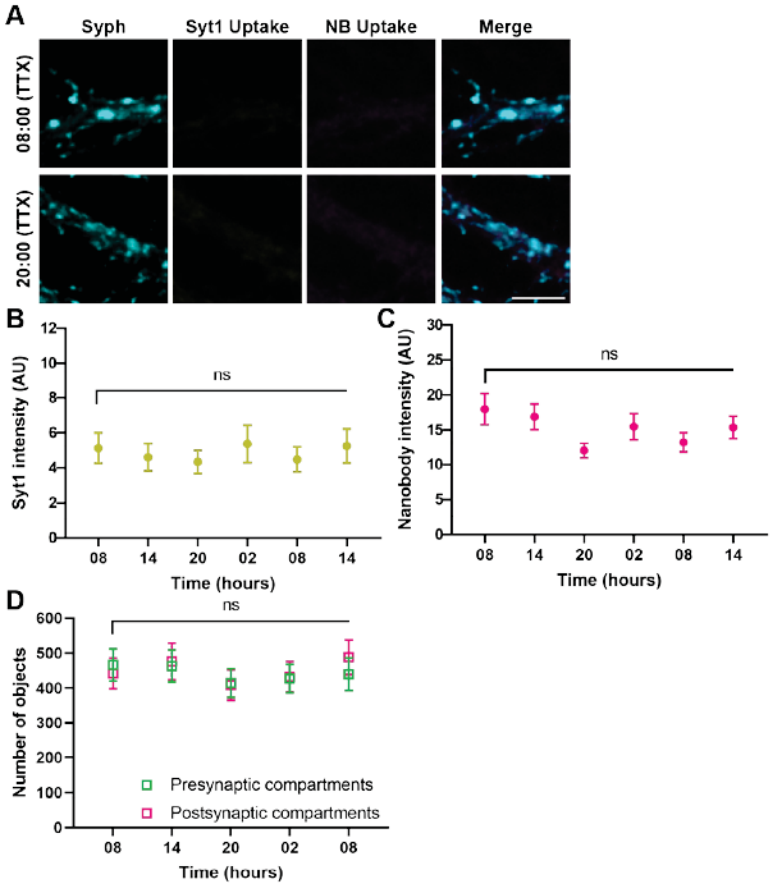

Supplementary Figure 3. Synaptotagmin1 and nanobody labeling show no significant differences throughout the day under TTX incubation. (A) We blocked network activity using tetrodotoxin (TTX), and then performed the same vesicle-labeling assay as in Fig. 2. Scale bar: 25 µm. **(B)** and **(C)** The analysis of Syt1 and NB staining was performed as described in Fig. 2. The symbols indicate means ± SEM. N=4 independent experiments. No significant differences were found when using one-way ANOVA tests, followed by Dunnet's multiple comparison test. **(D)** To determine whether the number of synapses vary throughout the day, we measured the numbers of Syph- and Homer1-positive objects from the images shown in Fig. 2. The graphs indicate the number of objects (synapses) per image (mean ± SEM). N=4 independent experiments. No significant differences were found when using one-way ANOVA tests, followed by Dunnet's multiple comparison test.

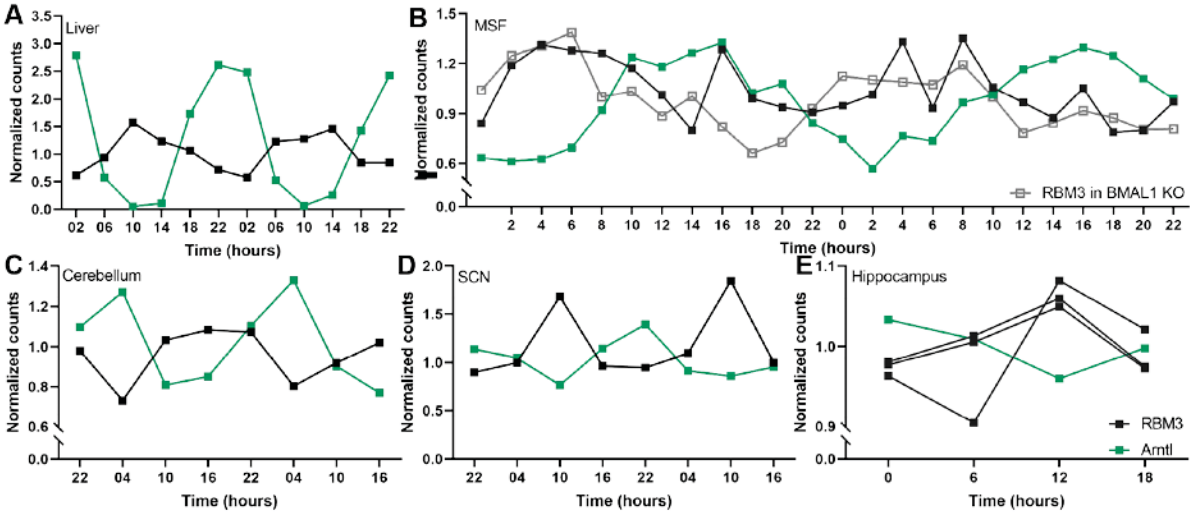

Supplementary Figure 4. RBM3 appears to have a rhythmic daily expression *in vivo*. We monitored the RBM3 expression patterns in *in vivo* circadian transcriptomics data that are available online. As a control, we also plot the expression of the gene for the core clock protein BMAL1 (gene depicted as Aryl hydrocarbon receptor nuclear translocator-like protein 1, Arntl). **(A)** The graph shows the expression pattern of Arntl and RBM3 throughout the day in the liver tissue (Terajima et al., 2017). **(B)** To determine the relationship between RBM3 and the molecular clock, we found a dataset that knocked out BMAL1. Mouse skin fibroblast (MSF) cell cultures were prepared from wild type (WT) and BMAL1 knock-out (BMAL1 KO) mice. RNA samples were collected every two hours, after 48 hours treatment with a circadian clock synchronizer (Dexamethasone). The RBM3 expression still exhibits daily rhythmicity throughout the day (GSE134333 (Ray et al., 2020)), especially in the absence of BMAL1. **(C)** The circadian mammalian atlas provides information on the expression patterns of Arntl and RBM3 throughout the day, and it indicates that RBM3 has a circadian expression in the cerebellum (GSE54651 (Zhang et al., 2014)). **(D)** The graph shows the median normalized expression pattern of Arntl and RBM3 throughout the day in the SCN tissue (GSE70391). **(E)** The graph shows the median normalized expression pattern of Arntl and 3 transcripts of RBM3 throughout the day in the hippocampus tissue (GSE66875 (Renaud et al., 2015)). The daily rhythmicity was confirmed via the MetaCycle (Wu et al., 2016). All time series shown have a significant daily rhythm, except for RBM3 in the wild-type MSF culture (panel b), p = 0.0667.

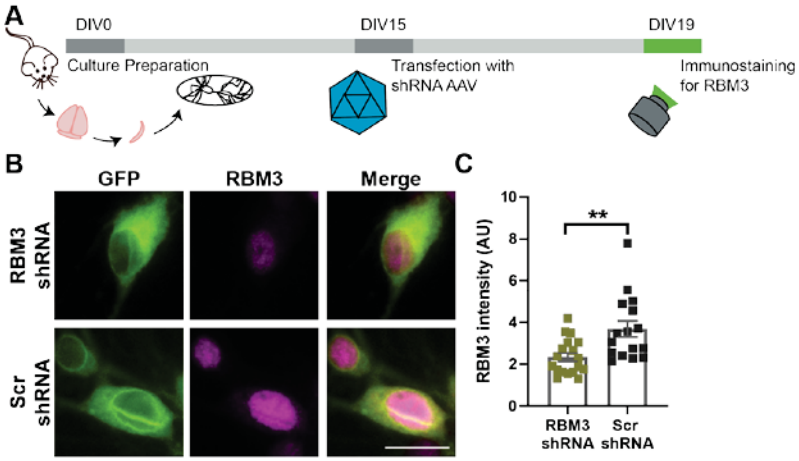

Supplementary Figure 5. The RBM3 abundance is reduced by the RBM3 shRNA virus expression. (A) A short-hairpin (shRNA) sequence that targets the RBM3 mRNA was designed. A scrambled sequence was used as a control. Adeno-associated virus (AAV) was chosen as the delivery method, at DIV15. After four days, neurons were fixed and immunostained for RBM3. **(B)** Exemplary RBM3 images are shown. The reporter for the shRNA virus is green fluorescent protein (GFP). Scale bar: 10 µm. **(C)** An analysis of the RBM3 abundance. Each dot represents the mean of an image, and the bar graph shows the mean ± SEM. N=3 independent experiments. A significant difference was detected (Mann-Whitney test). **p<0.005.

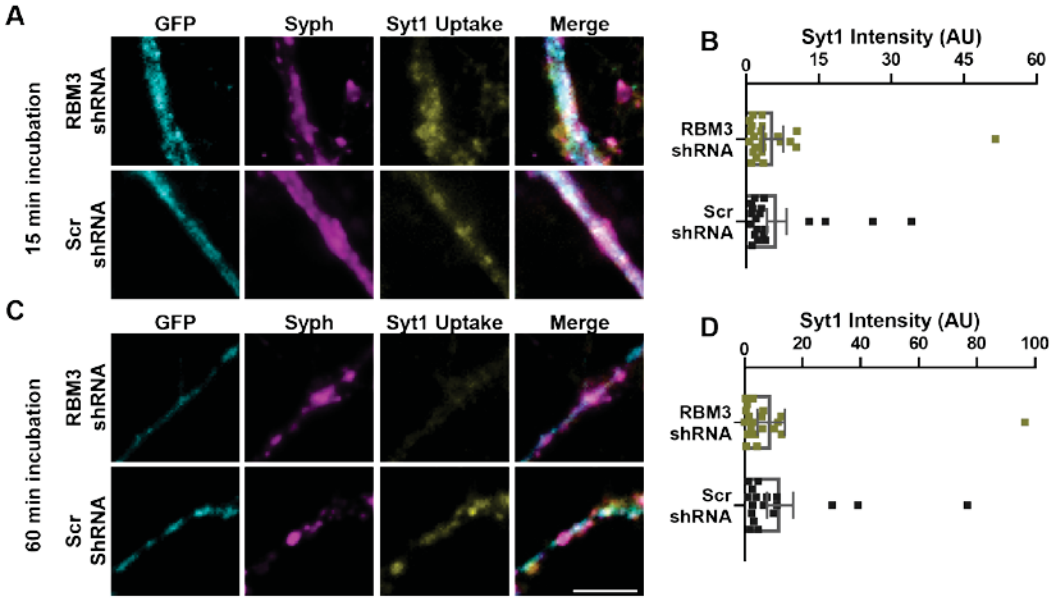

Supplementary Figure 6. Synaptotagmin1 and nanobody labeling show no significant differences in RMB3 knock-downs under TTX incubation. (A) and **(C)** We blocked network activity using tetrodotoxin (TTX), and then performed the same vesicle-labeling assay as in Fig. 6. Typical images are shown. Scale bar: 20 µm. **(B)** and **(D)** A quantification of the signals revealed no significant differences (Mann-Whitney tests). Each dot represents the mean of an image, and the bar graph shows the mean ± SEM. N=4 independent experiments.

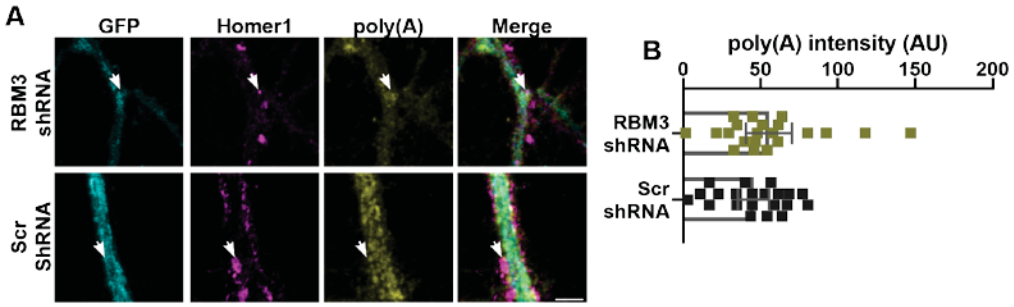

Supplementary Figure 7. The postsynaptic mRNA levels are not affected by RMB3 knock-downs. (A) To determine the mRNA levels at the postsynaptic compartments the oligo(dT) staining procedure was used as in Figs. 3 and 7, immunostaining the cells for the postsynaptic marker Homer1. Scale bar: 2.5 µm. **(B)** An analysis of the FISH signal indicates no significant difference between RMB3 knock-downs and controls (Kruskal-Wallis, followed by Dunn's multiple comparison test). Each dot represents the mean of an image, and the bar graph shows the mean ± SEM. N=4 independent experiments.

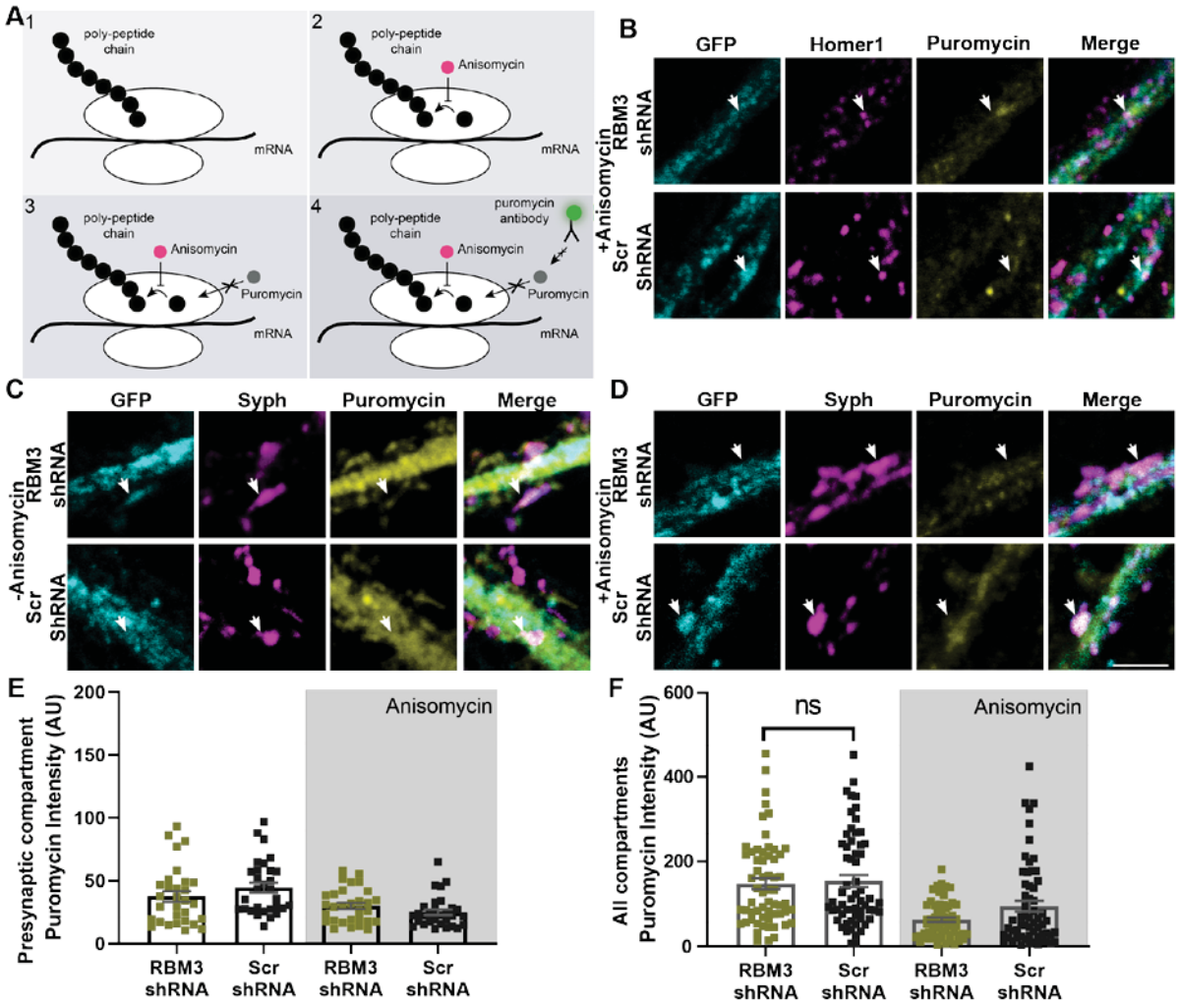

Supplementary Figure 8. Presynaptic and global translations are not affected by RBM3. (A) To measure the puromycin effect after protein synthesis inhibition, (1) we used anisomycin as a negative control prior to puromycin treatment. Anisomycin blocks the aminoacid transfer to the polypeptide chain (2). Therefore, puromycin cannot be incorporated into the polypeptide chain (3). A subsequent immunostaining for puromycin (4) enables an estimation of the amount of puromycin incorporation which have overcome the anisomycin effect. **(B)** Typical images for the negative control of the puromycin assay together with Homer1 (postsynaptic marker) staining. These were obtained in the conditions explained in Fig. 7. Scale bar: 2.5 µm. To measure local translation at the presynapse, we used the puromycin assay, as in Fig. 7, employing Syph as a synaptic marker, instead of Homer1. **(C)** and **(D)** Typical images with and without anisomycin treatment respectively. Example synapses are indicated by the arrows. Scale bar: 2.5µm. **(E)** Puromycin staining intensities are shown, calculated for the Syph areas. Each dot represents the mean of an image, and the bar graph shows the mean ± SEM. N=4 independent experiments. The RMB3 knock-downs appear to lower translation, but the overall levels in presynapses are too close to the negative controls (anisomycin) for this difference to be determined with precision (the difference was not significant when tested by a Kruskal-Wallis test, followed by Dunn's multiple comparison test). **(F)** An analysis of the global puromycin levels in RBM3 knock-downs and controls. Each dot represents the mean of an image, and the bar graph shows the mean ± SEM. N=4 independent experiments. No significant difference was observed by a Kruskal-Wallis test, followed by Dunn's multiple comparison test.

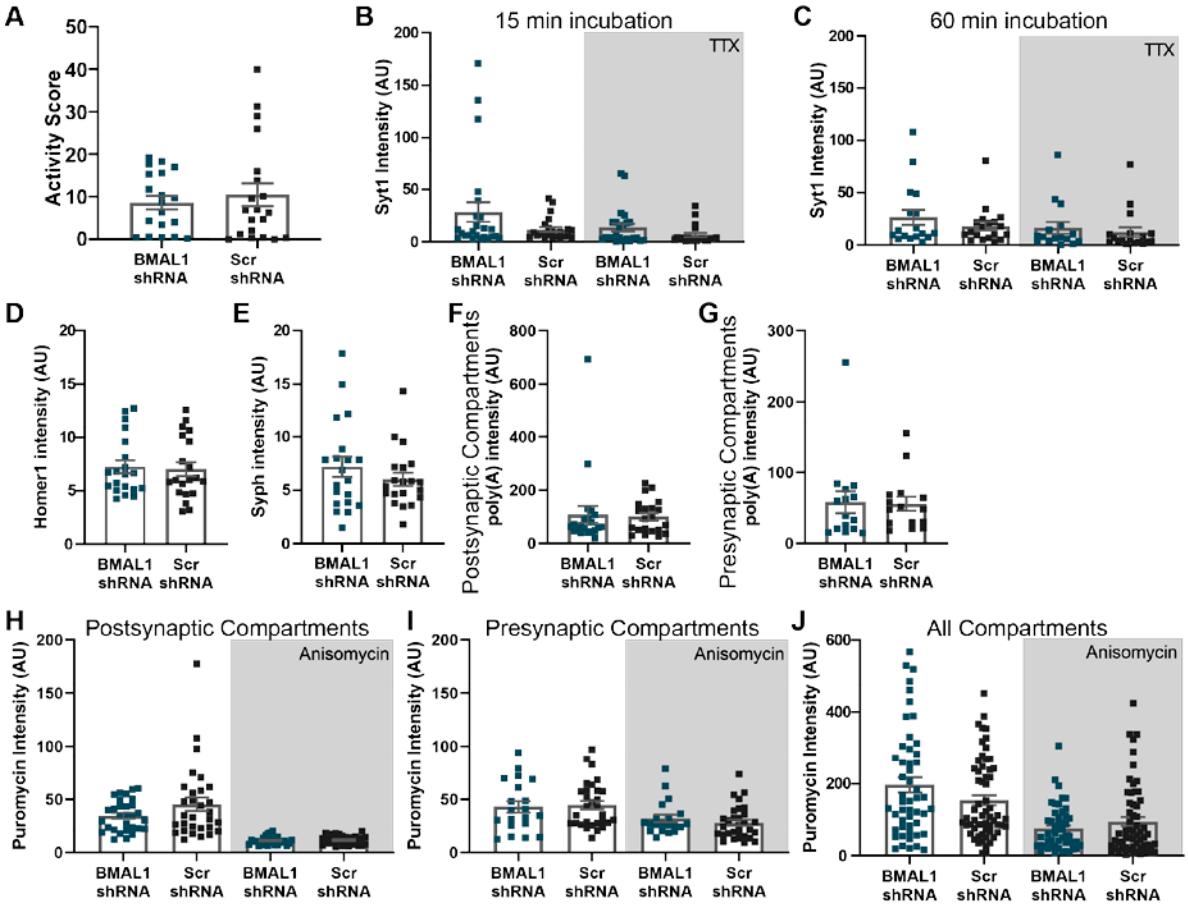

Supplementary Figure 9. The effect of BMAL1 on neurons. (A) To measure the contribution of the molecular clock in the primary hippocampal culture, we performed same assays with BMAL1 KD neurons. Again we knocked down BMAL1 in the cultures by shRNA expression (see Methods). Alternatively, a scrambled shRNA was expressed (Scr), as a control. To determine the firing patterns, we performed Ca^{2+} experiments, exactly as in Fig.1. The signals over the entire 5-minute recordings from the cells shown are plotted. We selected maximum 5 neurons from one coverslip, and performed 4 coverslips per experiment. N=3 independent experiments. **(B)** and **(C)** We performed Syt1 assay as described in Fig. 6. The Syt1 intensity was measured. The symbols represent the mean of each image, and the bar graph shows the mean ± SEM; N=4 independent experiments. The recycling vesicle pool size (measured with 60-minute incubations), as well the synaptic activity (measured with 15-minute incubations) do not show difference for the BMAL1 knock-downs (Mann-Whitney tests). **(D)** and **(E)** To monitor changes in the size or morphology of synapses, neurons were immunostained for Syph and Homer1. The graphs show the intensity of the Syph and Homer1 stainings, respectively. The symbols indicate the mean intensity of each image, and the bar graph indicates the mean ± SEM. N=4 independent experiments. The Homer1 intensity of BMAL1 KD is not different than in the controls (Mann-Whitney tests). **(F)** and **(G)** To determine the effects of BMAL1 on mRNA levels at the post (Homer1 as a marker) and presynapse (Syph as a marker) respectively. An analysis of the FISH signal indicates no significant difference between BMAL1 knock-downs and controls (Kruskal-Wallis, followed by Dunn's multiple comparison test). Each dot represents the mean of an image, and the bar graph shows the mean ± SEM. N=3 independent experiments. **(H)**, **(I)** and **(J)** To measure local translation at the postsynapse, we used the puromycin assay as described in Fig. 7. Puromycin staining intensities are shown, calculated for the Homer1, Syph and all areas respectively. Each dot represents the mean of an image, and the bar graph shows the mean ± SEM. N=4 independent experiments. The BMAL1 knock-downs do not show significant change in local translation (one-way ANOVA, followed by Dunnet's multiple comparison test).

Supplementary Table 1. The Biological Process pathways determined by analyzing difference among the transcriptomes measured at different time points. We performed a gene set enrichment analysis by comparing the transcriptomes obtained at different time points, using the Webgestalt database (Wang et al., 2017). The table shows up to ten non-redundant Biological Process pathways whose p-value and false-discovery rate (FDR) were smaller than 0.05.

	Description	Normalized Enrichment Score
08:00 vs 14:00	ribonucleoprotein complex subunit organization	-1.92
	RNA splicing	-2
	ribonucleoprotein complex biogenesis	-2.32
08:00 vs 20:00	ribonucleoprotein complex biogenesis	-2.23
	axon development	1.94
	cell morphogenesis involved in differentiation	1.95
	dendrite development	1.93
	synapse organization	2
	semaphorin-plexin signaling pathway	1.9
	cell part morphogenesis	1.91
	synaptic transmission, glutamatergic	1.97
	regulation of neuron projection development	1.88
	neuron projection organization	1.86
08:00 vs 02:00	vesicle-mediated transport in synapse	1.96
	synaptic vesicle cycle	1.97
	glutamate receptor signaling pathway	1.97
	response to ammonium ion	2
	serotonin receptor signaling pathway	1.93
	amine transport	2.02
	regulation of trans-synaptic signaling	1.92
	response to anesthetic	1.92
	synaptic transmission, GABAergic	2.03
	regulation of postsynaptic membrane neurotransmitter receptor levels	1.9
20:00 vs 14:00	defense response to other organism	1.99
	cytokine-mediated signaling pathway	1.98
	endothelium development	1.97
	integrin-mediated signaling pathway	1.96
	leukocyte migration	1.91
	humoral immune response	1.85
02:00 vs 14:00	cell adhesion mediated by integrin	2.25
	cilium organization	2.16
	smoothened signaling pathway	2.06
	extracellular structure organization	2.05
	integrin-mediated signaling pathway	1.96
	embryonic morphogenesis	1.87
	skeletal system development	1.87
	connective tissue development	1.84
	cardiovascular system development	1.82
	skin development	1.8
02:00 vs 20:00	cilium organization	2.38
	smoothened signaling pathway	2.29
	amine transport	-2.23
	synaptic transmission, GABAergic	-2.42
	gamma-aminobutyric acid signaling pathway	-2.16
	synaptic vesicle cycle	-2.03
	neurotransmitter transport	-2.03
	regulation of neurotransmitter levels	-1.99
	acid secretion	-1.96
	response to amine	-2

5| General Discussion

The primary hippocampal culture is a powerful *in vitro* model. It simplifies the complicated nervous system. Although it is widely used, some features have not been studied thoroughly. Here, I present the first characterization of sex-specific and temporal dynamics in primary hippocampal cultures. First, I found that male neurons have higher electrical activity as well as synaptic translation than female neurons, although the female transcriptome was enriched in synaptic transmission related transcripts. Second, despite desynchronization in the molecular clock gene expression, I found rhythmicity in the electrical activity, synaptic dynamics and synaptic mRNA amounts in the primary hippocampal neurons. I also determined a candidate protein, RNA-binding motif 3 (RBM3), as a regulator of the rhythmic electrical activity through post-synaptic translation.

5.1| The primary hippocampal culture shows sex-specific behaviors

Sex-specific differentiation has been seen in primary hypothalamus cultures (Reisert et al., 1989). Despite reports on sexual differentiation in the hippocampus, the primary hippocampal culture has never been investigated thoroughly in this regard. In this work, I investigated the transcriptome and proteome profiles between the two sexes. Although synaptic transmission related transcripts were enriched in female neurons, I found that male neurons have higher spontaneous electrical activity and response capacity to electrical stimulations. These findings were followed up by studying the synaptic dynamics. I found that male neurons have a larger active synaptic vesicle pool and more dynamic synaptic transmission. Such functional differences led me to study the synaptic organization by performing a series of synaptic protein immunostainings. Female neurons showed enriched bassoon stainings, whereas the males had elevated Synaptophysin signal. To determine a mechanism behind these functional differences, I investigated the local translation rate at the synapse and found that local translation constitutes a greater proportion of the male synapse than females.

Sex specific differentiation results in higher electrical and synaptic translation rate in male than female primary hippocampal neurons.

There is an overwhelming evidence that sexual differentiation in the brain is beyond hypothalamus and it includes hippocampus. Within the estrogen cycle the number of synapses at the CA1 region has been found to be oscillating (Woolley et al., 1990). The mechanism is thought to be the estrogen-NMDA receptor interaction (McEwen and Milner, 2017). Nevertheless, not many described the spontaneous firing rate in the hippocampus. The first

attempt with *in vivo* recordings has reported that male hippocampal neurons have higher spontaneous firing rate than female neurons (Osada et al., 1991). Despite not having constant estrogen or testosterone inputs from gonads, primary hippocampal neurons show similar patterns to these findings. In this work, the male neurons exhibited greater electrical activity and response capacity to electrical stimulations. The investigation on synaptic dynamics supported the observation on electrical activity by reporting larger active synaptic vesicle pools and higher synaptic vesicle activity in the favor of male neurons. These results might point out a structural differentiation at the pre- and post-synaptic compartments.

Even though the transcriptome data revealed that female neurons are enriched with synaptic transmission-related transcripts, these transcripts have not been seen as differentially abundant in the proteome. The distribution of the proteins in a neuron might be sex-specific. Therefore, I surveyed the synaptic proteins between the two sexes.

Synaptic organization is similar between female and male neurons except for Synaptophysin, and Bassoon.

The transcriptome is a suggestion of how the proteomic topology might look like. In the transcriptomics data, I have identified several synaptic transmission-related transcripts that are enriched in the female culture. However, these transcripts were not found in the proteome as sex-specific proteins. One reason to that might be the translation efficiency. To initiate translation, various initiation and elongation factors are required. The availability of these factors can control the translation rate of mRNAs. Furthermore, the Y chromosome locates several elongation and translation factors that can influence the translation rate of certain mRNAs. The enhancer effect of Y chromosome linked translation factors can explain the difference between RNA and protein levels. Another problem might be the distribution of these mRNAs and proteins in the neuron. The soma in a pyramidal neuron constitutes a very small portion of the cell volume (Altemus et al., 2005), and it is difficult to differentiate the local contributions from whole-cell transcriptome and proteome. To tackle this problem, I used immunofluorescence stainings, which enable to study the localization and abundance of a protein of interest. I surveyed the numerous synaptic proteins in the primary hippocampal cultures and found two proteins that are differentially abundant in the synapse: Synaptophysin (Syph), and Bassoon.

It has been shown that male synapses are denser in the human cortical neurons (Rabinowicz et al., 1999) and male neurons exhibit more elaborate branching than female neurons in the rat primary hippocampal culture (Burke et al., 2017). These reports suggest that male neurons have more synapses than females.

Synaptophysin is a gene that is located on the X chromosome. Several allelic variants have been identified with mental retardation (Tarpey et al., 2009). Synaptophysin has been found in the synapse interacting with cholesterol and VAMP2 (Takamori et al., 2006b; Thiele et al., 2000). Its function is thought to be related to vesicle fusion and synaptic vesicle protein sorting during endocytosis (Kwon and Chapman, 2011; Stevens et al., 2012). In the sexually differentiated brain, recent studies with adult animals have reported that Synaptophysin is enriched in the female compared to male hippocampus tissue (Bian et al., 2012; Kokras et al., 2019). Despite identifying the Synaptophysin as a female enriched transcript as well as protein in the primary hippocampal culture, immunofluorescence has pointed out the opposite. The Synaptophysin intensity at the synapse appeared to be enriched in male cultures. This result can be an indication for the synapse size or the synaptic abundance of the Synaptophysin.

Bassoon is a scaffold protein at the presynaptic compartment. It is part of a complex that organizes the cytomatrix at the active zone where the neurotransmitters will be released (Garner et al., 2000). The bassoon knock-out studies indicate that bassoon is not essential for the synapse formation but for the neurotransmitter release regulation and fast recovery after the stimulation (Altrock et al., 2003; Fejtova et al., 2010; Frank et al., 2010). While female neurons exhibit smaller active synaptic vesicle pool and less calcium activity in the primary hippocampal culture, they have bassoon enriched synapses. It might be a compensation mechanism for having a smaller synaptic vesicle pool than male neurons.

Sex-specific hormone receptors can influence the activity via Adenyl cyclase and ERK signaling pathways.

Another way to influence the neuronal activity is the distribution of the sex-specific hormone receptors in the neurons. Many studies have shown that estrogen and androgen receptor distribution is sex and cell-type dependent (McEwen and Milner, 2007, 2017). There are two mechanisms of action for sex-specific hormones: genomic and non-genomic activation. Genomic or nuclear receptors act as a transcription factors and induce expression of certain genes, whereas non-genomic or non-nuclear receptors act in the adenyl cyclase and/or ERK signaling pathway. Comparing sex-specific receptors between the two sexes in the transcriptome and proteome data showed us that estrogen related receptor gamma is enriched in female cultures (**Table 1**). It is mainly responsible for the non-nuclear receptor action of estrogen receptors (Frick et al., 2015).

Table 1. The female to male difference folds of sex-specific receptors are shown in mRNA level and protein abundancy. The sex-specific receptors are lists with the female to male difference fold in log 2 scale. The colored rows indicate adjusted p-value is smaller than 0,05 and empty rows indicate the unidentified proteins in the iBAQ experiment.

Gene name	Protein	Description	RNAseq	iBAQ
Ar		androgen receptor	0,38	
Esr1	ERα	estrogen receptor 1	-0,80	
Esrra		estrogen related receptor, alpha	0,13	
Esrrb		estrogen related receptor beta	0,41	
Esrrg		estrogen related receptor gamma	0,51	
Pgr		progesterone receptor	0,28	
Pgrmc1		progesterone receptor membrane component 1	0,01	-1,44
Pgrmc2		progesterone receptor membrane component 2	0,04	-0,92

There are two main types of estrogen receptors (ERs): ERα and ERß. ERα has been localized on acetylcholinergic synapses, the nucleus of GABAergic neurons, and glia processes (Towart et al., 2003; Weiland et al., 1997), while ERß has been identified at the synapses of pyramidal neurons (Milner et al., 2005). As these receptors can be nuclear, their non-nuclear activity is thought to be the mechanism behind the fast reaction to estrogen treatments. It has been shown that estrogen can interact with NMDA receptor as well as activate the ERK and/or adenyl cyclase signaling pathway in the synapses to induce plasticity. As a result, estrogen treatment can lead to the phosphorylation of the cyclic AMP response element binding protein (CREB) (Pozzo-Miller et al., 1999; Wade and Dorsa, 2003; Zhou et al., 2005) and enhance the synaptic protein expression (Murphy and Segal, 1997; Zhao et al., 2005). Alternatively, estrogen has a similar influence as the brain derived neurotrophic factor (BDNF) (Scharfman et al., 2003). It has been reported that the activation of a tyrosine kinase, called tropomyosin receptor kinase ß (Trkß) (Brito et al., 2004; Carrer et al., 2003), is essential for the neuronal growth through estrogen treatment and a non-nuclear estrogen receptor has been shown to transactivate Trkß (Wang et al., 2018). These reports are suggesting that the estrogen receptors can induce plasticity at the synapse through local translation.

The primary cultures are prepared from animals that have not completed sexual differentiation. Today it is still unclear, how it reflects the neuron development in the culture. Even though cultures from female and male rats are exposed to the same concentration of progesterone hormone, they present sex-specific morphological and physiological differences (Heyer et al., 2005; Keil et al., 2017; Reisert et al., 1989). In many studies including this work, estrogen and androgen receptors have not been found to be differentially expressed (**Table 1**) (Heyer et al., 2005; Keil et al., 2017). However, the female enriched transcript *Esrrg* might promote the non-nuclear receptor action of estrogen receptors and influence the synaptic plasticity.

The sexually dimorphic synaptic plasticity might be induced by differential local translation rate in synapses.

As discussed in the previous subsection, sexual differentiation might be playing a crucial role in synaptic plasticity. The synaptic activation pattern can induce changes in the synaptic strength and these changes are referred as synaptic plasticity. Briefly, in the case of high firing rates, post-synaptic NMDA receptors are activated. This will lead to AMPA receptor placement on the post-synaptic membrane. As the potentiation is getting higher with the receptor activation and placement, the synapse activates production of more proteins via local translation. The local translation is essential for late-phase LTP (Kang and Schuman, 1996), which is thought to be the molecular mechanism of learning and memory. In this work, other than showing higher electrical activity in the male neurons, the local translation has been found to be sex-specific, with higher rates in male synapses. Such findings suggest that male synapses have greater strength in the primary hippocampal culture.

Understanding the molecular differentiation in the primary hippocampal culture is a step towards understanding sex-specific behavior.

There is a rapidly growing literature that describes the sex-biased prevalence and severity of neurodegenerative (Vegeto et al., 2020) and neurodevelopmental diseases (May et al., 2019). The sexual differentiation in the brain is the origin for such contrast. Starting from the hypothalamus, multiple brain regions, including the hippocampus, undergo sexual differentiation and contribute to the sex-specific behavior. Especially hippocampal dependent memory formation such as water-maze, radial arm and contextual fear conditioning present sex bias, even female mice have different performances depending on the estrous cycle. Keil et al (2017) has illustrated that the morphological differences in the primary hippocampal culture between two sex is relevant to tissue structure *in vivo* (Keil et al., 2017). This thesis has demonstrated differences in synaptic translation rates including global and synaptic activity. It might be due to the sex-specific activation of the ERK and Trkß pathways at the synapse. As further studies are necessary to draw this conclusion, it can explain the sex-specific hippocampus dependent memory performances.

5.2| The primary hippocampal culture demonstrates synchronized and rhythmic network behavior

The primary hippocampal neurons present rhythmicity in synaptic activity and mRNA amounts in synapses.

Every mammalian cell has a daily rhythmic gene expression. The common components of this rhythmicity are called the molecular clock. They control many biological functions through transcription and translation, such as electrical activity. The central pacemaker is the suprachiasmatic nucleus (SCN) of the hypothalamus. It sets an example of how daily firing pattern can be regulated by the molecular clock. However, our knowledge on other brain regions is limited. It is still in question whether the daily molecular landscape and neuronal firing pattern have similar principles as in the SCN. For example, it is known that learning and memory processes are regulated by the circadian clock. However, we do not fully understand the underlying regulatory mechanisms that are taking place in the main memory consolidation center, the hippocampus. Therefore, it is crucial to explore molecular and electrophysiological processes in other brain regions throughout the day. In this work, I studied the firing pattern of an average primary hippocampal neuron, and found rhythmic changes in global activity, synaptic vesicle dynamics, synapse size and synaptic mRNA amounts. Moreover, the transcriptome data revealed that RNA-binding motif 3 has a rhythmic gene expression and abundance in the primary hippocampal culture. By knocking-down RBM3 expression, drastic changes in global and synaptic activity have been found, and the cause has been demonstrated to be the decrease in the local translation rate in synapses.

The network activity helps to sustain a rhythmicity in the primary hippocampal culture.

In this thesis, the long-term calcium imaging pointed out that dissociated hippocampal neurons have a rhythmic firing pattern throughout the day. Moreover, I showed that neurons from different preparations have a similar rhythmic BMAL1 promoter activity. These findings suggest that primary hippocampal cultures maintain a rhythmicity with a weak synchronicity. Other preparations like explants and cell lines can also sustain daily rhythmicity in molecular clock gene expression without an external input, but they will slowly desynchronize from one another (Balsalobre et al., 1998; Yamazaki et al., 2000). Together with rapidly growing literature, it was clear that cultured cells can present daily rhythms only if they have an external stimulus such as serum shock (Balsalobre et al., 1998), temperature shock (Brown et al., 2002; Ohnishi et al., 2014) and glucocorticoid treatments (Balsalobre et al., 2000b; Yoo et al., 2004). One exception was dispersed neurons from the SCN tissue. Dispersed SCN cultures have presented individual but rhythmic firing patterns (Welsh et al., 1995). Having higher density in the culture helped them to have synchronicity, which was an indication that network activity is a major player in synchronization (Honma et al., 1998). Observations on desynchronizing acute and dispersed SCN cultures after prolonged tetrodotoxin (TTX) treatments showed how

essential the synaptic connections were (Honma et al., 2000; Yamaguchi et al., 2003). As SCN is a very-well studied brain region in terms of temporal dynamics, other brain regions have not been explored yet. For the first time here a daily behavior of a dissociated culture from the hippocampus has been investigated. Cultured neurons present rhythmic electrical firing pattern, synaptic activity and changes in mRNA amounts in the synapse. Despite lack of external stimuli, how do they maintain weak but synchronous rhythmicity? According to literature, the network is one of the most important factors.

Astrocytes could be also playing an important role for the culture synchronization.

As the biggest portion of the culture, astrocytes could be another key player for the culture synchronization. The glia cells make up ~70% of the culture. The gap junctions allow astrocytes to form a very strong network (Sul et al., 2004; Tian et al., 2006), and their ability to interact with up to thousands of synapses (Bushong et al., 2002; Halassa et al., 2007) show their potential as a synchronizer. Many studies have shown circadian behavior in astrocytes such as releasing ATP (Marpegan et al., 2011), and expressing neurotransmitter transporters (Spanagel et al., 2005) together with molecular clock genes (Tso et al., 2017). Recent study on astrocytes in the SCN has demonstrated that astrocytes have capacity to entrain the molecular clock gene expression, and therefore, firing pattern in the SCN (Brancaccio et al., 2019). These findings strongly suggest that glia cells in the primary hippocampal culture might also play an important role to generate a rhythmic behavior by buffering ions and regulating neurotransmitters at the synaptic cleft. In summary, synaptic connections and astrocytes might have major contribution to the rhythm generation in the primary hippocampal cultures.

5.3| RBM3 is a candidate protein for regulating the rhythmic neuronal activity through out the day

RBM3 has a rhythmic gene expression in the SCN in vivo and in the primary hippocampal culture.

In this work, it was shown that dissociated hippocampal neurons have a daily rhythm in mRNA amounts in synapses. To identify these mRNAs, mRNA sequencing was performed. In the time-series transcriptome, I have identified only one single transcript that has robust rhythmic expression, RBM3. Investigating RBM3 with immunostainings pointed out that there are also rhythmic changes in the RBM3 abundance at synapses. The rhythmic gene expression of RBM3 has not been reported for the first time here. Many studies have demonstrated RBM3 has a circadian expression *in vivo* in the SCN, although their focus was not on RBM3 (Pembroke et al., 2015) and several more tissues (Almon, Richard R.; Yang, Eric; Lai, William; Androulakis, Ioannis P.; DuBois, Debra C.; Jusko, 2008; Terajima et al., 2017; Yan et al., 2008; Zhang et al., 2014). RBM3 was also found as a circadian transcript in the hippocampus tissue (Renaud et al., 2015). Observations on a rhythmic RBM3 expression *in vivo* suggests that dissociated hippocampal neurons preserve their circadian behavior in the primary culture.

RBM3 is regulating the pre- and postsynaptic activity through postsynaptic translation

RBM3 is a cold shock protein (Danno et al., 1997, 2000), which indicates its expression is induced by hypothermia. The rhythmic expression of RBM3 could be an evolutionary advantage for anticipating the temperature changes in the environment and the body. Recent studies have illustrated the neuroprotective contribution of RBM3. The synaptic stability can be sustained and apoptosis can be inhibited in neurodegenerative animal models (Peretti et al., 2015) and hypoxic conditions (Chip et al., 2011; Rosenthal et al., 2017; Yan et al., 2019) with the RBM3. In this work, it was shown that RBM3 abundance in synapses increases steadily after 20:00. It might be an indication that in the circadian system, RBM3 could anticipate the temperature change and impel the synapse.

Knocking down RBM3 pointed out that RBM3 can influence the pre- and postsynaptic activity. There are several functions for an RNA-binding protein such as polyadenylation, splicing, mRNA transport and translation. The literature on RBM3 suggests that the mechanism of action for RBM3 in synapses is promoting translation. Reports on interactions between ribosomal proteins (Smart et al., 2007b) and RBM3, increase in phosphorylation of eukaryotic translation initiation factors and the poly-ribosome complexes (Dresios et al., 2005) upon RBM3 overexpression suggests that as hypothermia halts the global translation, RBM3

induces protective mRNA translation. Here I demonstrated that RBM3 regulates the explicitly post-synaptic local translation. Overall, these observations suggest that daily rhythmic abundance of RBM3 regulates the local translation rate in post-synapses, and hence synaptic activity.

RBM3 contributes to the synaptic plasticity by promoting local translation

The synaptic plasticity is a dynamic process where synapse strength is arranged according to the synaptic activity. Extremely long arbors of a neuron (Ishizuka et al., 1995) do not allow the cell body to produce and transport proteins to distal parts fast enough. The local translation in synapses is therefore essential for a neuron. The translational machinery has been identified in synapses: polyribosomes (Ostroff et al., 2018; Steward and Levy, 1982), translation initiation and elongation factors (Steward and Levy, 1982; Sutton and Schuman, 2006; Tiedge and Brosius, 1996). Moreover, a study demonstrated how abundant the local translation in synapses is (Hafner et al., 2019). Recently, an investigation on the comparison between circadian transcriptome and proteome of the forebrain synaptosome showed that the sleep-wake cycle drives the rhythmic translation of transcripts (Noya et al., 2019). RNA-binding proteins and translation machinery contributes to the global proteome with local translation in synapses. In primary hippocampal culture, I identified an RNA-binding protein RBM3 whose abundance in synapses changes throughout the day. Knocking-down RBM3 has influenced the local translation rate but not the mRNA amount in synapses. These findings suggest that RBM3 does not transport mRNAs to synapses, but it regulates the local translation rate and therefore, synaptic plasticity.

5.4| Shortcomings of the technology that is used

As mRNA sequencing and mass-spectrometry rely on different technologies, it is challenging to combine the two datasets.

mRNA sequencing and mass-spectrometry are both very powerful techniques; however, they rely on two distinct technologies. mRNA sequencing is based on fast imaging of 50 basepair reads in a truncated RNA sequence. After the imaging session, the reads are aligned to a genome and calculated how many transcripts were identified. On the other hand, the iBAQ technique is based on mass-spectrometry. Truncated proteins are mixed with few polypeptides, whose sequences and concentrations are known. The samples will fly according to their mass/charge ratio and it allows us to calculate accurately how many proteins were in that sample. The first thing that draws our attention in a comparison between transcriptome and proteome is the coverage values (Figure 1). mRNA sequencing has identified 13835 transcripts whereas proteomics data has only 1657 proteins.

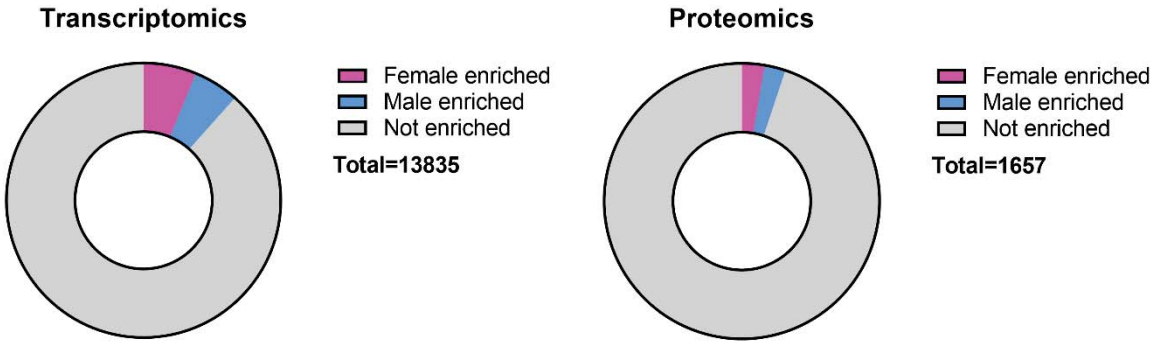

Figure 1. Mismatch between the number of identified transcripts and proteins due to technical challenges. The circles represent the total number of identified transcripts (left) and proteins (right). The colors as shown in the legend; pink is for female, blue is for male enriched transcripts and proteins. The portion of the colored parts suggest the portion of the enriched transcripts and proteins.

Moreover, the sex-specific transcripts have either not found or not shown the same trend. **Table 1** illustrates significantly enriched transcripts and proteins that are identified in both datasets, (N=24). The colored rows indicate the similar enrichment across the two techniques (N=13). It is not possible to conclude a gene set enrichment study with such small number of identified transcripts/proteins.

Table 1. The significantly enriched transcripts/proteins in both datasets do show similar expression and/or abundance profile. The significantly enriched transcripts/proteins are listed. RNAseq and iBAQ columns indicate the log2 scale of male to female ratio of transcriptomics and proteomics dataset, respectively. Blue is for male enrichment and pink is for female enrichment.

Gene symbol	Description	RNAseq	iBAQ
Pbxip1	PBX homeobox interacting protein 1	0,89	0,514508
Phgdh	phosphoglycerate dehydrogenase	0,64	0,20549
Atic	5-aminoimidazole-4-carboxamide ribonucleotide formyltransferase/IMP cyclohydrolase	0,35	0,371643
Hnrnpk	heterogeneous nuclear ribonucleoprotein K	0,29	0,123818
Itm2c	integral membrane protein 2C	0,38	0,623169
Rap1b	RAP1B, member of RAS oncogene family	0,28	0,23043
Cct5	chaperonin containing TCP1 subunit 5	0,26	0,156549
Eef1d	eukaryotic translation elongation factor 1 delta	0,41	0,210775
Sfxn5	sideroflexin 5	0,75	0,603598
Prdx4	peroxiredoxin 4	0,53	0,729555
Cstb	cystatin B	0,33	-0,33037
Fis1	fission, mitochondrial 1	0,32	-0,72266
Tmed2	transmembrane p24 trafficking protein 2	0,35	-0,48741
Psmc4	proteasome 26S subunit, ATPase 4	0,24	-0,40286
Reep5	receptor accessory protein 5	-0,61	-0,81655
Stxbp1	syntaxin binding protein 1	-1,23	-0,88866
Hnrnpd	heterogeneous nuclear ribonucleoprotein D	-0,91	-0,20506
Atp1b1	ATPase Na+/K+ transporting subunit beta 1	-0,52	0,248165
Psma3	proteasome subunit alpha 3	-0,34	0,257176
Uso1	USO1 vesicle transport factor	-0,24	0,461812
Tuba1a	tubulin, alpha 1A	-0,51	0,364783
Wasf1	WAS protein family, member 1	-2,46	0,508245
Rtn3	reticulon 3	-0,9	0,510715
Rac1	ras-related C3 botulinum toxin substrate 1	-0,22	0,259821

Primary hippocampal cultures constitute of glia cells and neurons.

Another limitation of such high-throughput datasets is the contamination with non-neuronal cells. Primary hippocampal cultures do not only have hippocampal neurons but also glia cells. It is possible to control the number of neurons in the culture, but it is almost impossible to control the number of seeded glia and its growth. They are not visible under the light microscope. It is, therefore, not easy to plate same number of glia cells on the coverslip. To control the growth of glia cells, a basal medium is used in this work. This medium is specialized for the neuron growth but not for glia. Yet, it is still possible to have different number of glia cells in the mature culture. This can reflect on the transcriptomics and proteomics data as well.

Table 2 shows the expression and abundance of glia specific protein (glia fibrillary acidic protein, GFAP) and neuron specific protein (tubulin beta 3, Tubb3). Nevertheless, these values are not showing any significant difference between female and male cultures, which is also suggesting that glia cells have a similar contribution to cultures from both sexes.

Table 2. The number of glia and neuron do not show significant difference across female and male hippocampal cultures. The glia biomarker (glia fibrillary acidic protein (GFAP)) and neuronal biomarker (tubulin beta 3 (Tubb3)) are shown in transcriptomics, proteomics and immunostaining datasets with the log2 scale of female to male ratio. The values do not indicate a statistically significant difference.

Gene symbol	RNAseq	iBAQ	IF
GFAP	0,09	-0,56	-0,11
Tubb3	0,53	0,66	0,02

Cholesterol metabolism is the next likely candidate for circadian behavior.

In this work, I present rhythmic changes in the mRNA amount at the synapse. To identify these mRNAs, I took advantage of mRNA sequencing. Despite the lack of external input, I have identified one single transcript that has robust rhythmic expression: RNA-binding motif 3 (RBM3). However, if the data was treated less strict and grouped the first 5‰ transcripts that are most likely to have rhythmicity, steroid metabolism related transcripts would have been enriched (**Table 3**). It is important to remember that these transcripts can be expressed in the glia cells as well. A closer look on expression profiles indicates similar patterns either to the RBM3 transcript or to the protein abundance of RBM3 (**Figure 2**).

What is the best way to analyze a time-series dataset? The research on circadian analysis methods is still ongoing. It is easy to detect high amplitude rhythms in a dataset. However, my time-series mRNA sequencing data was challenging to analyze. One problem, I encountered, is high variations between cultures. Secondly, the culture is not fully synchronized in terms of molecular clock. These two problems dampen the amplitude of an expression profile. Therefore, it is difficult to detect robust rhythmicity in the time-series transcriptome. Yet I applied bonferroni correction as a multiple-comparison test. The bonferroni correction is a very strict correction method. In such a big dataset, applying this correction might not be the best approach to analyze a time-series dataset. To explore the data more, I rearranged it according to adjusted p-values of transcripts, which is an indication for their rhythms.

Table 3. The steroid metabolic process is enriched in the time-series mRNA sequencing data. The time-series mRNA sequencing data was treated less strict and listed the transcripts according to adjusted p-values. To identify whether there is an enriched pathway, 5‰ transcripts (72 transcripts) with the smallest p-values were analyzed in the Webgestalt with the overrepresentation analysis. The p-value and FDR value are less than 0.05 as shown in the table.

Gene Ontology	Gene Symbol	Gene Name	p-value	FDR
Steroid metabolic process	Srebf2	sterol regulatory element binding transcription factor 2	0,000	0,005
	Sc5d	sterol-C5-desaturase		
	Sqle	squalene epoxidase		
	Mvd	mevalonate diphosphate decarboxylase		
	Hmgcs1	3-hydroxy-3-methylglutaryl-CoA synthase 1		
	Abca1	ATP binding cassette subfamily A member 1		
	Stard4	StAR-related lipid transfer domain containing 4		

Nevertheless, if the data was treated less strictly, it would be possible to find steroid metabolic process as an enriched pathway. It can be important for the energy and cholesterol metabolism. The steroid metabolic process has been described as a circadian pathway mainly in the liver tissue (Reinke and Asher, 2016). However, it has been also shown to be a part of the energy metabolism in the central nervous system (Ding et al., 2018). we need further studies to understand the rhythmic behavior of the steroid metabolism in hippocampal neurons.

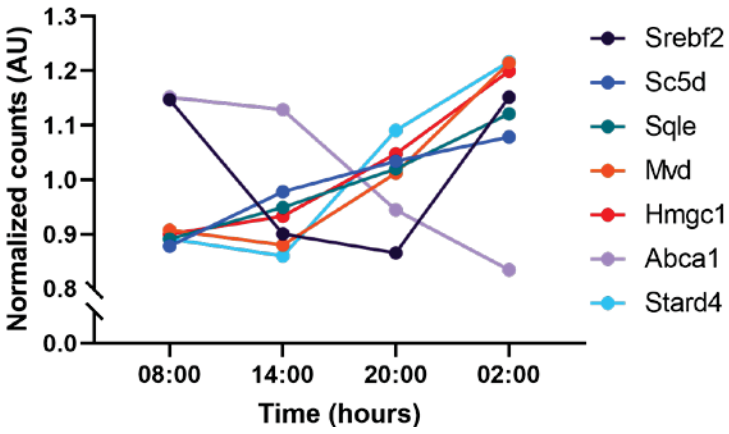

Figure 2. Expression profiles of seven transcripts that are part of the steroid metabolic process. Seven transcripts among 72 transcripts, which are the most likely to be daily rhythmic, are enriched in the steroid metabolic process. The graph shows the normalized count values of each transcript. Each colored line represents one transcript and the colormap is on the right side.

5.5| Outlook

SRY::GFP plasmid can be a useful tool to study sexual differentiation in a female-male mixed culture.

SRY is a sex-determining region Y protein. As it is explained in the introduction, it is essential for the masculinization of the fetus. I would like to design a new plasmid which has an *SRY* promoter and an enhanced-GFP sequence in the downstream. This plasmid will allow me to investigate sex-specific functional and morphological differences in a female-male mixed hippocampal culture.

Understainding sexual differentiation in the hippocampus might explain the sex-biased diseases such as Alzheimer's disease (AD).

Many studies have reported that memory performance is sex-dependent (Koss and Frick, 2017). The molecular studies have tried to explain these differences by investigating the neuron morphology (Keil et al., 2017) and sex-specific receptors (McEwen and Milner, 2017) in the hippocampus. These research contributes to our knowledge on neurodevelopmental and neurodegenerative diseases such as Alzheimer's disease (AD) and autism spectrum disorder (ASD) (Yagi and Galea, 2019). Other than showing sex-bias in prevalence, onset and severity, these diseases also show disturbances in memory performances. Therefore, it is important to understand sexual differentiation in the hippocampus.

The primary hippocampal culture is providing a great advantage for investigating molecular differences between the two sexes as well as therapeutic strategies. A comparison between our primary hippocampal cultures and any disease model might explain the mechanism behind the sex-dependendence. A study on aging with primary hippocampal cultures in relevance to our results can provide insights into how neurodegeneration develops. Our systematic investigation on sexual differentiation in primary hippocampal cultures can be a basis for any research on sex-biased disease.

Finding mRNA targets of RBM3 might reveal the mechanism for the neuroprotection.

A study on cold-shock proteins reveal that RBM3 regulates the alternative polyadenylation of molecular clock genes (Liu et al., 2013). They shared an mRNA list which have been found to bind RBM3 protein. They also shared an mRNA sequencing data for wildtype and RBM3 knock-down mouse embryonic fibroblasts. Combining these two datasets reveals possible mRNA targets of RBM3. There are axonal growth transcripts, cholesterol metabolism related

transcripts like a*bca5, acsl4, far1,* and *cav*2, and synaptic plasticity related transcripts such as *rhob, egr1, creb1* and *tlr4.* However, these experiments were performed on mouse embryonic fibroblasts. To understand the effects of RBM3 on hippocampal neurons, it would be exciting to repeat such experiments with our cultures and identify mRNAs whose translation is promoted by RBM3.

Since the influence of RBM3 in neuroprotection has been reported in many studies, researchers have started to explore RBM3 as a treatment for hypoxia and neurodegenerative diseases (Jackson and Kochanek, 2019; Rosenthal et al., 2017; Sureban et al., 2008; Yan et al., 2019; Zhu et al., 2019). As RBM3 plays an important role in neuroprotection, knowing target mRNAs can explain the mechanism of action for RBM3, and hence it can be used as a treatment for hypoxia or neurodegeneration diseases.

6| References

Almon, Richard R.; Yang, Eric; Lai, William; Androulakis, Ioannis P.; DuBois, Debra C.; Jusko, W.J. (2008). Circadian Variations in Liver Gene Expression: Relationships to Drug Actions. J Pharmacol Exp Ther. 700–716.

Altemus, K.L., Lavenex, P., Ishizuka, N., and Amaral, D.G. (2005). Morphological characteristics and electrophysiological properties of CA1 pyramidal neurons in macaque monkeys. Neuroscience *136*, 741–756.

Altrock, W.D., Tom Dieck, S., Sokolov, M., Meyer, A.C., Sigler, A., Brakebusch, C., Fässler, R., Richter, K., Boeckers, T.M., Potschka, H., et al. (2003). Functional inactivation of a fraction of excitatory synapses in mice deficient for the active zone protein bassoon. Neuron *37*, 787–800.

Aton, S.J., Colwell, C.S., Harmar, A.J., Waschek, J., and Herzog, E.D. (2005). Vasoactive intestinal polypeptide mediates circadian rhythmicity and synchrony in mammalian clock neurons. Nat. Neurosci. *8*, 476–483.

Balsalobre, A., Damiola, F., Schibler, U., and Gene, C.- (1998). A Serum Shock Induces Circadian Gene Expression in Mammalian Tissue Culture Cells. Cell *93*, 929–937.

Balsalobre, A., Marcacci, L., and Schibler, U. (2000a). Multiple signaling pathways elicit circadian gene expression in cultured Rat-1 fibroblasts. Curr. Biol. *10*, 1291–1294.

Balsalobre, A., Brown, S.A., Marcacci, L., Tronche, F., Kellendonk, C., Reichardt, H.M., Schutz, G., and Schibler, U. (2000b). Resetting of circadian time in peripheral tissues by glucocorticoid signaling. Science (80-.). *289*, 2344–2347.

Banker, G.A., and Cowan, W.M. (1977). Rat hippocampal neurons in dispersed cell culture. Brain Res. *126*, 397–425.

Barnes, C.A., McNaughton, B.L., Goddard, G. V, Douglas, R.M., and Adamec, R. (1977). Circadian rhythm of synaptic excitability in rat and monkey central nervous system. Science *197*, 91–92.

Benson, D.L., Watkins, F.H., Steward, O., and Banker, G. (1994). Characterization of GABAergic neurons in hippocampal cell cultures. J. Neurocytol. *23*, 279–295.

Besing, R.C., Rogers, C.O., Paul, J.R., Hablitz, L.M., Johnson, R.L., McMahon, L.L., and Gamble, K.L. (2017). GSK3 activity regulates rhythms in hippocampal clock gene expression and synaptic plasticity. Hippocampus *27*, 890–898.

Bian, C., Zhu, K., Guo, Q., Xiong, Y., Cai, W., and Zhang, J. (2012). Sex differences and

synchronous development of steroid receptor coactivator-1 and synaptic proteins in the hippocampus of postnatal female and male C57BL/6 mice. Steroids *77*, 149–156.

Bowman, R.E., Beck, K.D., and Luine, V.N. (2003). Chronic stress effects on memory: Sex differences in performance and monoaminergic activity. Horm. Behav. *43*, 48–59.

Brancaccio, M., Edwards, M.D., Patton, A.P., Smyllie, N.J., Chesham, J.E., Maywood, E.S., and Hastings, M.H. (2019). Cell-autonomous clock of astrocytes drives circadian behavior in mammals. Science (80-.). *363*, 187–192.

Brewer, G.J. (1995). Serum-free B27/neurobasal medium supports differentiated growth of neurons from the striatum, substantia nigra, septum, cerebral cortex, cerebellum, and dentate gyrus. J. Neurosci. Res. *42*, 674–683.

Brewer, G.J., Torricelli, J.R., Evege, E.K., and Price, P.J. (1993). Optimized survival of hippocampal neurons in B27-supplemented Neurobasal, a new serum-free medium combination. J. Neurosci. Res. *35*, 567–576.

Brito, V.I., Carrer, H.F., and Cambiasso, M.J. (2004). Inhibition of tyrosine kinase receptor type B synthesis blocks axogenic effect of estradiol on rat hypothalamic neurones in vitro. Eur. J. Neurosci. *20*, 331–337.

Brown, S.A., Zumbrunn, G., Fleury-Olela, F., Preitner, N., and Schibler, U. (2002). Rhythms of mammalian body temperature can sustain peripheral circadian clocks. Curr. Biol. *12*, 1574–1583.

Buijs, R.M., Scheer, F.A., Kreier, F., Yi, C., Bos, N., Goncharuk, V.D., and Kalsbeek, A. (2006). Organization of circadian functions: interaction with the body. Prog. Brain Res. *153*, 341–360.

Burke, S.M., Manzouri, A.H., and Savic, I. (2017). Structural connections in the brain in relation to gender identity and sexual orientation. Sci. Rep. *7*, 1–12.

Bushong, E.A., Martone, M.E., Jones, Y.Z., and Ellisman, M.H. (2002). Protoplasmic astrocytes in CA1 stratum radiatum occupy separate anatomical domains. J. Neurosci. *22*, 183–192.

Carrel, A. (1923). Method for the physiological study of tissues in vitro. J. Exp. Med. *38*, 407–418.

Carrer, H.F., Cambiasso, M.J., Brito, V., and Gorosito, S. (2003). Neurotrophic Factors and Estradiol Interact to Control Axogenic Growth in Hypothalamic Neurons. In Annals of the New York Academy of Sciences, (New York Academy of Sciences), pp. 306–316.

Cauller, L.J., Boulos, Z., and Goddard, G. V. (1985). Circadian rhythms in hippocampal responsiveness to perforant path stimulation and their relation to behavioral state. Brain Res. *329*, 117–130.

Chappell, S.A., Owens, G.C., and Mauro, V.P. (2001). A 5′ Leader of Rbm3, a Cold Stress-induced mRNA, Mediates Internal Initiation of Translation with Increased Efficiency under Conditions of Mild Hypothermia. J. Biol. Chem. *276*, 36917–36922.

Chaudhury, D., Wang, L.M., and Colwell, C.S. (2005). Circadian regulation of hippocampal long-term potentiation. J. Biol. Rhythms *20*, 225–236.

Chip, S., Zelmer, A., Ogunshola, O.O., Felderhoff-Mueser, U., Nitsch, C., Bührer, C., and Wellmann, S. (2011). The RNA-binding protein RBM3 is involved in hypothermia induced neuroprotection. Neurobiol. Dis. *43*, 388–396.

Chou, C.C., Zhang, Y., Umoh, M.E., Vaughan, S.W., Lorenzini, I., Liu, F., Sayegh, M., Donlin-Asp, P.G., Chen, Y.H., Duong, D.M., et al. (2018). TDP-43 pathology disrupts nuclear pore complexes and nucleocytoplasmic transport in ALS/FTD. Nat. Neurosci. *21*, 228–239.

Chow, J.C., Yen, Z., Ziesche, S.M., and Brown, C.J. (2005). Silencing of the Mammalian X Chromosome. Annu. Rev. Genomics Hum. Genet. *6*, 69–92.

Chowen, J.A., Freire-Regatillo, A., and Argente, J. (2018). Neurobiological characteristics underlying metabolic differences between males and females. Prog. Neurobiol.

Chun, L.E., Woodruff, E.R., Morton, S., Hinds, L.R., and Spencer, R.L. (2015). Variations in phase and amplitude of rhythmic clock gene expression across prefrontal cortex, hippocampus, amygdala, and hypothalamic paraventricular and suprachiasmatic nuclei of male and female rats. J. Biol. Rhythms *30*, 417–436.

Citri, A., and Malenka, R.C. (2008). Synaptic plasticity: multiple forms, functions, and mechanisms. Neuropsychopharmacology *33*, 18–41.

Colwell, C.S. (2000). Rhythmic coupling among cells in the suprachiasmatic nucleus. J. Neurobiol. *43*, 379–388.

Colwell, C.S. (2011). Linking neural activity and molecular oscillations in the SCN. Nat. Rev. Neurosci. *12*, 553–569.

Costanzi, C., and Pehrson, J.R. (1998). Histone macroH2A1 is concentrated in the inactive X chromosome of female mammals. Nature *393*, 599–601.

Cox, J., and Mann, M. (2008). MaxQuant enables high peptide identification rates, individualized p.p.b.-range mass accuracies and proteome-wide protein quantification. Nat.

Biotechnol. *26*, 1367–1372.

Cox, J., Neuhauser, N., Michalski, A., Scheltema, R.A., Olsen, J. V., and Mann, M. (2011). Andromeda: A peptide search engine integrated into the MaxQuant environment. J. Proteome Res. *10*, 1794–1805.

Danno, S., Nishiyama, H., Higashitsuji, H., Yokoi, H., Xue, J.H., Itoh, K., Matsuda, T., and Fujita, J. (1997). Increased transcript level of RBM3, a member of the glycine-rich RNA-binding protein family, in human cells in response to cold stress. Biochem. Biophys. Res. Commun. *236*, 804–807.

Danno, S., Itoh, K., Matsuda, T., and Fujita, J. (2000). Decreased expression of mouse Rbm3, a cold-shock protein, in Sertoli cells of cryptorchid testis. Am. J. Pathol. *156*, 1685–1692.

Dibner, C., Schibler, U., and Albrecht, U. (2010). The mammalian circadian timing system: organization and coordination of central. Annu. Rev. Physiol. *72*, 517–549.

Ding, G., Gong, Y., Eckel-Mahan, K.L., and Sun, Z. (2018). Central circadian clock regulates energy metabolism. In Advances in Experimental Medicine and Biology, (Springer New York LLC), pp. 79–103.

Dobin, A., Davis, C.A., Schlesinger, F., Drenkow, J., Zaleski, C., Jha, S., Batut, P., Chaisson, M., and Gingeras, T.R. (2013). STAR: Ultrafast universal RNA-seq aligner. Bioinformatics *29*, 15–21.

Doherty, C.J., and Kay, S.A. (2010). Circadian Control of Global Gene Expression Patterns. Annu. Rev. Genet. *44*, 419–444.

Döhler, K.D., Coquelin, A., Davis, F., Hines, M., Shryne, J.E., and Gorski, R.A. (1982). Differentiation of the sexually dimorphic nucleus in the preoptic area of the rat brain is determined by the preinatal hormone environment. Neurosci. Lett. *33*, 295–298.

Dotti, C.G., Sullivan, C.A., and Banker, G.A. (1988). The establishment of polarity by hippocampal neurons in culture. J. Neurosci. *8*, 1454–1468.

Dresios, J., Aschrafi, A., Owens, G.C., Vanderklish, P.W., Edelman, G.M., and Mauro, V.P. (2005). Cold stress-induced protein Rbm3 binds 60S ribosomal subunits, alter microRNA levels, and enhances global protein synthesis. Proc. Natl. Acad. Sci. U. S. A. *102*, 1865–1870.

Eagle, H. (1955). Nutrition needs of mammalian cells in tissue culture. Science (80-.). *122*, 501–504.

Eagle, H. (1959). Amino acid metabolism in mammalian cell cultures. Science (80-.). *130*, 432–437.

van Esseveldt, K.E., Lehman, M.N., and Boer, G.J. (2000). The suprachiasmatic nucleus and the circadian time-keeping system revisited. Brain Res. Brain Res. Rev. *33*, 34–77.

Fejtova, A., Schmidt, H., Weyhersmüller, A., Silver, R.A., Gundelfinger, E.D., and Eilers, J. (2010). Bassoon speeds vesicle reloading at a central excitatory synapse. Neuron *68*, 710–723.

Foy, M.R., Xu, J., Xie, X., Brinton, R.D., Thompson, R.F., and Berger, T.W. (1999). 17β-estradiol enhances NMDA receptor-mediated EPSPs and long-term potentiation. J. Neurophysiol. *81*, 925–929.

Frank, T., Rutherford, M.A., Strenzke, N., Neef, A., Pangršič, T., Khimich, D., Fetjova, A., Gundelfinger, E.D., Liberman, M.C., Harke, B., et al. (2010). Bassoon and the synaptic ribbon organize Ca2+ channels and vesicles to add release sites and promote refilling. Neuron *68*, 724–738.

Freeman, M.R., and Rowitch, D.H. (2013). Evolving concepts of gliogenesis: A look way back and ahead to the next 25 years. Neuron *80*, 613–623.

Frick, K.M., Kim, J., Tuscher, J.J., and Fortress, A.M. (2015). Sex steroid hormones matter for learning and memory: Estrogenic regulation of hippocampal function in male and female rodents. Learn. Mem. *22*, 472–493.

Fugger, H.N., Kumar, A., Lubahn, D.B., Korach, K.S., and Foster, T.C. (2001). Examination of estradiol effects on the rapid estradiol mediated increase in hippocampal synaptic transmission in estrogen receptor α knockout mice. Neurosci. Lett. *309*, 207–209.

Garner, C.C., Kindler, S., and Gundelfinger, E.D. (2000). Molecular determinants of presynaptic active zones. Curr. Opin. Neurobiol. *10*, 321–327.

Gegenhuber, B., and Tollkuhn, J. (2020). Signatures of sex: Sex differences in gene expression in the vertebrate brain. Wiley Interdiscip. Rev. Dev. Biol. *9*, 1–27.

Gekakis, N., Staknis, D., Nguyen, H.B., Davis, F.C., Wilsbacher, L.D., King, D.P., Takahashi, J.S., and Weitz, C.J. (1998). Role of the CLOCK protein in the mammalian circadian mechanism. Science *280*, 1564–1569.

Gerstner, J.R., and Yin, J.C.P. (2010). Circadian rhythms and memory formation. Nat. Rev. Neurosci. *11*, 577–588.

Green, D.J., and Gillette, R. (1982). Circadian rhythm of firing rate recorded from single cells

in the rat suprachiasmatic brain slice. Brain Res. *245*, 198–200.

Gu, Q., and Moss, R.L. (1996). 17β-Estradiol potentiates kainate-induced currents via activation of the cAMP cascade. J. Neurosci. *16*, 3620–3629.

Gu, Q., Korach, K.S., and Moss, R.L. (1999). Rapid action of 17β-estradiol on kainate-induced currents in hippocampal neurons lacking intracellular estrogen receptors. Endocrinology *140*, 660–666.

Guilding, C., and Piggins, H.D. (2007). Challenging the omnipotence of the suprachiasmatic timekeeper: are circadian oscillators present throughout the mammalian brain? Eur. J. Neurosci. *25*, 3195–3216.

Gutman, R., Genzer, Y., Chapnik, N., Miskin, R., and Froy, O. (2011). Long-lived mice exhibit 24 h locomotor circadian rhythms at young and old age. Exp. Gerontol. *46*, 606–609.

Hafner, A.S., Donlin-Asp, P.G., Leitch, B., Herzog, E., and Schuman, E.M. (2019). Local protein synthesis is a ubiquitous feature of neuronal pre- And postsynaptic compartments. Science (80-.). *364*.

Halassa, M.M., Fellin, T., and Haydon, P.G. (2007). The tripartite synapse: roles for gliotransmission in health and disease. Trends Mol. Med. *13*, 54–63.

Harbour, V.L., Weigl, Y., Robinson, B., and Amir, S. (2014). Phase differences in expression of circadian clock genes in the central nucleus of the amygdala, dentate gyrus, and suprachiasmatic nucleus in the rat. PLoS One *9*.

Harris, K.M., and Teyler, T.J. (1983). Age differences in a circadian influence on hippocampal LTP. Brain Res. *261*, 69–73.

Harrison, R.G., Greenman, M.J., Mall, F.P., and Jackson, C.M. (1907a). Observations of the living developing nerve fiber. Anat. Rec. *1*, 116–128.

Harrison, R.G., Greenman, M.J., Mall, F.P., and Jackson, C.M. (1907b). Observations of the living developing nerve fiber. Anat. Rec. *1*, 116–128.

Hastings, M.H., Reddy, A.B., and Maywood, E.S. (2003). A clockwork web: circadian timing in brain and periphery, in health and disease. Nat. Rev. Neurosci. *4*, 649–661.

Hendrickson, A.E., Wagoner, N., and Cowan, W.M. (1972). An autoradiographic and electron microscopic study of retino-hypothalamic connections. Zeitschrift Für Zellforsch. Und Mikroskopische Anat. (Vienna, Austria 1948) *135*, 1–26.

Herzog, E.D., Takahashi, J.S., and Block, G.D. (1998). Clock controls circadian period in isolated suprachiasmatic nucleus neurons. Nat. Neurosci. *1*, 708–713.

Heyer, A., Hasselblatt, M., von Ahsen, N., Häfner, H., Sirén, A.-L., and Ehrenreich, H. (2005). *In vitro* Gender Differences in Neuronal Survival on Hypoxia and in 17β-Estradiol-Mediated Neuroprotection. J. Cereb. Blood Flow Metab. *25*, 427–430.

Hojo, Y., and Kawato, S. (2018). Neurosteroids in adult hippocampus of male and female rodents: Biosynthesis and actions of sex steroids. Front. Endocrinol. (Lausanne). *9*, 183.

Holt, C.E., Martin, K.C., and Schuman, E.M. (2019). Local translation in neurons: visualization and function. Nat. Struct. Mol. Biol. *26*, 557–566.

Honma, S., Shirakawa, T., Katsuno, Y., Namihira, M., and Honma, K.I. (1998). Circadian periods of single suprachiasmatic neurons in rats. Neurosci. Lett. *250*, 157–160.

Honma, S., Shirakawa, T., Nakamura, W., and Honma, K.I. (2000). Synaptic communication of cellular oscillations in the rat suprachiasmatic neurons. Neurosci. Lett. *294*, 113–116.

Imahori, K., and Uchida, T. (1997). Physiology and pathology of tau protein kinases in relation to Alzheimer's disease. J. Biochem. *121*, 179–188.

Inouye, S.T., and Kawamura, H. (1979). Persistence of circadian rhythmicity in a mammalian hypothalamic "island" containing the suprachiasmatic nucleus. Proc. Natl. Acad. Sci. U. S. A. *76*, 5962–5966.

Ishizuka, N., Cowan, W.M., and Amaral, D.G. (1995). A quantitative analysis of the dendritic organization of pyramidal cells in the rat hippocampus. J. Comp. Neurol. *362*, 17–45.

Jackson, T.C., and Kochanek, P.M. (2019). A New Vision for Therapeutic Hypothermia in the Era of Targeted Temperature Management: A Speculative Synthesis. Ther. Hypothermia Temp. Manag. *9*, 13–47.

Jacobson, C.D., and Gorski, R.A. (1981). Neurogenesis of the sexually dimorphic nucleus of the preoptic area in the rat. J. Comp. Neurol. *196*, 519–529.

Jacobson, C.D., Shryne, J.E., Shapiro, F., and Gorski, R.A. (1980). Ontogeny of the sexually dimorphic nucleus of the preoptic area. J. Comp. Neurol. *193*, 541–548.

Jiang, Z.G., Yang, Y.Q., and Allen, C.N. (1997). Tracer and electrical coupling of rat suprachiasmatic nucleus neurons. Neuroscience *77*, 1059–1066.

Jilg, A., Lesny, S., Peruzki, N., Schwegler, H., Selbach, O., Dehghani, F., and Stehle, J.H. (2010). Temporal dynamics of mouse hippocampal clock gene expression support memory processing. Hippocampus *20*, 377–388.

Jones, K.J., Templet, S., Zemoura, K., Kuzniewska, B., Pena, F.X., Hwang, H., Lei, D.J., Haensgen, H., Nguyen, S., Saenz, C., et al. (2018). Rapid, experience-dependent translation

of neurogranin enables memory encoding. Proc. Natl. Acad. Sci. U. S. A. *115*, E5805–E5814.

Kaech, S., and Banker, G. (2006). Culturing hippocampal neurons. Nat. Protoc. *1*, 2406–2415.

Kang, H., and Schuman, E.M. (1996). A requirement for local protein synthesis in neurotrophin-induced hippocampal synaptic plasticity. Science (80-.). *273*, 1402–1406.

Kapitein, L.C., Yau, K.W., and Hoogenraad, C.C. (2010). Microtubule Dynamics in Dendritic Spines (Methods Cell Biol).

Keihani, S., Kluever, V., Mandad, S., Bansal, V., Rahman, R., Fritsch, E., Caldi Gomes, L., Gärtner, A., Kügler, S., Urlaub, H., et al. (2019). The long noncoding RNA neuroLNC regulates presynaptic activity by interacting with the neurodegeneration-associated protein TDP-43. Sci. Adv. *5*.

Keil, K.P., Sethi, S., Wilson, M.D., Chen, H., and Lein, P.J. (2017). In vivo and in vitro sex differences in the dendritic morphology of developing murine hippocampal and cortical neurons. Sci. Rep. *7*, 1–15.

Kerr, J.E., Allore, R.J., Beck, S.G., and Handa, R.J. (1995). Distribution and hormonal regulation of androgen receptor (ar) and ar messenger ribonucleic acid in the rat hippocampus. Endocrinology *136*, 3213–3221.

Kokras, N., Sotiropoulos, I., Besinis, D., Tzouveka, E.L., Almeida, O.F.X., Sousa, N., and Dalla, C. (2019). Neuroplasticity-related correlates of environmental enrichment combined with physical activity differ between the sexes. Eur. Neuropsychopharmacol. *29*, 1–15.

Kononenko, N.I., Kuehl-Kovarik, M.C., Partin, K.M., and Dudek, F.E. (2008). Circadian difference in firing rate of isolated rat suprachiasmatic nucleus neurons. Neurosci. Lett. *436*, 314–316.

Konopka, R.J., and Benzer, S. (1971). Clock mutants of Drosophila melanogaster. Proc. Natl. Acad. Sci. U. S. A. *68*, 2112–2116.

Koopman, P., Gubbay, J., Vivian, N., Goodfellow, P., and Lovell-Badge, R. (1991). Male development of chromosomally female mice transgenic for Sry. Nature *351*, 117–121.

Kos, A., Wanke, K.A., Gioio, A., Martens, G.J., Kaplan, B.B., and Aschrafi, A. (2016). Monitoring mRNA Translation in Neuronal Processes Using Fluorescent Non-Canonical Amino Acid Tagging. J. Histochem. Cytochem. *64*, 323–333.

Koss, W.A., and Frick, K.M. (2017). Sex differences in hippocampal function. J. Neurosci.

Res. *95*, 539–562.

Kraszewski, K., Mundigl, O., Daniell, L., Verderio, C., Matteoli, M., and De Camilli, P. (1995). Synaptic vesicle dynamics in living cultured hippocampal neurons visualized with CY3-conjugated antibodies directed against the lumenal domain of synaptotagmin. J. Neurosci. *15*, 4328–4342.

Kuhlman, S.J., and McMahon, D.G. (2004). Rhythmic regulation of membrane potential and potassium current persists in SCN neurons in the absence of environmental input. Eur. J. Neurosci. *20*, 1113–1117.

Kumar, A., Bean, L.A., Rani, A., Jackson, T., and Foster, T.C. (2015). Contribution of estrogen receptor subtypes, ERα, ERβ, and GPER1 in rapid estradiol-mediated enhancement of hippocampal synaptic transmission in mice. Hippocampus *25*, 1556–1566.

Kwon, S.E., and Chapman, E.R. (2011). Synaptophysin Regulates the Kinetics of Synaptic Vesicle Endocytosis in Central Neurons. Neuron *70*, 847–854.

Landfield, P.W. (1996). Aging-related increase in hippocampal calcium channels. In Life Sciences, (Elsevier Inc.), pp. 399–404.

Lee, J.T., and Jaenisch, R. (1997). Long-range cis effects of ectopic X-inactivation centres on a mouse autosome. Nature *386*, 275–279.

Lehman, M.N., Silver, R., Gladstone, W.R., Kahn, R.M., Gibson, M., and Bittman, E.L. (1987). Circadian rhythmicity restored by neural transplant. Immunocytochemical characterization of the graft and its integration with the host brain. J. Neurosci. *7*, 1626–1638.

Lephart, E.D., Lund, T.D., and Horvath, T.L. (2001). Brain androgen and progesterone metabolizing enzymes: Biosynthesis, distribution and function. In Brain Research Reviews, (Brain Res Brain Res Rev), pp. 25–37.

Li, X., Zhao, X., Fang, Y., Jiang, X., Duong, T., Fan, C., Huang, C.C., and Kain, S.R. (1998). Generation of destabilized green fluorescent protein as a transcription reporter. J. Biol. Chem. *273*, 34970–34975.

Liao, Y., Smyth, G.K., and Shi, W. (2019). The R package Rsubread is easier, faster, cheaper and better for alignment and quantification of RNA sequencing reads. Nucleic Acids Res. *47*, e47.

Liu, C., Weaver, D.R., Strogatz, S.H., and Reppert, S.M. (1997). Cellular Construction of a Circadian Clock: Period Determination in the Suprachiasmatic Nuclei. Cell *91*, 855–860.

Liu, Y., Hu, W., Murakawa, Y., Yin, J., Wang, G., Landthaler, M., and Yan, J. (2013). Cold-

induced RNA-binding proteins regulate circadian gene expression by controlling alternative polyadenylation. Sci. Rep. *3*, 1–11.

Loy, R., Gerlach, J.L., and McEwen, B.S. (1988). Autoradiographic localization of estradiol-binding neurons in the rat hippocampal formation and entorhinal cortex. Dev. Brain Res. *39*, 245–251.

Luine, V., Villegas, M., Martinez, C., and McEwen, B.S. (1994). Repeated stress causes reversible impairments of spatial memory performance. Brain Res. *639*, 167–170.

Luine, V., Martinez, C., Villegas, M., Magariños, A.M., and Mcewen, B.S. (1996). Restraint stress reversibly enhances spatial memory performance. Physiol. Behav. *59*, 27–32.

De Mairan, J.J.. (1729). Observation Botanique. Hist. l'Academie R. Des Sci. 35.

Marpegan, L., Swanstrom, A.E., Chung, K., Simon, T., Haydon, P.G., Khan, S.K., Liu, A.C., Herzog, E.D., and Beaulé, C. (2011). Circadian regulation of ATP release in astrocytes. J. Neurosci. *31*, 8342–8350.

Matteoli, M., Takei, K., Perin, M.S., Sudhof, T.C., and De Camilli, P. (1992). Exo-endocytotic recycling of synaptic vesicles in developing processes of cultured hippocampal neurons. J. Cell Biol. *117*, 849–861.

Matteoli, M., Verderio, C., Krawzeski, K., Mundigl, O., Coco, S., Fumagalli, G., and De Camilli, P. (1995). Mechanisms of synaptogenesis in hippocampal neurons in primary culture. J. Physiol. - Paris *89*, 51–55.

May, T., Adesina, I., McGillivray, J., and Rinehart, N.J. (2019). Sex differences in neurodevelopmental disorders. Curr. Opin. Neurol. *32*, 622–626.

McClure, C., Cole, K.L.H., Wulff, P., Klugmann, M., and Murray, A.J. (2011). Production and titering of recombinant adeno-associated viral vectors. J. Vis. Exp.

McEwen, B.S., and Milner, T.A. (2007). Hippocampal formation: Shedding light on the influence of sex and stress on the brain. Brain Res. Rev. *55*, 343–355.

McEwen, B.S., and Milner, T.A. (2017). Understanding the broad influence of sex hormones and sex differences in the brain. J. Neurosci. Res. *95*, 24–39.

Mclaren, A. (1988). Sex determination in mammals. Trends Genet. *4*, 153–157.

Mei, L., Fan, Y., Lv, X., Welsh, D.K., Zhan, C., and Zhang, E.E. (2018). Long-term in vivo recording of circadian rhythms in brains of freely moving mice. Proc. Natl. Acad. Sci. U. S. A. *115*, 4276–4281.

Mercer, T.R., Dinger, M.E., and Mattick, J.S. (2009). Long non-coding RNAs: Insights into functions. Nat. Rev. Genet. *10*, 155–159.

Meredith, A.L., Wiler, S.W., Miller, B.H., Takahashi, J.S., Fodor, A.A., Ruby, N.F., and Aldrich, R.W. (2006). BK calcium-activated potassium channels regulate circadian behavioral rhythms and pacemaker output. Nat. Neurosci. *9*, 1041–1049.

Meyer-Bernstein, E.L., and Morin, L.P. (1996). Differential serotonergic innervation of the suprachiasmatic nucleus and the intergeniculate leaflet and its role in circadian rhythm modulation. J. Neurosci. *16*, 2097–2111.

Miller, S., Yasuda, M., Coats, J.K., Jones, Y., Martone, M.E., and Mayford, M. (2002). Disruption of dendritic translation of CaMKIIα impairs stabilization of synaptic plasticity and memory consolidation. Neuron *36*, 507–519.

Milner, T.A., Ayoola, K., Drake, C.T., Herrick, S.P., Tabori, N.E., McEwen, B.S., Warrier, S., and Alves, S.E. (2005). Ultrastructural localization of estrogen receptor β immunoreactivity in the rat hippocampal formation. J. Comp. Neurol. *491*, 81–95.

Molnár, E. (2011). Long-term potentiation in cultured hippocampal neurons. Semin. Cell Dev. Biol. *22*, 506–513.

Montgomery, J.R., and Meredith, A.L. (2012). Genetic activation of BK currents in vivo generates bidirectional effects on neuronal excitability. Proc. Natl. Acad. Sci. U. S. A. *109*, 18997–19002.

Moore, R.Y., and Eichler, V.B. (1972). Loss of a circadian adrenal corticosterone rhythm following suprachiasmatic lesions in the rat. Brain Res. *42*, 201–206.

Moore, R.Y., and Lenn, N.J. (1972). A retinohypothalamic projection in the rat. J. Comp. Neurol. *146*, 1–14.

Moscona, A. (1952). Cell suspensions from organ rudiments of chick embryos. Exp. Cell Res. *3*, 535–539.

Moscona, A., and Moscana, H. (1952). The dissociation and aggregation of cells from organ rudiments of the early chick embryo. J. Anat. *86*, 287–301.

Munn, R.G.K., and Bilkey, D.K. (2012). The firing rate of hippocampal CA1 place cells is modulated with a circadian period. Hippocampus *22*, 1325–1337.

Murakami, S., and Arai, Y. (1989). Neuronal death in the developing sexually dimorphic periventricular nucleus of the preoptic area in the female rat: Effect of neonatal androgen treatment. Neurosci. Lett. *102*, 185–190.

Murphy, D.D., and Segal, M. (1997). Morphological plasticity of dendritic spines in central neurons is mediated by activation of cAMP response element binding protein. Proc. Natl. Acad. Sci. U. S. A. *94*, 1482–1487.

Nagoshi, E., Saini, C., Bauer, C., Laroche, T., Naef, F., and Schibler, U. (2004). Circadian gene expression in individual fibroblasts: cell-autonomous and self-sustained oscillators pass time to daughter cells. Cell *119*, 693–705.

Nakai, J. (1956). Dissociated dorsal root ganglia in tissue culture. Am. J. Anat. *99*, 81–129.

Nakamura, N.H., Rosell, D.R., Akama, K.T., and McEwen, B.S. (2004). Estrogen and ovariectomy regulate mRNA and protein of glutamic acid decarboxylases and cation-chloride cotransporters in the adult rat hippocampus. Neuroendocrinology *80*, 308–323.

Nakamura, T.J., Nakamura, W., Yamazaki, S., Kudo, T., Cutler, T., Colwell, C.S., and Block, G.D. (2011). Age-related decline in circadian output. J. Neurosci. *31*, 10201–10205.

Noya, S.B., Colameo, D., Brüning, F., Spinnler, A., Mircsof, D., Opitz, L., Mann, M., Tyagarajan, S.K., Robles, M.S., and Brown, S.A. (2019). The forebrain synaptic transcriptome is organized by clocks but its proteome is driven by sleep. Science (80-.). *366*.

Ohnishi, N., Tahara, Y., Kuriki, D., Haraguchi, A., and Shibata, S. (2014). Warm water bath stimulates phase-shifts of the peripheral circadian clocks in PER2::LUCIFERASE mouse. PLoS One *9*.

Olsen, J. V., de Godoy, L.M.F., Li, G., Macek, B., Mortensen, P., Pesch, R., Makarov, A., Lange, O., Horning, S., and Mann, M. (2005). Parts per million mass accuracy on an orbitrap mass spectrometer via lock mass injection into a C-trap. Mol. Cell. Proteomics *4*, 2010–2021.

Osada, T., Nishihara, M., and Kimura, F. (1991). Sex differences in the basal firing rate and the responsiveness to opioid peptides of rat hippocampal neurons. Jpn J Physiol *41*, 843–850.

Ostroff, L.E., Watson, D.J., Cao, G., Parker, P.H., Smith, H., and Harris, K.M. (2018). Shifting patterns of polyribosome accumulation at synapses over the course of hippocampal long-term potentiation. Hippocampus *28*, 416–430.

Partch, C.L., Green, C.B., and Takahashi, J.S. (2014). Molecular architecture of the mammalian circadian clock. Trends Cell Biol. *24*, 90–99.

Paul, J.R., DeWoskin, D., McMeekin, L.J., Cowell, R.M., Forger, D.B., and Gamble, K.L. (2016). Regulation of persistent sodium currents by glycogen synthase kinase 3 encodes daily rhythms of neuronal excitability. Nat. Commun. *7*.

Paul, J.R., Davis, J.A., Goode, L.K., Becker, B.K., Fusilier, A., Meador-Woodruff, A., and Gamble, K.L. (2019). Circadian regulation of membrane physiology in neural oscillators throughout the brain. Eur. J. Neurosci. 1–30.

Pembroke, W.G., Babbs, A., Davies, K.E., Ponting, C.P., and Oliver, P.L. (2015). Temporal transcriptomics suggest that twin-peaking genes reset the clock. Elife *4*, 1–15.

Pennartz, C.M.A., Bierlaagh, M.A., and Geurtsen, A.M.S. (1997). Cellular Mechanisms Underlying Spontaneous Firing in Rat Suprachiasmatic Nucleus: Involvement of a Slowly Inactivating Component of Sodium Current. J. Neurophysiol. *78*, 1811–1825.

Pennartz, C.M.A., De Jeu, M.T.G., Bos, N.P.A., Schaap, J., and Geurtsen, A.M.S. (2002). Diurnal modulation of pacemaker potentials and calcium current in the mammalian circadian clock. Nature *416*, 286–290.

Peretti, D., Bastide, A., Radford, H., Verity, N., Molloy, C., Martin, M.G., Moreno, J.A., Steinert, J.R., Smith, T., Dinsdale, D., et al. (2015). RBM3 mediates structural plasticity and protective effects of cooling in neurodegeneration. Nature *518*, 236–239.

Pfaff, D.W. (1968). Autoradiographic localization of radioactivity in rat brain after injection of tritiated sex hormones. Science (80-.). *161*, 1355–1356.

Pfaff, D., and Keiner, M. (1973). Atlas of estradiol-concentrating cells in the central nervous system of the female rat. J. Comp. Neurol. *151*, 121–157.

Picon, R. (1976). Testosterone secretion by foetal rat testes in vitro. J. Endocr. *71*, 231–238.

Pittendrigh, C.S. (1960). Circadian Rhythms and the Circadian Organization of Living Systems. Cold Spring Harb. Symp. Quant. Biol. *25*, 159–184.

Pozzo-Miller, L.D., Inoue, T., and Murphy, D.D. (1999). Estradiol increases spine density and NMDA-dependent Ca2+ transients in spines of CA1 pyramidal neurons from hippocampal slices. J. Neurophysiol. *81*, 1404–1411.

Rabinowicz, T., Dean, D.E., Petetot, J.M.D.C., and De Courten-Myers, G.M. (1999). Gender differences in the human cerebral cortex: More neurons in males; more processes in females. J. Child Neurol. *14*, 98–107.

Ray, S., Valekunja, U.K., Stangherlin, A., Howell, S.A., Snijders, A.P., Damodaran, G., and Reddy, A.B. (2020). Circadian rhythms in the absence of the clock gene Bmal1. Science *367*, 800–806.

Reinke, H., and Asher, G. (2016). Circadian Clock Control of Liver Metabolic Functions. Gastroenterology *150*, 574–580.

Reisert, I., Engele, J., and Pilgrim, C. (1989). Early sexual differentiation of diencephalic dopaminergic neurons of the rat in vitro. Cell Tissue Res. *255*, 411–417.

Renaud, J., Dumont, F., Khelfaoui, M., Foisset, S.R., Letourneur, F., Bienvenu, T., Khwaja, O., Dorseuil, O., and Billuart, P. (2015). Identification of intellectual disability genes showing circadian clock-dependent expression in the mouse hippocampus. Neuroscience *308*, 11–50.

Ringer, S. (1882). Concerning the Influence exerted by each of the Constituents of the Blood on the Contraction of the Ventricle. J. Physiol. *3*, 380–393.

Ritchie, M.E., Phipson, B., Wu, D., Hu, Y., Law, C.W., Shi, W., and Smyth, G.K. (2015). limma powers differential expression analyses for RNA-sequencing and microarray studies. Nucleic Acids Res. *43*, e47–e47.

Rizzoli, S.O., and Betz, W.J. (2005). Synaptic vesicle pools. Nat. Rev. Neurosci. *6*, 57–69.

Rosenthal, L.-M., Tong, G., Walker, C., Wowro, S., Krech, J., Pfitzer, C., Justus, G., Berger, F., and Schmitt, K. (2017). Neuroprotection via RNA-binding protein RBM3 expression is regulated by hypothermia but not by hypoxia in human SK-N-SH neurons. Hypoxia *Volume 5*, 33–43.

Sanada, K., Okano, T., and Fukada, Y. (2002). Mitogen-activated protein kinase phosphorylates and negatively regulates basic helix-loop-helix-PAS transcription factor BMAL1. J. Biol. Chem. *277*, 267–271.

Scarnati, M.S., Kataria, R., Biswas, M., and Paradiso, K.G. (2018). Active presynaptic ribosomes in the mammalian brain, and altered transmitter release after protein synthesis inhibition. Elife *7*, 1–28.

Scharfman, H.E., Mercurio, T.C., Goodman, J.H., Wilson, M.A., and MacLusky, N.J. (2003). Hippocampal Excitability Increases during the Estrous Cycle in the Rat: A Potential Role for Brain-Derived Neurotrophic Factor. J. Neurosci. *23*, 11641–11652.

Scoville, W.B., and Milner, B. (1957). Loss of recent memory after bilateral hippocampal lesions. J. Neurol. Neurosurg. Psychiatry *20*, 11–21.

Sherwin, B.B. (1988). Estrogen and/or androgen replacement therapy and cognitive functioning in surgically menopausal women. Psychoneuroendocrinology *13*, 345–357.

Simerly, R.B., Swanson, L.W., and Gorski, R.A. (1985a). The distribution of monoaminergic cells and fibers in a periventricular preoptic nucleus involved in the control of gonadotropin release: Immunohistochemical evidence for a dopaminergic sexual dimorphism. Brain Res. *330*, 55–64.

Simerly, R.B., Swanson, L.W., Handa, R.J., and Gorski, R.A. (1985b). Influence of perinatal androgen on the sexually dimorphic distribution of tyrosine hydroxylase-immunoreactive cells and fibers in the anteroventral periventricular nucleus of the rat. Neuroendocrinology *40*, 501–510.

Smarr, B.L., Jennings, K.J., Driscoll, J.R., and Kriegsfeld, L.J. (2014). A time to remember: The role of circadian clocks in learning and memory. Behav. Neurosci. *128*, 283–303.

Smart, F., Aschrafi, A., Atkins, A., Owens, G.C., Pilotte, J., Cunningham, B.A., and Vanderklish, P.W. (2007a). Two isoforms of the cold-inducible mRNA-binding protein RBM3 localize to dendrites and promote translation. J. Neurochem. *101*, 1367–1379.

Smart, F., Aschrafi, A., Atkins, A., Owens, G.C., Pilotte, J., Cunningham, B.A., and Vanderklish, P.W. (2007b). Two isoforms of the cold-inducible mRNA-binding protein RBM3 localize to dendrites and promote translation. J. Neurochem. *101*, 1367–1379.

Smith, C.C., and McMahon, L.L. (2005). Estrogen-induced increase in the magnitude of long-term potentiation occurs only when the ratio of NMDA transmission to AMPA transmission is increased. J. Neurosci. *25*, 7780–7791.

Smith, P.K., Krohn, R.I., Hermanson, G.T., Mallia, A.K., Gartner, F.H., Provenzano, M.D., Fujimoto, E.K., Goeke, N.M., Olson, B.J., and Klenk, D.C. (1985). Measurement of protein using bicinchoninic acid. Anal. Biochem. *150*, 76–85.

Snider, K.H., Sullivan, K.A., and Obrietan, K. (2018). Circadian Regulation of Hippocampal-Dependent Memory: Circuits, Synapses, and Molecular Mechanisms. Neural Plast. *2018*.

Spanagel, R., Pendyala, G., Abarca, C., Zghoul, T., Sanchis-Segura, C., Magnone, M.C., Lascorz, J., Depner, M., Holzberg, D., Soyka, M., et al. (2005). The clock gene Per2 influences the glutamatergic system and modulates alcohol consumption. Nat. Med. *11*, 35–42.

Stephan, F.K., and Zucker, I. (1972). Circadian rhythms in drinking behavior and locomotor activity of rats are eliminated by hypothalamic lesions. Proc. Natl. Acad. Sci. U. S. A. *69*, 1583–1586.

Stevens, R.J., Akbergenova, Y., Jorquera, R.A., and Troy Littleton, J. (2012). Abnormal synaptic vesicle biogenesis in Drosophila synaptogyrin mutants. J. Neurosci. *32*, 18054–18067.

Steward, O., and Levy, W.B. (1982). Preferential localization of polyribosomes under the base of dendritic spines in granule cells of the dentate gyrus. J. Neurosci. *2*, 284–291.

Stumpf, W.E. (1968). Estradiol-concentrating neurons: Topography in the hypothalamus by

dry-mount autoradiography. Science (80-.). *162*, 1001–1003.

Stumpf, W.E., and Sar, M. (1976). Steroid hormone target sites in the brain: The differential distribution of estrogen, progestin, androgen and glucocorticosteroid. J. Steroid Biochem. *7*, 1163–1170.

Sul, J.Y., Orosz, G., Givens, R.S., Haydon, P.G., and Haydon, P.G. (2004). Astrocytic Connectivity in the Hippocampus. Neuron Glia Biol. *1*, 3–11.

Sureban, S.M., Ramalingam, S., Natarajan, G., May, R., Subramaniam, D., Bishnupuri, K.S., Morrison, A.R., Dieckgraefe, B.K., Brackett, D.J., Postier, R.G., et al. (2008). Translation regulatory factor RBM3 is a proto-oncogene that prevents mitotic catastrophe. Oncogene *27*, 4544–4556.

Sutton, M.A., and Schuman, E.M. (2006). Dendritic Protein Synthesis, Synaptic Plasticity, and Memory. Cell *127*, 49–58.

Swiech, L., Heidenreich, M., Banerjee, A., Habib, N., Li, Y., Trombetta, J., Sur, M., and Zhang, F. (2015). In vivo interrogation of gene function in the mammalian brain using CRISPR-Cas9. Nat. Biotechnol. *33*, 102–106.

Tabori, N.E., Stewart, L.S., Znamensky, V., Romeo, R.D., Alves, S.E., McEwen, B.S., and Milner, T.A. (2005). Ultrastructural evidence that androgen receptors are located at extranuclear sites in the rat hippocampal formation. Neuroscience *130*, 151–163.

Takamori, S., Holt, M., Stenius, K., Lemke, E.A., Grønborg, M., Riedel, D., Urlaub, H., Schenck, S., Brügger, B., Ringler, P., et al. (2006a). Molecular anatomy of a trafficking organelle. Cell *127*, 831–846.

Takamori, S., Holt, M., Stenius, K., Lemke, E.A., Grønborg, M., Riedel, D., Urlaub, H., Schenck, S., Brügger, B., Ringler, P., et al. (2006b). Molecular Anatomy of a Trafficking Organelle. Cell *127*, 831–846.

Tarpey, P.S., Smith, R., Pleasance, E., Whibley, A., Edkins, S., Hardy, C., O'Meara, S., Latimer, C., Dicks, E., Menzies, A., et al. (2009). A systematic, large-scale resequencing screen of X-chromosome coding exons in mental retardation. Nat. Genet. *41*, 535–543.

Terajima, H., Yoshitane, H., Ozaki, H., Suzuki, Y., Shimba, S., Kuroda, S., Iwasaki, W., and Fukada, Y. (2017). ADARB1 catalyzes circadian A-to-I editing and regulates RNA rhythm. Nat. Genet. *49*, 146–151.

Thiele, C., Hannah, M.J., Fahrenholz, F., and Huttner, W.B. (2000). Cholesterol binds to Synaptophysin and is required for biogenesis of synaptic vesicles. Nat. Cell Biol. *2*, 42–49.

Tian, G.F., Takano, T., Lin, J.H.C., Wang, X., Bekar, L., and Nedergaard, M. (2006). Imaging of cortical astrocytes using 2-photon laser scanning microscopy in the intact mouse brain. Adv. Drug Deliv. Rev. *58*, 773–787.

Tiedge, H., and Brosius, J. (1996). Translational machinery in dendrites of hippocampal neurons in culture. J. Neurosci. *16*, 7171–7181.

Toft, D., and Gorski, J. (1966). A receptor molecule for estrogens: isolation from the rat uterus and preliminary characterization. Proc. Natl. Acad. Sci. U. S. A. *55*, 1574–1581.

Tom Dieck, S., Kochen, L., Hanus, C., Heumüller, M., Bartnik, I., Nassim-Assir, B., Merk, K., Mosler, T., Garg, S., Bunse, S., et al. (2015). Direct visualization of newly synthesized target proteins in situ. Nat. Methods *12*, 411–414.

Tornøe, C.W., Christensen, C., and Meldal, M. (2002). Peptidotriazoles on solid phase: [1,2,3]-Triazoles by regiospecific copper(I)-catalyzed 1,3-dipolar cycloadditions of terminal alkynes to azides. J. Org. Chem. *67*, 3057–3064.

Towart, L.A., Alves, S.E., Znamensky, V., Hayashi, S., McEwen, B.S., and Milner, T.A. (2003). Subcellular relationships between cholinergic terminals and estrogen receptor-α in the dorsal hippocampus. J. Comp. Neurol. *463*, 390–401.

Travnickova-Bendova, Z., Cermakian, N., Reppert, S.M., and Sassone-Corsi, P. (2002). Bimodal regulation of mPeriod promoters by CREB-dependent signaling and CLOCK/BMAL1 activity. Proc. Natl. Acad. Sci. U. S. A. *99*, 7728–7733.

Truckenbrodt, S., Viplav, A., Jähne, S., Vogts, A., Denker, A., Wildhagen, H., Fornasiero, E.F., and Rizzoli, S.O. (2018). Newly produced synaptic vesicle proteins are preferentially used in synaptic transmission. EMBO J. *37*.

Tso, C.F., Simon, T., Greenlaw, A.C., Puri, T., Mieda, M., and Herzog, E.D. (2017). Astrocytes Regulate Daily Rhythms in the Suprachiasmatic Nucleus and Behavior. Curr. Biol. *27*, 1055–1061.

Vegeto, E., Villa, A., Della Torre, S., Crippa, V., Rusmini, P., Cristofani, R., Galbiati, M., Maggi, A., and Poletti, A. (2020). The Role of Sex and Sex Hormones in Neurodegenerative Diseases. Endocr. Rev. *41*.

Wade, C.B., and Dorsa, D.M. (2003). Estrogen activation of cyclic adenosine 5′-monophosphate response element-mediated transcription requires the extracellularly regulated kinase/mitogen-activated protein kinase pathway. Endocrinology *144*, 832–838.

Wang, J., Vasaikar, S., Shi, Z., Greer, M., and Zhang, B. (2017). WebGestalt 2017: a more comprehensive, powerful, flexible and interactive gene set enrichment analysis toolkit.

Nucleic Acids Res. *45*, W130–W137.

Wang, L.M., Dragich, J.M., Kudo, T., Odom, I.H., Welsh, D.K., O'Dell, T.J., and Colwell, C.S. (2009). Expression of the circadian clock gene *Period2* in the hippocampus: possible implications for synaptic plasticity and learned behaviour. ASN Neuro *1*, 139–152.

Wang, W., Le, A.A., Hou, B., Lauterborn, J.C., Cox, C.D., Levin, E.R., Lynch, G., and Gall, C.M. (2018). Memory-related synaptic plasticity is sexually dimorphic in rodent hippocampus. J. Neurosci. *38*, 7935–7951.

Ward, I.L., and Weisz, J. (1980). Maternal Stress Alters Plasma Testosterone in Fetal Males. Science (80-.). *207*, 328–329.

Watanabe, K., Koibuchi, N., Ohtake, H., and Yamaoka, S. (1993). Circadian rhythms of vasopressin release in primary cultures of rat suprachiasmatic nucleus. Brain Res. *624*, 115–120.

Waters, E.M., Mitterling, K., Spencer, J.L., Mazid, S., McEwen, B.S., and Milner, T.A. (2009). Estrogen receptor alpha and beta specific agonists regulate expression of synaptic proteins in rat hippocampus. Brain Res. *1290*, 1–11.

Weiland, N., Orikasa, C., Hayashi, S., and McEwen, B. (1997). Distribution and Hormone Regulation of Estrogen Receptor Immunoreactive Cells in the Hippocampus of Male and Female Rats. J. Comp. Neurol. *388*.

Welsh, D.K., Logothetis, D.E., Meister, M., and Reppert, S.M. (1995). Individual neurons dissociated from rat suprachiasmatic nucleus express independently phased circadian firing rhythms. Neuron *14*, 697–706.

Welsh, D.K., Takahashi, J.S., and Kay, S.A. (2010). Suprachiasmatic Nucleus: Cell Autonomy and Network Properties. Annu. Rev. Physiol. *72*, 551–577.

West, M.O., and Deadwyler, S.A. (1980). Circadian modulation of granule cell response to perforant path synaptic input in the rat. Neuroscience *5*, 1597–1602.

Woolley, C.S., Gould, E., Frankfurt, M., and McEwen, B.S. (1990). Naturally occurring fluctuation in dendritic spine density on adult hippocampal pyramidal neurons. J. Neurosci. *10*, 4035–4039.

Wu, G., Anafi, R.C., Hughes, M.E., Kornacker, K., and Hogenesch, J.B. (2016). MetaCycle: An integrated R package to evaluate periodicity in large scale data. Bioinformatics *32*, 3351–3353.

Yagi, S., and Galea, L.A.M. (2019). Sex differences in hippocampal cognition and

neurogenesis. Neuropsychopharmacology *44*, 200–213.

Yamaguchi, S., Isejima, H., Matsuo, T., Okura, R., Yagita, K., Kobayashi, M., and Okamura, H. (2003). Synchronization of cellular clocks in the suprachiasmatic nucleus. Science *302*, 1408–1412.

Yamamoto, T., Nakahata, Y., Soma, H., Akashi, M., Mamine, T., and Takumi, T. (2004). Transcriptional oscillation of canonical clock genes in mouse peripheral tissues. BMC Mol. Biol. *5*, 18.

Yamazaki, S., Kerbeshian, M.C., Hocker, C.G., Block, G.D., and Menaker, M. (1998). Rhythmic properties of the hamster suprachiasmatic nucleus in vivo. J. Neurosci. *18*, 10709–10723.

Yamazaki, S., Numano, R., Abe, M., Hida, A., Takahashi, R.I., Ueda, M., Block, G.D., Sakaki, Y., Menaker, M., and Tei, H. (2000). Resetting central and peripheral circadian oscillators in transgenic rats. Science (80-.). *288*, 682–685.

Yan, J., Wang, H., Liu, Y., and Shao, C. (2008). Analysis of gene regulatory networks in the mammalian circadian rhythm. PLoS Comput. Biol. *4*, e1000193.

Yan, J., Goerne, T., Zelmer, A., Guzman, R., Kapfhammer, J.P., Wellmann, S., and Zhu, X. (2019). The RNA-Binding Protein RBM3 Promotes Neural Stem Cell (NSC) Proliferation Under Hypoxia. Front. Cell Dev. Biol. *7*.

Yang, H.J., Zhuang, R.J., Li, Y.B., Li, T., Yuan, X., Lei, B.B., Xie, Y.F., and Wang, M. (2019). Cold-inducible protein RBM3 mediates hypothermic neuroprotection against neurotoxin rotenone via inhibition on MAPK signalling. J. Cell. Mol. Med. *23*, 7010–7020.

Yao, T., and Asayama, Y. (2017). Animal-cell culture media: History, characteristics, and current issues. Reprod. Med. Biol. *16*, 99–117.

Yavin, E., and Yavin, Z. (1974). Attachment and culture of dissociated cells from rat embryo cerebral hemispheres on poly lysine-coated surface. J. Cell Biol. *62*, 540–546.

Yoo, S.-H., Yamazaki, S., Lowrey, P.L., Shimomura, K., Ko, C.H., Buhr, E.D., Siepka, S.M., Hong, H.-K., Oh, W.J., Yoo, O.J., et al. (2004). PERIOD2::LUCIFERASE real-time reporting of circadian dynamics reveals persistent circadian oscillations in mouse peripheral tissues. Proc. Natl. Acad. Sci. U. S. A. *101*, 5339–5346.

Young, M.W., and Kay, S.A. (2001). Time zones: a comparative genetics of circadian clocks. Nat. Rev. Genet. *2*, 702–715.

Van der Zee, E.A., Havekes, R., Barf, R.P., Hut, R.A., Nijholt, I.M., Jacobs, E.H., and

Gerkema, M.P. (2008). Circadian time-place learning in mice depends on Cry genes. Curr. Biol. *18*, 844–848.

Zhang, R., Lahens, N.F., Ballance, H.I., Hughes, M.E., and Hogenesch, J.B. (2014). A circadian gene expression atlas in mammals: Implications for biology and medicine. Proc. Natl. Acad. Sci. *111*, 16219–16224.

Zhao, L., Chen, S., Ming Wang, J., and Brinton, R.D. (2005). 17β-estradiol induces Ca2+ influx, dendritic and nuclear Ca2+ rise and subsequent cyclic AMP response element-binding protein activation in hippocampal neurons: A potential initiation mechanism for estrogen neurotrophism. Neuroscience *132*, 299–311.

Zhou, J., Zhang, H., Cohen, R.S., and Pandey, S.C. (2005). Effects of estrogen treatment on expression of brain-derived neurotrophic factor and cAMP response element-binding protein expression and phosphorylation in rat amygdaloid and hippocampal structures. Neuroendocrinology *81*, 294–310.

Zhu, X., Yan, J., Bregere, C., Zelmer, A., Goerne, T., Kapfhammer, J.P., Guzman, R., and Wellmann, S. (2019). RBM3 promotes neurogenesis in a niche-dependent manner via IMP2-IGF2 signaling pathway after hypoxic-ischemic brain injury. Nat. Commun. *10*, 1–14.

7| List of Abbreviations

a.u.	arbitrary unit
AVPV	anteroventral periventricular nucleus
BMAL	Brain and Muscle ARNT (Aryl hydrocarbon Receptor Nuclear Translocator) Like
BSA	bovine serum albumin
CA	cornu ammonis
CLOCK	Circadian Locomotor Output Cycles Kaput
Cry	cryptochrome
DG	dentate gyrus
DHT	dihydrotestosterone
DIV	day in vitro
DMEM	Dubelcco's Modified Eagle Medium
EGFP	enhanced green fluorescent protein
EPSP	excitatory post synaptic potential
FISH	fluorescence in-situ hybridization
GFP	green fluorescent protein
HBSS	Hank's balanced salt solution
HEPES	4-(2-Hydroxyethyl) piperazine-1-ethanesulfonic acid
KO	knock-out
LTP	long-term potentiation
NA	numerical aperature
NB	nanobody
PBS	phosphate-buffered saline
Per	period
PFA	paraformaldehyde
POA	pre-optic area
ROI	region of interest
RBM3	RNA-binding motif 3
RT	room temperature
SCN	suprachiasmatic nucleus
Scr	scrambled
SEM	standard error mean
shRNA	short-hairpin RNA
SRY	sex-determining region Y
Syph	Synaptophysin
Syt1	synaptotagmin 1
TTF	transcriptional translational feedback
TTX	tetrodotoxin

8| Acknowledgements

I would like to thank Silvio Rizzoli for giving me an opportunity to work on this project and supervising me throughout my PhD. His enthusiasm and passion are definitely contagious and they certainly motivated me through challenging times. I further thank him for providing me with the MATLAB scripts, which were the basis of my image analysis. I am very grateful that he gave me freedom to shape the project, but mostly I am grateful because he shared his knowledge on science and the world of academia. Thank you Silvio for all your efforts to raise a fully competent scientist.

I would like to thank my thesis committee members, Prof. Hannalore Ehrenreich and Prof. Henrik Bringmann for their input during the meetings. I also thank Prof. Peter Rehling and Roya Yousefi for their generous gift of puromycin, anisomycin and puromycin antibody. I further thank Transcriptome and Genome Analysis Laboratory (TAL) and Dr. Orr Shomroni for the RNA sequencing experiments and their analysis. I am very grateful to Prof. Christopher Colwell. He was a true inspiration to me. I would like to thank him for our constructive discussions, his support and encouragement. I also thank my medical doctoral student Wiebke Blumenstein, my lab rotation student Cagatay Aydin and my bachelor students Malena von Elling-Tammen and Janina Pasch for their help with the project.

Furthermore, I would like to thank the IMPRS Neuroscience office for their tireless work to organize the greatest graduate programme that I can imagine. Dear Micheal Hörner, thank you for sharing your vision with us and giving me the opportunity to be part of the Neuro family. Dear Sandra, I really appreciate your hard-work and thank you for that. And my fellow Neuro and MolBio friends, you are the reason why Göttingen is so beautiful. I will cherish all the memories that we gathered together. I would like to thank especially Kanishka Waghmare, Rashad Yusifov and Lukas Weiss for their unconditional friendship and endless support. Also I would like to thank my small Turkish family in Göttingen: Burak Bali, Burak Gür, Deniz Yüzak, Yunus Can Erol, Özge Demet Özcete and Özge Uslu. Benim fındık kıranlarım sizi cok seviyorum!

I would like to continue with the Turkish family and thank the dearest companions who are closest to my heart, my lovely family. Sizlere ve bütün emeklerinize tesekkür ediyorum canım annem Semra Sertel, babam Behcet Sertel, ve abicim Gökhan Sertel! Ablam Sinem Sertel ve yegenim Defne Sertel'e de paylastiklari mutluluklar icin tesekkür ederim. I would also like to thank my dear friends Özlem Cal, Mustafa Kücükkuru, Cem Emre Akbas, Burak Sahinbas, Simge Koc and Aynur Özlem for their unconditional love and support. Even though we are living in different countries, they always have time to share their beautiful smiles and thoughts.

Their determined characters and inspiring visions on life were a motivation to seek what I want from my life. Thank you for countless valuable lessons.

I am very grateful to be part of the greatest lab that I can wish for: Rizzoli lab. I would like to thank everyone for creating such an amazing atmosphere. First of all, I would like to thank Christina Schäffer-Zeising, Nicole Hartelt and Christina Patzelt. Your smile and your hard-work are greatly appreciated. Secondly, I am grateful to Dr. Eugenio Fornasiero for his scientific and non-scientific discussions. His door was always open for help. I would like to thank Verena Klüver for her help with molecular biology experiments, but mainly I am grateful for her friendship. I thank Dr. Martin Helm and Tal Dankovich for being the greatest office mates and for their scientific discussions. I thank Dr. Katharina Richter for her support throughout my PhD and her friendship. I cannot express my gratitude for Dr. Shama Sograte-Idrissi! Dear Shamita, thank you for your support and love.

Last but not least, I would like to thank Dr. Sebastian Jähne! Every day is beautiful with you. Every day I learn something from you. Every day I appreciate your love and friendship. Thank you for making my everyday life more meaningful.